DISLOCATIONS IN SEMICONDUCTORS

James R.K. Bigger

St. Catherine's College, Oxford.

A thesis submitted for the Degree of Doctor of Philosophy at the University of Oxford.
Trinity Term 1992.

DISLOCATIONS IN SEMICONDUCTORS

James R.K. Bigger

St. Catherine's College, Oxford

Submitted for the Degree of Doctor of Philosophy

Trinity Term 1992

ABSTRACT

A set of codes with 3D periodic boundary conditions has been developed to model dislocations in semiconductors. Several schemes have been used to investigate the atomic structure of dislocations; classical potentials incorporated in a Molecular Dynamics framework, a tight-binding k-space scheme and ab initio pseudopotential codes developed at Cambridge and Edinburgh.

An error has been detected in previous work that modelled dislocations using periodic boundary conditions. It is demonstrated, for the 90° and 30° Shockley partials, that a mismatch at the periodic boundaries leads to erroneous atomic and particularly electronic structures. A new approach is proposed which through its geometry obviates this problem.

The Stillinger Weber potential has been found to predict a completely new type of reconstruction for the 90° partial. Recent work by other authors confirms this and predicts significantly different results to earlier work. A thorough investigation has been made into the bonding processes involved in the core of the 90° partial. This study has involved reproducing much of the earlier work to understand why there has been such poor agreement between various authors. The reconstruction of the 90° partial is found to involve a symmetry lowering displacement intimately connected to its electronic structure. The band-gap is predicted to be clear of states, except for the possibility of shallow states at both band edges, which contradicts the findings of the most recent work on this partial by other authors.

The interaction of phosphorous with the 90° partial has been studied using the tight-binding model. The Hamiltonian has been parameterised by comparing the predictions to an earlier ab initio cluster method study. Good qualitative agreement with the ab initio work is obtained, including the prediction of a strong dislocation locking effect by phosphorous. Preliminary studies on the unreconstructed 30° partial show that phosphorous is strongly bound to the three-fold coordinated sites resulting in no states in the indirect band-gap.

The modelling of interstitial copper at the core of the 90° partial has been initiated. The ab initio codes have been used and new silicon and copper pseudopotentials tested. The first attempt to model copper located interstitially in the core was not successful and the reasons for this have been identified. However, it is evident from this investigation that the neutral copper strongly repels and does not form bonds with the surrounding silicon atoms.

A review is given of two techniques that have been developed to obtain the thermally averaged structure and concentration of vacancies at dislocations, together with a preliminary investigation on the Frank partial.

PREFACE

This thesis is an account of the work undertaken by the author in the Department of Materials, Oxford University, between October 1989 and September 1992, under the supervision of Dr. A.P. Sutton. The work has been supported by a Science and Engineering Research Council award.

This thesis has not been previously submitted for a degree at this or any other university. Part of the work contained in this thesis has or will be submitted for publication[1]. The work of others has been freely drawn upon and is duly acknowledged in the text. A full list of references is compiled at the back of this thesis.

---

[1] Bigger JRK, McInnes DA, Sutton AP, Payne MC, Stich I, King-Smith RD, Bird DM, and Clarke LJ, (1992), *submitted to Phys. Rev. Lett.*

Bigger JRK, McInnes DA and Sutton AP, (1992), *to be submitted to Acta. Metall.*

ACKNOWLEDGEMENTS

I would like to firstly thank my supervisor, Adrian Sutton, for all his help and encouragement throughout this project. I have greatly benefited from his knowledge and insight in this field of study. I shall also always smile when remembering several exhaustive walks (for Adrian) while over in Plymouth, New Hampshire, in which advice was flowing on matters far removed from science. I will really miss those eye opening discussions along with jokes of the quality of the now famous "salmon rusty". I wish him well in all future endeavours.

My thanks go to Duncan M^{c}Innes for a lively collaboration and friendship. Having swapped chemical "bonds" for the more lucrative kind I wish him every success in his new career.

I must thank Jon Wilson for his friendship and advice both in the labs and on the snooker table. I wish him success out in Holland and particularly with his ambition to marry and "make beautiful babies", and on this point it is with concern that I remind him of his snooker performances which consisted of half an hours excitement every six months.

There have been times when theoretical complications or diagnostic messages such as "panic" appearing on the Stardent computer lead to concern over the ability to obtain results for impurity interactions with dislocations; I am grateful to Peter Wilshaw and Tim Fell for reminding me of the problems associated with the experimental work in this field. I have thoroughly enjoyed their honesty and frankness in several illuminating conversations on the state of current work. I would also like to thank Tim Fell for his help in the experimental review in chapter 1.

The photographs in this thesis have been produced by Mohammad Taheri and the microfiches through Carol Bateman. Many thanks to them both for their help and time.

I am grateful to David Bird for his help in understanding the subtleties associated with the ab initio parallel code, and for all his help throughout the copper work. My thanks also go to the Cambridge crowd, Mike Payne, Ivan Stich, Ming-Hsien Lee, for their help in providing suitable pseudopotentials for the simulations undertaken here. I am particularly grateful to Victor Milman for his patience while I was checking for problems when

implementing the ab initio code on the Stardent here at Oxford.

I am grateful to Professor Sir Peter Hirsch and The Department of Materials for the use of the departmental facilities, and SERC together with The Worshipful Company of Ironmongers for financial support.

My thanks to Marta Ramos and Hashem Rafii-Tabar for several lively group "discussions" that invariably were started by Hashem with comments like "This damn computer must be female". I am also grateful to Chris Goringe for allowing me virtually exclusive use of the Stardent computer in the later stages of this work, with only the odd sneaky ab initio job appearing from time to time. I wish Ian Blackham well with the future and thank him for ensuring I am not even a close second for the longest serving Catz student.

I would like to thank all my other friends for the invaluable distractions of rowing, scuba diving, rock climbing, tennis, squash and beer. Finally I would like to dedicate this thesis to Heidi Avery, Jennifer Needham and my family for all their love and unwavering support which has been such a source of strength to me over the last three years.

TABLE OF CONTENTS

CHAPTER 4

CHAPTER 5

CHAPTER 6

CHAPTER 1

Introduction

1.1 Introduction

At the most fundamental level, the reliability of many electrical devices will be dependent on the properties of the p-n junction and the transistor. A direct correlation between the density of dislocations in the active region of a diode and the reverse current of the device has been established (Ravi, 1981). A similar correlation has been obtained for the Si bipolar transistor and dislocations are also correlated with premature junction breakdown (Bull *et al.*, 1979). There is thus an unambiguous relationship between dislocations and the electrical characteristics of the device. The efficiency and dependability of these devices are intimately linked to these basic properties and as a result material defects, such as dislocations, are generally one of the most common causes of device failure (Huff and Shimira, 1985).

Dislocations and impurities are inescapably linked. For example, metal contamination during processing reduces the nucleation barrier for dislocation formation (Bergholz *et al.*, 1991). Furthermore, once the dislocation is formed the impurities tend to getter there. The major effects observed are consequently related to a collective influence of dislocations and impurities.

An investigation of the electrical activity associated with dislocations is an area of intense study. The intention here is to give a review of the experimental, section 1.3, and theoretical, section 1.4, progress to date and to illuminate the areas that need further investigation. This leads to my thesis objectives, outlined in section 1.5. As a precursor to this, section 1.2 is intended to illustrate the type of dislocations that have been studied experimentally and

theoretically with a bias for those that will be studied in the remainder of this thesis. There is considerable justification for this bias, since these types of dislocations are one of the most commonly occurring in plastically deformed Si (Alexander, 1979; Weronek *et al.*, 1992).

1.2 The origin of Shockley partials in silicon

An introduction to the terminology and simple results of dislocation theory is presented here and is intentionally brief. For a fuller introduction to dislocations the reader is referred to Hirth and Lothe (1982) and Hull and Bacon (1984).

Application of stress to a crystal can nucleate dislocations which are line defects representing the boundary at which slip between adjacent atomic planes has taken place. Once formed, dislocations can move and the stress required to propagate them is the Peierls stress. The atomic displacement associated with the dislocation is represented by the Burgers vector, $\boldsymbol{b}$. The elastic energy of a dislocation is proportional to b^2 and this leads to *Franks rule* for the dissociation of a dislocation with Burgers vector, $\boldsymbol{b}_1$, to dislocations with Burgers vectors $\boldsymbol{b}_2$ and $\boldsymbol{b}_3$. His criterion is that the dissociation is energetically favourable if

$$b_1^2 > b_2^2 + b_3^2 \tag{1.1}$$

One immediate consequence of this is that dislocations with Burgers vectors that are multiples of perfect dislocations[1] are unstable. In an FCC crystal the shortest primitive lattice vectors are $1/2\langle 1\,1\,0\rangle$, and thus the energetically most stable perfect dislocations have Burgers vectors $1/2\langle 1\,1\,0\rangle$. Further, since the Peierls stress is least for the dislocation with the smallest magnitude Burgers vector (Hirth and Lothe, 1982), slip will occur most easily for perfect $1/2\langle 1\,1\,0\rangle$ dislocations. This stress is also least for those atomic planes with the greatest interplanar spacing, and these correspond to the closest-packed planes of the crystal (in FCC these are the $\{1\,1\,1\}$ planes). The principal glide system in FCC crystals is therefore

[1] A perfect dislocation has a Burgers vector that corresponds to a lattice vector of the crystal.

of the $\{1\,1\,1\}\,<1\,1\,0>$ type. Since the diamond cubic structure has an FCC lattice with a basis of two atoms, this is also the glide system for Si.

Glide dislocations lying along $<1\,1\,0>$ directions are either screw[2] or "60°" dislocations, $\boldsymbol{b}$ lying parallel or at 60° to the dislocation line respectively. Fig. 1.1a depicts the $\{1\,1\,1\}$ stacking sequence in the diamond cubic structure. The consequence of the two atom primitive unit cell is that the $\{1\,1\,1\}$ lattice planes are comprised of two atomic planes and their stacking sequence is ..AaBbCcAaBbCc.., as shown. A 60° perfect dislocation is formed by cutting out material, as illustrated by either of the dotted lines 1234 and 1564, and displacing the sides of the cut so that they join. This displacement places atoms such as II in the holes left by atoms like I. Note that atom II lies on a different $(20\bar{2})$ atomic plane to atom I, as illustrated by the squares and circles, so that the net displacement is

$$\boldsymbol{b}=\frac{1}{4}[1\bar{2}1]+\frac{1}{4}[10\bar{1}]=\frac{1}{2}[1\bar{1}0] \tag{1.2}$$

Due to this double-layer arrangement of the diamond cubic structure there exist two sets of dislocations with identical Burgers vectors. Using the notation of Hirth and Lothe, if material bounded by the surface 1234 is removed the extra half-plane ends between widely spaced planes, like Bb, forming the *shuffle set* dislocation. Alternatively, removing material bounded by the surface 1564 implies the half-plane ends between closely spaced layers, like aB, and the *glide set* dislocation is formed. The 60° perfect dislocations generated are illustrated in fig. 1.1b. A shift of the cut surface along the glide plane in fig. 1.1a, or equivalently, shifting bonds in both dislocations of fig. 1.1b, demonstrates that perfect dislocations of either set are glissile. Shockley (1953) suggested that the 60° dislocation would belong to the shuffle set since the number of bonds which have to be broken when the

---

[2] The work presented here describes the dissociation products of the 60° perfect dislocation only. However, the screw dissociates into two 30° *Shockley partials* and, as we shall see, this partial is one of the products of the 60° dissociation.

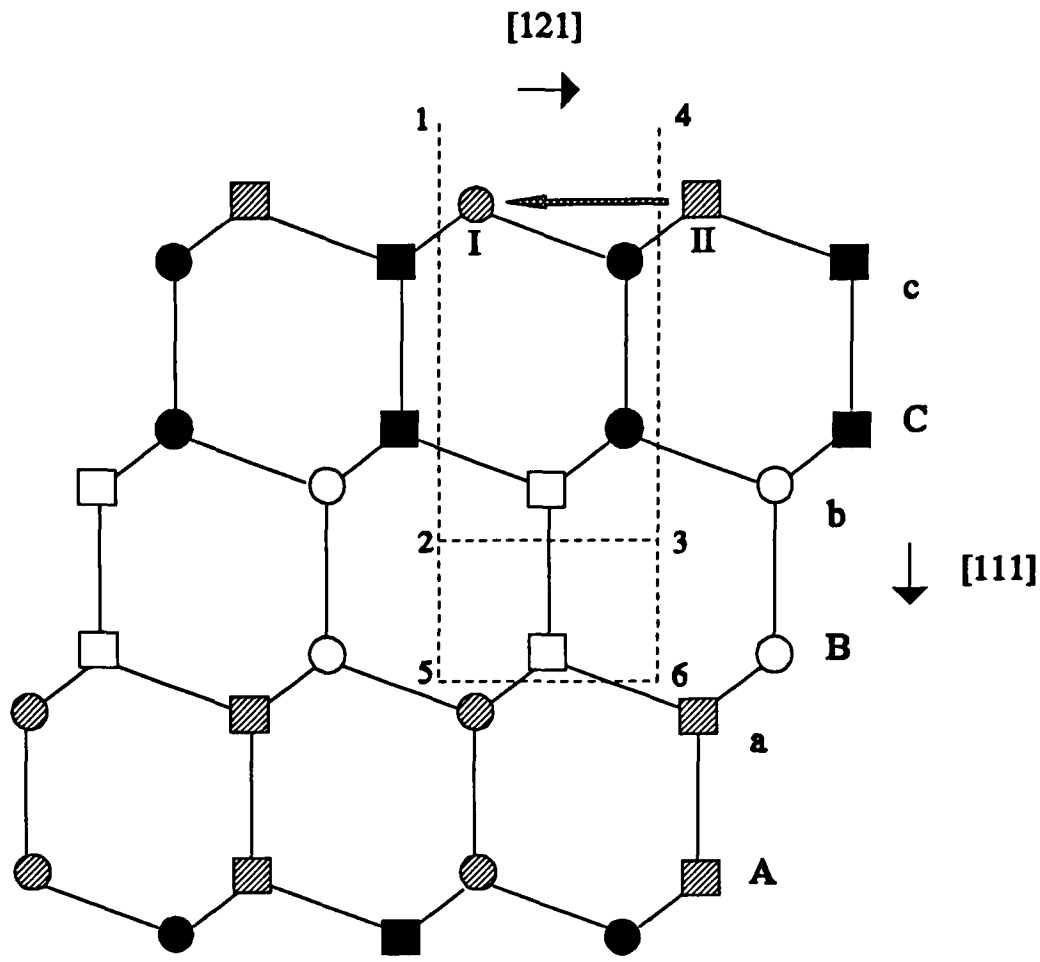

Fig. 1.1a Stacking of double layers in Diamond Cubic projected normal to $(10\bar{1})$ - Circles represent atoms in plane of paper and squares represent atoms in plane below.

Fig. 1.1b Perfect 60° dislocations of the Glide and Shuffle set.
(from Hirth and Lothe, 1968)

dislocation moves is one third of that for a dislocation of the glide set.

These perfect 60° dislocations can dissociate into Shockley partials which, using Frank's criterion, lowers the strain energy. However, the dissociation mechanism is different in the two cases. For the glide set, the vector dissociation of a perfect 60° glide dislocation forms the 90° and 30° Shockley partials

$$\frac{1}{2}[1\bar{1}0] \Rightarrow \frac{1}{6}[1\bar{2}1] + \frac{1}{6}[2\bar{1}\bar{1}] \tag{1.3}$$

These partials bound an intrinsic stacking fault (see below) which is a low energy fault that does not change the local tetrahedral bonding. This can be seen by imagining the Cc pairs in fig. 1.1a, and all pairs that continue above, to be shifted one step to the right in the stacking sequence. This transforms the Cc atoms into Aa positions, preserving the tetrahedral bonding with the Bb layer below, but producing a fault in the stacking sequence which has become ..AaBbAaBbCc..

From fig. 1.1a it can be seen that faults formed between adjacent layers of the *same* letter do not restore tetrahedral bonding and as a consequence have a high energy. For this reason dissociation of the shuffle set perfect dislocation cannot occur directly since it would lead to this type of high energy fault. Hornstra (1958) suggested a dissociation mechanism in which shuffle set dislocations associate themselves with a pair of Shockley partials on the neighbouring glide plane.

The application of the weak-beam method of electron microscopy showed that dislocations in Si and Ge are generally dissociated into partials (Ray and Cockayne, 1971; Häussermann and Schaumburg, 1973; Gomez *et al.*, 1975). However it was not possible from the image contrast to differentiate between simple dissociation of glide set dislocations and the Hornstra mechanism for shuffle set dissociation. By observing that dislocations glide in the dissociated configuration during plastic deformation (Gomez and Hirsch, 1977), doubt was cast on the shuffle set configurations since, as discussed by Hirth and Lothe (1982), these are likely to be much less mobile than the simple glide set partials. As noted by Hirsch (1985),

the shuffle configurations associated with a row of interstitials would be difficult to move without first constricting them, which is inconsistent with the observation that dislocations glide in the dissociated form. High Resolution electron images have been compared to computed images of the shuffle and glide cases (Anstis *et al.*, 1981; Olsen and Spence, 1981; Northrup *et al.*, 1981), and it was found that the experimental images favour the glide model.

Louchet and Thibault-Desseaux (1987) have questioned the assumption that dissociated dislocations are generated from perfect dislocations. They argue that dislocation sources can produce directly dissociated dislocations and hence that shuffle partials can in principle exist independently of whether or not a perfect shuffle dislocation ever existed. Evidence from HREM (Bourret *et al.*, 1983) found images of the 30° partial to be inconsistent with partials of the glide set *only*. Louchet and Thibault-Desseaux went on to propose that these results suggested that long segments of these partials exist in the shuffle form. One of their proposed forms of the core, the vacancy 30° shuffle partial, has been studied theoretically by Heggie and Jones (1987). They found the core energy associated with this partial to be much higher than that of the 30° glide partial. The majority of evidence is thus in favour of dissociation of dislocations into Shockley partials of the glide set and it is these that will be considered here.

The dissociation described by equation 1.3 is illustrated in fig. 1.2a. The intermediary position between the 90° partial slip and the restoring 30° displacement involves C atoms in A positions. This shear fault is *intrinsic* since it implies a {1 1 1} stacking sequence of ..AaBbAaBbCc..

The displacements that form the 90° and 30° partials are illustrated in fig. 1.2b. The central layer of C atoms corresponds to the slipped layer in fig. 1.2a. The 90° partial has a Burgers vector at right angles to the dislocation line and hence the displacement is in the $[1\bar{2}1]$ direction only and gives rise to 5 and 7 membered rings. By following the vertical {1 1 1} stacking sequence it can be seen that the intrinsic stacking fault has been introduced to the left of this partial.

The 30° partial is formed by a displacement both in the $[1\bar{2}1]$ direction and along the

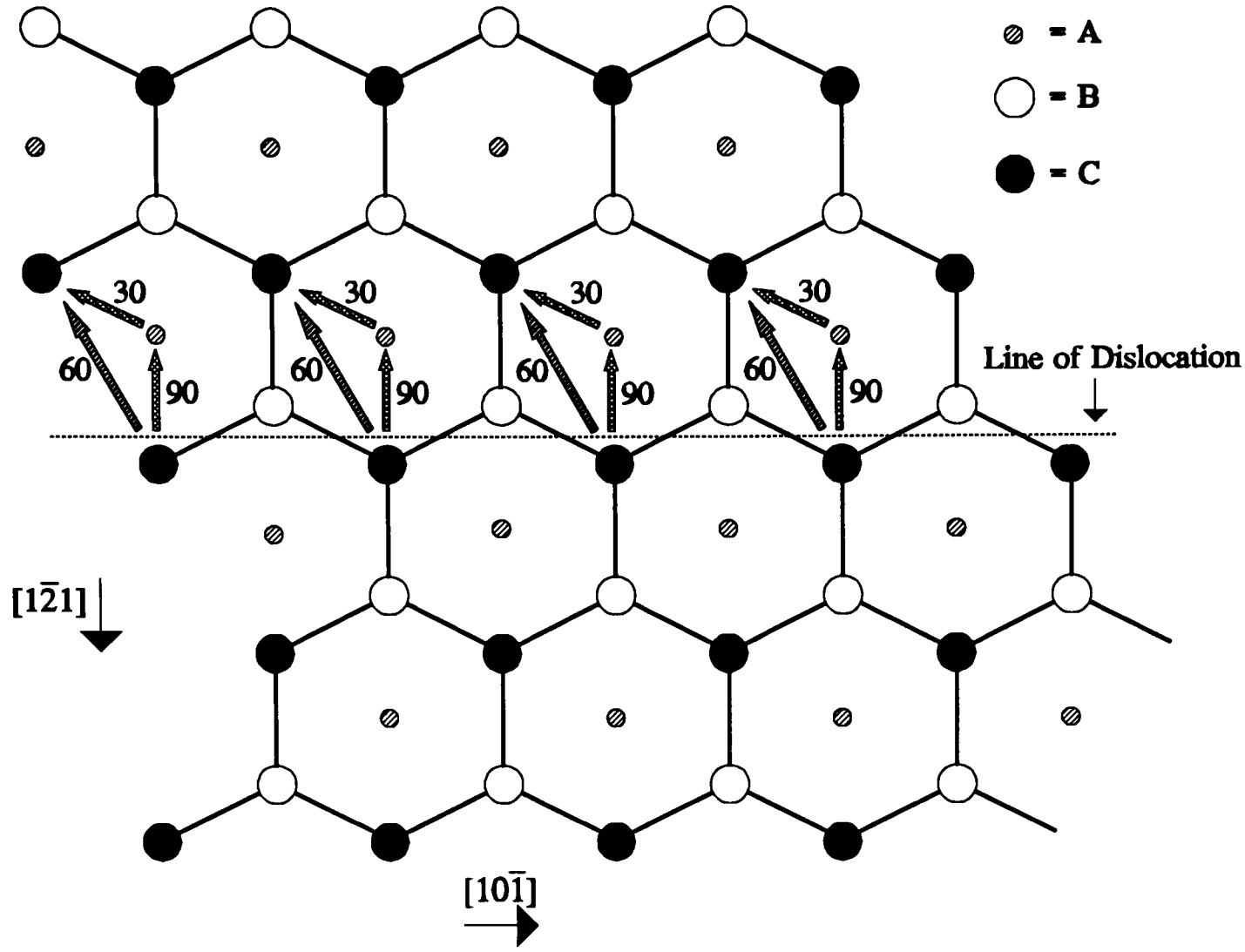

Fig. 1.2a Projection of atomic positions along [1 1 1] to show the relative movement of the half plane generating a 60° perfect dislocation. Also shown is the equivalent displacement in two stages which consists of forming a 90° partial and then a 30° partial. The intermediary position involves a fault in the (111) stacking sequence.

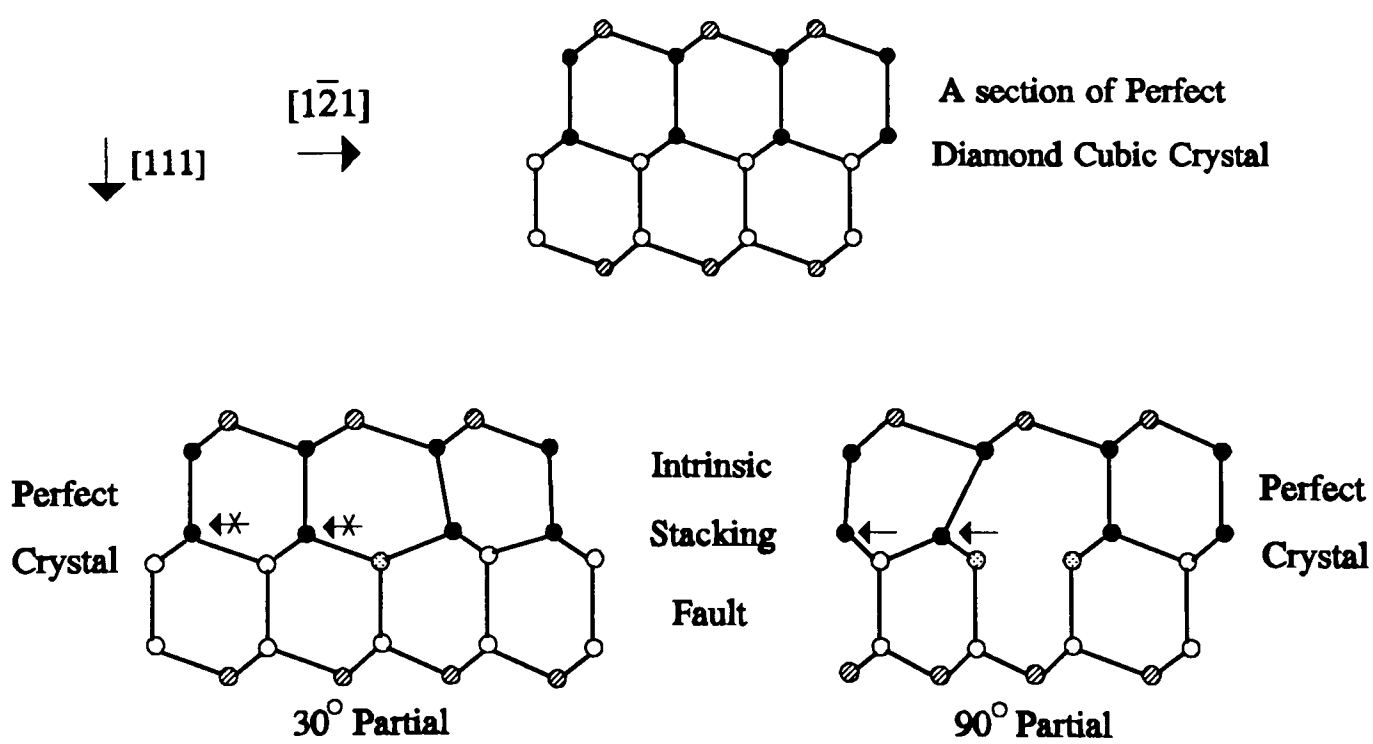

Fig. 1.2b [1 0 $\bar{1}$] projection of fig. 1.2a showing the formation of the 90° and 30° partials. A small section of perfect crystal is shown above the partials for reference. Only part of the intrinsic stacking fault formed between them is shown. The atoms filled with dots are only three-fold coordinated.

dislocation line (depicted by the cross). On its own, this also introduces a stacking fault, but the combined effect of the two partials is to reinstate the perfect crystal stacking as in fig. 1.2a.

In general then, as the two partials form there exists an elastic strain field that acts to move them apart. This movement is opposed by the ribbon of intrinsic stacking fault that is drawn out between the partials. Equilibrium will occur when the elastic repulsive force per unit length of dislocation balances the attractive force per unit length of dislocation arising from the creation of an increased area of stacking fault.

Fig. 1.2b also illustrates that both partials have atoms at the core which are three-fold coordinated as a result of the slip (the dotted atoms). The perspective view of the *unreconstructed* 90° partial is shown in fig. 1.3a. Each unit cell along the dislocation line has two dangling bonds, each of which contains one electron. This suggests that if these dangling bonds interact a full band results (Hirsch, 1979). However, atomic displacements across and along the dislocation core can eliminate the dangling bonds, as shown in fig. 1.3b (Hirsch, 1979; Jones, 1979). The appealing feature of this proposed reconstruction is that orbital overlap is increased and four-fold coordination recovered. However, this effect must compete with the extra shear strain involved and the question of core stability has been widely studied theoretically.

The unreconstructed 30° partial is depicted in fig. 1.4a. The periodicity in this structure involves one electron per cell and should thus be associated with a half-filled band (Hirsch, 1979). Reconstruction is again possible by bonding *along* the core where each alternate dangling-bond is displaced in the opposite direction (see fig. 1.4b). This results in a doubling of the periodicity along the dislocation line and the splitting of the half-filled band into two bands one of which is full and the other empty.

1.3 Experimental work on the electrical activity of dislocations

The intention of this section is to provide the reader with the essential experimental

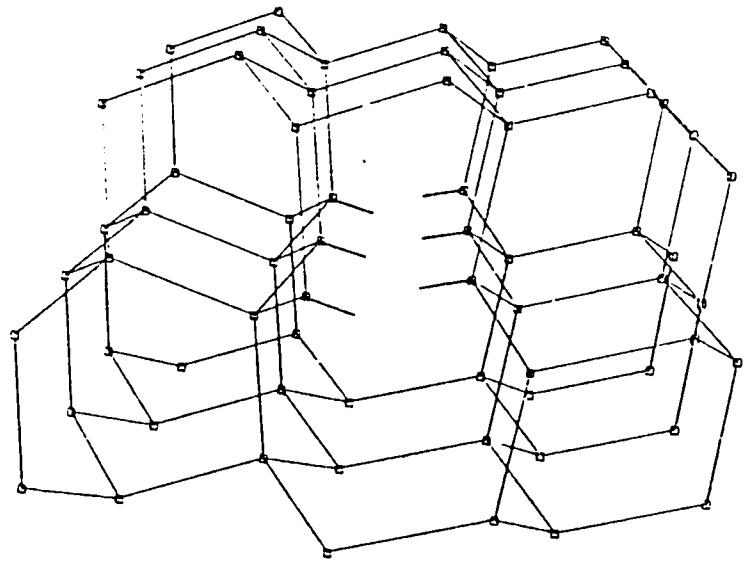

Fig. 1.3a Perspective view of the unreconstructed 90° partial.

(from Marklund, 1980)

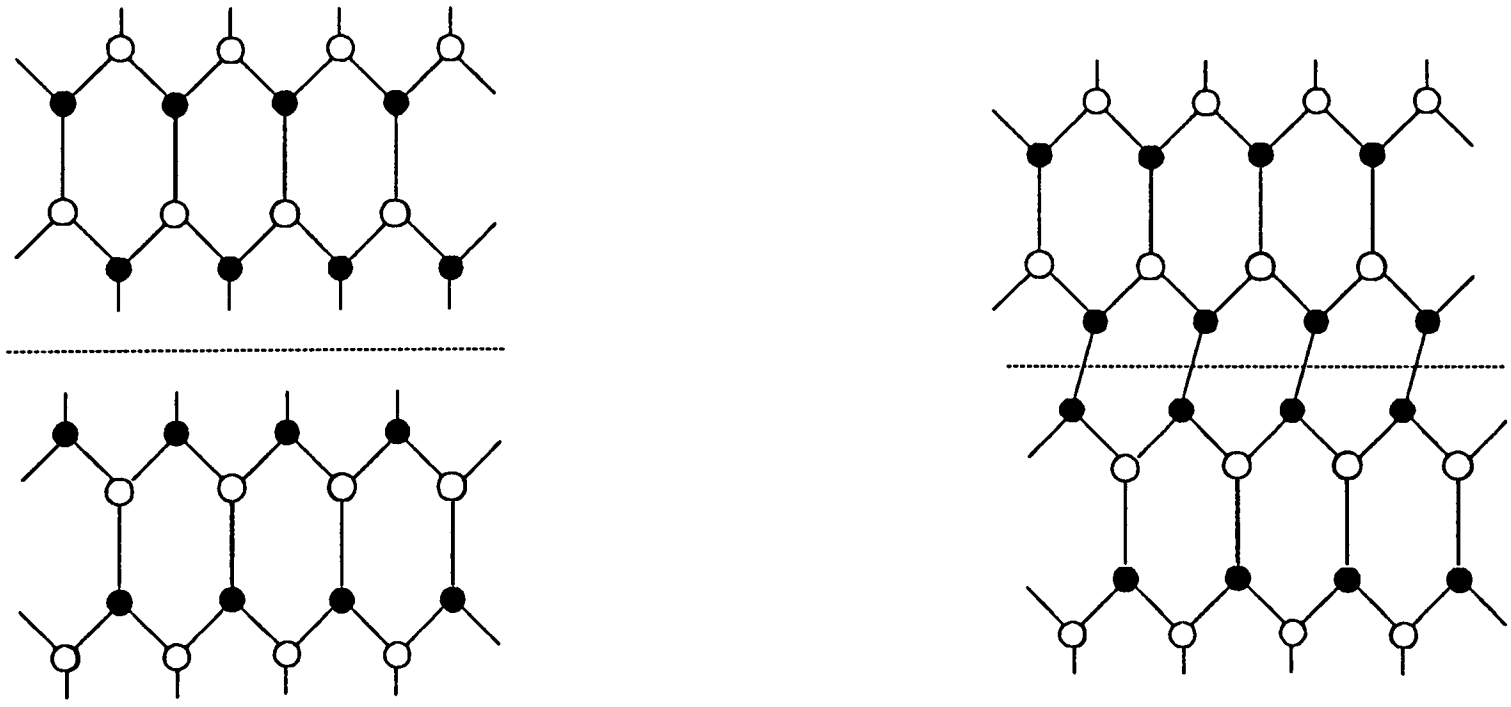

Fig. 1.3b Core structures of the unreconstructed and reconstructed 90° partial on the {1 1 1} plane. The solid and open symbols represent atoms on either side of the slip plane.

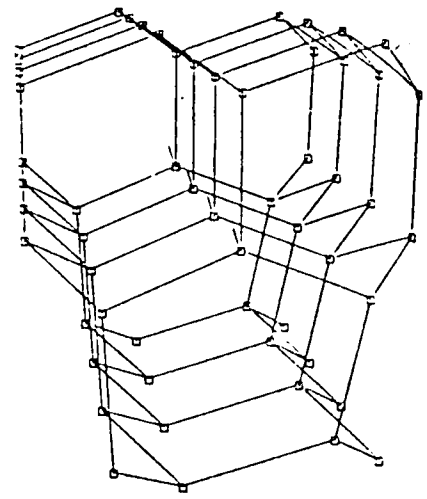

Fig. 1.4a Perspective view of the unreconstructed 30° partial.
(from Marklund, 1980)

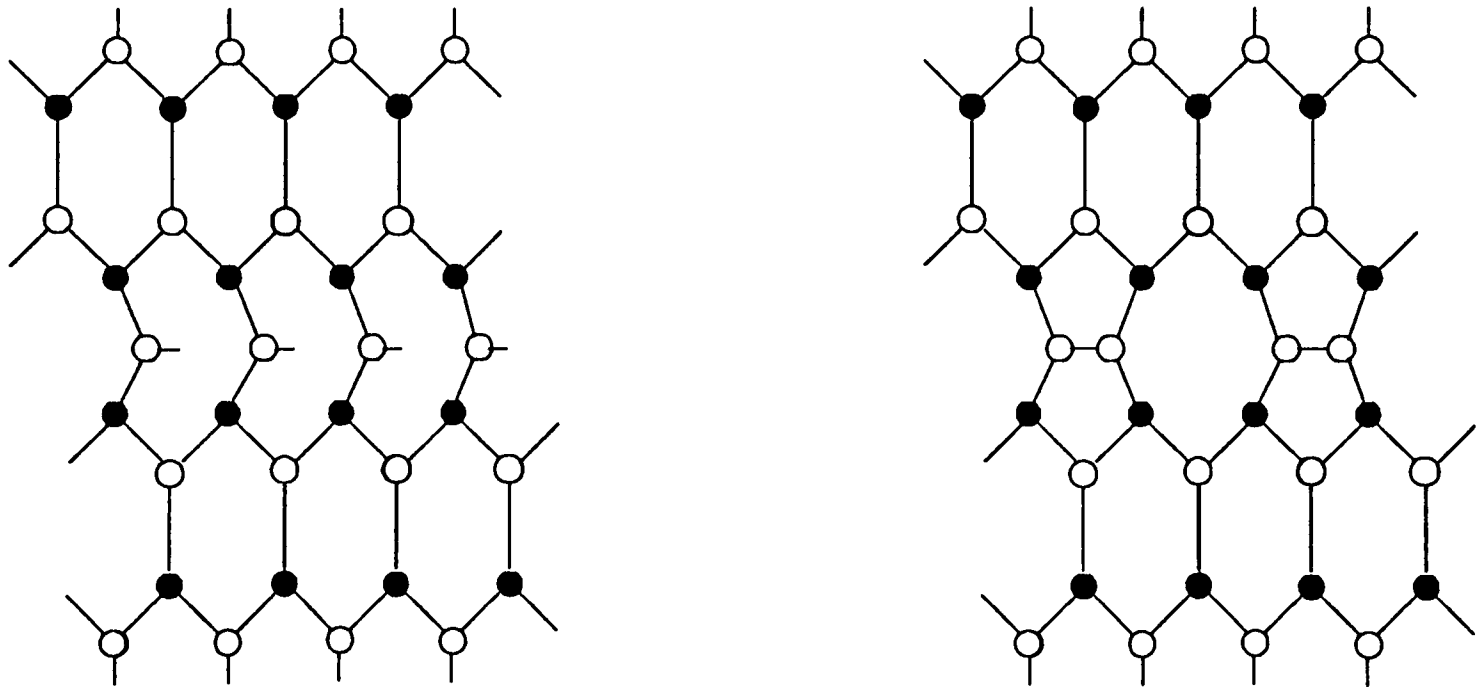

Fig. 1.4b Core structures of the unreconstructed and reconstructed 30° partial on the {1 1 1} plane. The solid and open symbols represent atoms on either side of the slip plane.

findings in this field. For more extensive reviews see Hirsch (1985), Alexander (1986) and Fell (1992).

Electron Paramagnetic Resonance (EPR) involves the use of radiation of microwave frequency to induce transitions between the levels of electrons with unpaired spins split using a magnetic field. It has thus been used for investigating the occurrence of singly occupied dangling bonds at the dislocation core. Several EPR spectra have been observed and correlated with dislocations and there is general agreement within the field (Weber and Alexander, 1979; 1983; Schröter *et al.*, 1980; Grazhulis *et al.*, 1981; Suezawa *et al.*, 1981). A defect containing two dangling bond sites can explain two of the EPR spectra. This can be in three charge states associated with zero, one (Si-K1 spectra) or two electrons (Si-K2 spectra). A broad line (Si-Y), associated with the greatest number of unpaired spins, is correlated to dangling-bond defects in various surroundings. Whether or not the dislocation core is correlated to Si-Y or just Si-K1, Si-K2 is uncertain (Grazhulis *et al.*, 1981; Weber and Alexander, 1983), but either way EPR predicts only a fraction of bonds can be broken which strongly suggests that these dislocations are reconstructed except for a few unknown defect situations. Other EPR spectra, Si-K3,K4,K5, seem to be randomly distributed through the bulk and are attributed to point defect clusters. All the above mentioned spectra are found *only* for samples deformed at 650°C, disappearing for higher and lower temperature deformations. However, in boron and phosphorous doped silicon two further signals are found (Si-K6 and Si-K7) and these exist in both high and low temperature deformation conditions and have been correlated to the dislocation core.

Deep Level Transient Spectroscopy (DLTS) results in four deep levels, E1,E2,E3,E4, under the 650°C deformation conditions. There are large inconsistencies in the position of these deep levels as measured by several workers (Kimerling *et al.*, 1981; Szielko *et al.*, 1981; Kveder *et al.*, 1982; Omling *et al.*, 1985; Kisielowski-Kemmerich *et al.*, 1987). The levels E1 and E4 are also found to be present only in the 650°C deformation conditions and further Omling *et al.* have observed the DLTS spectrum to be dominated by E4 in samples

which exhibit the EPR Si-K1,K2 spectra. Alexander (1986) has concluded that E4 and Si-K1,K2 are related and possibly belong to a defect produced by a dislocation-dislocation interaction present at 650°C. He explains the temperature dependence of these signals by proposing that at 420°C this defect is not generated whereas at higher temperatures it anneals out. Alexander (1986) has also proposed that the generation of Si-K1,K2 in the dislocation core is related to the production of point defects in the bulk, since the deformation temperature dependence and densities of these lines are similar to those of Si-K3,K4,K5. The two other DLTS levels (E2 and E3) exist at all three deformation conditions and are produced in direct proportion to the dislocation density (Patel and Kimerling, 1981). The proposal is that they are located at the dislocations and are most probably caused by impurity contamination. A significant finding by Peaker *et al.* (1991) is that it is possible to reproduce the whole range of deep DLTS states by varying the degree of impurity decoration on a single stacking fault. The implication is that there has been general disagreement in the positions of deep levels because different workers have had varying degrees of unintentional contamination.

Photoluminescence has revealed four characteristic lines (D1,D2,D3 and D4) associated with dislocations. They are remarkably reproducible and have been correlated to curved dislocations (Sauer *et al.*, 1985). The question of whether these PL D lines originate from impurity decoration of dislocations is of current controversy. Lightowlers *et al.* (1989) and Higgs *et al.* (1992) have shown that very low contamination of transition metal impurities leads to strong D1,D2 luminescence not observed with "clean" dislocations. Higher levels of contamination eventually quenched the luminescence and at this stage metallic precipitates on the dislocations were observed by TEM. Higgs *et al.* proposed that these precipitates absorb the centres responsible for D band emissions. These results were largely unaffected by the identity of the transition metal used. However, Weronek *et al.* (1992) have come to the opposite conclusion finding a drastic *decrease* of the luminescence on contaminating with copper and iron. They also showed that by decreasing the concentration of iron and copper the D band emissions could be made to reappear.

In all these experimental techniques so far mentioned, signals are obtained from *all* deformation defects and as a consequence correlation to a particular defect has been difficult. This problem has been largely circumvented with the development of Si deformation procedures, since it is now possible to create specimens containing predominantly one type of defect. However, the advent of new techniques now offers the spatial resolution needed to investigate individual dislocation segments. Electron Beam Induced Current (EBIC) is able to give information on either the energy position of dislocation states within the band gap, or the concentration of these states along the dislocation line. This type of analysis has revealed one state approximately every 100Å at individual straight screw and 60° dislocations deformed in the 420° regime (Wilshaw and Booker, 1985, 1987). Woodham and Booker (1987) have confirmed this state density using the same samples but performing SDLTS (Scanning-DLTS). States of this density are clearly inconsistent with the dangling-bond model of a dislocation core. Wilshaw and Fell (1989) have also found no increase in the number of charged states associated with curved over straight segments on hexagonal loops. This also implies a general absence of dangling-bonds from kinks. Further evidence for bond reconstruction was provided by Wilshaw and Fell (1990) who showed that "clean" oxygen induced stacking faults and their bounding Frank partial dislocation do not act as recombination centres. However, the introduction of copper and iron results in an EBIC signal, the recombination activity being dependent on the impurity atom and of greater strength at the bounding partial than at the stacking fault.

There is thus clear experimental evidence that the basic $<110>$ 60° and screw dislocations, which implies also the 30° and 90° partials, are reconstructed with the possible exception of a small number of unknown defects containing dangling-bonds. Against this weight of evidence, Pohoryles (1986, 1987, 1988a, 1988b, 1989) has developed the case for *mainly* unreconstructed dislocation cores. Pohoryles (1986) had the idea of overcoming the experimental difficulties associated with the separation of effects intrinsic to the dislocation core from those due to decoration by impurities, by causing a change of the core structure and

observing this change. He has shown that helium atoms under pressure can penetrate the interior of Ge and Si via dislocation pipes in which the diffusivity may be several orders of magnitude higher than in the bulk. Using a simple statistical argument, Pohoryles (1988a) has shown that He atoms diffusing along the dislocation core push atoms away from their unreconstructed positions, and at a point when the He density is high enough, will eventually cause complete reconstruction. Pohoryles (1987) has concluded that the 90° partial contains dangling bonds whereas the 30° is mainly reconstructed except at steps/kinks. Of course this whole model of driven reconstruction is based on the assumption that the unreconstructed core is the one of lowest energy, which will be shown is *not* the theoretical conclusion. Further, this model rests on finding an effect intrinsic to the dislocation core why dangling-bonds are not experimentally observed.

It is certain from this experimental evidence that impurities, notably transition metals, segregate to dislocations and have a dramatic effect on their electrical activity. Another area of experimental work concerned with impurity-dislocation interactions is the profound "pinning" effect of dislocations by certain impurities. In particular, atoms with a valency other than 4 are especially effective at locking dislocations. For example, C exhibits virtually no dislocation pinning (Imai and Sumino, 1983; Sumino and Imai, 1983), whereas O has a strong locking effect while also introducing donor states (Yonenaga and Sumino, 1985; Sato and Sumino, 1985). N and P also lock dislocations, the N, and possibly too the P, appearing electrically inactive at the dislocation (Kamiyama and Sumino, 1985; Sumino and Imai, 1983). The strength of immobilisation increases in the order O, P and N. However, due to the high diffusivity and solubility of O at high temperatures, this immobilisation of dislocations proceeds most efficiently in oxygen-doped silicon (Sumino, 1989). Perhaps a surprising result is that rather than behaving in a similar way to N and P, B is actually found to have a very weak locking strength (Imai and Sumino, 1983). This could be related to the fact that B is the first element in group III and electron deficient, which might give it a different chemistry in Si to the group V elements.

1.4 Theoretical work

The question of core reconstruction has been the subject of intense theoretical study. Hirsch (1979) used a "ball and stick" model to gauge how much strain was involved in reconstructing the 90° and 30° partials. From these models Hirsch concluded that the 30° partial is likely to reconstruct, but reconstruction of the 90° partial would be less certain because of the large shear strain involved (see fig. 1.3b).

Initial work on the 90° partial used a tight-binding approach to analyse the band-energy as a function of the displacement across the core which leads to reconstruction (Marklund, 1979; Jones, 1979). Their results indicated a lowering of this energy the larger the displacement from the unreconstructed state, indicating reconstruction to be favoured. However, Chadi (1979a) showed that a structure minimising the total energy did not generally minimise the band-energy.

Marklund (1980) used simple interatomic potentials (Keating, 1966; Koizumi and Ninomiya, 1978) to compare the relative stabilities and concluded that the unreconstructed state seemed energetically favourable. Indeed the latter potential was unable to even stabilise the reconstructed core. Altmann *et al.* (1982; 1983) using a modified form of the Lifson Warshell (1968) potential came to the opposite conclusion. They found the reconstructed state to be lower in energy, although the description of the dangling-bond interaction across the core was only represented by a van der Waals coupling (Altmann *et al.*, 1983). All these approaches relied upon an estimate of the dangling-bond energy for an energetic comparison, a quantity not known with any precision. More recent work has used techniques that can make a direct energy comparison. Heggie and Jones (1987) used the modified form of the Tersoff (1986) potential to show the reconstructed core is energetically favourable. Bonapasta *et al.* (1988) came to the same conclusion using an ab initio calculation on small clusters of 5, 9 and 10 Si atoms.

There is little doubt that the core of the 90° partial is reconstructed but the atomic structure of the core is much less certain. Recent work by Duesbery *et al.* (1991) has found a core

reconstruction involving weak five-fold bonding using two classical potentials (Stillinger and Weber, 1985; Kaxiras and Pandey, 1988). Using the Tersoff (1989) potential, with a larger than prescribed cutoff radius, results in a shift back to a four-fold reconstructed core, but with a reconstructed bond of 11%. Both these structures are significantly different to that obtained in the earlier work. This work of Duesbery *et al.* has been investigated thoroughly in chapter 5. A recent inconsistency occurs in the work of Marklund and Wang (1992) who have used the same potential as Heggie and Jones (1987) but obtained a considerably different core structure. This too is investigated in chapter 5.

The question of the electrical activity associated with the reconstructed and unreconstructed cores has produced inconsistent results. The work of Jones (1979) and Marklund (1979) showed that the unreconstructed core introduces two deep energy levels, which split as the atoms were displaced towards the reconstructed state. The unreconstructed core is consistently associated with broad bands of states in the gap, though agreement in their placement and splitting is less certain (Marklund, 1983; Teichler and Veth, 1983; Lodge *et al.*, 1983, 1984; Veth and Teichler, 1984; Teichler and Marheine, 1987; Wang and Teichler, 1989). This is mainly because of the differences in the treatment of the dangling-bond interactions across the core. Marklund (1983), using the tight-binding Hamiltonian of Pandey and Phillips (1976), considered this interaction as either zero, or as a second neighbour interaction or as a weak first neighbour interaction (five-fold coordination). The effect of the first two approaches was just a difference in the position of the overlapping bands. However in the case of weak five-fold coordination the bands were found to split into a full and empty one. Persson (1983) has questioned the reliability of using parameters fitted to perfect crystal properties to evaluate electron states at a defect such as a dangling-bond. His calculations, which involved a recalculation of the matrix elements for the dangling-bond environment, showed that the bands were sensitive to this process. Teichler and Marheine (1987) have used an LCAO scheme with full inclusion of s and p states and d states treated in the approximation of Louie (1980). They found that there exists a marked interaction across the core resulting in a large splitting of the

dangling-bond bands. This splitting has been confirmed by Wang and Teichler (1989), this time with full inclusion of the d orbitals also. Teichler (1989a), using a bond order model similar to that of Harrison (1980), has also found that the dangling-bond interaction across the core is far from insignificant. He does, however, find the reconstructed state to be lower in energy.

Such a high density of states is not observed experimentally and provides further evidence that the 90° partial is reconstructed. The question arises as to whether the band splitting that occurs on reconstruction is sufficient to clear the indirect band-gap of states. Marklund (1983) and Veth and Teichler (1984) have used a tight-binding scheme and the Pandey and Phillips (1976) Hamiltonian, and conclude that reconstruction does clear the band-gap of states. However, Lodge *et al.* (1984) using an extended Hückel theory scheme (Hoffmann, 1963) and Chelikowsky and Spence (1984), using an ab initio pseudopotential approach, both found that broad bands of states remained within the band-gap. In later work, Lodge *et al.* (1989) used a pseudopotential method and found the band-gap to be essentially clear, except for some stacking fault states. However, recent work by Marklund and Wang (1992), using the LCAO scheme of Wang and Teichler (1989), has predicted a band of states leaving the conduction band and penetrating as deep as mid-gap.

It is clear that the atomic and electronic structure of the reconstructed 90° partial remains largely unresolved. It is one of the main objectives of this thesis to understand and predict both of these.

The 30° partial has provided much more consistent theoretical results. Jones (1979) and Marklund (1979) showed that the unreconstructed core yields a wide single dangling-bond band extending across the whole gap. No experimental evidence exists for such a band. This result was reproduced by Northrup *et al.* (1981) using a pseudopotential technique. These electronic structure results thus suggest the 30° partial is reconstructed. Both Jones and Marklund found that on reconstruction, which doubles the periodicity along the dislocation line (see fig. 1.4b), two narrow bands split out of the wide single band, one occupied the other

empty. Chelikowsky (1982) found that this splitting was sufficient to clear the indirect band-gap of states.

Marklund (1980) found the reconstructed core to be energetically favourable over the unreconstructed state in agreement with the prediction of Hirsch (1979). Further work confirmed the existence of the broad band in the unreconstructed case which splits and clears the band-gap upon reconstruction (Marklund, 1983; Veth and Teichler, 1984).

There is one other partial which has also been studied and is mentioned here for completeness. Two 60° partials are the dissociation products of edge dislocations predominantly formed in compressed specimens (Hirsch, 1979). Hirsch (1979, 1980) has discussed possible core structures, and relaxed configurations have been obtained by Jones and Marklund (1980) and Veth and Teichler (1984). Possible core structures that contain dangling-bonds gave rise to states in the gap (Veth and Teichler). A fully reconstructed partial produced an empty state in the upper half of the band-gap (Jones and Marklund), whereas Veth and Teichler found this same configuration to clear the gap. For further details the reader is referred to these papers. The 60° partial has not been studied here.

Pseudopotential calculations on the bands associated with these dislocations indicated a minimum width of 0.5eV (Kirton and Jaros, 1981; Jaros and Kirton, 1982). These authors concluded that since the experimentally observed deep levels have sharply defined energies they are likely to be associated with localised defects rather than with the atomic geometry of perfect straight dislocations. The antiphase defect (Hirsch, 1980), or the soliton as named by Jones (1981), is a localised defect equivalent to a lone dangling-bond site that can occur during reconstruction. Fig. 1.3b and 1.4b show that any dangling-bond atom can bond with one of two neighbours in equivalent positions which are energetically degenerate. The system spontaneously moves in one of these two directions and this could result in both neighbours nearest an atom moving away to bond with their other neighbours, leaving the original atom unbonded. In a series of papers (Heggie and Jones, 1982, 1983a, 1983b, 1983c) the soliton was shown to produce energy levels around mid-gap which were very sensitive to the local

environment. This sensitivity led Heggie and Jones to conclude that the soliton was a negative U-centre and diamagnetic. By considering a vacancy-soliton complex as a paramagnetic defect Heggie and Jones tried to correlate the EPR results with a model of solitons and vacancies interacting at the core. However repeated calculations, which involved a tight-binding scheme that included the crystal potential change around the soliton (Jones and King, 1983), contradicted the earlier work by finding the mid-gap level to be insensitive to the geometry (Jones, 1985). Teichler (1989b) has found the neutral soliton to be paramagnetic introducing a level at 0.77eV above the valence band edge.

The importance of the soliton will depend critically on its *formation* and *migration* energies. Estimates of the formation energy vary from 0.4eV (Jones, 1981) to more than 2eV (Teichler, 1989b). A migration energy lower than kT will result in mobile solitons of opposite sign annihilating each other. This would leave just the equilibrium density which for a high formation energy will be small. However, if the migration energies are higher than kT, as postulated by Heggie and Jones (1982, 1983c), then solitons produced at elevated temperatures could easily be frozen in with non-equilibrium concentrations.

Another possible source of states in the gap is the kink. However, calculations on reconstructed kinks have shown that no deep levels are introduced into the gap (Jones, 1981; Heggie and Jones, 1982, 1983a; Klenova and Moloskii, 1986). Migration of the kink involves momentary saddle point configurations and these do give rise to deep states (Heggie and Jones, 1983b; Jones, 1985). These results predict the 30° partial to have a substantially lower mobility than the 90° partial.

Theoretical studies of impurity interactions with dislocations have been limited to the study of the locking effect associated with phosphorous. Heggie (1987) had postulated that group III and V elements could passivate a reconstruction soliton by taking up the position of the triply coordinated Si atom there. Robertson (1983a) had used a tight-binding scheme to show that most group III and all group V elements are neutral under three-fold coordination in amorphous Si and have no levels in the gap, B being the exception. There is also evidence

from NMR (Greenbaum and Carlos, 1984) that B, P and As exist predominantly in a three-fold state within amorphous Si. Calculations were undertaken on the interaction of P with a soliton in crystalline Si (Heggie *et al.*, 1989) using a cluster method with local density functional pseudopotential theory. The P was indeed found to sit preferentially at a 90° partial soliton (binding energy 1.5eV) and in taking up this site the gap was cleared of states. Heggie *et al.* (1991) have also shown that P binds to a 90° partial through a second mechanism, where two P atoms take up sites on either end of the reconstructed bond. The bond breaks to allow each P atom to adopt three-fold coordination and the binding energy for this process is 2.3eV. Only two filled levels close to the valence band edge, corresponding to weak P-P interaction, are found in the band-gap. These results indicate that the observed strong locking effect of P does not have to imply the formation of precipitates but can be explained in terms of just two P atoms migrating to the core.

1.5 Thesis objectives

It is clear that most of the theoretical work to date has involved the study of clean dislocations. However, there still exist major discrepancies about the predicted atomic and electronic structure of a clean reconstructed 90° partial. It is also demonstrated, in chapter 4, that previous work in which dislocations have been modelled using 3D periodic boundary conditions has involved an error that is shown to affect both the atomic and electronic structures. This implies that results on the 30° partial, using this technique, will also be in error.

Consequently, an initial objective of this thesis will be to make a detailed study of the clean dislocations. The intention is to develop and test the programs needed against the reference of previous work. Much of this process will be geared towards understanding the different results obtained for the 90° partial and predicting the reliability of various types of model. For example, simple classical potentials have been used almost exclusively to obtain the atomic structure of these dislocation cores. There is a need to investigate and compare the

predictions of more accurate techniques such as tight-binding and ab initio methods and this is undertaken here. This investigation into the reliability of these techniques will allow the completion of a second objective, namely to understand why significant differences have been obtained in previous work and then to predict the actual core structure for the 90° partial.

Impurity interactions with dislocations are a new area of study. Experimentally, techniques such as EBIC are now providing information on how the electrical properties of "clean" dislocations are modified by impurities. There is a need for the parallel development of theoretical models which can hopefully provide an explanation at the atomic level for the experimental observations. A possible outcome of this work could be an understanding of how to control or modify the electronic properties of dislocations. This would provide an immediate focus for a large area of research that is dedicated to finding ways of rendering dislocations electrically inactive (eg. Lee and Morrison, 1988). The final objective of this thesis is to start the theoretical investigation of how impurities affect the atomic and electronic structure of clean dislocations.

CHAPTER 2

Interatomic forces

2.1 Introduction

An accurate description of interatomic forces is essential to describe the properties of defects in semiconductors. Effects such as hybridisation and charge transfer intimately couple the atomic and electronic structures. While accurate quantitative answers have obvious merits, a reliable qualitative description of bonding, that incorporates the physics of such effects, can be just as illuminating.

There exists a very wide range of descriptions of interatomic forces each constructed on certain simplifying approximations. The work here has involved several such methods ranging from a self-consistent density functional pseudopotential formalism to simple empirical interatomic potentials. This chapter is intended to illuminate the degree of approximation associated with each method used as a precursor to understanding why failures can and have occurred in later work. The mathematical details for these various methods can be found in the references cited.

2.2 The Born-Oppenheimer approximation

The many-body problem consists of describing the interactions of the electrons and atomic nuclei within the solid. The solution entails constructing the Hamiltonian and solving

Schrödinger's Equation:

$$H\psi = E\psi \tag{2.1}$$

The Born-Oppenheimer approximation amounts to saying that the electronic and nuclear degrees of freedom may be decoupled. This implies the electrons are always in their ground state as the atoms of the solid vibrate thermally. This is usually an excellent approximation since the lighter electrons have a relaxation time typically three orders of magnitude smaller than the atomic nuclei. It can break down, for example during chemical reactions, but not in cases considered here.

2.3 Outline of density functional theory

Although the electron and nuclear motions have been decoupled the problem now faced is how to describe the multi-electron wavefunction, which represents the state of all the electrons interacting with each other. This many-body problem is clearly a hopeless task since the wavefunction of the system will be a function of roughly 10^{23} variables in a cubic centimetre of a typical solid.

In 1964, Hohenberg and Kohn proved that all aspects of the electronic structure of interacting electrons, in the *ground state*, are completely represented by the electronic charge density $\rho(\underline{r})$. They also proved that the ground state energy of the interacting electrons is a unique functional of $\rho(\underline{r})$ and that this functional is minimised when the charge density reaches its true value. This result implies mathematically there is a *variational principle* for finding the charge density. The multi-electron wavefunction has thus been replaced by the charge density as the quantity to be determined, $\rho(\underline{r})$ being a function of only three variables.

The second major simplification came in 1965 when Kohn and Sham proved that a system of N interacting electrons can be *exactly* mapped onto a system of N one-electron equations. This means that each electron is moving *independently* of the others, but experiences an *effective* potential, V_{eff}, which exactly emulates the interactions with all the other electrons.

Kohn and Sham further showed that V_{eff} is a unique functional of the charge density. These one particle equations are known as the Kohn-Sham equations:

$$-\frac{\hbar^2}{2m}\nabla^2\Psi_j(r)+V_{eff}(r)\Psi_j(r)=E_j^{KS}\Psi_j(r)$$

$$V_{eff}(r)=V_H(r)+V_N(r)+V_{XC}(r) \qquad (2.2)$$

$$\rho(r)=\sum_{j\ occupied}|\Psi_j(r)|^2$$

where V_H is the Hartree potential which is related to the electronic charge density through Poisson's equation, V_N is the electrostatic potential arising from the fixed nuclei and V_{XC} is the exchange-correlation potential. V_{XC} represents the two forms of correlated motion of electrons. The first arises from Coulomb repulsion between electrons and this leads to an energy lowering called the correlation energy. Secondly, the Pauli exclusion principle implies electrons of the same spin will avoid each other, and this leads to an energy lowering called the exchange energy. Both effects lower the energy since there is less Coulomb repulsion as a result of the electrons being further apart on average. These equations are self-consistent since the wavefunctions are defined by the effective potential V_{eff} which is a functional of the charge density, which itself is defined by the wavefunctions. The equations are solved when the output charge density is the same as the input charge density.

2.3.1 The local density approximation

The Kohn-Sham equations are an *exact* solution of the many-body interacting system described by equation 2.1, under the Born-Oppenheimer approximation only. The only problem is that the exchange-correlation potential and energy are unknown for a spatially varying charge density as will be the case in any solid. In the *local density approximation* the exchange-correlation potential at position $\underline{r}$ is assigned the value of the exchange-correlation potential in a *uniform* electron gas which has the same density as that calculated at $\underline{r}$. Clearly this is an approximation since all non-local contributions to the exchange-correlation potential,

arising from the variation of the charge density in the vicinity of $\underline{r}$, are neglected. At first it was believed that only cases that involved a charge density which was a slowly changing function of position could be at all well described by the local density approximation. However it was found to be remarkably successful in cases that significantly departed from this condition. The local density approximation has been very successful in describing the properties of semiconductors, such as the lattice parameter, bulk modulus and crystal stability (see for example, Yin and Cohen, 1982a). Large discrepancy from experiment is obtained in the calculation of band gaps which are found to be underestimated by $\sim 50\%$, with Ge predicted to be metallic (Louie, 1989). This however is a failing of density functional theory and *not* a consequence of the local density approximation.

2.3.2 The frozen core and pseudopotential approximations

The problem can be further simplified by recognising that the valence electrons play the dominant role in chemical bonding. Core electrons are in deeper shells and in the *frozen core approximation* they are grouped with the nucleus and assigned to their isolated atomic states. In this approximation only the valence electron states respond to changes in the atomic environment and the problem has thus been reduced to solving the Kohn-Sham equations for valence states only.

The term pseudopotential describes the weak effective potential felt by an electron in the vicinity of an ion core. The *real* attractive potential of the ions is largely cancelled by an *effective* repulsive potential that arises from the increase in kinetic energy at the core. This occurs because the exclusion principle demands that the valence electron state be orthogonal to the localised core states and this introduces many new oscillations as a result. The kinetic energy, which is proportional to the second derivative of the wavefunction, consequently increases.

The degree of cancellation is dependent on the core states to which the valence electron state has to be orthogonal. For the 3d transition metals the atomic cores contain only s and p

electrons. While the orthogonality requirement provides good cancellation to the attraction of the valence state to the core for both the s and p components, it does not for the d component. Consequently the s and p components of the pseudopotential are "weak" but the d component is "strong".

The pseudopotential thus replaces the full ionic potential by an effective potential which reproduces the correct scattering behaviour of the valence states. The pseudopotential and the screened ionic potential are identical outside a core radius, r_c, and hence the pseudopotential gives the true valence wavefunctions in this region. The bonding energy in a solid is principally determined by the electron density in the regions outside the core and hence bonding should be well described in the pseudopotential approximation. These pseudopotentials can be constructed for any element in the periodic table (Bachelet *et al.*, 1982) and are termed "non-local" because they are angular momentum dependent. A key advantage is that the pseudopotential wavefunctions are smooth in the core in contrast to the true wavefunctions which must oscillate rapidly as described above. It is thus possible to expand the valence wavefunctions in a plane wave basis set, although the number of plane waves required for an adequate fitting increases dramatically for "hard" pseudopotentials such as those of the 3d transition metal series.

This then is essentially all the approximations involved in the ab initio total energy pseudopotential codes (CETEP and CASTEP) developed at Cambridge and Edinburgh, although two further points should be considered. Firstly, the valence wavefunctions are expanded in a *finite* plane wave basis set. The severity of this approximation is considered in chapter 3. Secondly, the electronic energy of the system is obtained by calculations at a *finite* number of **k**-points using the scheme of Monkhurst and Pack (1978). This is also considered in more detail in chapter 3. These codes represent our benchmark against which less accurate approaches can be compared.

2.3.3 Non-self-consistent solution

The Kohn-Sham energy functional is minimised at the correct value of the charge density and this implies a variational principle. An error in the charge density, $\Delta\rho$, will result in an error in the total energy of order $(\Delta\rho)^2$. The Harris-Foulkes scheme (Harris, 1985; Foulkes, 1987) exploits this consequence to obtain a reasonable estimate of the total energy without iteration. At the self-consistent charge density, the Harris-Foulkes and Kohn-Sham functionals are equivalent. The accuracy of this scheme is therefore dependent on a suitable input charge density, such as the superposition of atomic charges in the case of covalent materials. With a suitable choice the total energy is estimated from a single iteration with errors occurring to second order.

2.4 Tight-binding methods

This represents the starting point for the tight-binding bond (TBB) model of Pettifor and Podloucky (1986), Pettifor (1987) and Sutton *et al.* (1988). By rearranging the Harris-Foulkes functional, Sutton *et al.* have derived a physically transparent expression for the cohesive energy of the solid:

$$E_{coh}=E_{cov}+E_{pro}+\Delta E_{es}+\Delta E_{xc} \tag{2.4}$$

E_{cov} represents the energy gained during bond formation and is given by a sum over individual covalent bond energies. E_{pro}, the promotion energy, is the change in energy associated with moving charge into the bonding configuration of the solid from the free atomic states. The last two terms represent the change in the total electrostatic and exchange-correlation energies on forming the solid from isolated atoms. Sutton *et al.* showed that these last two terms could be treated as a sum of pair potentials to the same degree of error implicit throughout. The Band model developed by Chadi (1978, 1979a, 1979b, 1984) is closely related to the TBB model, although it was empirically derived rather than rigorously justified

and differs in its treatment of the pair potentials.

Within the tight-binding approximation the one-electron wavefunction is expanded in a *limited basis set* as a linear combination of atomic orbitals:

$$\psi_i = \sum_\beta c_{i\beta}\phi_\beta \tag{2.5}$$

where β denotes both the orbital symmetry (s, p, d etc.) and the atomic site on which it is centred. Substituting this expression into Schrödinger's equation allows the problem to be reduced to a secular form:

$$\sum_\beta (H_{\alpha\beta} - \epsilon_i S_{\alpha\beta})c_{i\beta} = 0 \tag{2.6}$$

where $H_{\alpha\beta}$ and $S_{\alpha\beta}$ represent the integrals $<\phi_\alpha|H|\phi_\beta>$ and $<\phi_\alpha|\phi_\beta>$ respectively. These Hamiltonian integrals consist of a number of types of interaction:

(1) The crystal field integral - this couples two orbitals on the same atom through the potential on another.

(2) Two centre hopping integral - this couples a state on one site with a state on another through the potential on one of these sites.

(4) Three centre integral - this couples two states on differing sites through the potential on a third site.

The approximations made in the tight-binding scheme are as follows: the atomic basis functions ϕ_β are assumed to form an orthonormal set so that the overlap matrix, $S_{\alpha\beta}$, is the identity matrix. This seemingly gross simplification has been justified using chemical pseudopotential theory (see Heine, 1980). All three centre integrals are ignored. This is a matter of convenience rather than a knowledge that they are small (Slater and Koster, 1954) but Pettifor (1977) has shown the leading correction terms to the energy are of second order. The two centre hopping integrals are limited to first nearest-neighbour interactions only. Use of a limited basis set is also clearly an approximation, but for the calculation of valence

electron properties it is necessary only to include orbitals in the expansion which have comparable energies with the valence electrons. However for excited states a much poorer description is obtained unless the basis set is expanded. For example, in the case of Si leaving d-electrons out of the expansion leads to a poor description of the conduction bands.

Slater and Koster also concluded that the remaining integrals were still numerous and difficult to evaluate. Consequently they treated these integrals as parameters that are fitted to the energy bands, obtained experimentally or from accurate calculations, at points of high symmetry in the Brillouin zone. The assumption is that these matrix elements are transferable to a defect environment where the effective potential acting will be significantly different to that of the perfect crystal. This approximation has been shown to lead to inconsistent answers. As discussed in chapter 1, section 1.4, Heggie and Jones (1982, 1983a), using the Pandey and Phillips (1976) parameterised Hamiltonian, found the mid-gap energy levels of the soliton to be very sensitive to the local environment, suggesting this defect is a negative U-centre. However, a method that involved explicit calculation of the crystal potential and analytic evaluation of the integrals (Jones and King, 1983), has predicted a soliton energy level that is insensitive to the local geometry (Jones, 1985). Nonetheless, chemical pseudopotential theory has shown that localised atomic like orbitals can be defined in which the influence of the atomic environment occurs as only a weak perturbation.

Since there is no explicit evaluation of any integrals in simple tight-binding schemes some sort of scaling with bond length must be defined. Harrison (1980) proposed that the magnitude of the hopping integrals decays with the inverse square of the bond length. This inverse square scaling is justified by Harrison (1980), but at high atomic separation the overlap is expected to be near exponential so that a $1/d^2$ overweights second neighbour interactions. The energies and equilibrium volumes of close-packed structures are in error as a result (Paxton and Sutton, 1989). By rescaling the hopping parameters Goodwin *et al.* (1989) attempted to provide a more consistent description of the overlap at both first and higher order neighbours and improved the fit to the ab initio structural energy curves of Yin and Cohen (1982a).

2.4.1 Bond order potentials

There is an obvious motivation for developing empirical potentials which have a functional form derived from quantum mechanical origins. For example, even within the tight-binding approximation the Hamiltonian must still be solved either in k-space using matrix diagonalisation[1] or in real space using the recursion method (Haydock *et al.*, 1972). These are both time consuming calculations. Pettifor (1989, 1990) has introduced the idea of a bond order potential which promises an empirical form that maintains the physics incorporated in the TBB model. This is possible since the bond order potential has a functional form that is derived from the TBB model and consequently it can and is being systematically improved (Pettifor and Aoki, 1991).

2.5 Classical potentials

Finally there is the concept of a classical interatomic potential. One class of such potentials is often termed a Valence Force Field (VFF) since the crystal potential energy is expressed in terms of the valence coordinates, ie. bond lengths and bond angles. They are appealing because they offer considerable computational simplicity and speed, but they make no attempt to solve the Schrödinger equation; instead, they are constructed using *assumed* functional forms and fitted empirically by matching some macroscopic properties of the crystal, such as elastic constants, phonon dispersion curves, etc. These properties are in general long-ranged and yet these VFFs are by their construction short-ranged. As a result of this inconsistency even the short-range terms for which these fields are primarily valid can be poorly described (Ball and Hajaig, 1981). There is a conflicting problem in simultaneously describing the elastic constants and the softening of the transverse acoustic modes characteristic of Si (Baraff *et al.*, 1980), since fitting to the former implies an angular stiffness to the potential which is too strong to reproduce the latter. For example, the Keating (1966) potential was accurately fitted to the elastic constants, but in order to simulate the phonon softening Baraff *et al.* had to

---

[1] The time taken to diagonalise scales as N^3 for an NxN matrix.

reduce the bond bending parameter by a factor of 3.

More recent work has identified the need for a better link with the Schrödinger equation (Jones, 1987; Stoneham *et al.*, 1988). Jones (1987) and Tersoff (1986) fitted their potentials to the results of highly accurate Local Density Functional theory calculations of the energies of polytypes of Si. These calculations have been extremely successful in predicting many ground state properties of semiconductors in strained environments (Yin and Cohen, 1982a; Yin and Cohen, 1982b; Nielsen and Martin, 1983). Thus in contrast to simple VFFs which are only fitted to equilibrium bulk properties, these potentials are hopefully applicable far from equilibrium and therefore are useful for making structural predictions near defect sites. However, in general workers like Halicioglu *et al.* (1988) have concluded that these potentials are applicable to highly strained environments only in the regime where they were fitted.

Three classical potentials have been used to obtain relaxed structures of the dislocation core. The first is a modified form of the 1968 Lifson Warshell potential due to Altmann *et al.*, 1983. This potential includes the usual bond stretching and bending terms but also includes more distant neighbours through van der Waals non-bonding interactions, interactions between two atoms joined to a common atom as well as torsional terms. In comparison to other simple VFFs used in modelling the structure of dislocations (Keating, 1966; Koizumi and Ninomiya, 1978) this potential gave more reliable results in treating dangling bonds (Marklund, 1983). Stoneham *et al.* (1988) have noted that the greatest disagreement between various VFFs will occur when modelling dangling-bonds, since authors cannot agree on points such as whether bond angle terms should be included when one of the bonds involved is "broken". This inadequacy led to the desire for potentials which could treat coordinations other than four, with particular emphasis on transferability.

Stillinger and Weber (1985) introduced a potential that aimed to meet these requirements. It must be emphasised that the functional form for this potential, like the VFFs, was constructed on intuitive ideas rather than being based in quantum mechanics. Indeed the Stillinger Weber potential is unable to describe electronic effects such as rehybridisation and

consequently has proved unsuccessful at modelling surfaces (Wilson *et al.*, 1990). Nonetheless this potential is extremely popular in Si modelling and it has been used here to investigate its ability to describe the bonding processes present in dislocation cores.

The third classical potential considered is that due to Tersoff (1988a, 1988b). Tersoff formulated his potential around intuitive ideas of how the bond order is affected by the local atomic environment. It is remarkable that his ideas generated a potential which possesses the same type of functional form as the simplest approximation to the bond order potentials of Pettifor. Part of this thesis is concerned with investigating the reliability of Tersoff's potential compared with the two other classical potentials described and the tight-binding scheme (M^{c}Innes, 1992). The predictions of all these schemes are then compared to the results of the pseudopotential LDF method which is taken as the benchmark.

CHAPTER 3

Computational modelling of dislocations

3.1 Introduction

A set of fully 3D periodic boundary codes have been implemented to generate and model dislocations in Si. The intention here is to provide a brief description of each method. Details on their use, and all other related programs that have been developed, can be found in appendices A-D. All the programs have been written in Fortran and their use on several computers confirms their portability. Full listings are provided on the microfiche at the back of this thesis.

3.2 Generating the elastic solution

The form of the starting geometry can be key to the results obtained, particularly when using static and simple energy minimisation methods. The use of anisotropic elasticity theory should ensure a better starting solution and allows these programs to be used in crystals whose

anisotropy causes the simpler isotropic theory to break down. There are two stages, and programs, to obtaining the elastic solution.

A 3D unit cell of perfect diamond cubic crystal is constructed using the program **GEN3D**[1]. It generates *orthogonal* unit cells only and its interactive use is self-explanatory. Directions for the box edges are input and new coordinate axes are set up along these box vectors. The box is thus defined by $(\pm boxx/2,0,0)$, $(0,\pm boxy/2,0)$ and $(0,0,\pm boxz/2)$ where *boxx*, *boxy* and *boxz* are the repeat periods entered along the x, y and z directions respectively. Atomic coordinates are stored in terms of this box coordinate system.

The anisotropic elastic solution is obtained using **AESOL** and the other related programs (see appendix B). The method is essentially based on the work of Eshelby *et al.* (1953) and is extended and described in detail in Hirth and Lothe (1982). Periodic repetition of the unit cell will generate a superlattice of dislocations (see Chapter 4, section 4.2). Thus for any position within the central unit cell the distance to all periodic dislocation images are evaluated and the displacement predicted by each is calculated. The actual displacement is then given by the sum of all these individual displacements. In theory there is an infinite number of dislocations within the superlattice but the displacements tend to cancel, due to the geometrical arrangement of the dislocations, fairly rapidly with distance from any dislocation. The summation is therefore finite and over the number of neighbouring cells input. A mesh of 20x20 is adequate in all cases considered, but this can be easily checked by increasing the number of neighbouring cells included and comparing the displacements that result.

3.3 Classical relaxation

Elasticity theory provides a continuum solution that is well represented for regions away from the core of the dislocation. However, near the core the atomic structure becomes critically important and the core forces become strongly influenced by local atomic

---

[1] This program is based on the construction package, **CON3D**, developed and written by A.P. Sutton and involves only minor modifications.

interactions. In chapter 2 a variety of prescriptions for calculating the interatomic forces have been reviewed. The atomic structure can be predicted by choosing one of these techniques and minimising the total energy. Here the classical schemes used in this work are described. All three classical potentials are used within a molecular dynamics framework to obtain the minimum energy configuration.

3.3.1 Molecular Dynamics

Given a scheme which provides the energy and forces for a particular atomic configuration, there exist two main areas of techniques for minimising the total energy. Static minimisation is guaranteed to find a *local* minimum and a large range of techniques has been developed for improving the efficiency by which this minimum is reached (see Press *et al.*, 1986).

An alternative scheme is dynamic minimisation. In molecular dynamics (MD) the system evolves under Newton's classical laws of motion. The forces are described as before but in addition the atoms have kinetic energy. It is this kinetic energy, provided it is high enough, that gives the system freedom to access different regions of phase space and thus to escape local minima and seek the global minimum. The minimisation proceeds in two steps. Firstly a high temperature anneal for several thousand time steps samples the configurational phase space. Secondly slow *cooling* or *quenching* extracts the minimum this anneal has found.

3.3.1.1 A Molecular Dynamics time-step

The original code for the core of this MD scheme was developed by A.P. Sutton. However it has been largely rewritten here and expanded upon. At its heart lies the technique used to integrate, with respect to time, the classical equations of motion. If the classical trajectory is continuous, then an estimate of the positions and velocities at time $t+\delta t$ may be obtained by using the "Velocity Verlet" algorithm (Swope *et al.*, 1982). This algorithm is more effective at minimising the round-off error than the original Verlet (1967) form. Its implementation involves two stages, assuming the positions, velocities and accelerations at

time t are known. Firstly, the new positions at time $t+\delta t$, and the velocities at *mid-step* are calculated using

$$\begin{aligned} \boldsymbol{r}(t+\delta t) &= \boldsymbol{r}(t) + \delta t \boldsymbol{v}(t) + 1/2 \delta t^2 \boldsymbol{a}(t) \\ \boldsymbol{v}(t+1/2\delta t) &= \boldsymbol{v}(t) + 1/2 \delta t \boldsymbol{a}(t) \end{aligned} \tag{3.1}$$

The forces at $t+\delta t$, and hence accelerations, are computed for the new positions and the velocity move completed

$$\boldsymbol{v}(t+\delta t) = \boldsymbol{v}(t+1/2\delta t) + 1/2 \delta t \boldsymbol{a}(t+\delta t) \tag{3.2}$$

The kinetic energy can now be calculated at time $t+\delta t$ and the potential energy has been calculated in the force loop. The system has thus been moved forward in time.

3.3.1.2 Neighbour lists

A key factor required to allow different regions of configurational phase space to be sampled using MD is a flexible neighbour list. Prior decisions on which atoms will interact immediately lock the system into a particular state. One simple solution is to choose a cutoff[2], r_c, and then for each atom to calculate the distances to all other atoms in the simulation cell. All bond lengths that are greater than r_c are ignored. However, this logical testing of every atom pair in the system is inefficient, particularly as the size of the system increases.

A better approach is to use the cell index and linked lists method (Hockney and Eastwood, 1981). This technique is described in detail in Allen and Tildesley (1987). The essential difference is to section the unit cell into a mesh of link cells. A routine **NNCELL()** was developed by A.P. Sutton to evaluate the connectivity of these cells. For each cell, the routine calculates and stores in a two dimensional array all cells that lie within r_c. This routine needs

---

[2] This cutoff is usually a parameter built into the functional form of the classical potential so that all derivatives are continuous at this boundary (Stillinger and Weber, 1985; Tersoff, 1988a). This is essential in MD since neighbours to a particular atom must be able to move smoothly in an out of the range of the potential without introducing discontinuous forces into the simulation.

only to be called once in an entire simulation. An improved version of **NNCELL()** has been developed here and relies on the fact that a cell-cell interaction need only be considered and stored once. The two dimensional array is replaced by a one dimensional array which halves the storage requirements and is accessed sequentially improving efficiency.

Once the cell connectivity has been established, the atoms are sorted into their appropriate cells using a routine **LNKCEL()**. This must be called for each MD step since atoms can move in or out of particular cells. **LNKCEL()** also generates the linked lists, which amounts to choosing one particular atom, for each cell, as the head of a chain which links all other atoms in that cell. The atom connectivity is then evaluated as follows: loop through all link cells; for each cell, c, an atom may only interact with another one further down the chain and the bond length r_{ij} is calculated. This ensures the ij interaction is considered only once. Bond lengths with atoms in the neighbouring cells to c are calculated in the same manner. Consequently, each atom needs to only consider a small fraction of the simulation cell to obtain its neighbours, rather than all the other atoms.

Finally the bond lengths r_{ij} need to be compared with r_c, retaining all those within this cutoff. The original version of the MD codes were based on the *minimum image convention* (Metropolis *et al.*, 1953), which implies that any particular atom can only interact with the closest periodic image of all the others. This restricts the possible number of bonds associated with an atom pair, ij, to one but as a consequence demands a minimum physical size to the simulation cell. This has been found to be too restrictive a requirement since the crystal periodicity along the dislocation line is unchanged, except on reconstruction of the 30° partial, at only $a_0/\sqrt{2}$, where a_0 is the lattice constant. The cutoff, r_c, of the classical potentials used is comparable to this repeat distance and thus 2-3 periods along the dislocation need to be considered in order to satisfy the minimum image condition. Lifting the restriction that atom i may only interact with the closest periodic images of all the others has eliminated this problem. In general, an atom pair ij may have several bonds which differ by integer multiples of superlattice vectors. This allows simulations to be performed on unit cells with only one,

or any number of, repeat periods along the dislocation line.

3.3.1.3 Energy and momentum conservation

Starting the simulation involves assigning an initial velocity to each atom. These are chosen randomly from a Maxwell-Boltzmann distribution with magnitudes conforming to the required temperature and adjusted to ensure no overall momentum. The choice of the time increment, δt, is gained from experience; too large a value leads to a lack of conservation of the total energy. However, the smaller the value the longer it takes for the system to evolve. A time-step of $\delta t = 10^{-15}$ seconds has been used for all simulations here, giving a conservation of energy to typically 1 part in 10^4 over several thousand MD iterations.

Conservation of momentum is guaranteed with 3D periodic boundary conditions provided they are implemented correctly. Violation of momentum conservation is thus usually related to an error in the neighbour lists which must keep track of interactions across the boundaries.

3.3.1.4 Energy minimisation

As it stands the scheme can be used for annealing a system, but in order to extract a minimum configuration two techniques have been added. The first is the usual approach of *temperature cooling*. This involves the slow removal of temperature from the system by reducing *all* velocities by the *same* amount each time step. This scheme was found to be unreliable in obtaining the minimum system state. This is because by reducing the velocities by a constant amount each time step forces the system to become motionless after a definite number of MD iterations. Unless the cooling is slow enough, and this implies a prior knowledge of how far from a minimum the system lies, the final configuration will not have arrived at the lowest energy state.

The main inadequacy with this technique is that there is no discrimination between atoms. Those that still need to move are cooled at the same rate as those that are already near their lowest energy position. A different method (Finnis, 1990) has been applied which has been called *quenching* since in certain circumstances the velocity of an atom is "quenched" by

setting it to zero. The method involves the calculation of $\boldsymbol{F}.\boldsymbol{v}$ for each atom and is most easily understood with reference to fig. 3.1. For an atom that is moving "uphill" in energy, regardless of direction, $\boldsymbol{F}.\boldsymbol{v} < 0$ and its velocity is set to zero (fig. 3.1a). If however the atom is moving "downhill" in energy (fig. 3.1b) then $\boldsymbol{F}.\boldsymbol{v} > 0$ and its velocity is left untouched. The system rapidly approaches the minimum configuration using this technique and the kinetic energy remaining within the system gives a direct indication of how far from this state the system is. This technique has been used throughout the work in this thesis.

3.3.2 Classical potentials

Three classical potentials have been programmed and are used within the MD scheme described. The functional forms for these potentials and their parameters are given in appendix A and the resource files for their use in appendix C.

The modified Lifson Warshell potential (Altmann *et al.*, 1982, 1983) has been used to provide a comparison with the predictions of the more "transferable" classical potentials of Stillinger and Weber (1985) and Tersoff (1988a, 1988b). Analytic expressions for the forces have not been evaluated for the modified Lifson Warshell potential. Forces are calculated as the numerical derivative of the energy with respect to position.

For any potential to be used effectively for predicting core structures it must be able to treat configurations with coordinations other than four. For example, the unreconstructed 90° partial involves three-fold coordinated atoms at the core. Simple VFFs provide an ambiguous description in this case, since they are constructed for an explicit assumption of four-fold coordination.

Stillinger and Weber (1985) introduced a potential that aimed to provide more "transferable" properties. Since the diamond-cubic structure is *not* stable with respect to a shear under the action of a conventional pair potential, the new potential also included three body interactions. Stillinger and Weber chose their parameters based on several criteria. They first required that the diamond structure be the most stable periodic configuration at zero

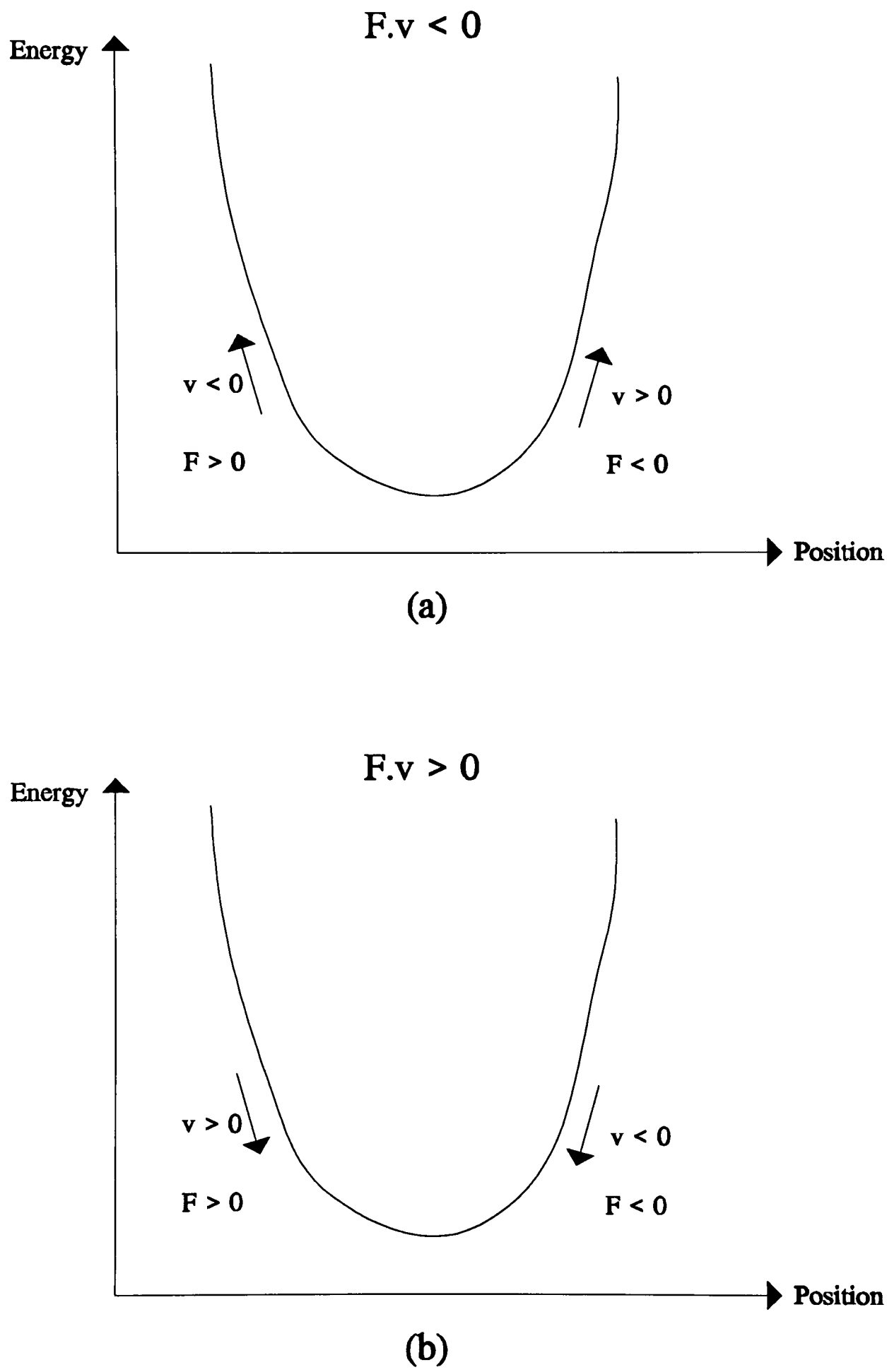

Fig. 3.1 Velocity quenching algorithm: (a) velocity set to zero, (b) velocity unchanged.

temperature and pressure. They then required that the melting point and the liquid structure of the melt be in reasonable accord with experiment.

Teichler (1989c) has noted that, as with most classical potentials, the Stillinger Weber potential has problems simultaneously modelling the elastic properties and the transverse acoustic phonon branch flattening. Specifically, the Stillinger Weber potential gives too much contribution to three-body interactions and as a result phonon frequencies are systematically higher then the experimental results (Jian *et al.*, 1990). By reducing the parameter, λ, and slightly modifying the form of the three-body potential, Jian *et al.* have obtained a better phonon frequency description. Their functional form and choice of parameters has been investigated here. Unfortunately it has been found that the effect of reducing the stiffness of the original potential no longer stabilises the diamond cubic structure with respect to closer-packed higher coordination structures. Hairie (1992) has also reduced the stiffness of the Stillinger Weber potential to fit experimental results on grain boundaries but has also recently found that the diamond cubic structure is no longer the lowest energy phase.

Only the original form of the Stillinger Weber potential will be used throughout this thesis.

In its original form the Tersoff (1986) potential reproduced many properties of Si well but did not find the diamond cubic structure to be the energetically most favourable (Dodson, 1987). Tersoff (1988a) modified the form of his original potential in several respects to overcome this shortcoming. The new physics incorporated in this potential is a description of the bond order (ie. the strength of each bond). The potential tries to describe the real effect that an atom with many neighbours forms weaker bonds than an atom with few neighbours. This key role of bond order is absent from most other classical prescriptions.

Heggie and Jones (1987) and Marklund and Wang (1992) have used this form of the Tersoff potential in simulations on the 90° partial. However, this form of the potential was found to give a poor description of the elastic constants (Tersoff, 1988b) and as a result significantly underestimates the bond-bending versus bond-stretching stiffness and thus shear deformation contributions (Teichler, 1989c). Tersoff (1988b) developed a new parameter set

to provide a better description of bond-bending forces. Both parameter sets are used here to investigate the differences they predict and throughout this thesis the two forms will be referred to as Tersoff (1988a) and Tersoff (1988b).

3.4 Tight-binding relaxation

A semi-empirical tight-binding code has been developed by M^{c}Innes (1992). The scheme is based on 3D periodic supercells and thus the Hamiltonian is solved in reciprocal-space by matrix diagonalisation. The method is essentially that due to Chadi (1979a, 1979b), but rather than expanding the repulsive pair-potential as a quadratic it is used in the form A/r^4, with A determined by the equilibrium condition for the bulk Si crystal at the experimentally observed lattice parameter. The disadvantage of Chadi's scheme is that an atom is unable to lose or gain a neighbour without introducing a discontinuity in the force and so a fixed crystal connectivity must be maintained throughout the relaxation. Force discontinuities are avoided in M^{c}Innes' program by ensuring the radial variation of the hopping integrals and the repulsive pair potential, and their derivatives, fall smoothly to zero at a chosen cutoff radius, r_t. This is indicated schematically in fig. 3.2. A fifth order polynomial is matched to the scaling law at some nodal distance, r_n. First and second order derivatives are continuous at r_n, while the polynomial smoothly falls to zero at the cutoff radius r_t. The nodal point is typically chosen to reduce the scaling to zero over a range of 0.2Å. The choice of the Hamiltonian cutoff, r_t, is also arbitrary and various choices have been considered in this work (see chapter 5).

A key advantage of the reciprocal-space formalism adopted here, over say the real space (recursion) method, is that the analytic forces are the *exact* derivatives of the energy. Both the force and the energy are approximations within the model and subject to a finite Brillouin zone sampling, but they are internally consistent. Relaxation is terminated when these forces typically fall below 10^{-6}eV/Å, and is performed as a static minimisation using the *variable metric method* (see Press *et al.*, 1986). The model also allows an explicit determination of the

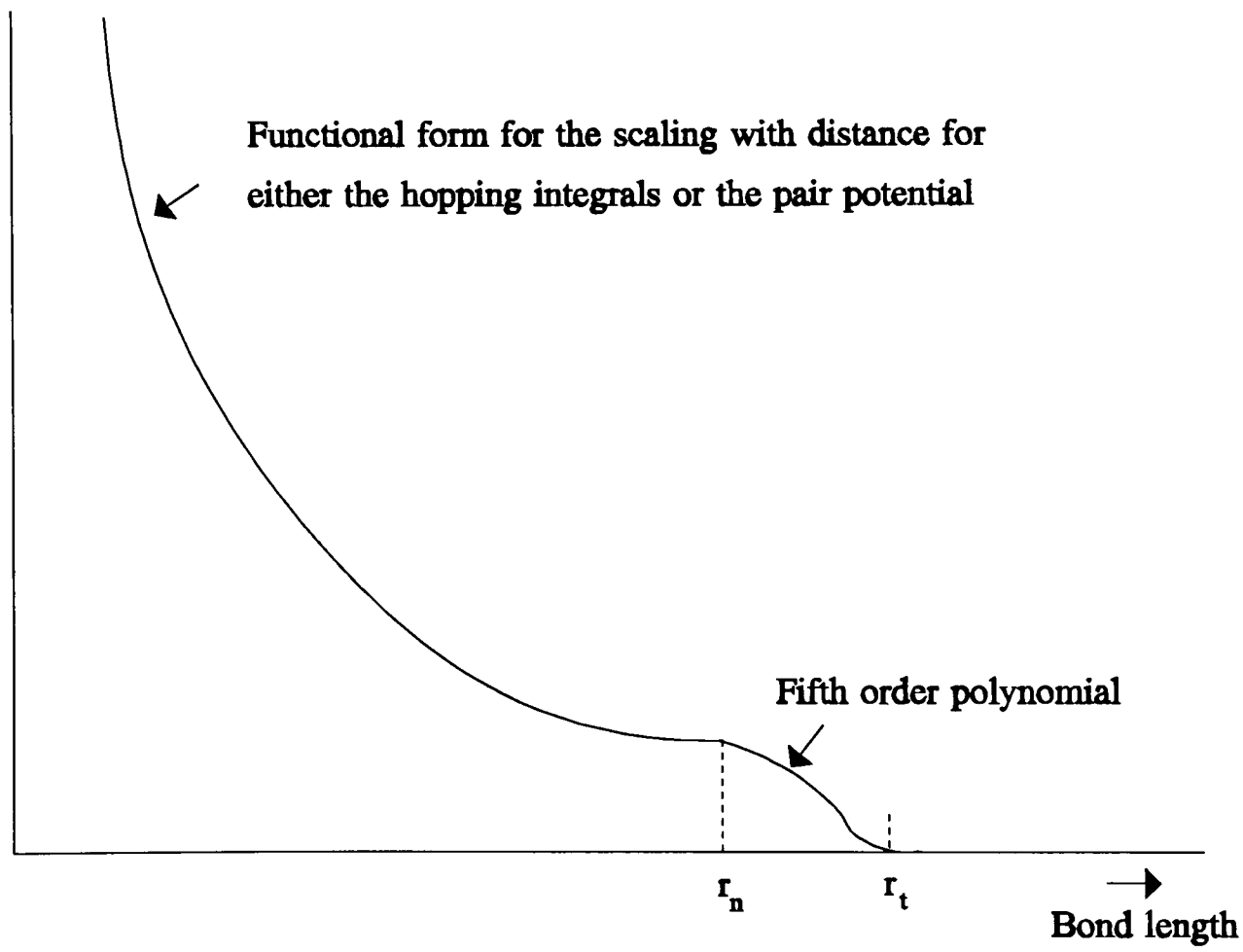

Fig. 3.2 Smooth termination to the scalings used for the hopping integrals and the pair potential within the tight-binding scheme of M^{c}Innes (1992). Atoms can move in and out of r_t without introducing discontinuities in the forces.

band-structure which is particularly suited to a discussion of shallow states.

3.4.1 Tight-binding Hamiltonians

Various tight-binding parameters for Si have been proposed and three sets have been considered here. The parameter set used by Chadi (1984) is a minimal sp^3 basis and used with an inverse square scaling law (Harrison, 1980). Chadi and Cohen (1975) have pointed out that such a minimal basis will not correctly reproduce the indirect band-gap in Si. Further, for an accurate description of the conduction bands d orbitals should be included (Kane, 1976). However, by incorporating an excited s-state into their parameterisation, Vogl *et al.* (1983) have significantly improved the *lower* conduction bands and reproduced the indirect nature of the band-gap. The scaling of the hopping parameters is again taken to be proportional to $1/d^2$. This Hamiltonian has been used mainly for band-structure calculations. By conducting a rescaling of the hopping parameters, Goodwin *et al.* (1989) have developed a Hamiltonian with a more realistic description of the overlap at both first and higher order neighbours than a simple inverse square or exponential (Pandey and Phillips, 1974a, 1974b, 1976) scaling can provide.

The angular dependence of the hopping integrals is given by the geometric factors evaluated by Slater and Koster (1954).

3.4.2 Temperature

Simulations can also be performed at temperature for which the internal energy, U, is replaced by the Helmholtz free energy, $F=U-TS$, as the function to be minimised. Quantities such as the band energy involve summations over all *occupied* states. At 0°K this simply involves populating each energy level with two electrons, starting from the lowest level until all electrons have been accounted for. The motivation for introducing temperature is that many structures have a degeneracy, or extremely closely spaced levels, in their highest occupied state. For example, consider two levels A and B which lie just below and above the Fermi

level. At 0°K level *A* will be occupied and *B* unoccupied. However, during relaxation atomic distortions could cause these states to reverse their ordering, so that at 0°K level *B* is now occupied and *A* unoccupied. Such an effect will lead to a discontinuity in the density matrix and consequently the forces. This can be avoided by introducing a temperature into the system and populating all energy levels according to Fermi-Dirac statistics. There is now a mixing between states *A* and *B* and they can smoothly reverse their ordering. The summation is now over *all* energy levels in the system.

3.4.3 Code development and changes

While the writing of virtually all the tight-binding code is the work of M°Innes (1992) much of its development has been linked with the work here. For example, the neighbour lists used in the program have been taken from the linked-lists approach of the MD schemes, described above. Inclusion of code to allow impurity atoms to be introduced has also been developed for this work. A recent development was the introduction of molecular dynamics to the code. Again, although rewritten by M°Innes to conform to the rest of the code, these routines are based entirely on the MD scheme developed in this work. Here I mention those changes that I have performed since M°Innes left.

3.4.3.1 k-point sampling

Electronic states are only allowed at a set of k-points determined by the boundary conditions of the solid. In an infinite crystal there exists an infinite number of k-points, and an infinite number of atomic orbitals needed to describe the problem. Use of Bloch's theorem (Bloch, 1928) allows a smaller repeat unit cell with the underlying periodicity of the infinite lattice to represent the original problem. This periodicity in real space leads to the concept of a reciprocal lattice and the Brillouin zone[3]. A consequence of Bloch's theorem is that only

[3] See any standard text book for an introduction to the concepts of **k**-space and Brillouin zones, eg. Ashcroft and Mermin (1976) *Solid State Physics* or Kittel (1986) *Introduction to Solid State Physics.*

k-points within the first Brillouin zone give rise to unique values for the electronic energy levels of the system. The problem has thus been reduced to calculations on a finite number of atoms and orbitals over an infinite number of k-points within the first Brillouin zone of the repeating unit cell. Since the occupied states at each k-point contribute to the electronic energy, in principle an infinite number of calculations is still required. However for k-points close to one another the resulting energy levels from the second point will be well represented by those at the first point. It is thus possible to get an estimate of the electronic energy from calculations at a finite number of k-points. One such technique has been developed by Monkhurst and Pack (1978) in which a uniform symmetric mesh is generated for performing this averaging over the Brillouin Zone. The convergence can be investigated as the approximation to the true average is improved by making the size of the mesh finer. The implementation of the technique is described by M^{c}Innes (1992).

In general, since the energy levels vary with k (dispersion), a symmetric uniform mesh is only efficient for a near-cubic Brillouin zone. For example, in most of the unit cells considered here there exists translational symmetry parallel to the dislocation line and this repeat vector is $\underline{z}=[10\bar{1}]/2$ which in terms of the cubic lattice parameter a_0 has period $c=a_0/\sqrt{2}$. Since the other box sides are much longer the *reciprocal* unit cell should only have significant dispersion in one direction. It is now necessary to ensure effective k-point sampling in this direction *only*. The code has been changed so that rather than generate a uniform mesh in all three reciprocal directions, specific k-points can be entered which sample along high dispersion directions only. By choosing $q<0$ in the resource file (see M^{c}Innes, 1992) k-points are no longer generated internally but are read in from the atomic configuration file (see appendix C). In chapter 5 an investigation of the structural and energy convergence is performed as obtained using a set of specific k-points compared to a uniform mesh.

3.4.3.2 Other changes

Two forms of the tight-binding code have been developed by M^{c}Innes. The second version

involves no assumptions on the form of the hopping integrals so in the interaction of two different atomic species it is possible, for example, to model $sp\sigma$ having a different value from $ps\sigma$. This version of the code has also been extended to incorporate the 5 orbital Hamiltonian due to Vogl *et al.* (1983). The routines required to introduce temperature to this version of the code were incomplete. This has been completed here to allow the Vogl *et al.* Hamiltonian to be used to investigate the stability of a structure that involves a degeneracy at the Fermi level (see Chapter 5, section 5.4.3.1).

The final change has been the incorporation of codes to study a *non-orthogonal* unit cell which will be described in Chapter 4. These codes have been introduced to all the classical MD schemes as well. It should be noted that they do not allow the modelling of any general non-orthogonal unit cell.

3.5 CETEP and CASTEP relaxation

CETEP (parallel code) and CASTEP (serial code) are ab initio total energy pseudopotential packages developed at Cambridge and Edinburgh. They have been treated as "black boxes" and as such only a description of how they are used is given here, except for a brief synopsis of the method.

These codes are based on density functional theory, with the Perdew-Zunger (1981) parameterisation of the exchange-correlation energy, and with the occupied valence orbitals expanded in plane waves. The total energy functional is minimised with respect to the plane-wave coefficients of the occupied orbitals and the ionic degrees of freedom. Kerker (1980) pseudopotentials are applied in the form of Kleinman and Bylander (1980), with the s-wave component treated as local, retaining three p and five d projectors. In CASTEP this projection is in k-space whereas in CETEP a real-space technique is used, which significantly increases the efficiency of large-scale calculations (King-Smith *et al.*, 1991). The electronic minimisation is similar to the technique of Car and Parrinello (1985) but use of a conjugate-gradient technique significantly improves the rate of convergence (Teter *et al.*, 1989). The

ionic relaxation uses a steepest descent algorithm in CETEP and a conjugate-gradient technique in CASTEP. k-point averaging is performed using the method of Monkhurst and Pack (1978). For a review of the pseudopotential method see Ihm *et al.* (1979), Denteneer and van Haeringen (1985) and Payne *et al.* (1992).

The serial code has been implemented on a Stardent Series GS2000 computer here at Oxford. The codes have been written in single precision and had to be converted to double precision. The resulting code has been tested thoroughly against results obtained in Cambridge.

The expansion of the valence orbitals in a limited number of plane waves needs further clarification. The number of plane waves in the expansion is controlled by an energy cutoff parameter. The truncation of the plane wave basis set at a finite energy cutoff leads to an error in the computed total energy. The magnitude of this error is reduced by including more plane waves. In principle, the cutoff energy should be increased until the calculated total energy has converged. However, taking the structural curves of Si (Yin and Cohen, 1984) as an example, only an accurate description of the shape, curvature and relative positions of the minima of these curves is necessary and not the absolute placement of these curves on a total energy scale. These required properties are related to energy *differences* which converge much more rapidly than absolute total energies.

Fig. 3.3 shows the curves obtained by calculating the total energy as a function of the bond length of a Si dimer situated at the centre of a unit cell of sides 7.5Å using CASTEP. Two curves are shown corresponding to a plane wave energy cutoff of 125eV and 175eV. The essential point is that the shape of the curve and the position of its minimum (0.4% error) are well described by using a cutoff of just 125eV, but the curve lies 0.95eV higher than that obtained with a 175eV cutoff, indicating total energies are still unconverged.

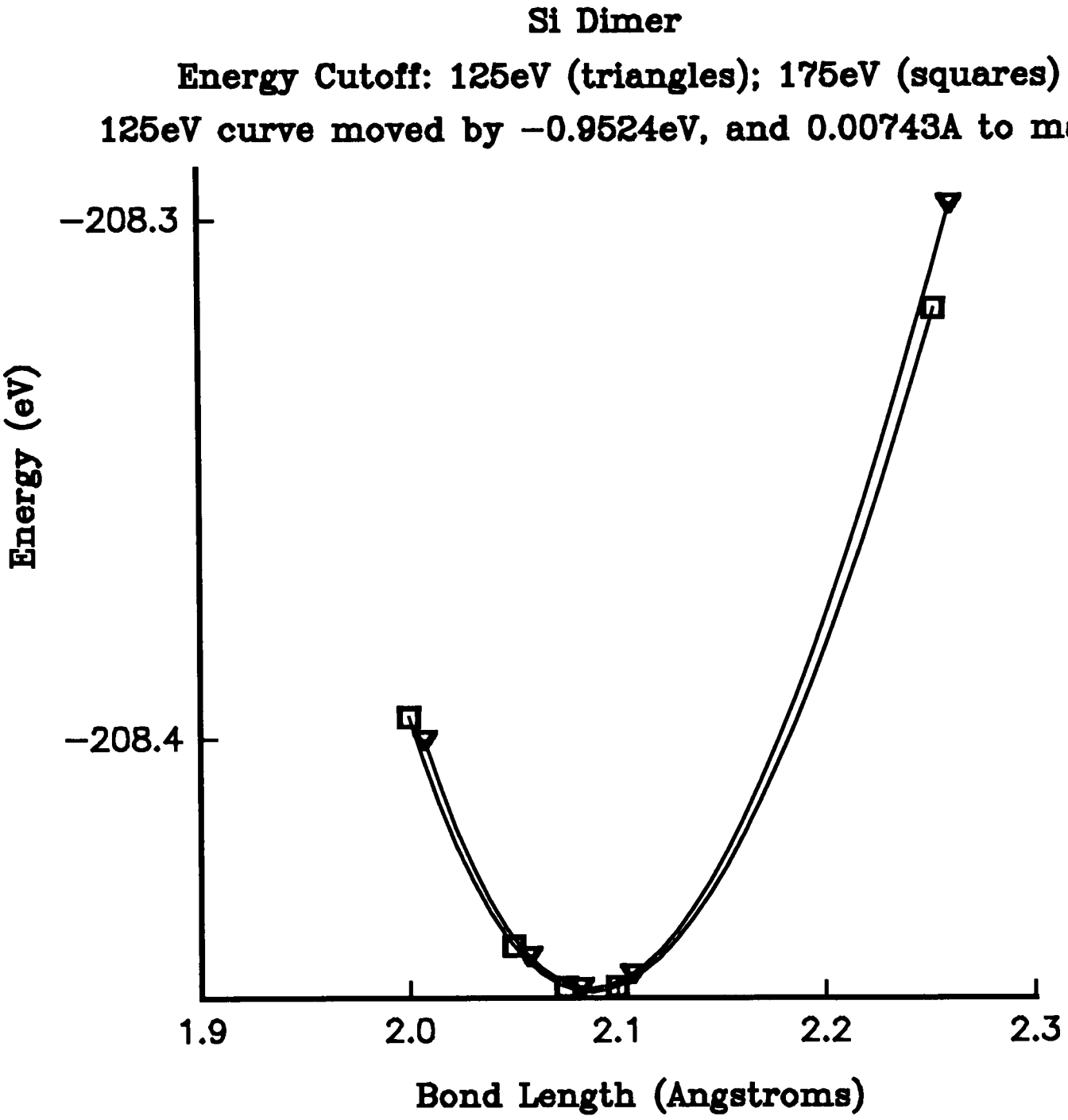

Fig. 3.3 Si dimer calculations using **CASTEP**.

CHAPTER 4

Boundary conditions

4.1 Introduction

Dislocations are extended defects which preserve the translational symmetry of the lattice parallel to the dislocation line and destroy it in a plane orthogonal to their line direction. There exist short range forces acting in the core region which tend to constrict the core and a long range elastic field which favours a wide core (Peierls, 1940; Nabarro, 1947). The structure of a dislocation core is thus determined by a balance between these two effects and due to the long-range nature of the elastic field the dislocation should ideally be embedded in an infinite medium.

Practically, any theoretical simulation is restricted to a finite and relatively small number of atoms and two approximate methods have emerged that both involve an artificial representation of this embedding:

(1) a finite cluster of atoms surrounding a *single* dislocation core

(2) the Large Unit Cell method developed by Marklund (1978) which involves forming a superlattice by periodically repeating unit cells containing *pairs* of dislocations with equal and opposite Burgers vectors.

The strength of the first method lies in its ability to treat an isolated dislocation, but the use of a cluster destroys all translational symmetry. This implies that the Schrödinger equation be solved in real space and limits the electronic structure information obtained to a set of

discrete levels. In all the early work (Jones, 1979; Jones and Marklund, 1980; Heggie and Jones, 1983a) the LDOS was calculated for a central atom in the dislocation core using the recursion method of Haydock *et al.* (1972). This had a rather limited energy resolution and could only address the position of deep levels within the indirect band gap.

By using a basis of Bloch functions with wave vectors parallel to the dislocation line, Veth and Teichler (1984) were able to consider much larger clusters and also to address the dispersion of the dislocation bands along this line direction. They obtained the band structure by calculating the LDOS for different k values along the dislocation line.

It is quite possible for shallow states in the band gap, which appear below the valence band maximum or above the conduction band minimum, to be buried in the Local Density of States (LDOS) under the band edges. To reveal the existence of such states it is necessary to carry out a k-space band-structure calculation. Exactly this scenario was found in two studies on silicon grain-boundaries by Paxton and Sutton (1988, 1989) and Kohyama *et al.* (1988a, 1988b), in which only the latter group who used a k-space approach were able to make conclusive statements about states in the gap near the band edges. Cluster calculations suffer from the additional problem of termination of the cluster, and there are two aspects to this.

Firstly, surface atoms associated with dangling bonds (Jones, 1979; Jones and Marklund, 1980) give rise to levels in the gap which are difficult to distinguish from defect levels. Heggie and Jones (1983b) used a topological ploy in which an inverse of their cluster was connected to the original to reduce the problem of these surface dangling bonds. Recently Heggie *et al.* (1989, 1991), using a local density functional pseudopotential scheme, have saturated the cluster surface atoms with hydrogen. Unfortunately they found the H atoms have bonding and anti-bonding states which couple strongly with states at the top of the valence band and at the bottom of the conduction band and artificially enlarge the gap (eg. 4.5eV for a 56 atom cluster $Si_{26}H_{30}$). The use of such small clusters results in the band gap being sensitively dependent on cluster size, and it is assumed that the positions of any defect levels relative to the band edges scale uniformly with their separation.

The second problem associated with cluster termination involves the competing effects of the short range forces acting in the core and the long range elastic field. As noted earlier, it is the balance of these two effects that determines the dislocation core structure and while much attention has been focused on the first aspect there is a real need to simulate the embedding of the cluster in an elastic medium. In such cases the decision as to whether the surface of the cluster should be fixed at the elastically generated positions or permitted to move will affect the degree to which the elastic field is coupled to the relaxation of the core. Jones (1985) found that the results obtained for a relaxed 90° partial containing a double kink were very sensitive to which of these two types of boundary condition was used, even for clusters of 2774 atoms. For the H terminated clusters (Heggie *et al.*, 1989, 1991), all the Si atoms and those H atoms lying in the glide plane were allowed to relax. The remaining H atoms were fixed to simulate a larger cluster embedding.

In this thesis the large unit cell method of Marklund (1978) has been used. The use of 3D periodic boundary conditions requires the unit cell to contain *two* dislocations of equal and opposite Burgers vectors so that the strain field remains finite. The disadvantages to this approach are that firstly, as in the cluster method, only a limited number of atoms within the unit cell can be treated and secondly that *two* dislocations have to be considered. This raises the question of how severely the interactions of these two dislocations affect the atomic and electronic structure results, and this has been investigated in chapter 5. It is also necessary to treat both dislocations symmetrically when considering point defect interactions for two main reasons. Firstly, contamination of only one dislocation core could lead to unreliable results. For example, the total energy might be minimised by structural changes in both the contaminated and clean dislocation core, and this would lead to a different core structure than would be obtained for the contaminated dislocation in isolation. Furthermore, interpretation of the band-structure results will be difficult when each core has been modelled differently. The disadvantage of this requirement is that impurity atoms have to be that much closer to one another.

If a small cluster is compared to a unit cell the latter should better describe the embedding of the dislocation in an infinite medium because *all* atoms in the unit cell are allowed to respond to the elastic field. Furthermore, increasing the size of the unit cell, as greater computing power will allow, will eliminate all of the above problems for the unit cell approach. This is not so clear for the cluster technique since even large clusters are affected by their termination as discussed above.

While in principle periodic repetition of these unit cells should result in the elimination of uncertain surface effects, there has seemed to be an historical problem with matching the boundaries of a unit cell with its neighbouring cells. Marklund (1979, 1983) used isotropic elasticity theory (Hirth and Lothe, 1982) to generate initial atomic positions within the unit cell. Following his earlier work (Marklund, 1978), he produced a better fit between adjacent cells by superimposing on each unit cell the elastic strain field from its neighbouring cells. Chelikowsky and Spence (1984) set up the starting configuration directly from near-atomic-resolution electron micrographs. They found it necessary to distort some of the bond lengths and bond angles at the boundary of their unit cell in order to create a periodic structure. Lodge *et al.* (1984) constructed a 64 atom cell from the centre of a relaxed 500 atom cluster containing a dipole. As with Marklund (1978) and Chelikowsky and Spence (1984) they found distorted bonds at the boundary of their unit cell and followed the approach of Marklund and superimposed neighbouring cell strain fields in order to produce a better fit. They noted that this technique distorted bonds from the values found originally in the *cluster*, though the distortion was fairly even over the unit cell.

Wang and Teichler (1989) took the basis vectors for the supercell lattice from the corresponding distances of simulations for an *isolated* partial dislocation and then imposed periodic boundary conditions during the relaxation. Relaxation using periodic boundary conditions has the disadvantage that any errors that might occur in matching atoms across a cell boundary will be absorbed into the relaxed structure. As a consequence the final configuration obtained could well mask the existence of an improper starting geometry. For

example, Lodge *et al.* (1989) used anisotropic elasticity theory (Hirth and Lothe, 1982) to generate the initial atomic positions in the unit cell and used periodic boundary conditions during the relaxation. All bond lengths and bond angles appeared to be sensible after relaxation but further analysis revealed that a residual net stress was still present in their cell even after relaxing the atomic coordinates. To relax this stress they allowed the shape of the periodic cell to change.

4.2 Geometry of unit cells - grain boundaries

What causes this stress? Lodge *et al.* (1989) were the first to quantify the magnitude of this problem by identifying the existence of an overall shear strain of the order of 0.1 in the relaxed configuration of Chelikowsky and Spence (1984). Using the work of Seeger (1982) they showed that a shear strain of that size in perfect crystalline Si would raise the valence band edge by the order of 0.2eV while leaving the conduction band edge unchanged. They proposed that its presence in the dislocation geometry may well have a similar effect on the dislocation bands.

The origin of this problem has been identified here and is illustrated by considering the 90° partial dislocation. Fig. 4.1 shows the *dipolar* lattice that is generated by periodically repeating the dipole in the rectangular unit cell. Tilt grain boundaries (solid lines) of equal and opposite misorientations are generated. *Unless the height of the repeat cell, d, is commensurate with the periodicity of the grain boundaries a misfit is introduced at the horizontal cell boundaries.*

Consideration of an example will make this point clearer. Fig. 4.2 illustrates a $<101>$ projection of an FCC lattice and it can be seen that the repeat period in the vertical, $<111>$, direction is three $\{111\}$ planes. This has been labelled, d_0. Part of a second interpenetrating FCC lattice and the formation of diamond cubic is also shown. It is seen that $d_0 = 3\{111\}$ planes is also the repeat period for diamond cubic, where each $\{111\}$ plane now involves one atom from each FCC sub-lattice. Arbitrarily, a unit cell height of d_0 will be considered. Each

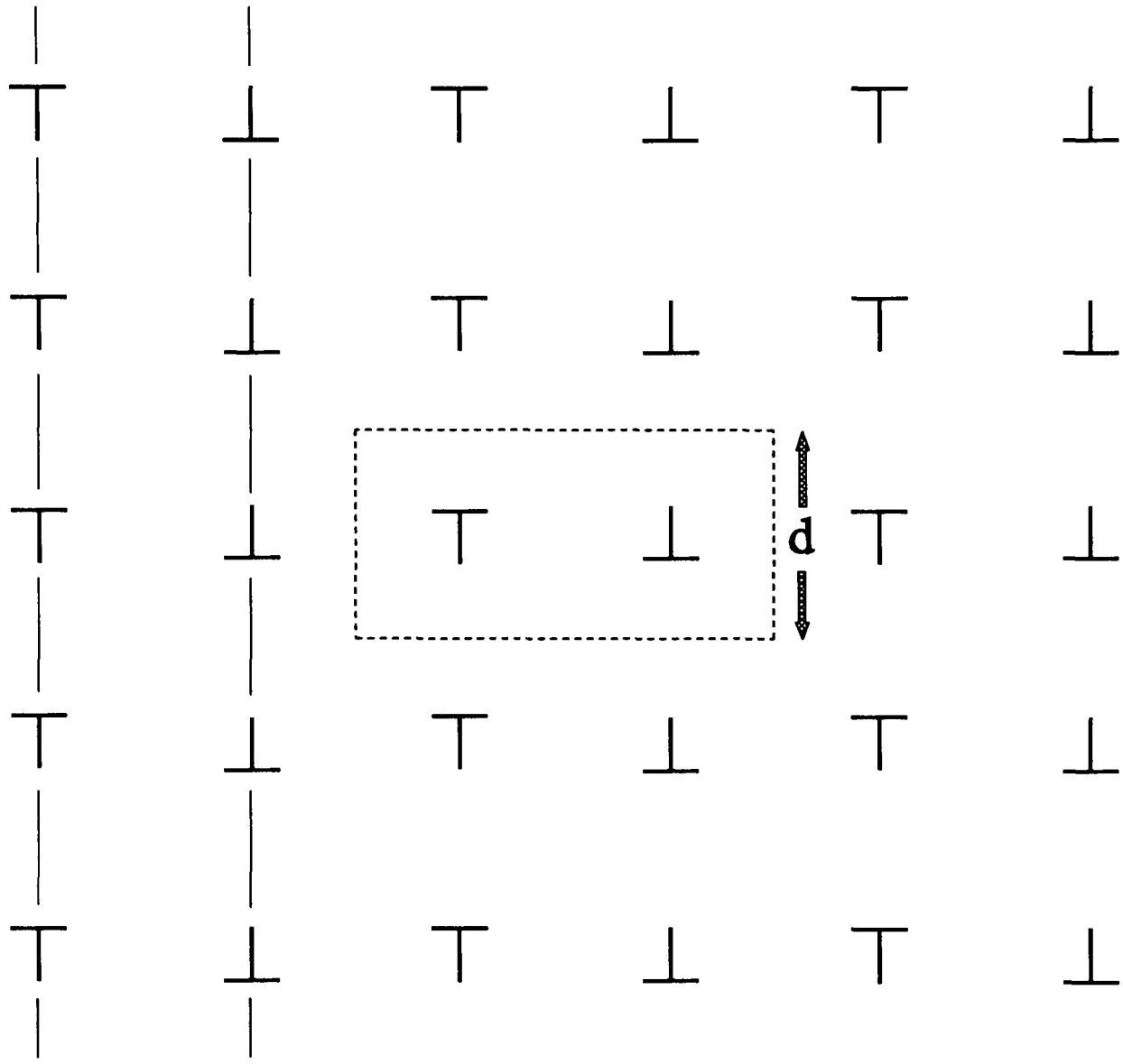

Fig. 4.1 Dipolar superlattice formed by periodically repeating the unit cell containing the dislocation dipole. The solid lines illustrate the formation of alternating tilt grain boundaries.

cell contains two opposing partials which when periodically repeated will generate two opposing grain boundaries each having a vertical partial separation of d_0. One such grain boundary is illustrated in fig. 4.2, passing vertically through atoms 1 and 2. The Burgers vector for each partial in this grain boundary is $\underline{b}=1/6<121>$, the other grain boundary being composed of the partials of opposing Burgers vector $-\underline{b}$. Considering the lattice site 2, the grain boundary will impart an equal and opposite atomic displacement of $|\underline{b}|/2$ to each grain. It can be seen that this displacement does not separate lattice sites and by imagining the triangular wedge of material enclosed to be removed it is clear that there no longer exists a periodic image of atom 1. This implies that a unit cell height of three $\{111\}$ planes, as used by Chelikowsky and Spence (1984), will possess a misfit across the $<111>$ boundary.

The required unit cell height to obtain correct boundary matching can be calculated with reference to fig. 4.3. Using, $d_0=3\times1/3[\bar{1}\bar{1}\bar{1}]$ and that $\boldsymbol{b}=1/6[1\bar{2}1]$ for the 90° partial gives

$$\begin{aligned} \boldsymbol{p}_u &= [\bar{1}\bar{1}\bar{1}]-\frac{1}{12}[1\bar{2}1]=\frac{1}{12}[\bar{1}3\,\bar{1}0\,\bar{1}3] \\ \boldsymbol{p}_l &= [\bar{1}\bar{1}\bar{1}]+\frac{1}{12}[1\bar{2}1]=\frac{1}{12}[\bar{1}\bar{1}\,\bar{1}4\,\bar{1}1] \end{aligned} \qquad (4.1)$$

The grain boundary repeat vectors are consequently $6\boldsymbol{p}_u=1/2[\bar{1}3\,\bar{1}0\,\bar{1}3]$ and $6\boldsymbol{p}_l=1/2[\bar{1}\bar{1}\,\bar{1}4\,\bar{1}1]$. This implies that a correct boundary matching first occurs for a unit cell height of $6\times d_0$ in which there exists a misorientation angle, $\theta=13.4°$.

This can be also understood from fig. 4.2. The first lattice site nearest 2 is atom 3, but the square signifies it lies on a different $\{202\}$ plane to atom 2. Hence the first equivalent atom site to atom 2 is atom 4 which lies a displacement of $6\times\underline{b}/2$ away. Consequently the grain boundary vector will start and finish on an equivalent site every 6 dislocations or $6\times d_0=18\,\{111\}$ planes. This implies that for a desired vertical partial separation of $3\,\{111\}$ planes, periodic boundary conditions are satisfied only for a unit cell height which is a

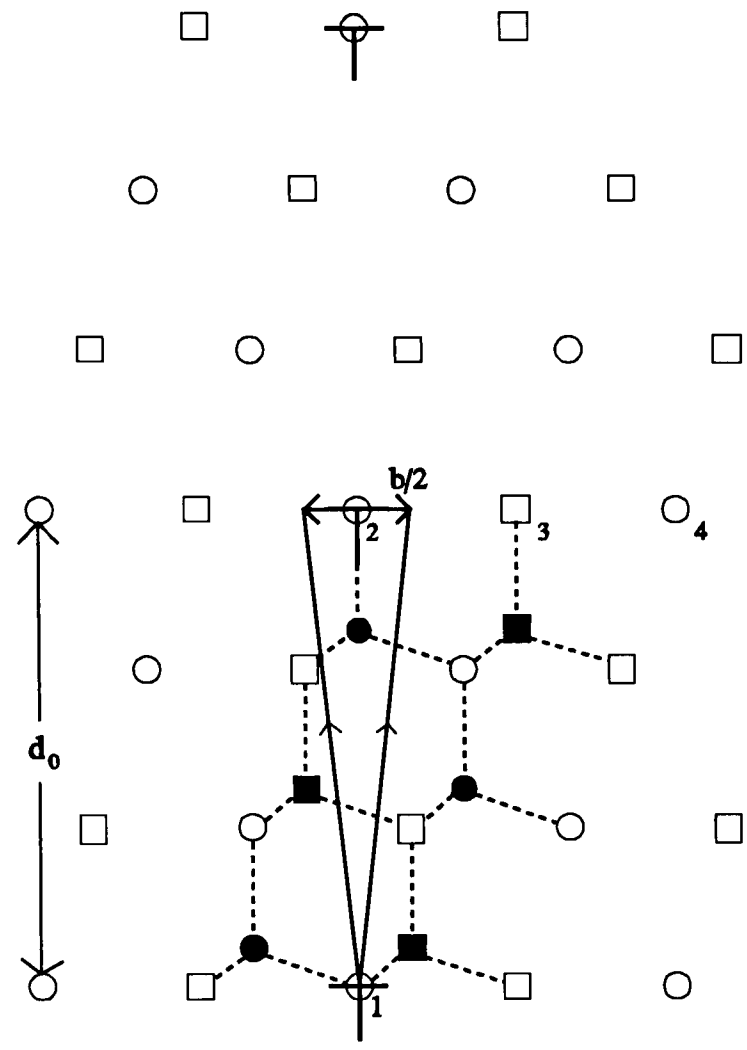

Fig. 4.2 <101> projection of an FCC lattice represented by the hollow symbols. The solid symbols illustrate the second interpenetrating FCC lattice and the formation of diamond cubic. The grain boundary rises vertically through atoms 1 and 2. The circles and squares represent atoms on different {202} planes.

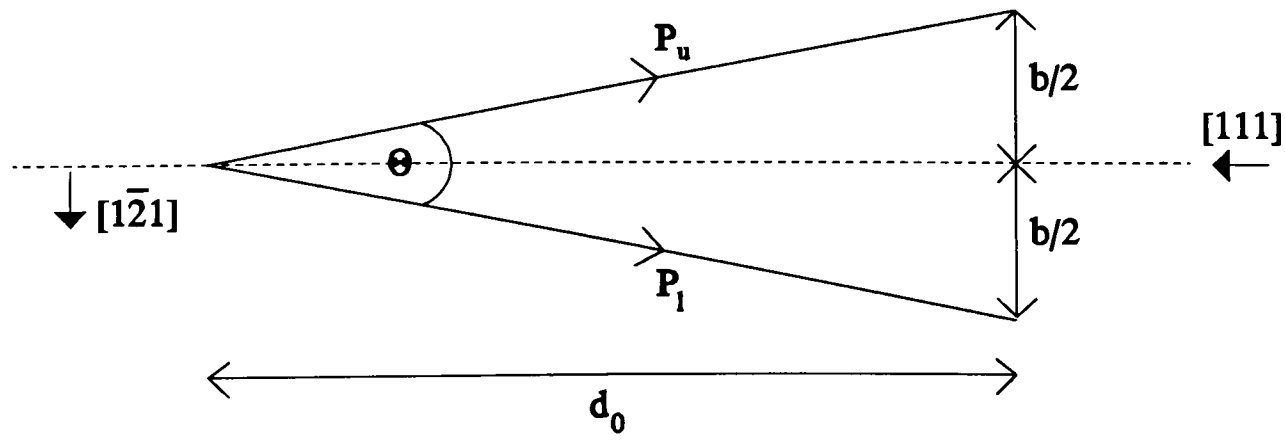

Fig. 4.3 Illustration of the grain boundary vectors in the upper and lower grain.

multiple of 18 {1 1 1} planes. The smallest such cell contains 6 dislocation dipoles and is illustrated in fig. 4.4!

It can be seen from fig. 4.2 that there is never an equivalent site to atom 1 with a Burgers vector displacement of just $\underline{b}/2$. As a result, whatever the <1 1 1> height chosen for the unit cell, the consequence of only containing one dislocation dipole is that there will always be a boundary mismatch. This implies that all previous simulations on the 90° partial using the large unit cell technique of Marklund (1978) have had some degree of artificial stress present in their system.

Recent authors have found an improvement to the fit of neighbouring cells by the use of non-orthogonal crystal vectors (Wang and Teichler, 1989; Lodge *et al.*, 1989; Marklund and Wang, 1992). This is not surprising since the system is clearly in a state of strain at the boundary in a rectangular cell, but the consequences of allowing a skewness into the cell leads to another problem, illustrated in fig. 4.5. The grain boundaries are now at an angle as in fig. 4.5a. In fig. 4.5b the displacement imparted by one of these grain boundaries is represented in its two resolved components. The set of partial dislocations on the right hand side of this figure results in displacements *along* the boundary line which necessarily give rise to a long-range average stress. There thus exists two competing stresses, one which works to distort the unit cell for proper boundary matching and the other that arises as a result of this distortion.

By relaxing the stress within their unit cell, Lodge *et al.* (1989) have obtained a structure in which these two competing stresses have cancelled and eliminated the shear strain previously located at the cell boundary. Without this strain the system gives rise to a significantly different electronic structure, as will be seen, but the superlattice being modelled is physically incorrect for two reasons. Firstly, it corresponds to an inclined boundary containing only one type of partial which is stabilised by imposing a periodic displacement, t, as illustrated in fig. 4.5a. Secondly, the crystal structure must change across these inclined boundaries, as a consequence of the epitaxial component, and this implies that part of the unit

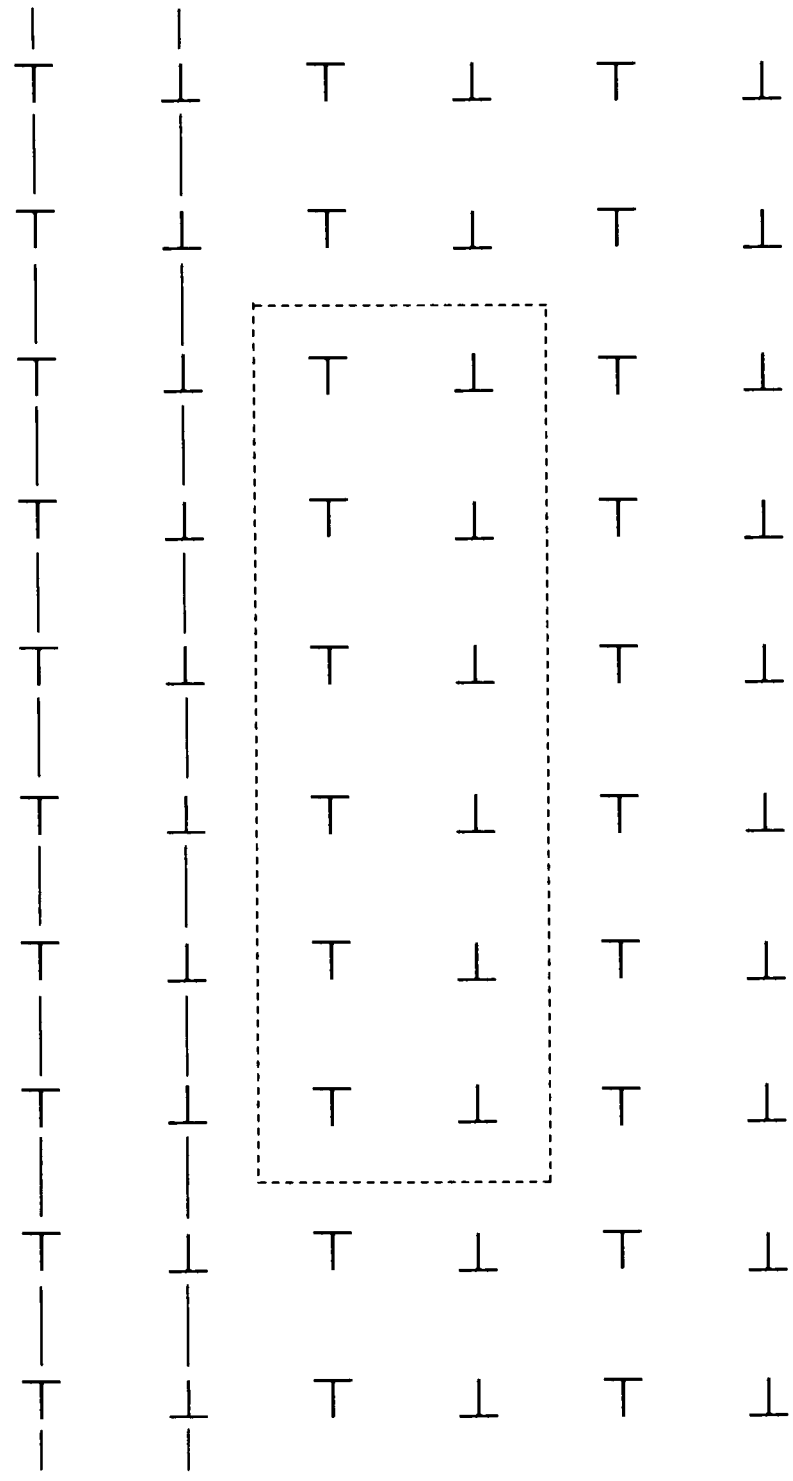

Fig. 4.4 Solution to the boundary matching problem which arises due to the generation of the alternating tilt grain boundaries (solid lines).

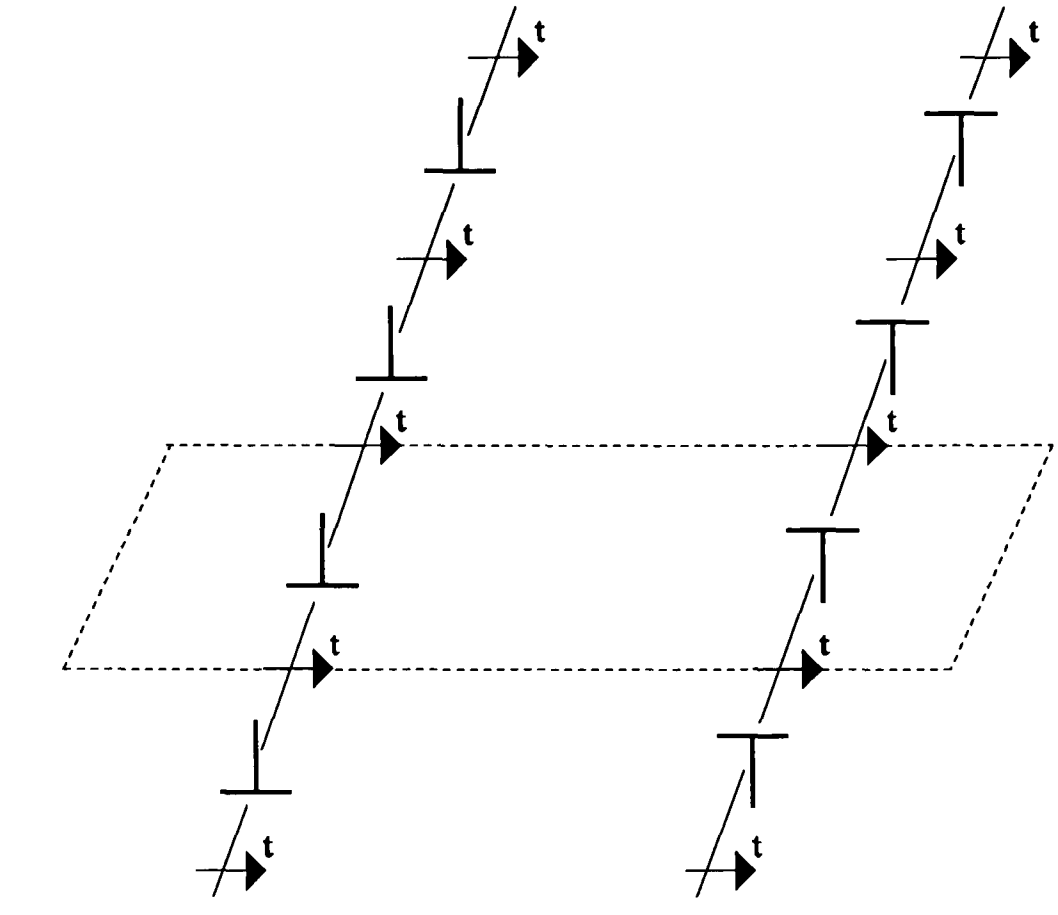

(a)

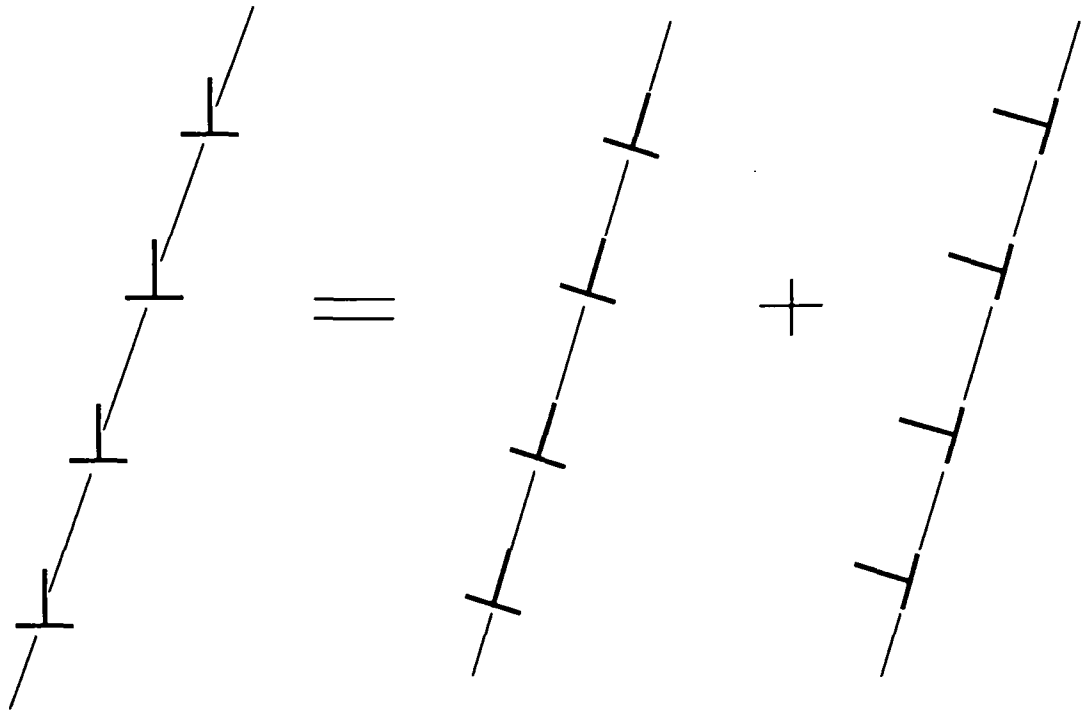

(b)

Fig. 4.5 Skew unit cells leading to another source of stress within the system, (a) the dislocation superlattice generated by the skew unit cell and (b) a representation of the dislocation components parallel and perpendicular to the line direction.

cell consists of a non-diamond cubic phase.

Considering our goal is to model the structure of an isolated 90° partial it is clearly highly undesirable to have to consider a unit cell containing 12 such partials (fig. 4.4) in order to be commensurate with our choice of periodic boundary conditions. There is however an alternative solution which also avoids either of these two unphysical stresses. The rectangular cell depicted in fig. 4.6 contains a dislocation quadrupole and generates a superlattice with partials of alternating Burgers vectors both horizontally *and* vertically, which avoids the generation of grain boundaries altogether. The <1 1 1> boundary layer will now match correctly because the displacements produced by the lower dipole will be exactly cancelled by the upper one.

Care must be taken in choosing the height of this unit cell since the diamond cubic repeat period in the <1 1 1> direction, d_0, must be taken into consideration. This period is often represented in terms of a <1 1 1> stacking sequence ...AaBbCcAaBbCc.., the repeated symbols Aa, etc., reflecting the presence of two atoms in the primitive unit cell[1]. This period immediately implies that a unit cell of perfect diamond cubic can only wrap correctly at the <1 1 1> boundary if its length in this direction is a multiple of d_0. For the quadrupole in fig. 4.6, any path from the bottom to the top of the cell passes through one stacking fault. Consider then a unit cell of height $2d_0$ which if perfect diamond cubic would wrap correctly, AaBbCcAaBbCc. The presence of the stacking fault in the quadrupole geometry modifies this stacking sequence to AaBbAaBbCcAa. While symmetry has ensured that the atomic positions across the boundary will be equivalent there exists an incorrect stacking sequence AaAa. The solution is to add two {1 1 1} planes BbCc, so that the height of the unit cell is now 8{1 1 1} planes and the stacking sequence has become AaBbAaBbCcAaBbCc. In general any quadrupole geometry which has two extra pairs of {1 1 1} atomic planes on top of a unit cell involving any multiple of three of these planes (eg 5,8,11,14 etc.) will match in a correct

[1] See fig. 1.1a in chapter 1 if this is not clear.

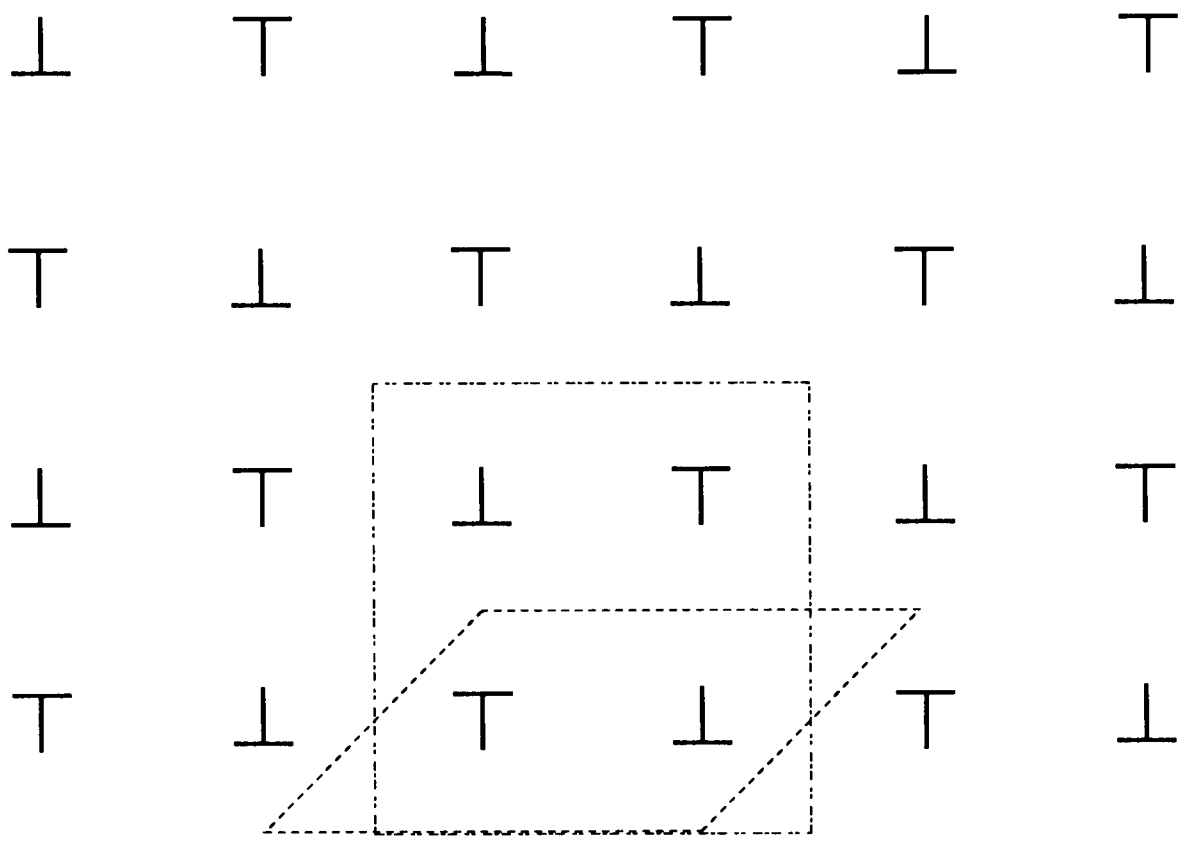

Fig. 4.6 Quadrupolar superlattice formed by periodically repeating either the rectangular unit cell containing a dislocation quadrupole or the oblique unit cell containing a dislocation dipole.

diamond cubic stacking sequence across the boundary.

Fig. 4.6 also shows how a particular non-orthogonal unit cell containing once again a single dislocation *dipole* can be created with periodic properties that reproduce the *quadrupolar* superlattice[2]. However, this reduction of the quadrupole unit cell to this oblique form is possible only when the partials can be *exactly* symmetrically placed within it. For example, if the partials in the central unit cell are moved nearer together horizontally they lie correspondingly further away from their periodic images (fig. 4.7a). However, the skew unit cell now gives rise to a very different superlattice (fig. 4.7b).

In the case of the 90° partial the atomic displacements that give rise to the two partials do allow their *exact* symmetrical placement. The oblique cell has the same $\underline{X}$ (along $<121>$) and $\underline{Z}$ (along $<101>$) box vectors as the quadrupole cell but has a skew $\underline{Y}$ vector which is calculated as follows: the height of the oblique dipole cell in the $<111>$ direction is half that of the quadrupole, ie. $\underline{Y}/2$. Fig. 4.6 illustrates that as an atom leaves the bottom of the oblique cell it moves by $\underline{Y}/2$ to the top but is also translated by $\underline{X}/2$. The vector $\underline{y}=(\underline{Y}+\underline{X})/2$ ensures periodic image of the oblique unit cell reproduces the quadrupole atomic positions in the $<121>$ and $<111>$ directions. There is however one further problem; in any $\{111\}$ layer alternate atoms of the same FCC sub-lattice lie on different $\{202\}$ planes as illustrated by the circles and squares in fig. 4.2. The oblique unit cell has the property that the periodic image of the bottom layer of atoms actually all lie on the wrong $\{202\}$ plane for correct marrying with the top layer of atoms. By shifting all atoms that periodically wrap from the lower to upper surface by $<101>/4$ they can be translated to lie on the other $\{202\}$ plane.

To recapitulate: a rectangular unit cell containing two opposing 90° partials results in a boundary mismatch and the introduction of artificial stress. This misfit can be eliminated by increasing the unit cell length in the $<111>$ direction to be a multiple of the grain boundary

---

[2] I am grateful to M. Heggie for pointing this out.

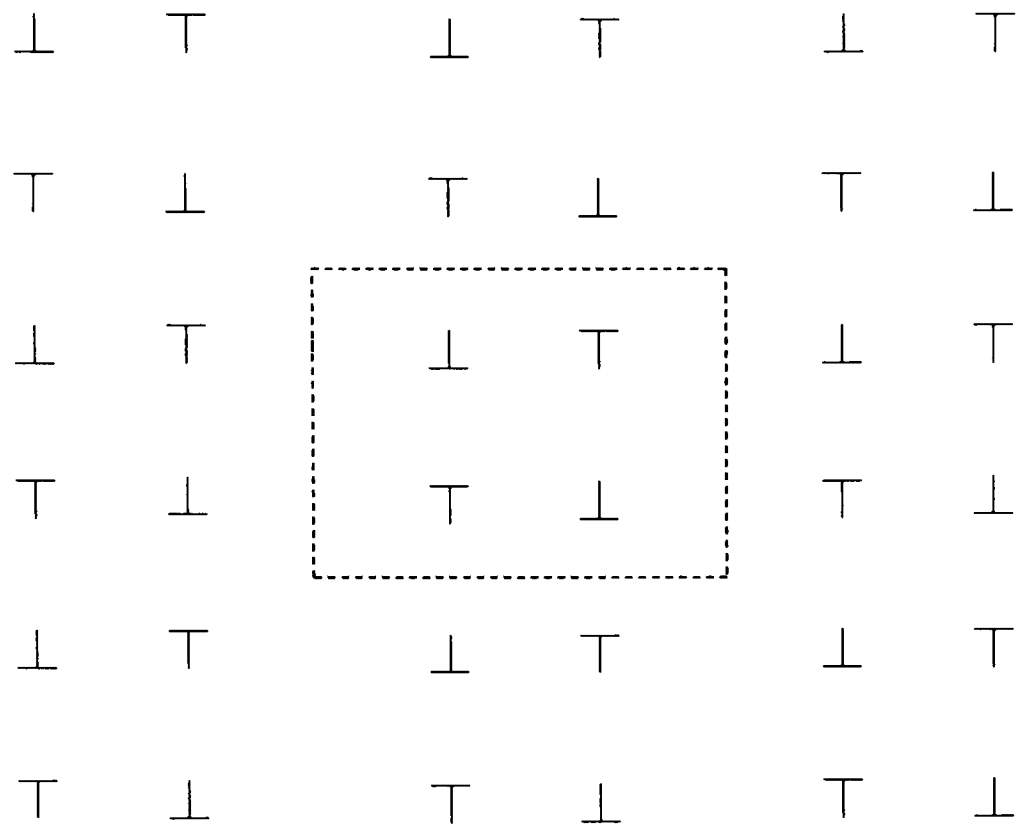

(a)

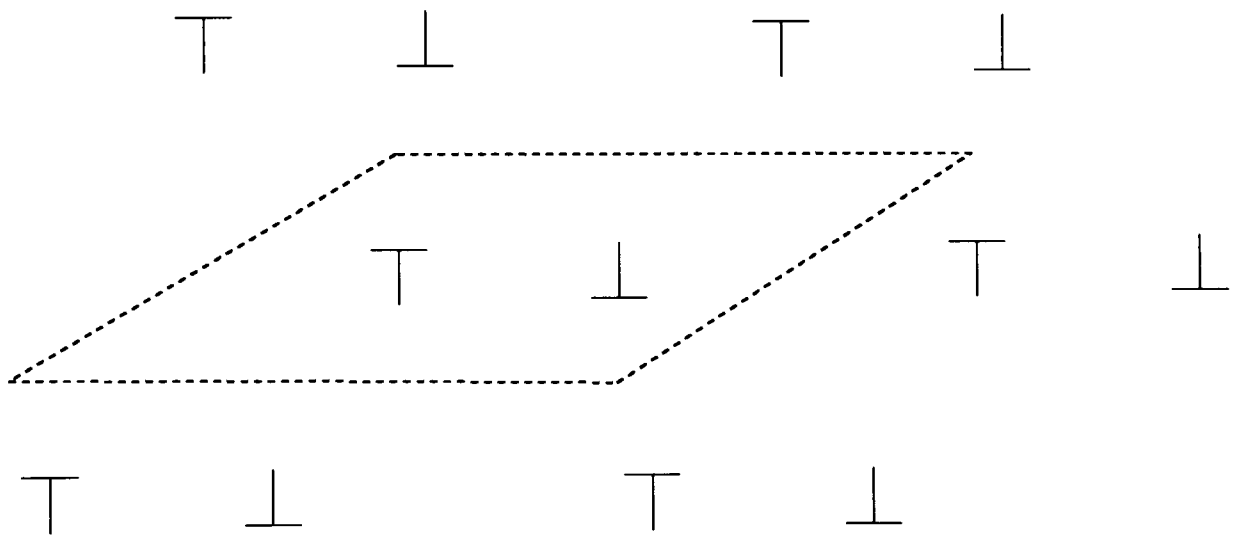

(b)

Fig. 4.7 Asymmetrical placement of partials within the unit cell, (a) the quadrupolar lattice generated and (b) the skew unit cell generating a very different superlattice.

period in that direction. This however, involves constructing unit cells containing 12 partials. Use of the rectangular quadrupole geometry, which avoids grain boundaries altogether, allows the modelling of cells with only four partials. A special case arises when the atomic positions of the atoms at the dislocation cores are symmetrically placed. It is then possible to create from the rectangular quadrupole unit cell with box vectors $\underline{X}$, $\underline{Y}$ and $\underline{Z}$ an oblique dipole unit cell with box vectors $\underline{X}$, $(\underline{Y}+\underline{X}+\underline{z'})/2$ and $\underline{Z}$, where $\underline{z'}=1/2<101>$. The oblique cell contains only two partials and half as many atoms as the quadrupole. The program **SKEW_FROM_QUAD** takes as its input a rectangular cell containing the quadrupole and generates its related oblique unit cell.

There still exists one subtle point which is related to the reconstruction of the 90° partial which can occur in two senses which are mirror images of one another[3]. The oblique unit cell can be generated only from a quadrupole unit cell which has the partials reconstructed in a particular symmetry. This is when partials diagonally related have the *same* reconstruction sense, since this is how the oblique unit cell will generate the superlattice on periodic repetition. Under this constraint it has been confirmed that a fully relaxed quadrupole unit cell generates an oblique unit cell with an identical atomic structure which is *also* fully relaxed. If it were not already fully relaxed this would imply an asymmetry in the system, and this is incidentally how the need to ensure that diagonally opposite partials in the quadrupole have the same reconstruction sense was discovered!

The 30° partial contains both some edge and screw character. The simple rectangular *dipole* unit cell fails again since there now involves a mismatch similar to the 90° partial *and* a superlattice with parallel screw dislocations which on their own are unstable. Use of the rectangular quadrupolar unit cell eliminates both of these problems through its symmetry. Unfortunately the 30° partial does not allow the problem to be reduced to an oblique unit cell since the atomic displacements lead to a very slightly asymmetrically placed partial, and hence

---

[3] Analysis of fig. 1.3b in chapter 1 will illustrate that reconstruction can occur either to the right, as shown, or equivalently to the left.

the problem shown in fig. 4.7.

4.3 Implementation of oblique unit cells for the 90° partial

All the methods described in chapter 3 have been developed for modelling orthogonal unit cells. Various oblique cells of different sizes and shapes have been considered here, but in all cases the periodic properties are such that the *X* and *Z* directions wrap identically to an orthogonal unit cell, as does the *Y* direction except for the displacements described above. It is thus possible to remain in an orthogonal coordinate system and reference to the obliqueness of the unit cell needs only to occur when calculating bond lengths with neighbours across the <1 1 1> boundary. This approach has been coded and added to the Molecular Dynamics schemes and the tight-binding method. The Cambridge and Edinburgh codes (**CETEP** and **CASTEP**) already have the ability to treat any non-orthogonal unit cell. In this case the program **SKEW_TB_TO_CSTP** converts the atomic configuration file of the oblique unit cell as used by the MD and tight-binding methods to that needed by **CETEP** and **CASTEP**.

4.4 Boundary mismatch consequences

An investigation of the effect that occurs as a result of this artificial strain introduced by a boundary mismatch is undertaken here. It is directed towards understanding why there has been poor agreement on the position of the dislocation bands for the reconstructed 90° partial modelled in a supercell.

Only the asymmetric four-fold reconstructed state as proposed by Hirsch (1979) and Jones (1979) will be considered here. A more rigorous analysis of the atomic and electronic structure is detailed in chapter 5. For example, the reliability of both the atomic and electronic structure results given here are investigated in chapter 5 by using different relaxation techniques and sizes and shapes of the unit cells. It is intended here only to understand the consequences of the unit cell geometry.

Two unit cells are used for this purpose. A *rectangular* unit cell of 96 atoms with box

vectors $2[1\bar{2}1]$, $2[\bar{1}\bar{1}\bar{1}]$ and $[10\bar{1}]/2$, and an *oblique* unit cell of 64 atoms with box vectors $2[1\bar{2}1]$, $[1\bar{2}1]+4/3[\bar{1}\bar{1}\bar{1}]+[10\bar{1}]/4$ and $[10\bar{1}]/2$.

4.4.1 Atomic structure of the 90° partial

Both these cells have been relaxed using two methods; the classical potential of Tersoff (1988b) *and* with tight-binding using the Goodwin *et al.* (GSP) Hamiltonian, both schemes restricted to the four-fold first neighbour cutoff. The relaxed unit cells are illustrated in fig. 4.8a and 4.8b.

Table 4.1 shows the bond length and bond angle changes that occur when moving from the *rectangular* to the *oblique* dipole unit cell, using the *same* method of relaxation in each cell. There is a consistent bond rearrangement in both the classical and tight-binding simulations which indicates that this is a consequence of the change in *cell* geometry and not the relaxation technique employed.

The main effect that occurs involves the back bonds off the reconstructed bond 1, depicted in fig. 4.9. In the *rectangular* unit cell the bonds 2 and 2' on the normal crystal side are longer than those on the stacking fault side, 3 and 3', and as a consequence a significant asymmetry of the bond angles exists. This core asymmetry is typical of that obtained in other rectangular cell geometries (Chelikowsky and Spence, 1984; Lodge *et al.*, 1984).

In the *oblique* unit cell the back bonds are much closer in length on either side of the reconstructed bond and the resulting bond angles far more symmetrical. In moving to a more symmetric state, bonds 4, 8 and 12 all stretch to accommodate the reduction of the back bonds, 2 and 2', on the normal crystal side. Analysis of fig. 4.9 shows that in a relaxation where each atom sees only four nearest neighbours the atomic environment seen by atoms 1 and 2 on either side of the core are very similar. It thus seems reasonable that there will exist symmetry around the reconstructed bond in this case and two results indicate this is the correct geometry. Firstly, Lodge *et al.* (1989) also obtained symmetrical back bonds when they allowed their unit cell to change shape and relax the shear strain present in its right-sided

Fig. 4.8a 96 atom *rectangular* unit cell containing a 90° partial dislocation dipole.

Fig. 4.8b 64 atom *oblique* unit cell containing a 90° partial dislocation dipole.

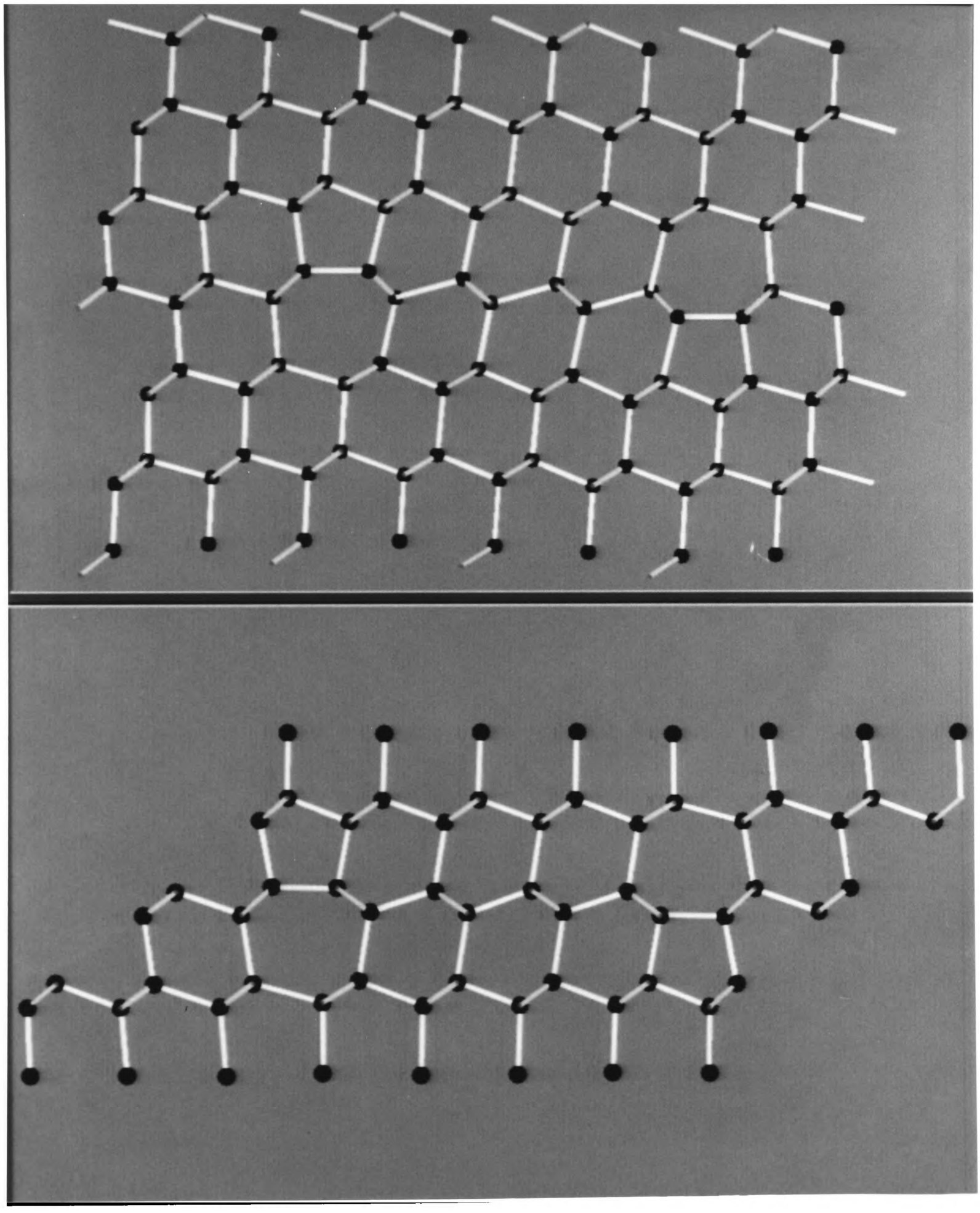

Bond	GSP r_t=3.0Å *Rectangular*	GSP r_t=3.0Å *Oblique*	Change Å	Tersoff (1988b) *Rectangular*	Tersoff (1988b) *Oblique*	Change Å
Bond 1	2.428	2.431	**0.003**	2.455	2.458	**0.003**
Bond 2	2.327	2.308	**-0.019**	2.335	2.320	**-0.015**
Bond 2'	2.421	2.409	**-0.012**	2.423	2.403	**-0.02**
Bond 3	2.389	2.403	**0.014**	2.385	2.399	**0.014**
Bond 3'	2.301	2.309	**0.008**	2.316	2.320	**0.004**
Bond 4	2.375	2.390	**0.015**	2.372	2.391	**0.019**
Bond 5	2.390	2.385	**-0.005**	2.388	2.382	**-0.006**
Bond 6	2.353	2.345	**-0.008**	2.362	2.352	**-0.01**
Bond 7	2.356	2.346	**-0.01**	2.357	2.353	**-0.004**
Bond 8	2.401	2.424	**0.023**	2.403	2.424	**0.021**
Bond 9	2.423	2.416	**-0.007**	2.428	2.421	**-0.007**
Bond 9'	2.358	2.363	**0.005**	2.363	2.368	**0.005**
Bond 10	2.369	2.347	**-0.022**	2.347	2.324	**-0.023**
Bond 10'	2.318	2.310	**-0.008**	2.322	2.311	**-0.011**
Bond 11	2.306	2.313	**0.007**	2.310	2.313	**0.003**
Bond 12	2.386	2.410	**0.024**	2.385	2.409	**0.024**
Bond 13	2.405	2.405	**0.0**	2.405	2.405	**0.0**
Bond 14	2.352	2.332	**-0.02**	2.356	2.335	**-0.021**
Bond 14'	2.370	2.352	**-0.018**	2.371	2.349	**-0.022**
Bond 15	2.342	2.349	**0.007**	2.342	2.347	**0.005**
Bond 15'	2.324	2.330	**0.006**	2.330	2.334	**0.004**
Bond 16	2.377	2.405	**0.028**	2.373	2.398	**0.025**
Bond 17	2.395	2.399	**0.004**	2.389	2.396	**0.007**
Normal Crystal Side						
Angle 213	97.8	96.6	**-1.2**	96.9	95.3	**-1.6**
Angle 214	134.6	134.1	**-0.5**	136.1	135.3	**-0.8**
Angle 215	99.6	103.8	**4.2**	98.7	103.5	**4.8**
Angle 314	108.0	109.0	**1.0**	107.6	108.8	**1.2**
Angle 315	117.3	114.4	**-2.9**	117.3	114.5	**-2.8**
Angle 415	100.7	99.4	**-1.3**	101.4	99.8	**-1.6**
Stacking Fault Side						
Angle 127	95.4	96.6	**1.2**	93.9	95.5	**1.6**
Angle 126	132.1	134.3	**2.2**	132.8	135.6	**2.8**
Angle 128	107.2	104.2	**-3.0**	107.6	104.1	**-3.5**
Angle 627	109.9	109.2	**-0.7**	109.5	108.9	**-0.6**
Angle 728	114.7	116.1	**1.4**	114.1	115.3	**1.2**
Angle 628	98.3	97.4	**-0.9**	99.4	98.2	**-1.2**

Table 4.1 Change in bonding around the core of one of the 90° partials as a result of moving from a 96 atom *rectangular* to a 64 atom *oblique* unit cell. Different columns are labelled by the technique used to obtain the relaxed core structure and the unit cell used. The bond and angle notation used is as depicted in fig 4.9, where, for example, angle 123 means the angle subtended by atoms 1 and 3 at atom 2. Bond lengths are given in Å.

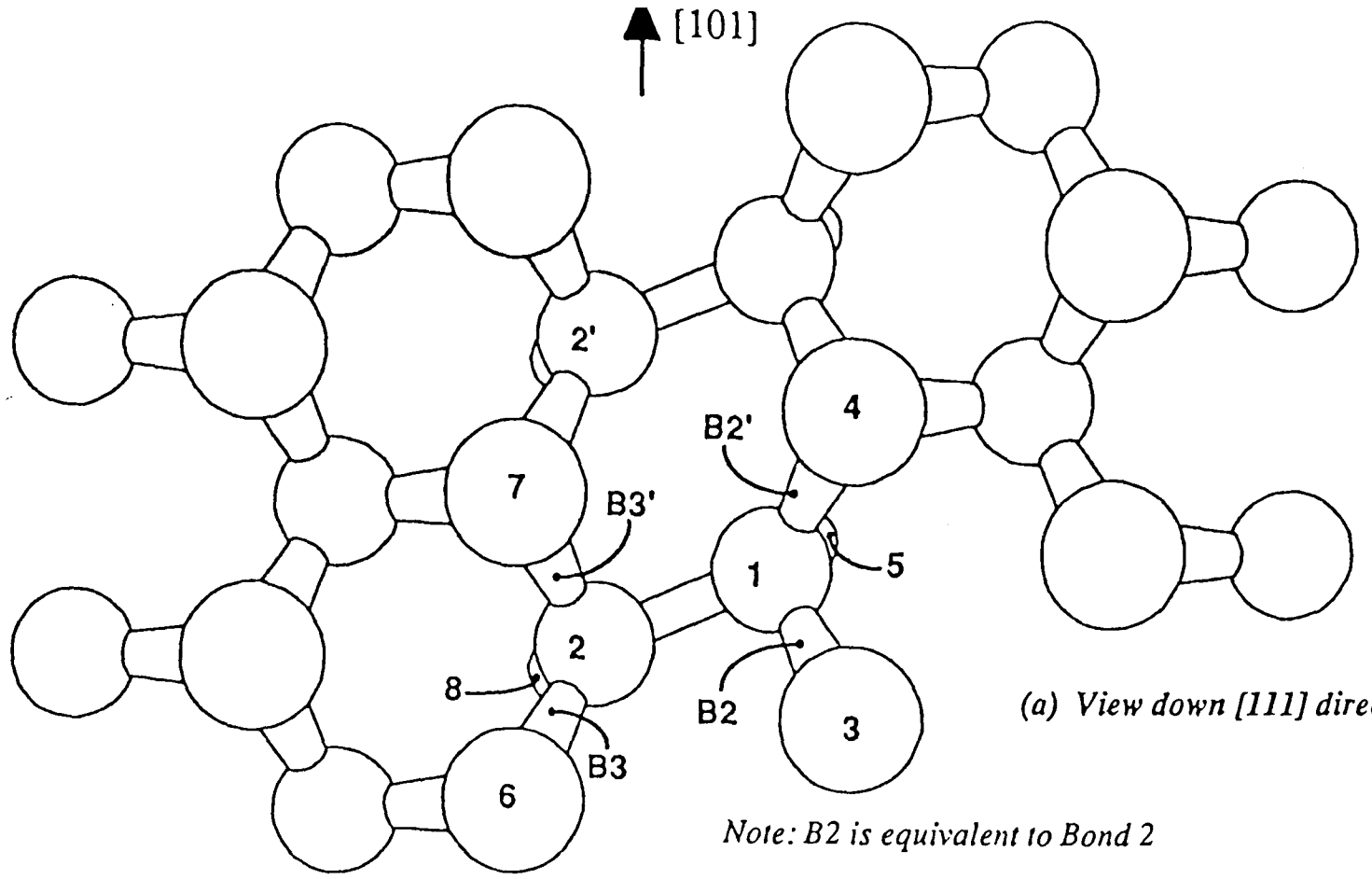

(a) View down [111] direction

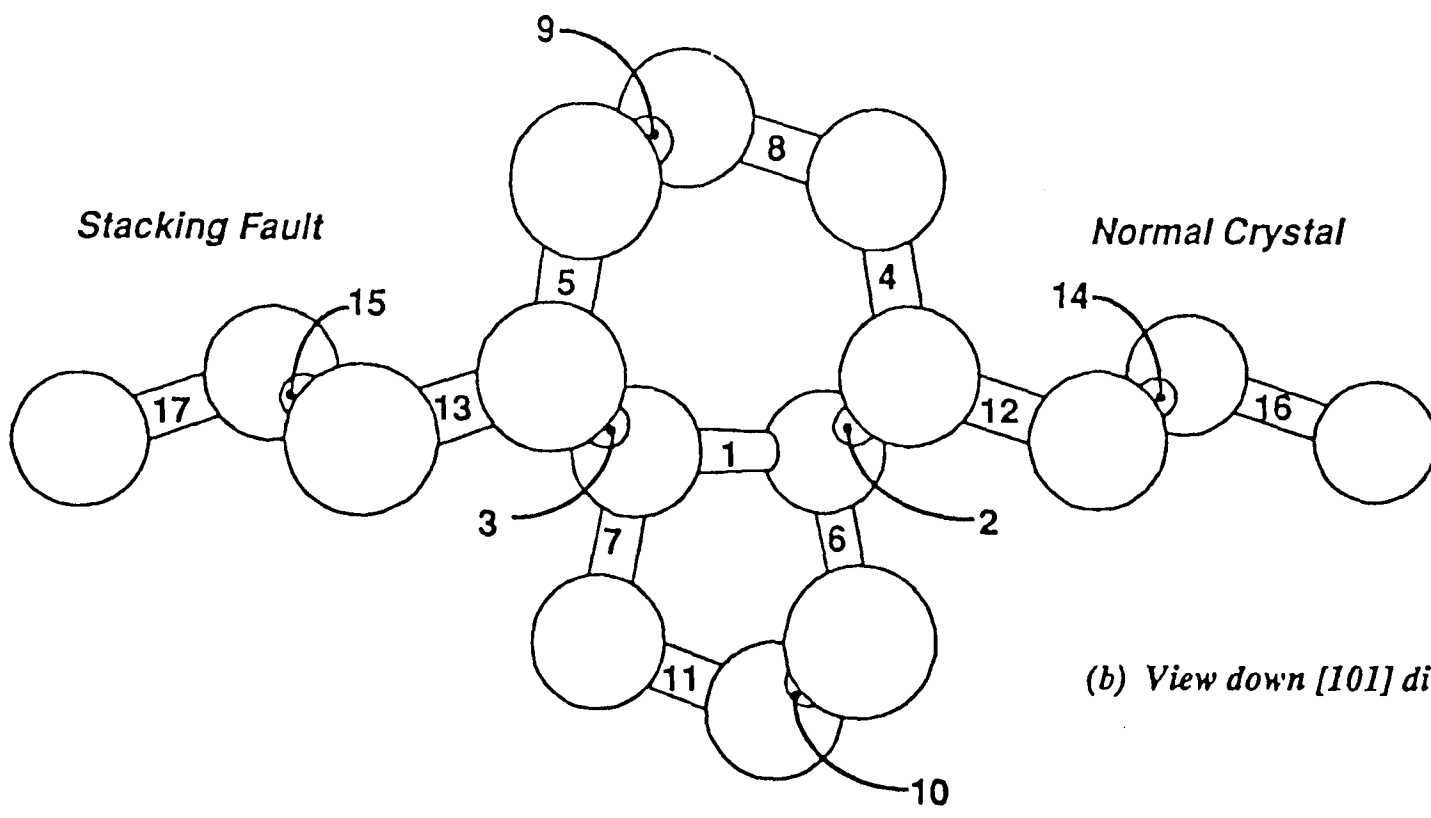

(b) View down [101] direction

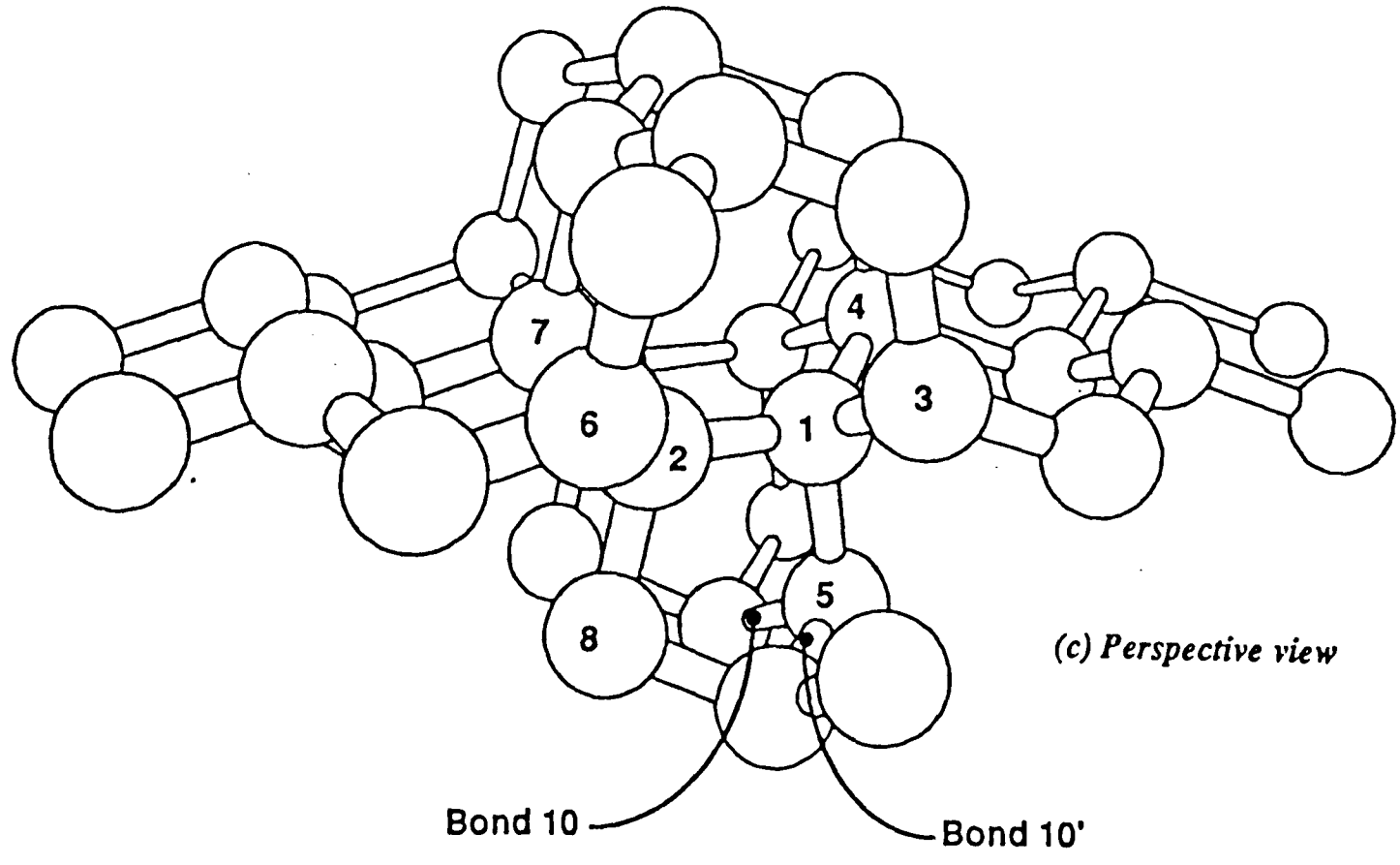

(c) Perspective view

Fig. 4.9 Views of the reconstructed core of the 90° partial dislocation (from M°Innes, 1992).

form. In earlier work they used a right-sided cell (Lodge *et al.*, 1984) which *did* predict a core asymmetry. Secondly, there is no asymmetry in the core for the cluster calculation of an *isolated* 90° partial of Marklund (1980, 1983).

It should be noted that when interactions outside the four-fold first neighbour shell are considered this symmetry is lifted, which is a consequence of the more distant atomic geometry being different on either side of the core due to the presence of the stacking fault. This will be considered in chapter 5. Nonetheless, the boundary mismatch present in the *rectangular* unit cells has been shown to distort the atomic geometry of the core. Within a nearest neighbour model, the *oblique* unit cell produces a core geometry more consistent with an *isolated* dislocation.

4.4.2 Electronic Structure of the 90° partial

Comparison of results for the perfect crystal and various dislocation geometries is achieved by looking at the projected band-structure down the dislocation line direction, $[10\bar{1}]$. The repeat vector along the dislocation line direction is $[10\bar{1}]/2$ which in terms of the cubic lattice parameter a_0 has period $c=a_0/\sqrt{2}$. In both the rectangular and oblique dipole cells k_z is chosen to sample 50 states along the dislocation line in the region $0 < k_z < \pi/c$. The cells used wrap in all three directions which means there will be some dispersion in any general direction of k. Improved sampling of the Brillouin zone is obtained by averaging over the plane perpendicular to k_z. Initial calculations involved a 9 k-point average, corresponding to $q=3$ in the Monkhurst and Pack (1978) scheme, over this plane for each value of k_z. However it became apparent that the difference between setting $q=3$ and $q=1$, where sampling is restricted to the dislocation line only, was negligible[4].

The approach here is to give the results in a sequence analogous to the path taken to initially interpret them. This might seem a little laborious but represents a large section of the

[4] This will be demonstrated in chapter 5, section 5.2.2.

work performed in this thesis and will hopefully guide the reader to a better understanding of the strain effects discussed.

This consequently involves starting with the *rectangular d*ipole unit cell results first and their implications. Band-structures calculated with the Chadi parameter set are presented in fig. 4.10 for both classically, using the modified Lifson Warshell and Tersoff (1988b) potentials, and tight-binding, using the Chadi and GSP Hamiltonians with r_t=3.0Å, relaxed rectangular dipole structures. The solid lines in each case represent the projected bulk band-edges which are obtained by simulations on a perfect repeatable block of diamond cubic for an equivalent k-point sampling. The plots show that for all the geometries a shallow band lies ~0.2eV above the valence band edge in disagreement with the large unit cell results of Marklund (1983) and Lodge *et al.* (1989). This band of states is clearly independent of the relaxation technique employed.

There were three areas of possible discrepancy with the work of Marklund and Lodge *et al.*. A first cause of concern lay in the use of the Chadi Hamiltonian and its weakness at describing even the lowest conduction bands. Marklund had used the tight-binding parameters of Pandey and Phillips (1976) while Lodge *et al.* had used a pseudopotential approach. To improve the band-structures the sp^3s^* Hamiltonian due to Vogl *et al.* (1983) was developed and used. Fig. 4.11 illustrates these results and while it should be noted that there are less states near the conduction band edge there is still a high degree of penetration into the gap off the valence band edge.

A second possible discrepancy lay in the fact that for an isolated 90° partial two equivalent reconstruction modes are possible, which are mirror images of one another. Lodge *et al.* (1989) had chosen to reconstruct in such a way as to preserve the inversion symmetry of the structure, while the other possibility has been used here. Switching the reconstruction sense of one of the partials resulted in negligible changes to the band-structure.

Perhaps a more plausible possibility lay in the fact that the cell used here was a different shape to that used by either Marklund or Lodge *et al.*, though the present work considered

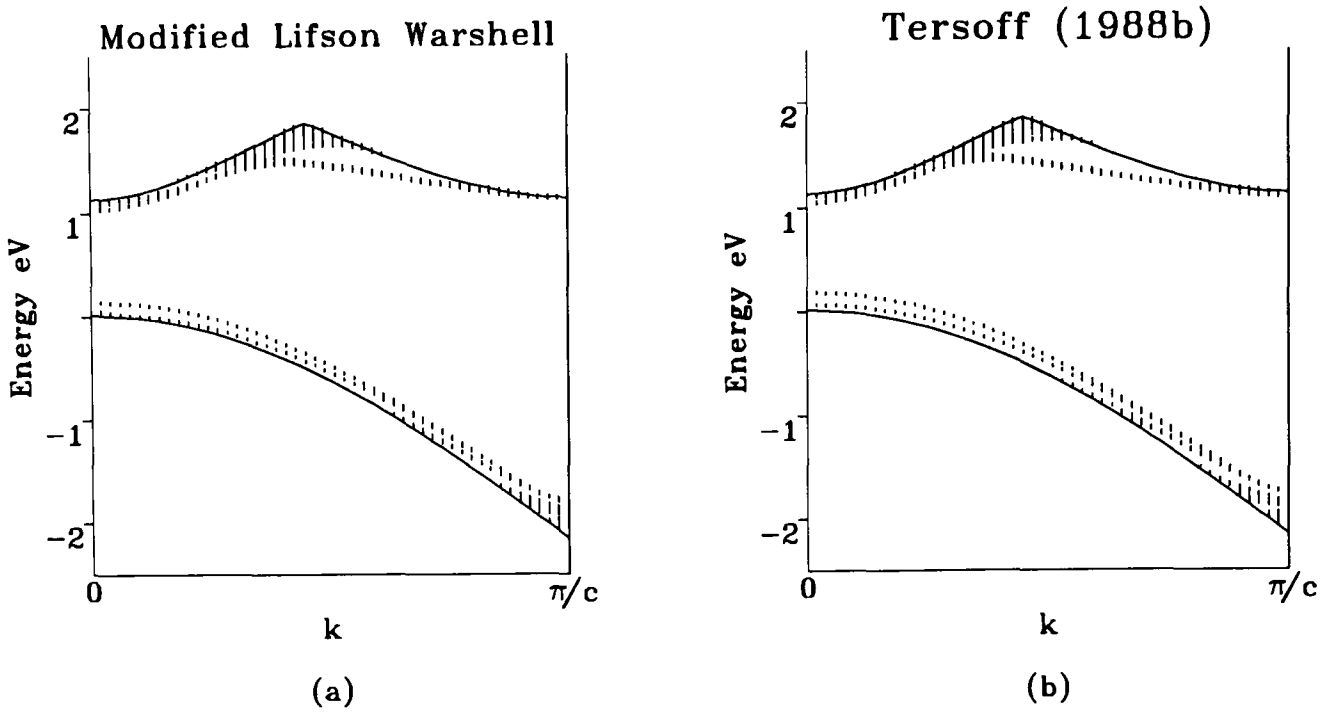

Fig. 4.10 Projected band-structures in eV for the reconstructed 90° partial along the dislocation line. The solid lines show the edges of the bulk valence and conduction bands. $c=a_0/\sqrt{2}$ is the repeat period along the dislocation. The band-structures are calculated using the Chadi Hamiltonian and the rectangular 96 atom unit cell. (a) Modified Lifson Warshell relaxed, (b) Tersoff (1988b) relaxed, (c) Chadi Hamiltonian relaxed, and (d) GSP Hamiltonian relaxed.

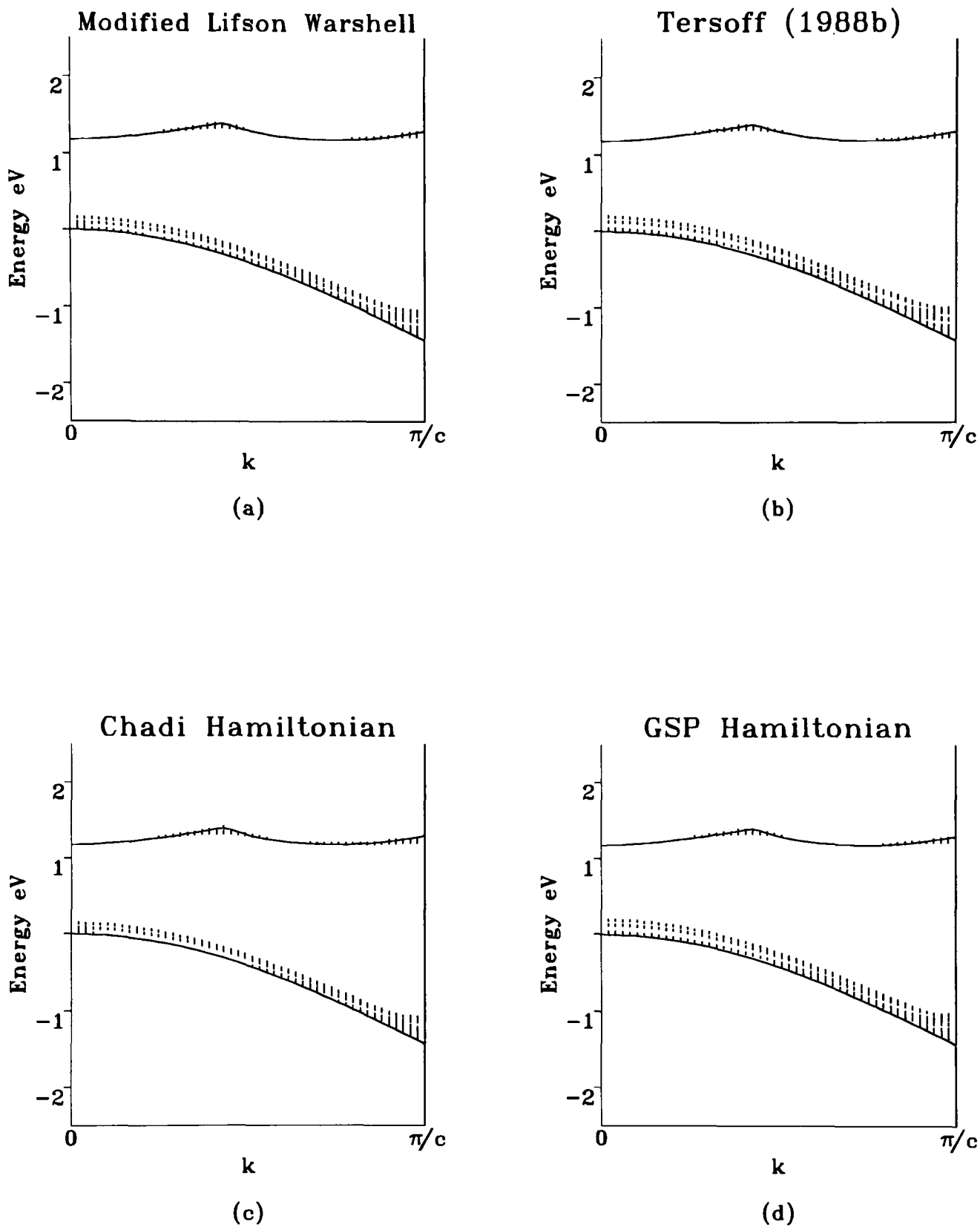

Fig. 4.11 Band-structures calculated using the Vogl Hamiltonian and the rectangular 96 atom unit cell. (a) Modified Lifson Warshell relaxed, (b) Tersoff (1988b) relaxed, (c) Chadi Hamiltonian relaxed, and (d) GSP Hamiltonian relaxed.

a greater number of atoms. Using the information published in their paper the skew unit cell of Lodge *et al.* (1989) was reconstructed. The band-structure for this cell, as calculated using both the Chadi and Vogl Hamiltonians, is shown in fig. 4.12. The essential point is that the indirect band gap is cleared apart from a small curved band above the valence band edge at $k_z=0$ when using Vogl's parameters, a state also obtained by Lodge *et al.*, although they found it deeper, and attributed by them to stacking fault states. Both Chadi's and Vogl's parameters reproduce the shallow tail of states at $k_z=\pi/c$ off both band edges also observed by Lodge *et al.*. The mid-zone states predicted in the tight-binding scheme lie outside the indirect band gap.

These results directly imply that the lack of activity in the indirect band gap obtained by Lodge *et al.* (1989) is related to their atomic geometry and *not* the electronic structure technique used. The key difference, as explained earlier, is that Lodge *et al.* also allowed the unit cell vectors to be variables in the energy minimisation. This technique was motivated by their observation that the unit cell of Chelikowsky and Spence (1984) contained a net shear strain after relaxation which they proposed could affect the band-structure results. This unit cell of Chelikowsky and Spence was reconstructed from their tabulated coordinates to investigate the consequence of this strain.

In agreement with the results of Chelikowsky and Spence, who had used a pseudopotential approach, a band of states that penetrated some 0.3eV into the gap above the valence band edge was found (fig. 4.13). States below the conduction band were also obtained, although they penetrated much less significantly than the findings of Chelikowsky and Spence. This difference is most probably related to the comments by Lodge *et al.* (1989) on the problems associated with the band-structure of Chelikowsky and Spence. Notably, an error in the d-orbital approximation of Louie (1980) was present in their work, which was later corrected by Lodge (1986).

These results clearly indicate that there is a net strain present in *rectangular* dipole unit cells. By allowing their unit cell to change shape Lodge *et al.* (1989) relieved this strain but,

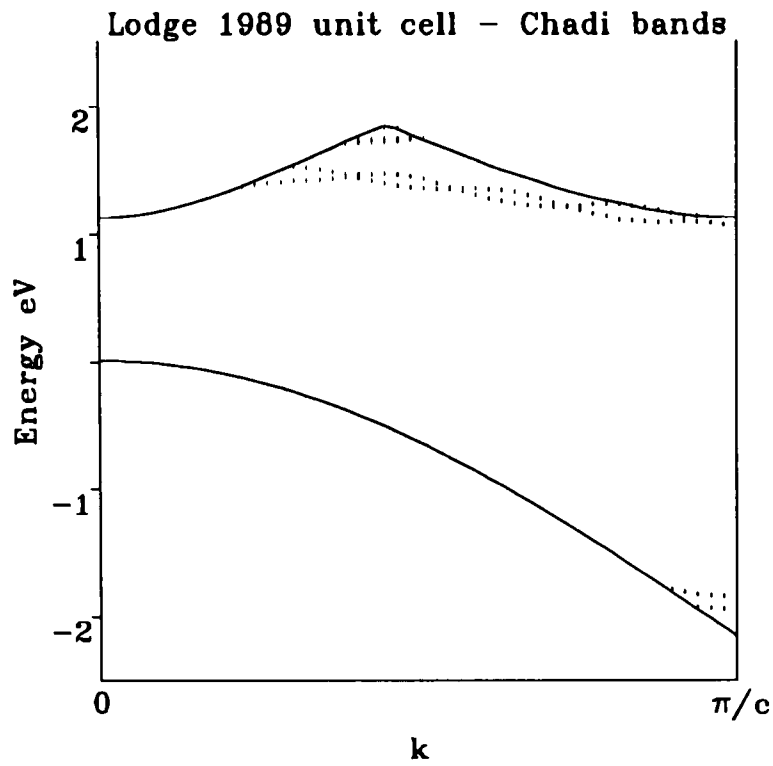

(a)

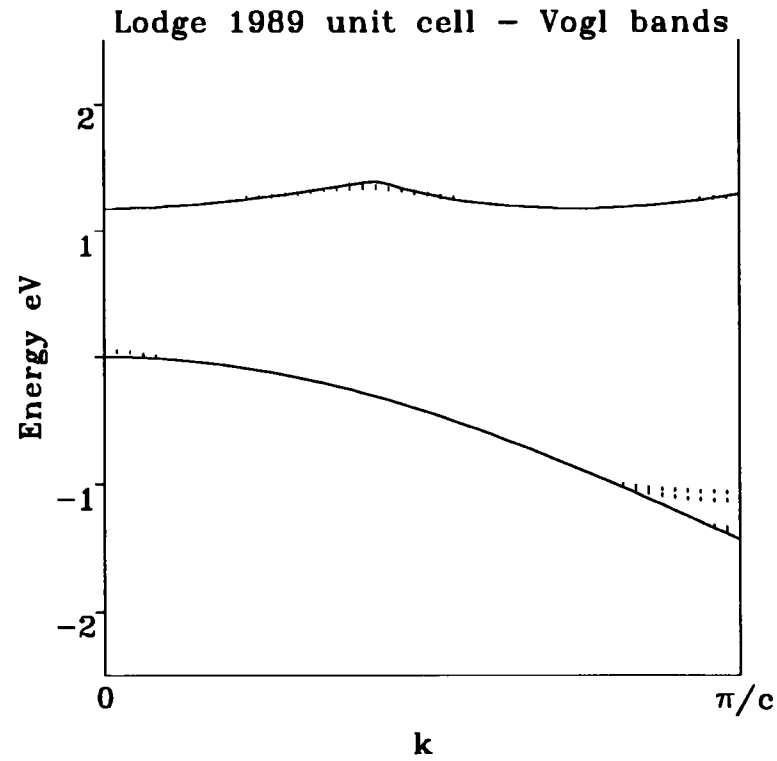

(b)

Fig. 4.12 Band-structures calculated using the 64 atom unit cell of Lodge *et al.* (1989). (a) using the Chadi Hamiltonian, and (b) using the Vogl Hamiltonian.

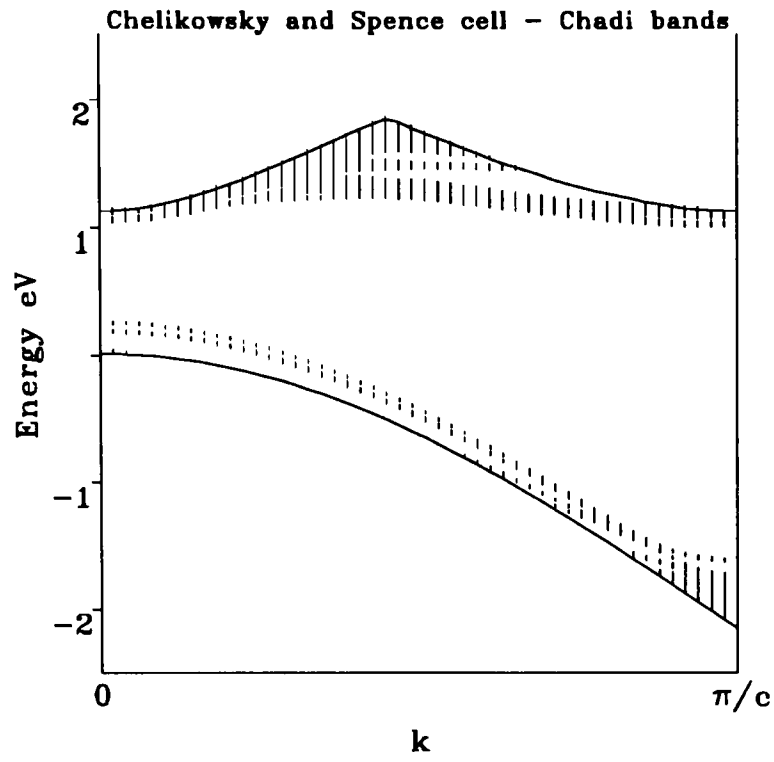

Fig. 4.13 Band-structures calculated on the 48 atom unit cell of Chelikowsky and Spence (1984). (a) using the Chadi Hamiltonian, and (b) using the Vogl Hamiltonian.

as discussed in section 4.2, the system that results is physically incorrect. Despite this, removal of this strain has been shown to have significant consequences to the band-structure.

It can be seen from fig. 4.2 that the length of the unit cell in the $<111>$ direction dictates the degree of boundary mismatch imposed and presumably therefore the amount of artificial strain introduced to the geometry. Analysis of this picture indicates that a unit cell with a height that is a multiple of the diamond cubic repeat period in this direction, 3 {1 1 1} planes, will have a similar boundary mismatch. All our cells and that due to Chelikowsky and Spence had this property. The unit cells of Marklund and Lodge, however, had non-diamond cubic repeat heights of 5 and 4 {1 1 1} planes respectively. It seemed instructive to analyse the electronic effects for *rectangular* cells of this shape.

Fig. 4.14a illustrates the band-structure for a 64 atom cell relaxed using the Tersoff (1988b) potential. The important feature is the disappearance of states for values of $k_z > \pi/(2c)$ not obtained with the 96 atom unit cell considered above. As a note, this result differs significantly from the band-structure obtained by Lodge *et al.* (1984) who used the same sized unit cell constructed from a cluster containing a dislocation dipole. Using the Extended Hückel Theory (EHT) they found the valence band edge clear but the empty upper dislocation band of states filling a major part of the gap. It seems there could be a problem in the vertical placement of these bands - Wang and Teichler (1989), looking at the bound states due to the unreconstructed core, also identified this discrepancy with the EHT work of Lodge *et al.* (1984).

Marklund (1983) reported no states within the indirect band gap using an 80 atom unit cell. Again the Tersoff (1988b) potential is used to obtain a relaxed structure for an equivalent cell. It can be seen from fig. 4.14b that the strain related states have become highly localised around $k_z=0$. It seems that choosing a non-diamond cubic repeat period height for a *rectangular* unit cell, as in the 64 and 80 atom cases, introduces *less* stress/strain to the geometry.

These band-structures, although markedly improved for this 80 atom cell, still contains

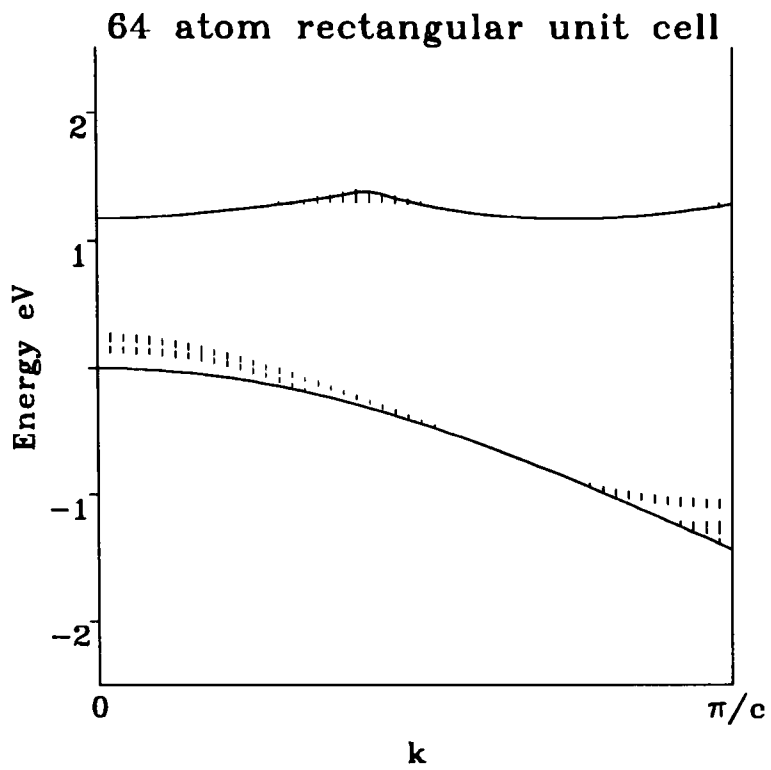

Fig. 4.14 Band-structures calculated using the Vogl Hamiltonian and unit cells relaxed with the Tersoff (1988b) potential. (a) 64 atom rectangular unit cell, and (b) 80 atom rectangular unit cell.

states within the indirect band gap, not found by Marklund (1983). However, Marklund had used a tight-binding scheme with a different Hamiltonian, that due to Pandey and Phillips (1976) which includes both first and second neighbour interactions. This parameterisation was also considered and the band gap was found to be broadly cleared. The band-structures obtained with β set to 0.5 and r_c to 3.84Å and 3.96Å are given in fig. 4.15. Only shallow states centred at k_z=0 are found above the valence band edge, but the starting conditions and the form of relaxation is quite different in our case compared to the approach of Marklund. The conclusion is that the Marklund (1983) result is not in disagreement with the results presented here and is a consequence of the particular choice of boundary conditions and parameterisation.

So to summarise, it has been shown that the incorrect boundary conditions associated with the *rectangular* dipole geometry give rise to bands of states located above the valence band edge, as suggested by Lodge *et al.* (1989). The degree of mismatch at the $<1\,1\,1>$ boundary dictates the amount of strain imposed and the depth of penetration of these states.

For the *oblique* dipole geometry this strain has been eliminated and the 64 atom oblique unit cell described in section 4.4 is used here. As before with the *rectangular* unit cells several classically and tight-binding relaxed structures were obtained. Using both the Chadi, fig. 4.16, and Vogl, fig. 4.17, Hamiltonians band-structures are found to contain only shallow states at $k_z=\pi/c$ and around k_z=0 remaining above the valence band edge. The depth of these states is now dependent on the particular structure analysed. No broad band of states is observed.

4.4.3 The 30° partial

A similar investigation into the effects on the band-structure has been started for the 30° partial. It was shown in chapter 1, section 1.2, that the periodicity down the dislocation line doubles when the 30° partial reconstructs and as such the unit cells used here must contain two periods in this direction. This leads to a rectangular unit cell of 192 atoms containing a dislocation *dipole*, rather than 96, and for comparison a *quadrupole* unit cell containing 256

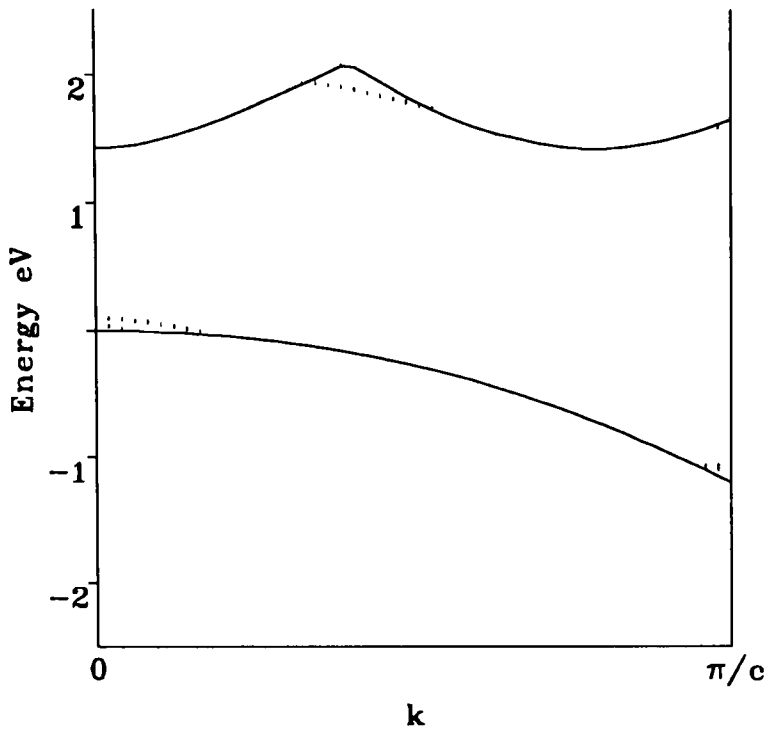

Fig. 4.15 Band-structures calculated using the Pandey and Phillips Hamiltonian and an 80 atom rectangular unit cell relaxed with the Tersoff (1988b) potential. (a) β=0.5 and r_c=3.84Å (b) β=0.5 and r_c=3.96Å.

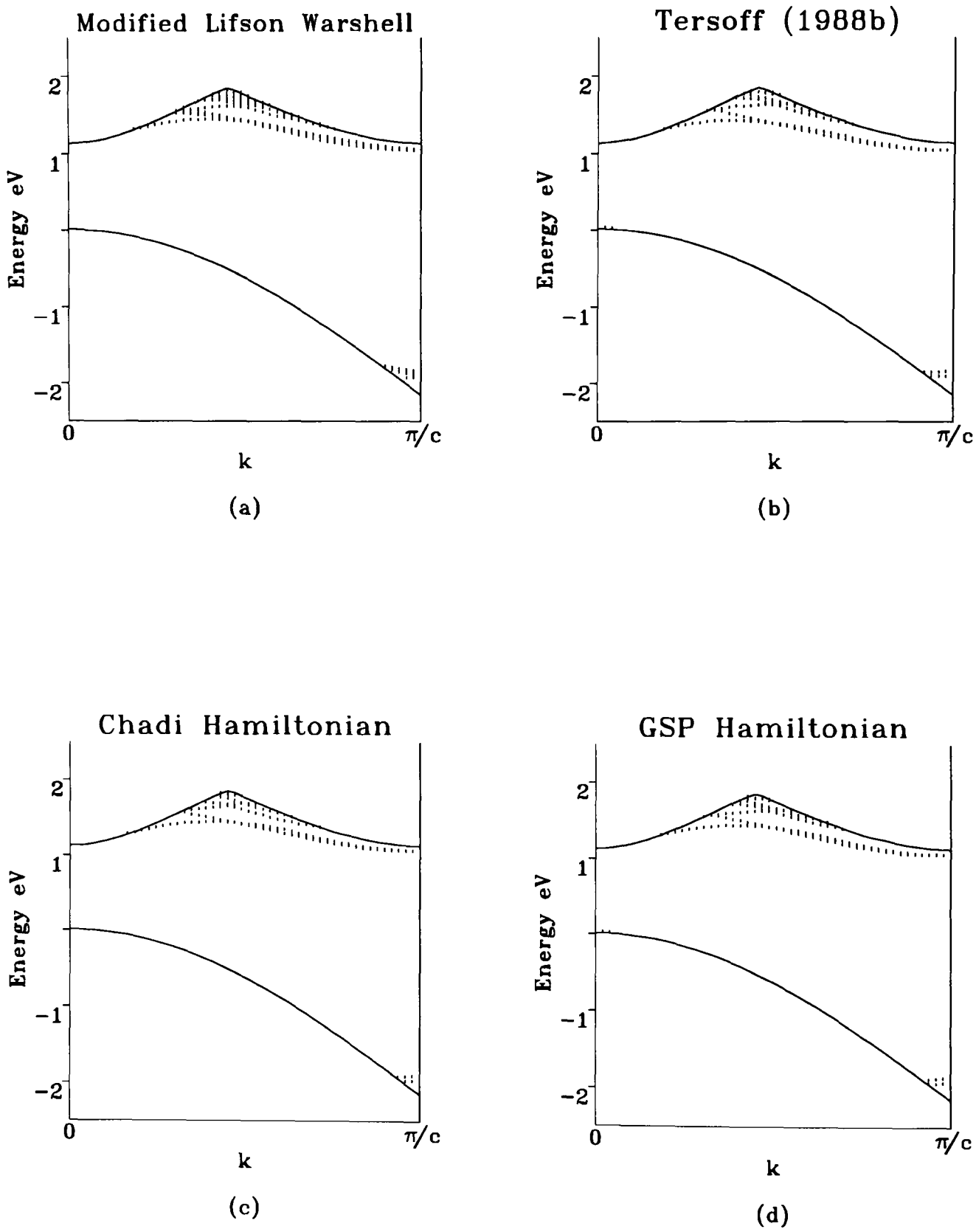

Fig. 4.16 Band-structures calculated using the Chadi Hamiltonian and the oblique 64 atom unit cell. (a) Modified Lifson Warshell relaxed, (b) Tersoff (1988b) relaxed, (c) Chadi Hamiltonian relaxed, and (d) GSP Hamiltonian relaxed.

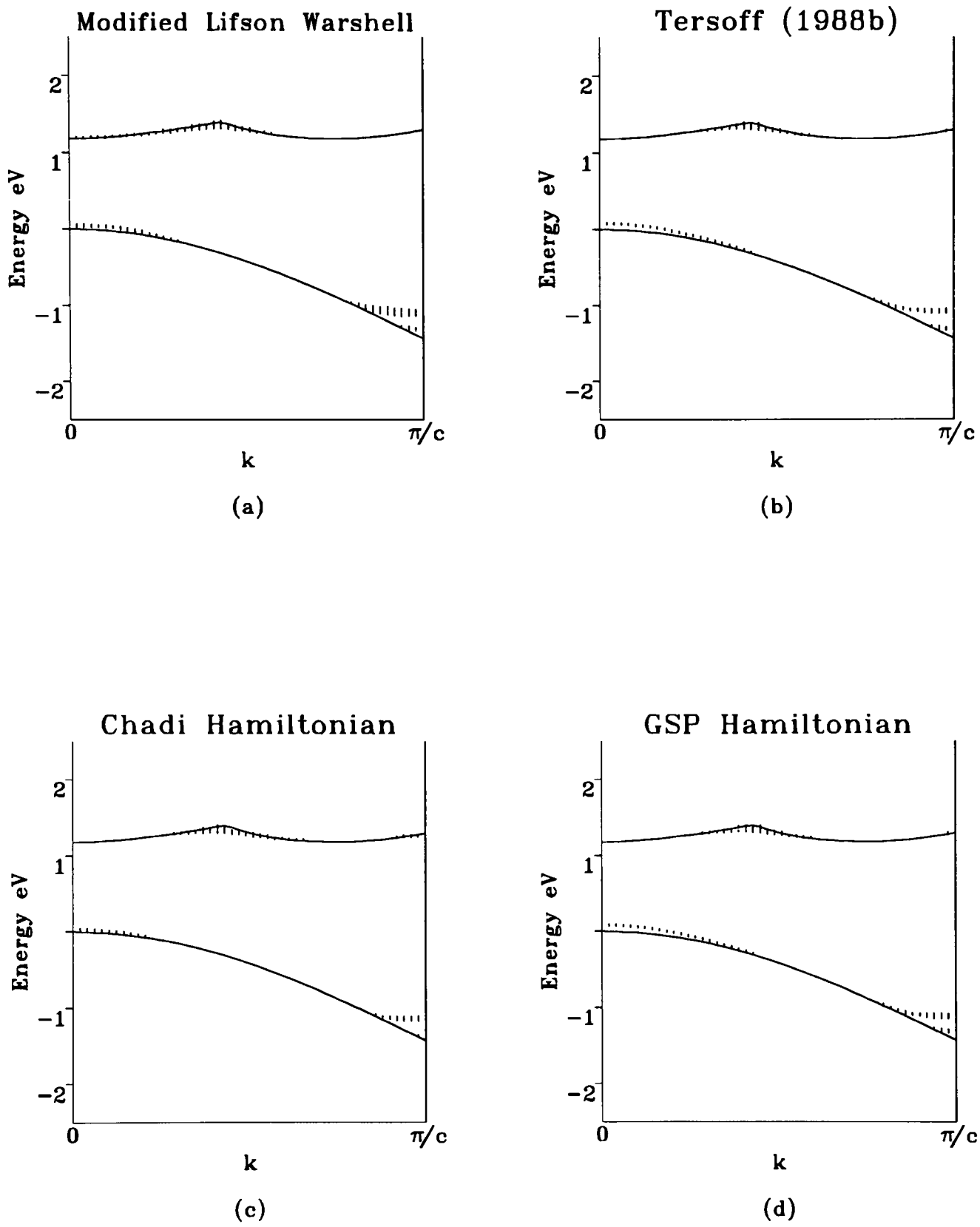

Fig. 4.17 Band-structures calculated using the Vogl Hamiltonian and the oblique 64 atom unit cell. (a) Modified Lifson Warshell relaxed, (b) Tersoff (1988b) relaxed, (c) Chadi Hamiltonian relaxed, and (d) GSP Hamiltonian relaxed.

atoms with box vectors, $2[1\bar{2}1]$, $8/3[\bar{1}\bar{1}\bar{1}]$ and $[10\bar{1}]$. These two unit cells are shown in fig. 4.18. A unit cell of 256 atoms represents the limit for tight-binding relaxations and band-structures of the current computing power at Oxford. Results given here, and in chapter 6, for the 30° partial have been obtained by working on both the Stardent Series GS2000 machine and the University Convex.

The dispersion of the bands for the 90° partial is easily obtained since upon reconstruction there is no change in periodicity down the dislocation line. As discussed earlier, the repeat vector along the dislocation line direction is $[10\bar{1}]/2$ which has period $c=a_0/\sqrt{2}$. By using a unit cell with only one repeat period in this direction and sampling states in the region $0 < k_z < \pi/c$ allows the one dimensional bands to be obtained. However the reconstructed 30° partial requires a unit cell length of $2c$ along the dislocation direction. The doubling of the unit cell length implies twice as many atoms and consequently double the number of bands at each k-point. It also implies the shrinking of the Brillouin zone to half its original length in this direction, and thus sampling now occurs in the region $0 < k_z < \pi/2c$. All information contained for $\pi/2c < k_z < \pi/c$ is *folded* back into the reduced region. For this reason, Chelikowsky (1982) chose to calculate the LDOS to investigate the existence of states within the gap for his periodic unit cell containing a reconstructed 30° partial dipole. However, it is possible to still consider the band-structure approach since the act of *folding* does not affect the energy of the bands. The band-structure obtained will provide no information on the dispersion of the states but will indicate immediately the existence of any states within the *indirect* band-gap. The edges of the *folded* bulk valence and conduction bands are obtained by calculating the band-structure for a unit cell of perfect diamond cubic Si containing two periods in the $[10\bar{1}]$ direction.

Relaxed configurations have been obtained for both the 192 and 256 atom unit cells using the Stillinger Weber and Tersoff (1988b) classical potentials and the tight-binding scheme with the Chadi Hamiltonian. For each of these relaxation techniques, the atomic structure at the

Fig. 4.18a 192 atom rectangular unit cell containing a 30° partial dislocation *dipole*.

Fig. 4.18b 256 atom rectangular unit cell containing a 30° partial dislocation *quadrupole*.

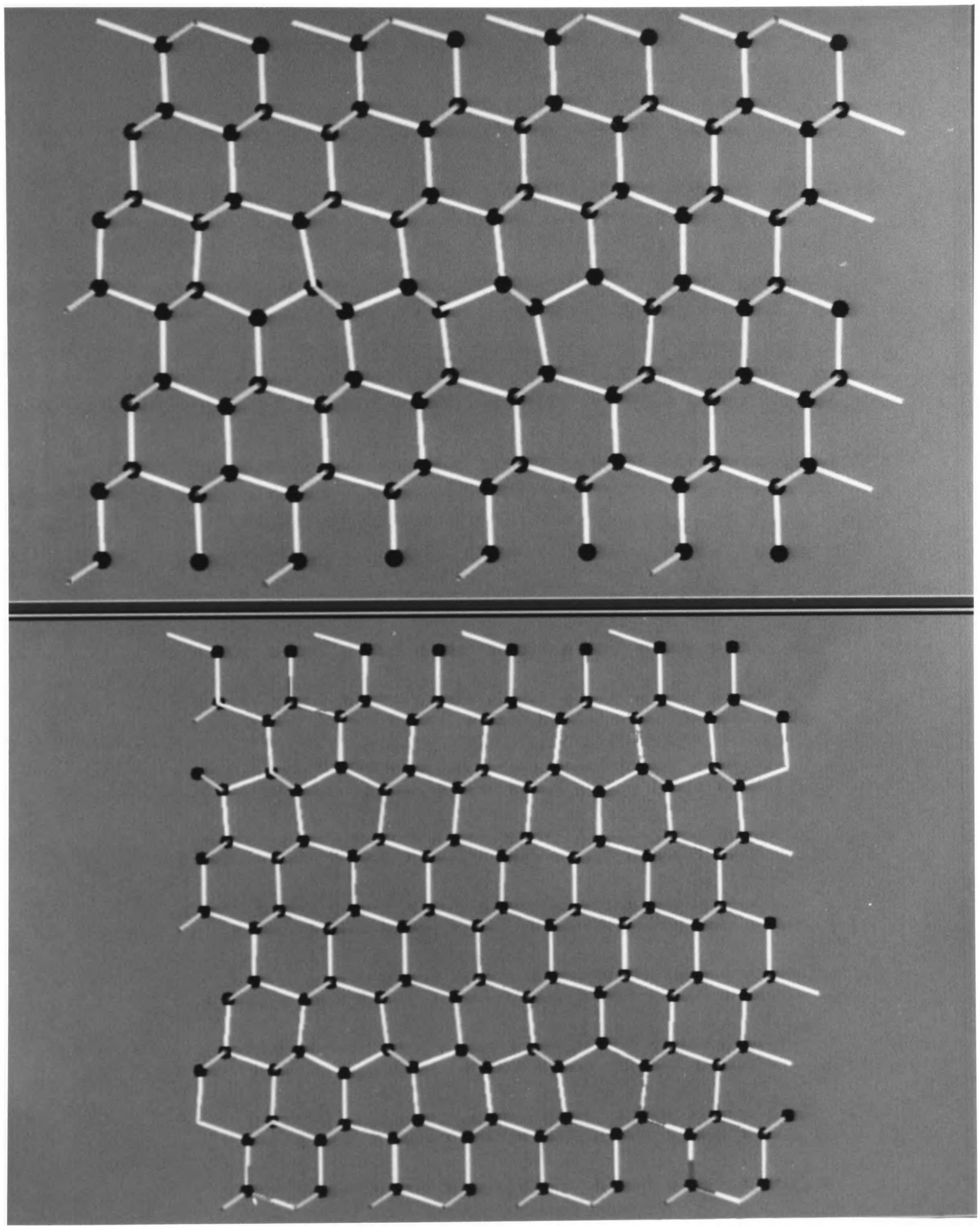

Fig. 4.18a 192 atom rectangular unit cell containing a 30° partial dislocation *dipole*.

Fig. 4.18b 256 atom rectangular unit cell containing a 30° partial dislocation *quadrupole*.

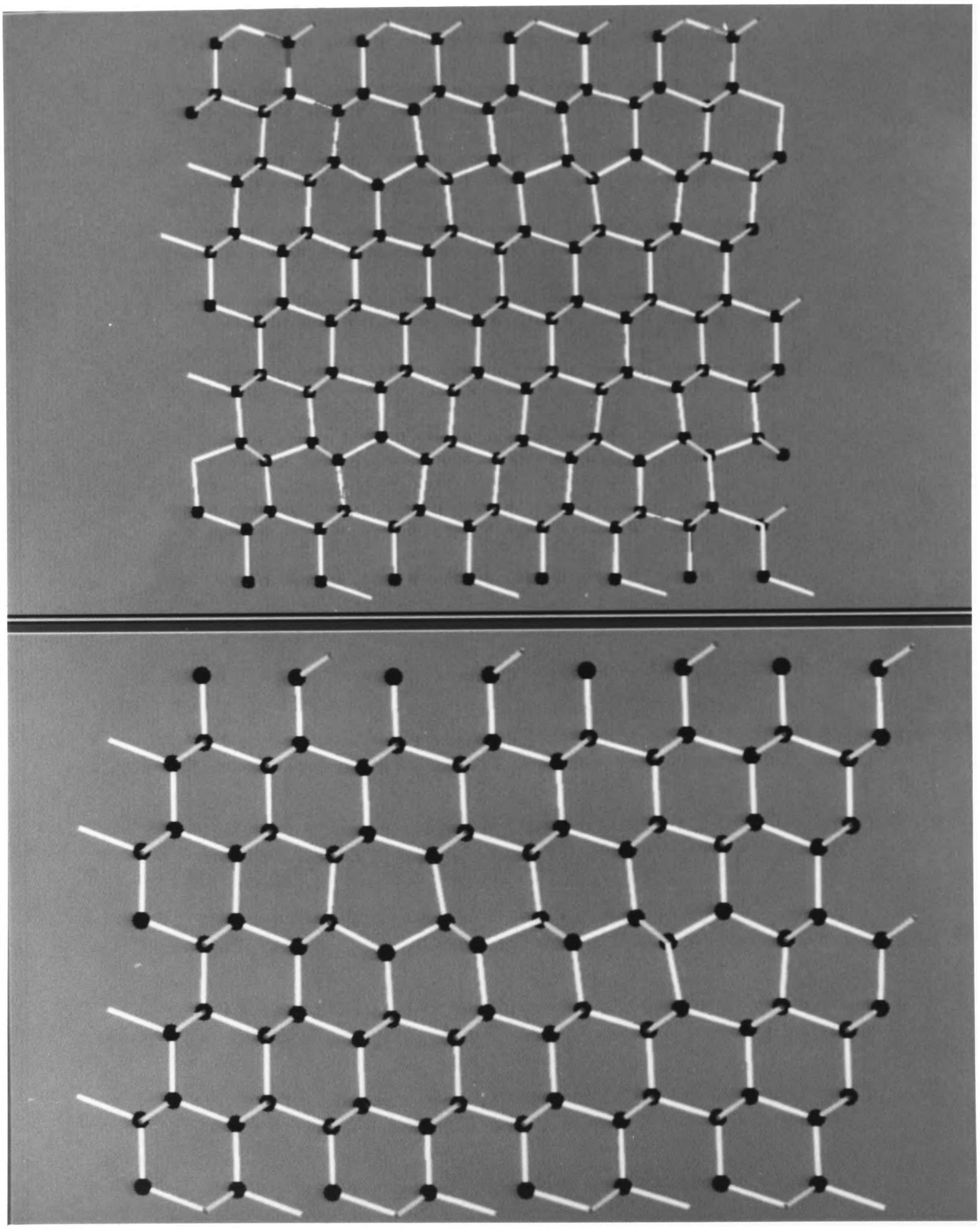

core is found to be similar in both unit cells, which indicates that the boundary mismatch present in the 192 atom *dipole* unit cell does not affect the core as significantly as found with the 90° partial. There are slight differences however, most notably a consistent 1° *less* bond angle distortion around the core found in the 256 atom *quadrupole* relaxed unit cells.

The band-structures indicate a greater consequence of the boundary error present in the 192 atom unit cell. It can be seen from fig. 4.19 that all three relaxation techniques predict a similar band-structure for this unit cell containing a 30° dislocation *dipole*. Specifically, a band of states located above the valence band edge is consistently found, which is a similar finding to that obtained with the 96 atom unit cell containing a 90° dislocation dipole.

The band-structure results for the 256 atom *quadrupole* unit cell are illustrated in fig. 4.20, for the three different relaxation methods. In comparing these band-structures to those of fig. 4.19 it can be seen that the band of states above the valence band edge has effectively disappeared.

In conclusion, a similar electronic structure result has been found for the 30° partial as was obtained for the 90° partial. The boundary mismatch present in the *dipole*, 192 atom, unit cell gives rise to a band of states above the valence band edge. By analogy with the 90° partial work, these states result from an artificial strain imposed on the system due to this boundary error. Using a quadrupolar geometry which eliminates this problem, the electronic structure of the reconstructed 30° partial gives rise to an essentially clear indirect band-gap.

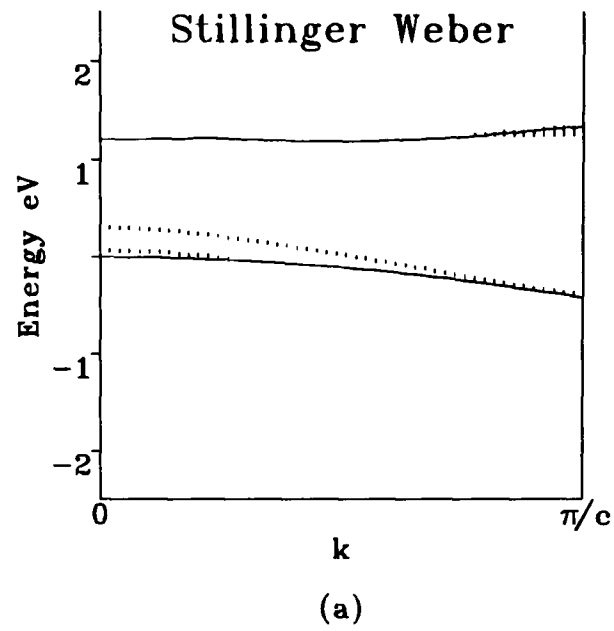

(a)

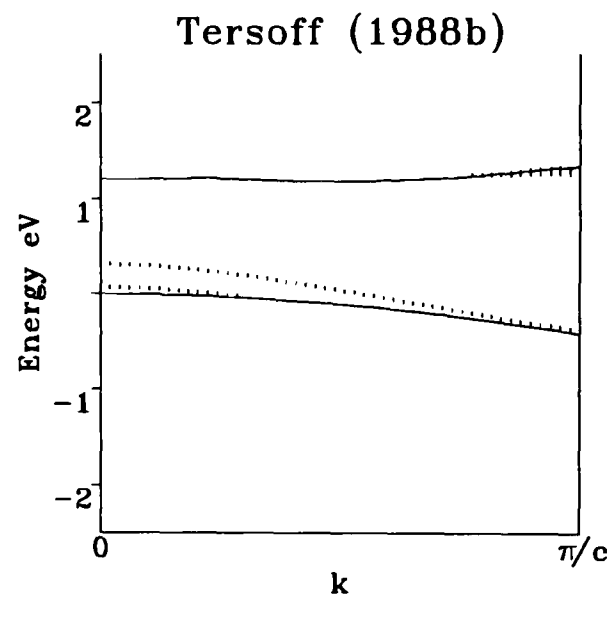

(b)

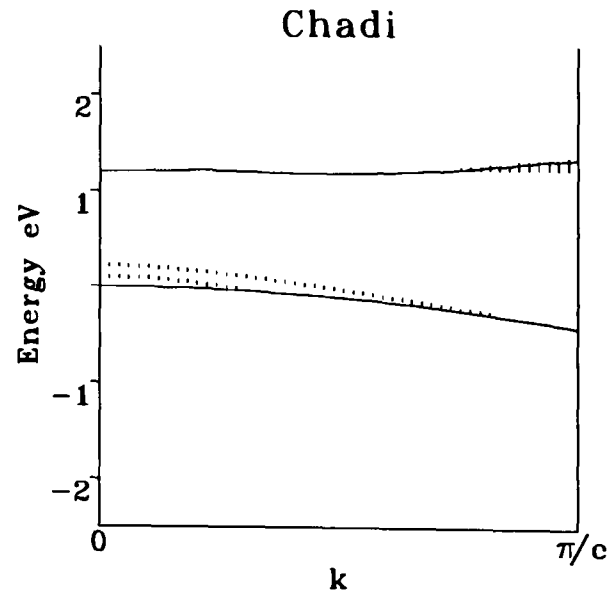

(c)

Fig. 4.19 Band-structures calculated using the Vogl Hamiltonian and the 192 atom unit cell containing a 30° dislocation *dipole*. (a) Stillinger Weber relaxed, (b) Tersoff (1988b) relaxed, and (c) Chadi Hamiltonian relaxed.

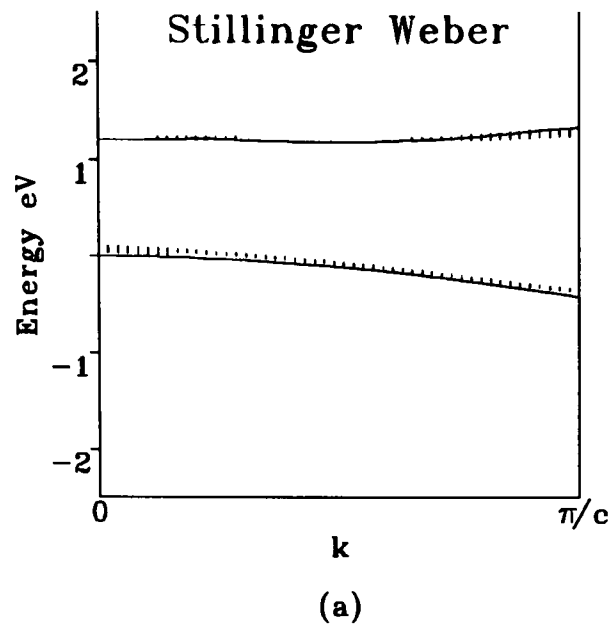

(a)

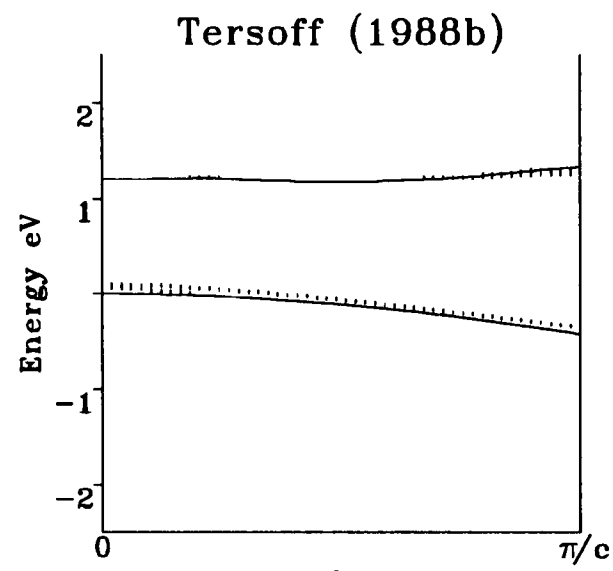

(b)

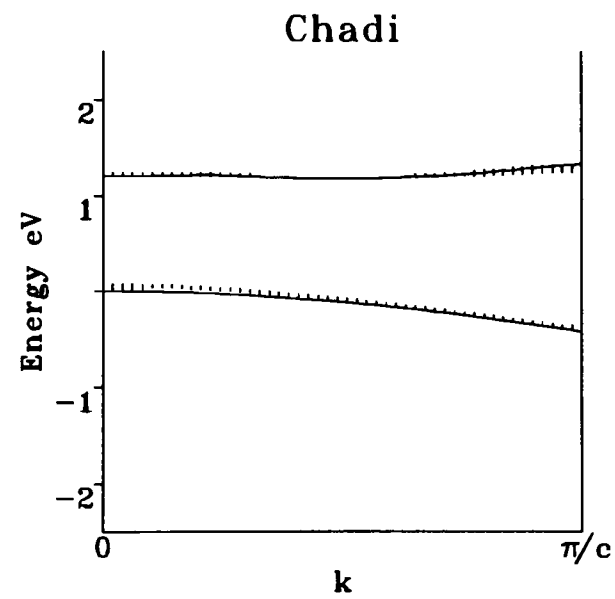

(c)

Fig. 4.20 Band-structures calculated using the Vogl Hamiltonian and the 256 atom unit cell containing a 30° dislocation *quadrupole*. (a) Stillinger Weber relaxed, (b) Tersoff (1988b) relaxed, and (c) Chadi Hamiltonian relaxed.

CHAPTER 5

The clean reconstructed 90° partial

5.1 Introduction

In chapter 4 the consequences of incorrectly treating the periodic boundary conditions were investigated. This demonstrated that a band of states associated with the *rectangular dipole* cells essentially disappears when using a rectangular unit cell containing a *quadrupole*, or in the case of the 90° partial, an equivalent *oblique dipole* unit cell. The indirect band-gap is clear except for the possibility of very shallow states. All simulations described here are for *oblique* dipole unit cells only.

In this chapter a detailed analysis of the bonding present in the core of a 90° partial is undertaken. Specifically, the recent results of Duesbery *et al.* (1991) and Marklund and Wang (1992) are addressed which both contradict the conclusions from earlier work.

5.2 Reliability of the results

To provide some confidence in the results that will be obtained here it is necessary to justify the conditions used to generate them. In chapter 3 the various interatomic force

prescriptions that have been used were described together with the tight-binding Hamiltonians used in band-structure calculations. There is no reliance on one particular method at any stage and comparison of the predictions of similar schemes should provide a better understanding and more reliable proposals for the atomic and electronic structure of the 90° partial. There are however two aspects to the problem that need further justification; the choice of the unit cell and the convergence of the k-point sampling.

5.2.1 Block size effects

As discussed earlier, the major disadvantage of the 3D unit cell technique is the need to consider 2, or even 4, partials in the unit cell. There will exist some interaction between the partials and this is investigated here. Five different unit cell sizes have been considered, ranging from 32 to 224 atoms. All these oblique dipole unit cells are created in the same way from their corresponding quadrupole unit cell which contains twice as many atoms. This has been described in detail in chapter 4 but is mentioned here for reference. For a rectangular quadrupole unit cell with box vectors $\underline{X}$, $\underline{Y}$ and $\underline{Z}$, taken here along the $[1\bar{2}1]$, $[\bar{1}\bar{1}\bar{1}]$ and $[10\bar{1}]$ directions respectively, the oblique dipole unit cell has box vectors $\underline{X}$, $(\underline{Y}+\underline{X}+\underline{z}')/2$ and $\underline{Z}$, where $\underline{z}' = [10\bar{1}]/2$. Similar size effects have been obtained with all the classical schemes and the Tersoff (1988b) potential has been chosen to describe these results.

Table 5.1 illustrates the atomic structure dependence on box size. The bonds and bond angles referred to are as depicted in chapter 4, fig. 4.9.

The 32 atom cell has a partial separation of just one repeat vector in the $\underline{X}$ direction, $\underline{x}=[1\bar{2}1]/2$. Its result is deliberately sectioned off since table 5.1 illustrates that it is significantly different to all the larger cells, indicating this partial separation is too small. Comparison of the 32 atom unit cell core structure to that of the others shows that the core is more compressed and the bond angles less distorted as a result. This is consistent with the fact that each core is unable to "breathe" due to the close proximity of the other.

Bond	**64 Atom Unit Cell**	**112 Atom Unit Cell**	**128 Atom Unit Cell**	**224 Atom Unit Cell**	**32 Atom Unit Cell**
Bond 1	2.458 (4.5)	2.453 (4.3)	2.464 (4.8)	2.459 (4.6)	2.431 (3.4)
Bond 2	2.320 (-1.4)	2.323 (-1.2)	2.320 (-1.4)	2.322 (-1.2)	2.327 (-1.0)
Bond 2'	2.403 (2.2)	2.403 (2.2)	2.404 (2.2)	2.405 (2.3)	2.391 (1.7)
Bond 3	2.399 (2.0)	2.401 (2.1)	2.401 (2.1)	2.402 (2.1)	2.390 (1.6)
Bond 3'	2.320 (-1.4)	2.321 (-1.3)	2.319 (-1.4)	2.320 (-1.3)	2.328 (-1.0)
Bond 6	2.352 (0.0)	2.356 (0.2)	2.350 (-0.1)	2.354 (0.1)	2.360 (0.4)
Bond 7	2.353 (0.0)	2.353 (0.0)	2.350 (-0.1)	2.351 (0.0)	2.360 (0.4)
Normal Crystal Side					
Angle 213	95.3	95.5	94.2	94.3	98.7
Angle 214	135.3	134.7	136.3	135.6	131.7
Angle 215	103.5	103.5	103.0	103.1	104.3
Angle 314	108.8	108.7	108.8	108.7	109.0
Angle 315	114.5	115.2	114.7	115.2	115.8
Angle 415	99.8	100.0	100.4	100.6	98.2
Stacking Fault Side					
Angle 127	95.5	95.7	94.3	94.6	98.9
Angle 126	135.6	135.0	136.5	136.0	132.1
Angle 128	104.1	103.5	103.3	103.1	104.5
Angle 627	108.9	108.8	108.9	108.8	109.0
Angle 728	115.3	115.3	115.3	115.4	116.4
Angle 628	98.2	99.1	99.2	99.7	97.0

Table 5.1 Local bonding around the reconstructed bond 1 for 5 *oblique* unit cells of different size and shape. All core structures have been obtained using the Tersoff (1988b) potential. The bond and angle notation used is as depicted in chapter 4, fig 4.9, where, for example, angle 123 means the angle subtended by atoms 1 and 3 at atom 2. The bond lengths are given in Å and the percentage distortions from the perfect Si bond length (2.3517Å) are in brackets.

The difference between the structures obtained with a partial separation of $2\underline{x}$, as in the 64 atom cell, and $4\underline{x}$, as in the 128 atom cell, is negligible and indicates that $2\underline{x}$ is a suitable minimum separation of the partials (this was as used by Marklund, 1983; Lodge *et al.*, 1984; Chelikowsky and Spence, 1984). The 112 atom cell has a partial separation of $2\underline{x}$ but contains 3 extra (1 1 1) planes increasing the partial separation in the $\underline{Y}$ direction. The changes to the core structure remain small, as they do for the 224 atom block where the partial separation is $2\sqrt{6}a_0$ (26.6Å) in the $[1\bar{2}1]$ and $7a_0/\sqrt{3}$ (21.9Å) in the $[\bar{1}\bar{1}\bar{1}]$ directions respectively.

These results indicate that the atomic structure results predicted using the 64 atom *oblique* unit cell are reliable.

The problem of interaction between the partials and its effect on the placement of the dislocation bands is well known (see Northrup *et al.*, 1981; Chelikowsky and Spence, 1984). A similar block size analysis is performed using the same 32, 64, 112, 128 and 224 atom oblique unit cells all relaxed with the Tersoff (1988b) potential.

Fig. 5.1 shows the band-structure of all five unit cells obtained using the Vogl Hamiltonian. In agreement with the atomic structure results it can be seen that a partial separation of just $\underline{x}$, as in the 32 atom cell, produces a significantly different band-structure to all the other cells. In fact fig. 5.1 illustrates that the 32 atom cell has cleared all states from the indirect band gap and this is because the partials are so strongly coupled that the bonding and anti-bonding dislocation states are split unphysically.

There is negligible difference in the band-structures obtained for the 64 atom cell, with a separation of $2\underline{x}$, and the 128 atom cell with a separation of $4\underline{x}$. This implies that the electronic structure, like the atomic result, is well represented for a minimum partial separation of $2\underline{x}$. The 112 atom cell which is longer in the $[\bar{1}\,\bar{1}\,1]$ direction shows slightly less penetration of states above the valence band edge. This implies that it is important to ensure the partials are well separated in both the $[1\,\bar{2}\,1]$ and $[\bar{1}\,\bar{1}\,1]$ directions for the band-structure, a feature not considered in earlier work (Marklund, 1983; Lodge *et al.*, 1984; Chelikowsky and Spence, 1984). The 224 atom cell actually leads to the greatest penetration of states since the partials are well separated in both the $[1\,\bar{2}\,1]$ and $[\bar{1}\,\bar{1}\,1]$ directions and hence the coupling has been significantly reduced compared to all the other unit cells. However, comparison of the 64 and 224 atom band-structures illustrates this effect is small.

The conclusion from this work is that a reliable prediction for both the atomic and electronic structure of the 90° partial is provided by the 64 atom oblique unit cell. This is used exclusively to obtain results in the rest of this thesis.

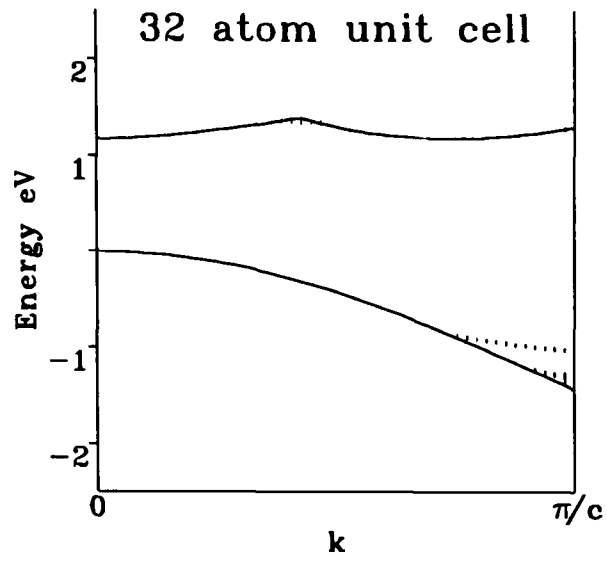

(a)

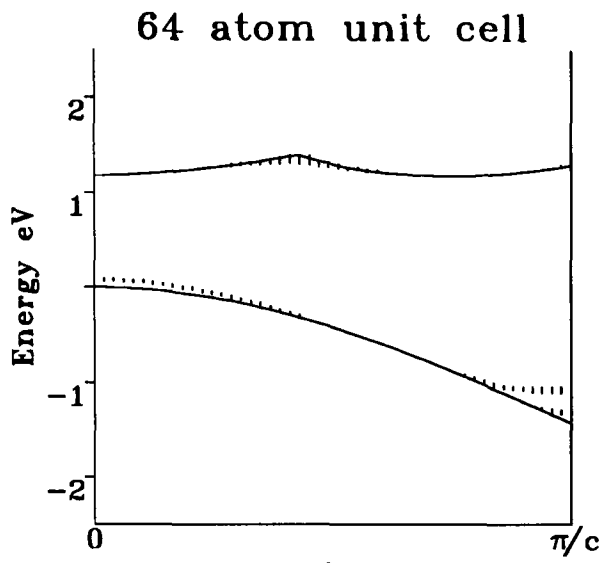

(b)

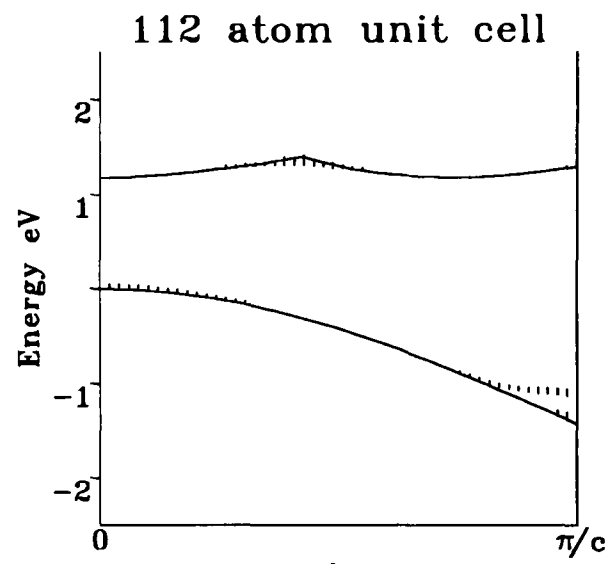

(c)

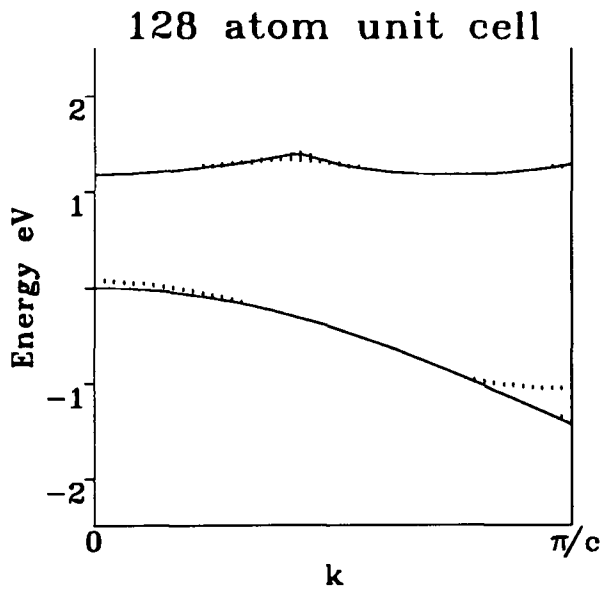

(d)

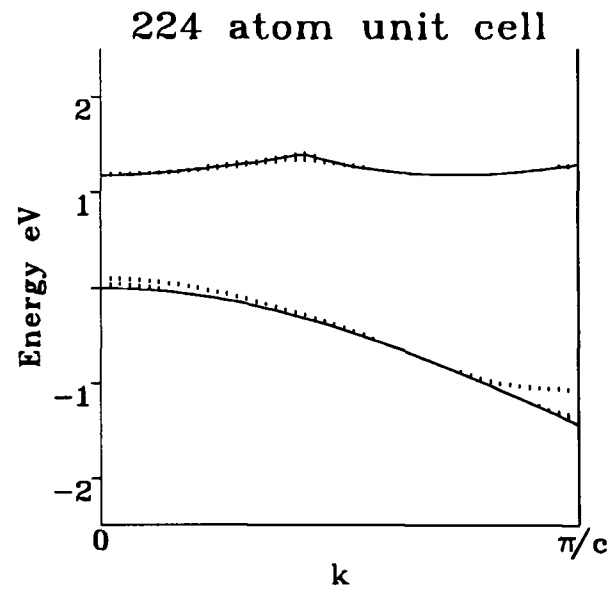

(e)

Fig. 5.1 Projected band-structures in eV for the reconstructed 90° partial along the dislocation line. The solid lines show the edges of the bulk valence and conduction bands. $c=a_0/\sqrt{2}$ is the repeat period along the dislocation. The band-structures are calculated using the Vogl Hamiltonian and various oblique unit cells relaxed with the Tersoff (1988b) potential. (a) 32 atom cell, (b) 64 atom cell, (c) 112 atom cell, (d) 128 atom cell, and (e) 224 atom cell.

5.2.2 k-point convergence

The k-point averaging scheme of Monkhurst and Pack (1978) has been described in chapter 3, section 3.4.3.1. In the original form of the code (M°Innes, 1992) k-points are generated by specifying an integer, q, in the resource file which gives a granularity of $1/q$ in *all three* directions of the Brillouin zone. For example, q=2 has a granularity of half the Brillouin zone and thus generates 2x2x2=8 k-points. Taking account of time-reversal symmetry[1] reduces this example to only 4 unique k-points each doubly weighted. Odd values of q include the gamma-point, which has no time-reversal symmetry partner. Its weighting is therefore half that of all other k-points which can make use of this symmetry.

For comparison, specific k-points generated to sample high dispersion directions are also considered. As discussed in chapter 3, section 3.4.3.1, the motivation for developing this approach is that in the unit cells used throughout this work there is likely to be only significant dispersion in one reciprocal lattice direction.

Table 5.2 illustrates the total energy and structural convergence as a function of the k-point sampling used. The convergence of the core structure is represented by the maximum and minimum bond and angle distortions for brevity. A fuller breakdown provides no further information in this case. The relaxations have been performed using the Chadi and Goodwin *et al.* (GSP) Hamiltonians, both with cutoffs of r_t=3.0Å.

Both tight-binding Hamiltonians show the same convergence trends. These can be summarised as follows, noting that the single k-point in *set 1* is equivalent to a one dimensional q=2 sampling and the two k-points in *set 2* are equivalent to a one dimensional q=4 sampling:

(1) sampling at the Brillouin centre only (q=1) produces poor binding energy and structural values. This implies there is significant dispersion in at least one reciprocal lattice direction.

---

[1] Time-reversal symmetry implies that diagonalisation at **k** and **-k** generates identical results.

Hamiltonian	k-point sampling	Binding Energy (eV)	Max/min Bond Lengths	Max/min Bond angles
Chadi	q=1 (ie. 0,0,0)	-3.842	6.75% -4.25%	135.0° 95.9°
Chadi	q=2 (4 k-points)	-4.783	5.39% -4.00%	133.5° 96.8°
Chadi	q=3 (14 k-points)	-4.696	5.67% -3.79%	133.5° 96.6°
Chadi	q=4 (32 k-points)	-4.710	5.57% -3.84%	133.5° 96.7°
Chadi	q=5 (63 k-points)	-4.707	5.61% -3.82%	133.5° 96.6°
Chadi	*set 1* (weight=1) (0,0,1/4)	-4.782	5.34% -3.99%	133.5° 96.8°
Chadi	*set 2* (weights=1/2) (0,0,1/8) (0,0,3/8)	-4.710	5.58% -3.84%	133.5° 96.7°
Chadi	*set 3* (weights=1/4) (0,0,1/16) (0,0,3/16) (0,0,5/16) (0,0,7/16)	-4.707	5.61% -3.82%	133.5° 96.6°
GSP	q=1 (ie. 0,0,0)	-3.443	4.64% -2.69%	136.1° 95.4°
GSP	q=2 (4 k-points)	-4.663	3.22% -2.27%	134.6° 96.2°
GSP	q=3 (14 k-points)	-4.572	3.47% -2.05%	134.2° 96.5°
GSP	q=4 (32 k-points)	-4.591	3.36% -2.16%	134.4° 96.5°
GSP	q=5 (63 k-points)	-4.585	3.40% -2.11%	134.3° 96.6°
GSP	*set 1* (weight=1) (0,0,1/4)	-4.663	3.25% -2.26%	134.6° 96.2°
GSP	*set 2* (weights=1/2) (0,0,1/8) (0,0,3/8)	-4.590	3.40% -2.16%	134.5° 96.4°
GSP	*set 3* (weights=1/4) (0,0,1/16) (0,0,3/16) (0,0,5/16) (0,0,7/16)	-4.586	3.43% -2.13%	134.5° 96.4°

Table 5.2 k-point convergence for both the Chadi and GSP Hamiltonians with r_t=3.0Å. q represents a uniform Brillouin zone sampling, whereas *sets 1-3* are specific k-points sampling along the high dispersion direction only.

(2) comparing *set 1* to q=2, and *set 2* to q=4, illustrates that the binding energy and structural results are almost identical in each case. The conclusion is that there is indeed negligible dispersion in the other two reciprocal lattice directions and a uniform mesh is unnecessary.

(3) structural convergence is adequate for just one k-point (*set 1*) but the binding energy requires a finer sampling[2]. It approaches convergence for q=5 (63 k-points! - 62 inversion partners and the gamma point) but also for *set 2* and *set 3* which consist of two and four k-points respectively. This clearly demonstrates the advantage of using the new scheme.

The other aspect of k-point convergence is related to the accuracy of the band-structure obtained. It was stated in chapter 4, section 4.4.2, that averaging over a plane at right angles to the dislocation line provided negligible changes to just restricting k-points to this line. This is illustrated here. $\boldsymbol{k}_z$ samples down the dislocation line but at each value of $\boldsymbol{k}_z$ two different approaches are taken. In the first a 9 k-point average is performed over the $\boldsymbol{k}_x\boldsymbol{k}_y$ plane (this corresponds to a two dimensional q=3 mesh) and in the second no averaging over this plane is performed.

Fig. 5.2 illustrates these two cases. In fig. 5.2a the averaging over the plane implies more states per $\boldsymbol{k}_z$ point and this can be seen by comparing fig. 5.2b. However, there is clearly no important information being obtained by performing this plane averaging since the two band-structures are so similar. This is consistent with the lack of dispersion in the $\mathbf{k}_x$, $\mathbf{k}_y$ directions indicated by the structural and energy convergence tests outlined above. All further band-structure results are calculated by sampling k-points restricted to the dislocation line.

5.3 Four-fold interaction only

Several empirical potentials have been used to model the atomic structure of the 90° partial

---

[2] This again illustrates the more rapid convergence of quantities dependent on energy differences compared to the rate of convergence of absolute energies.

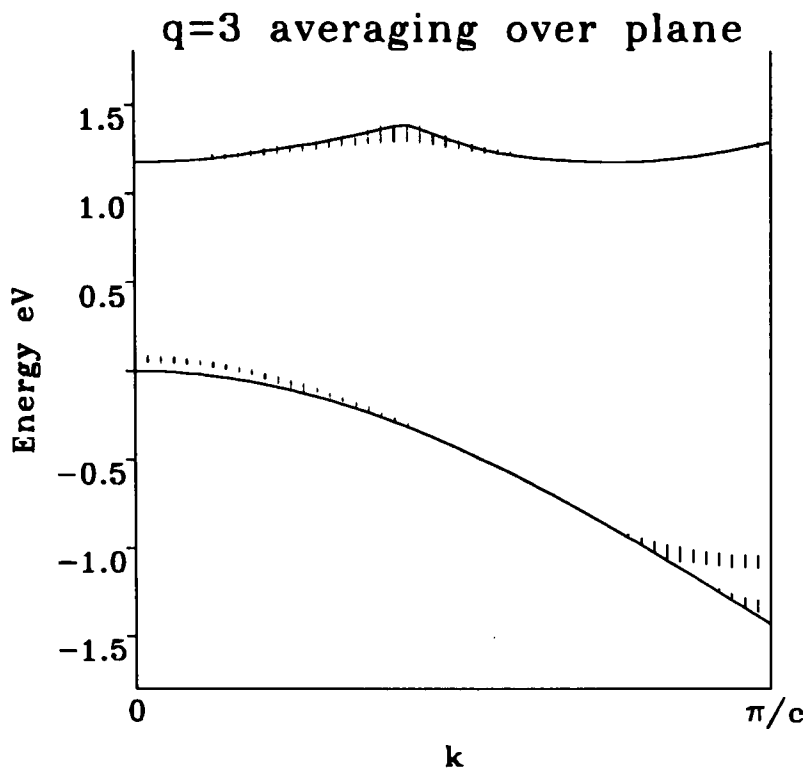

Fig. 5.2 Band-structures calculated using the Vogl Hamiltonian for the 64 atom oblique unit cell relaxed with the Tersoff (1988b) potential. (a) q=3 (9 k-point) averaging performed over a plane normal to the dislocation line (b) no plane averaging.

in Si. The harmonic potential due to Keating (1966), the anharmonic potential due to Koizumi and Ninomiya (1978) and the Lifson and Warshell (1968) potential used in a modified form by Altmann *et al.* (1983). By the nature of their construction these potentials are applicable to a four-fold environment only. In modelling the three-fold coordinated unreconstructed core the Keating and Koizumi and Ninomiya potentials relied upon the "pseudo atom" technique (Marklund, 1980) to saturate the dangling bonds and restore a four-fold environment to each atom. This approach implicitly restricts the description of the *bond order* increase that will draw the three-fold coordinated atoms back into the bulk, widening the core as a result. This is exactly what Altmann *et al.* (1983) found by avoiding the pseudo atom approach and treating the interaction across the core as a van der Waals coupling, although this is still an approximation to the true character of the dangling-bond interaction.

The methods that will be used here have been described in chapter 3. In general these are not restricted to a four-fold environment and this allows the use of techniques such as Molecular Dynamics to let the system evolve over time and hopefully extract the global rather than a local minimum. This extra freedom for the system has revealed different results to the restrictive analysis of the simple VFFs.

It is however instructive to restrict *initially* all the classical and tight-binding models to a *four-fold* nearest neighbour shell since it illustrates a reasonably consistent atomic structure in agreement with the earlier work. The results obtained using this neighbour list restriction are shown in table 5.3. The bonds and bond angles again refer to those depicted in chapter 4, fig. 4.9. The results obtained using the Tersoff (1988a) potential have been deliberately sectioned off since they do show significant differences to the other results. Specifically, the bond stretches are in general much smaller at the expense of wider bond angle deviations at the core. This is an interesting result and its implications are discussed further in section 5.5.

Concentrating on all the other relaxed structures it can be seen that the general atomic arrangement is reasonably consistent for both classical and tight-binding simulations. The similarities can be summarised as follows:

Bond	Chadi r_t=3.0Å	GSP r_t=3.0Å	Modified Lifson-Warshell	Tersoff (1988b)	Tersoff (1988a)
Bond 1	2.483 (5.6)	2.431 (3.4)	2.404 (2.2)	2.458 (4.5)	2.405 (2.3)
Bond 2	2.264 (-3.7)	2.308 (-1.9)	2.335 (-0.7)	2.320 (-1.4)	2.342 (-0.4)
Bond 2'	2.445 (3.9)	2.409 (2.4)	2.411 (2.5)	2.403 (2.2)	2.401 (2.1)
Bond 3	2.435 (3.6)	2.403 (2.2)	2.408 (2.4)	2.399 (2.0)	2.402 (2.1)
Bond 3'	2.264 (-3.7)	2.309 (-1.8)	2.336 (-0.6)	2.320 (-1.4)	2.339 (-0.5)
Bond 4	2.396 (1.9)	2.390 (1.6)	2.376 (1.0)	2.391 (1.7)	2.379 (0.9)
Bond 5	2.393 (1.8)	2.385 (1.4)	2.371 (0.8)	2.382 (1.3)	2.371 (0.8)
Bond 6	2.329 (-0.9)	2.345 (-0.3)	2.339 (-0.6)	2.352 (0.0)	2.353 (0.0)
Bond 7	2.329 (-1.0)	2.346 (-0.2)	2.341 (-0.4)	2.353 (0.0)	2.352 (0.0)
Bond 8	2.484 (5.6)	2.424 (3.1)	2.412 (2.6)	2.424 (3.1)	2.402 (2.1)
Bond 9	2.443 (3.9)	2.416 (2.8)	2.419 (2.9)	2.421 (2.9)	2.393 (1.8)
Bond 9'	2.352 (0.0)	2.363 (0.5)	2.387 (1.5)	2.368 (0.7)	2.369 (0.7)
Bond 10	2.366 (0.6)	2.347 (-0.2)	2.328 (-1.0)	2.324 (-1.2)	2.366 (0.6)
Bond 10'	2.278 (-3.1)	2.310 (-1.8)	2.304 (-2.0)	2.311 (-1.7)	2.335 (-0.7)
Bond 11	2.291 (-2.6)	2.313 (-1.7)	2.314 (-1.6)	2.313 (-1.6)	2.336 (-0.7)
Bond 12	2.429 (3.3)	2.410 (2.5)	2.410 (2.5)	2.409 (2.4)	2.385 (1.4)
Bond 13	2.418 (2.8)	2.405 (2.3)	2.404 (2.2)	2.405 (2.3)	2.384 (1.4)
Bond 14	2.312 (-1.7)	2.332 (-0.9)	2.334 (-0.8)	2.335 (-0.7)	2.351 (0.0)
Bond 14'	2.348 (-0.2)	2.352 (0.0)	2.353 (0.1)	2.349 (-0.1)	2.358 (0.3)
Bond 15	2.345 (-0.3)	2.349 (-0.1)	2.351 (0.0)	2.347 (-0.2)	2.359 (0.3)
Bond 15'	2.310 (-1.8)	2.330 (-0.9)	2.331 (-0.9)	2.334 (-0.8)	2.351 (0.0)
Bond 16	2.422 (3.0)	2.405 (2.3)	2.406 (2.3)	2.398 (2.0)	2.387 (1.5)
Bond 17	2.411 (2.5)	2.399 (2.0)	2.401 (2.1)	2.396 (1.9)	2.385 (1.4)
Normal Crystal Side					
Angle 213	96.6	96.6	97.4	95.3	90.0
Angle 214	133.1	134.1	133.4	135.3	145.3
Angle 215	103.1	103.8	103.8	103.5	104.3
Angle 314	109.2	109.0	108.0	108.8	108.1
Angle 315	115.8	114.4	116.5	114.5	107.0
Angle 415	99.8	99.4	98.9	99.8	98.5
Stacking Fault Side					
Angle 127	96.7	96.6	97.2	95.5	90.6
Angle 126	133.5	134.3	133.2	135.6	146.3
Angle 128	103.1	104.2	104.3	104.1	104.4
Angle 627	109.6	109.2	108.1	108.9	108.2
Angle 728	116.3	116.1	115.7	115.3	105.5
Angle 628	98.7	97.4	99.3	98.2	97.4

Table 5.3 Bonding around the core of one of the 90° partials within an *oblique* unit cell of 64 atoms. Different columns are labelled by the technique used to obtain the relaxed core structure. The bond and angle notation used is as depicted in chapter 4, fig 4.9, where, for example, angle 123 means the angle subtended by atoms 1 and 3 at atom 2. The bond lengths are given in Å and their percentage distortion relative to the perfect Si bond length (2.3517Å) in brackets.

1) bonds are stretched typically between -3% and +5% with bond angle deviations between 95° and 135°.

2) bond angles around the reconstructed bond are comparable between all core structures indicating that the central geometry is similar in all cases.

3) the bonds 8 and 9, in the region of elastic expansion, are highly stretched whereas the bonds 10 and 11, in the compressive region, are generally the shortest.

The similarities are also demonstrated in calculations of the electronic structure. Reference to chapter 4, figs. 4.16 and 4.17, illustrates the band-structures obtained using the Chadi and Vogl Hamiltonians respectively. The results for both the classical and tight-binding relaxed cells are virtually indistinguishable. They indicate, for a nearest four-fold neighbour description *only*, that the asymmetric core reconstruction (Hirsch, 1979; Jones, 1979) can be well described by simple classical potentials, excluding the Tersoff (1988a) result, and essentially clears the indirect band-gap of dislocation states. There is however the possibility of very shallow states near the valence and conduction band edges.

5.4 More distant interactions

Lifting the restriction that atoms may only interact with four neighbours has resulted in simulations on the reconstruction associated with the core of the 90° partial revealing results dependent on the model used to describe this reconstruction. Either the dangling bonds reconstruct in the usual way so that all atoms are four-fold coordinated, fig. 5.3b, or the core predicted by elasticity theory, fig. 5.3a, contracts resulting in two remote neighbours coming within range of the three-fold coordinated atoms, as in fig. 5.3c. This latter reconstruction mechanism was observed by Duesbery *et al.* (1991) and is discussed in section 5.4.3.

5.4.1 CETEP results

The ab initio pseudopotential codes have the valence wavefunctions expanded in a plane wave basis set. The ground state of the system is located by minimising the total energy with

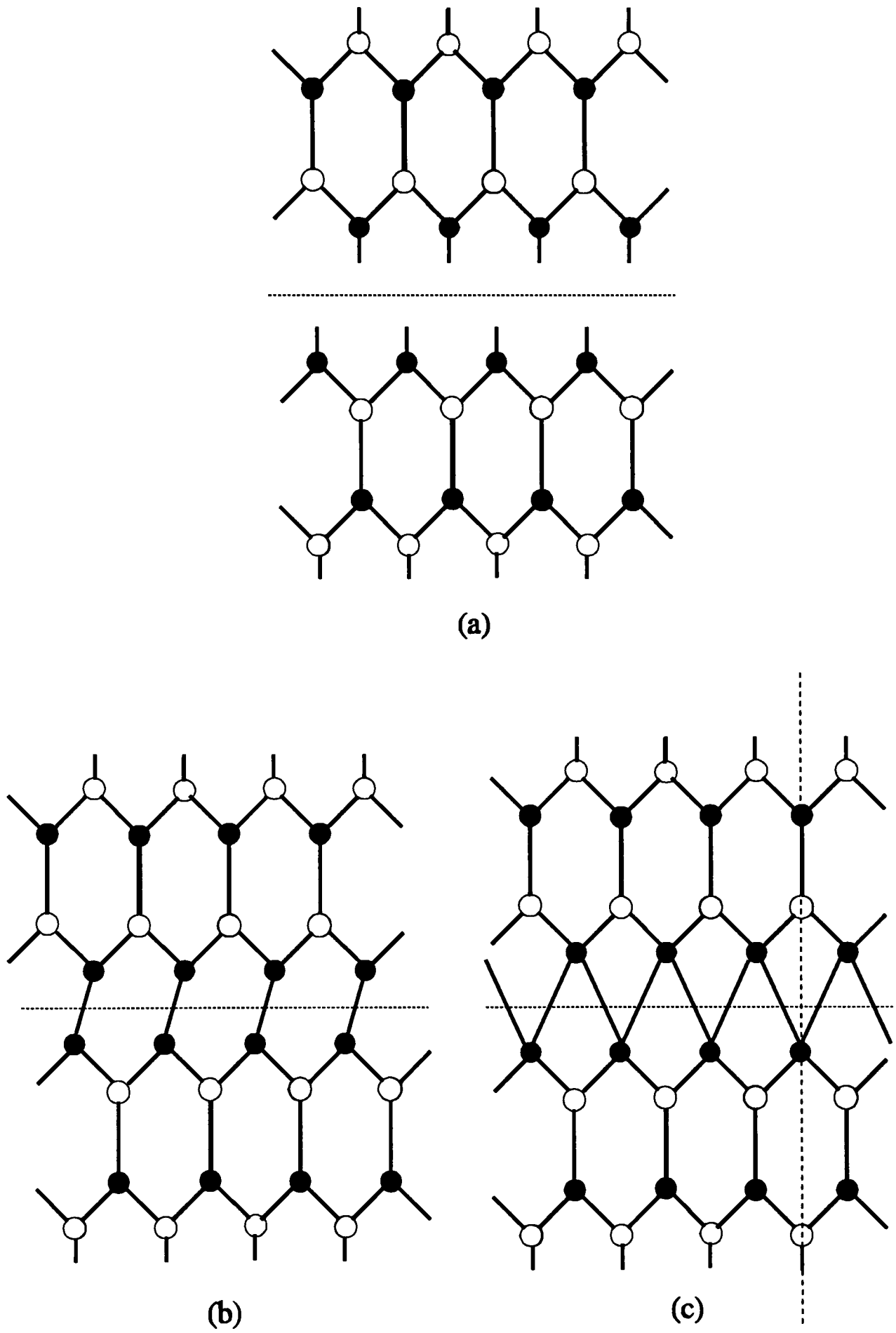

Fig. 5.3 Schematic illustration of the atomic coordinates within the core of a 90° partial dislocation on the (111) slip plane. The dislocation lies along the dotted line:
(a) three-fold unreconstructed, (b) asymmetric four-fold reconstruction, and (c) symmetric quasi-five-fold reconstruction, the dashed line showing the mirror plane.

respect to both the electronic and ionic coordinates. One of the advantages to this scheme is that no prior assumptions on the connectivity of the system has to be made. All interactions are taken into account in an unambiguous way[3].

All calculations described here have been performed on the Meiko parallel computer in Edinburgh. The relaxations were on the 64 atom oblique unit cell using a two k-point sampling which has been shown to provide good structural and energy convergence (*set 2* in table 5.2). The Si pseudopotential, as tested and used in earlier work (Stich *et al.*, 1992), was used at a cutoff of 120eV. Relaxation was terminated when forces fell to below 0.1eV/Å.

The starting point for the CETEP calculation was the relaxed tight-binding unit cell obtained with the Chadi Hamiltonian (table 5.3). This structure is compared with the CETEP result in table 5.4.

It can be seen that CETEP has reduced the reconstructed bond 1 stretch from 5.6% to 2.6%. Whereas in the tight-binding and classical simulations (table 5.3) the reconstructed bond is in general the most distorted in the structure, the CETEP result finds the reconstructed bond to be less stretched than some of its adjoining back bonds. There is also the introduction of asymmetry around the core, shown by the difference in the length of the back bonds and the angles on either side of the core. The bond angle deviations have increased as a result (96.0° to 138.5°). Bond 8, in the 7-membered ring, remained highly stretched at 5.5%.

In chapter 4, section 4.4.1, this question of core asymmetry was described and it was shown that the shear strain in the *rectangular* unit cells had given rise to different bond angles on either side of the core also obtained in earlier work (Chelikowsky and Spence, 1984; Lodge *et al.*, 1984). Use of the oblique unit cell resulted in a more symmetric core and the reason for this was discussed there. However, with CETEP, also in the *oblique* unit cell, an asymmetry is introduced due to the implicit inclusion of all interactions. By reference to

---

[3] In a classical prescription the connectivity is limited to that specified in the neighbour list. In the tight-binding scheme the density matrix, and thus the band energy and forces, is determined by *all* atoms in the system even though the Hamiltonian couples only nearest neighbours directly.

Bond	**Chadi (r_t=3.0Å)**	**CETEP**
Bond 1	2.483 (5.6)	2.412 (2.6)
Bond 2	2.264 (-3.7)	2.328 (-1.0)
Bond 2'	2.445 (3.9)	2.440 (3.8)
Bond 3	2.435 (3.6)	2.423 (3.0)
Bond 3'	2.264 (-3.7)	2.315 (-1.5)
Bond 6	2.329 (-0.9)	2.342 (-0.4)
Bond 7	2.329 (-1.0)	2.359 (0.3)
Normal Crystal Side		
Angle 213	96.6	96.2
Angle 214	133.1	134.9
Angle 215	103.1	103.7
Angle 314	109.2	107.3
Angle 315	115.8	115.2
Angle 415	99.8	100.2
Stacking Fault Side		
Angle 127	96.7	98.4
Angle 126	133.5	138.4
Angle 128	103.1	102.5
Angle 627	109.6	108.3
Angle 728	116.3	112.9
Angle 628	98.7	95.9

Table 5.4 Comparison of the local bonding around the reconstructed bond 1 for the Chadi Hamiltonian relaxed structure and the CETEP result. The bond and angle notation used is as depicted in chapter 4, fig 4.9, where, for example, angle 123 means the angle subtended by atoms 1 and 3 at atom 2. The bond lengths are given in Å and the percentage distortions from the perfect Si bond length (2.3517Å) are in brackets.

chapter 4, fig. 4.9c, it can be seen that for interactions outside the four nearest neighbours, atoms 1 and 2 directly "see" a different atomic environment due to the presence of the stacking fault. The bond angles on the stacking fault side are especially different to those obtained with the Chadi Hamiltonian and this is consistent with the fact that more distant interactions in this region do depart from the normal diamond-cubic stacking. It is significant that a nearest neighbour tight-binding Hamiltonian, which still couples *all* the atoms through the density matrix, predicts a result consistent with a simple nearest neighbour connectivity only. The consequences of considering more distant interactions directly through the Hamiltonian are considered in the next section.

The electronic structure is very similar to those calculated for all the structures listed in table 5.3, and is considered further in section 5.4.3.2.

This CETEP result implies that use of classical and tight-binding models, where restriction to a four-fold interaction is justified, produces reliable results. However, perturbing effects that are a consequence of higher neighbour interactions, such as the asymmetry around the core, cannot be obtained with a nearest neighbour model.

The atomic coordinates and cell vectors of this CETEP relaxed structure are tabulated in appendix E.

In their work on P and its interaction with a 90° partial, Heggie *et al.* (1989, 1991) also performed ab initio calculations on the clean dislocation embedded in a *cluster*. They reported a reconstructed bond stretch of less than 1% which is contrary to the results obtained in this work. However, recent more accurate calculations on a slightly larger cluster (Umerski, 1992) has revealed a reconstructed bond stretch of 3.5% which is in much better agreement with the present findings.

5.4.2 A highly stretched reconstructed bond

Can this asymmetry at the core predicted by CETEP be obtained by using the classical and tight-binding models with longer cutoffs to lift the nearest neighbour restriction? This is tested on the classical Tersoff (1988b) potential with a cutoff extended to 3.77Å, following the work of Duesbery *et al.* (1991)[4], and the tight-binding scheme using the GSP Hamiltonian with the same cutoff.

The classical and tight-binding methods both predict a similar effect and the local bonding around the core that results is listed in table 5.5.

Inclusion of more distant Hamiltonian matrix elements, or "hopping", has resulted in the

---

[4] Duesbery *et al.* (1991) actually used the Tersoff (1989) potential. However, this form of the potential is identical to that of Tersoff (1988b), except for one parameter, λ_3 (see appendix A), which is set to zero in the (1989) paper to simplify the analytic form of the forces. As mentioned by Tersoff (1988b) and verified here, setting this parameter to zero has negligible effect on the results obtained.

Bond	**GSP**	**Tersoff (1988b)**
Bond 1	2.544 (8.2)	2.653 (12.8)
Bond 2	2.312 (-1.7)	2.315 (-1.6)
Bond 2'	2.436 (3.6)	2.394 (1.8)
Bond 3	2.445 (4.0)	2.417 (2.8)
Bond 3'	2.319 (-1.4)	2.322 (-1.3)
Bond 6	2.373 (0.9)	2.368 (0.7)
Bond 7	2.392 (1.7)	2.395 (1.8)
Normal Crystal Side		
Angle 213	93.5	95.0
Angle 214	139.8	136.2
Angle 215	102.8	100.8
Angle 314	107.9	109.3
Angle 315	109.1	112.3
Angle 415	101.7	102.5
Stacking Fault Side		
Angle 127	92.8	94.8
Angle 126	138.6	135.3
Angle 128	103.3	103.2
Angle 627	107.4	108.2
Angle 728	116.2	117.5
Angle 628	99.5	99.3

Table 5.5 The local bonding around the reconstructed bond 1 for the classical Tersoff (1988b) and the GSP Hamiltonian tight-binding relaxed structures. Both schemes have been used with an extended cutoff, r_t=3.77Å. The bond and angle notation used is as depicted in chapter 4, fig 4.9, where, for example, angle 123 means the angle subtended by atoms 1 and 3 at atom 2. The bond lengths are given in Å and the percentage distortions from the perfect Si bond length (2.3517Å) are in brackets.

reconstructed bond 1 becoming considerably more stretched (8% from 3.5% in the tight-binding case; 12% from 4.5% in the classical case). This greater bond stretch is accommodated by the core "breathing" and a more open core results. This long reconstructed bond agrees with the findings of Duesbery *et al.* (1991) (c.f. 11%). Asymmetry, in the back bonds and bond angles around the core, has also been introduced.

Intuitively this result seems reasonable. Inclusion of more distant interactions (r_t=3.77Å) will weaken the local nearest neighbour bond orders, resulting in the repulsive pair potential contribution to the total bond energy dominating.

The electronic effect of these highly stretched reconstructed bonds is illustrated in fig. 5.4. The band-structures shown have been calculated using the Vogl Hamiltonian, similar results being predicted by the Chadi Hamiltonian. The results indicate slightly greater penetration of the dislocation states at both band edges than is obtained by their equivalent relaxed structures using the restricted cutoff (see chapter 4, fig. 4.17). It is perhaps surprising that there is not greater state penetration since the bonds are so highly stretched and the hopping integrals correspondingly weaker. However, it should be noted that these structures are still *locally* four-fold coordinated, the *next* nearest neighbour bond distance being roughly 3.5Å in both cases which is second shell like. While the reconstructed bonds have significantly increased, the bond angles have only become about 2-3° more distorted than those given in table 5.3 and thus the directional bonding is only slightly changed on increasing the cutoff to include more distant neighbours. The importance to the electronic structure of this competing effect between bond bending and stretching is considered further in section 5.5.

Relaxation from the Chadi configuration using CETEP (section 5.4.1) gave no indication of this core opening observed here, but the ionic relaxation occurs using energy minimisation by steepest descent and it could be that a local minimum was found. To check this, another CETEP relaxation was performed starting from the open core GSP configuration. The result was a closing of the core and a reduction of the 8% stretched reconstructed bond back to 3.5% at which point the relaxation was terminated.

This result is highly significant. It implies that the extent to which the local bond orders are weakened by including higher order neighbours is too great in both the tight-binding and classical prescriptions used here. It should be noted that Tersoff (1988a) indicated that there might be problems including interactions outside the "nearest neighbour shell" based on the simple ideas of bond order around which he constructed his potential. Thus by choosing an extended cutoff, Duesbery *et al.* (1991) were incorrectly using the Tersoff potential and it has been shown here that it leads to erroneous results to that predicted with the prescribed cutoff (table 5.3).

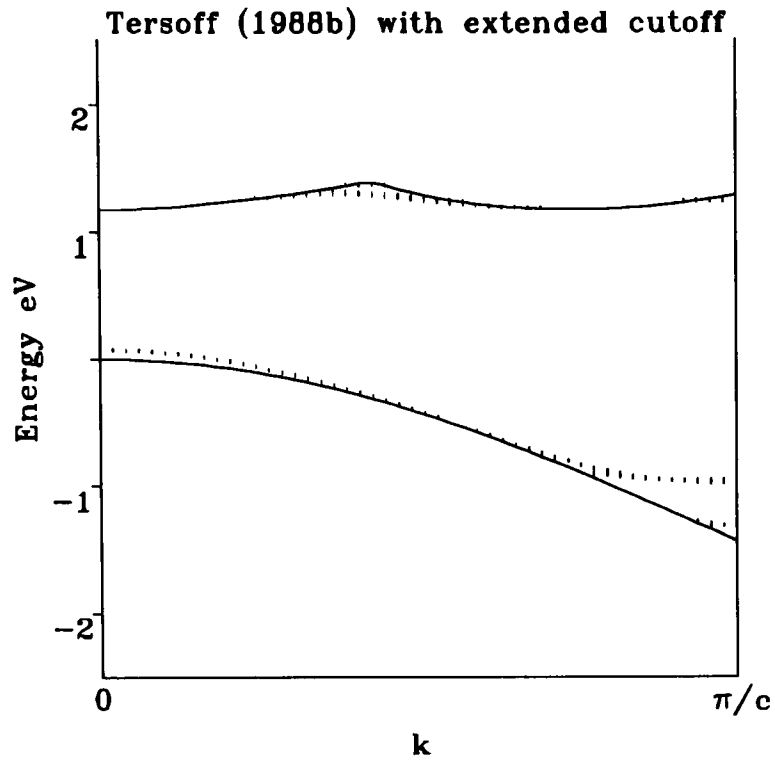

Fig. 5.4 Band-structures calculated using the Vogl Hamiltonian and the oblique 64 atom unit cell. (a) Tersoff (1988b) relaxed with r_t=3.77Å and (b) GSP Hamiltonian relaxed with r_t=3.77Å.

The result obtained with the Goodwin *et al.* (1989) Hamiltonian is perhaps more surprising since the scaling was derived to better describe these second neighbour interactions. In recent work (Kohyama, 1991; M^{c}Innes, 1992) there has been difficulty reproducing the structural energy curves calculated by Goodwin *et al.* in which *all non-zero Hamiltonian interactions* are included. Kohyama has reported problems obtaining these curves using the published parameters. M^{c}Innes has found that by restricting the GSP Hamiltonian to nearest neighbour interactions only much better agreement with the published curves is obtained. It thus seems likely that the published parameters are valid for only a nearest neighbour Hamiltonian and that although the scaling is physically plausible the parameters were fitted without second neighbour interactions being taken into account. The results obtained here support this suggestion, with the nearest neighbour model producing a reliable core structure (table 5.3) but extension to higher neighbours producing an unphysical core opening.

5.4.3 A symmetric quasi-five-fold reconstruction

The Stillinger Weber potential has a cutoff of 3.77Å, which allows the three-fold coordinated atoms to interact directly across the core. Anisotropic elasticity theory provides starting atomic positions and the system evolves using Molecular Dynamics. This scheme should ensure that much of the configurational guesswork is taken out of the starting requirements.

Using this scheme a *symmetric* reconstruction was obtained, where each three-fold coordinated atom has moved across the core perpendicular to the line direction to become *five-fold* coordinated (see Fig. 5.3c). Back bonds to these atoms are stretched by 2.4%, 2.4% and 0.9% while the two symmetric cross-core bonds are stretched by 17.2%. The bond angles are severely distorted and range from 77° to 153°. Even after breaking the symmetry and shifting these atoms into the usual four-fold coordinated reconstructed structure, a second simulation moved them back to the symmetric state.

Duesbery *et al.* (1991) have also obtained this symmetric reconstruction with the Stillinger

Weber potential, although the bond lengths reported there are in error (Duesbery, 1991). It is significant that this same quasi-five-fold reconstruction mechanism is predicted by the long ranged (5.5Å cutoff) potential due to Kaxiras and Pandey (1988) (Duesbery *et al.*, 1991).

The Lifson Warshell potential has also been applied to the quasi-five-fold structure in this work, but due to the limitations of the functional form this approach has little justification[5]. For a comparison with the Stillinger Weber and Kaxiras and Pandey potentials these highly stretched cross core bonds have been treated as covalent by using the full form of the modified Lifson Warshell potential. The energy of the Stillinger Weber relaxed quasi-five-fold structure was calculated using this modified potential in this manner and compared to the energy of the relaxed four-fold structure obtained with the same potential (table 5.3). The quasi-five-fold structure was found again to be *lower* in energy than the four-fold relaxed core.

As discussed already, Duesbery *et al.* found the Tersoff potential to predict a four-fold coordinated core to be more stable, although the use of a longer than prescribed cutoff led to erroneous results. By using the correct cutoff the stability of the two reconstructions can be re-analysed. The asymmetric reconstruction is listed in table 5.3. Starting from the symmetric core, the Tersoff (1988b) potential reduces the length of the cross core bonds from 17.2% to 15.0%, increasing the bond angle deviation (76° to 155°). Although the quasi-five-fold structure corresponds to an energy minimum, it is energetically unstable with respect to the asymmetric four-fold core by 0.064eV per dislocation, per repeat period along the dislocation line. Although this energy difference is small it is significant that the classical Tersoff potential predicts the four-fold core to be lower in energy, while three other classical potentials come to the opposite conclusion.

5.4.3.1 Tight-binding and CETEP relaxations

There is evidence that the interaction between the three-fold coordinated atoms across the

---

[5] The question of whether the cross-core interactions should be treated using the covalent bonding parts of the potential or just the van der Waals term has been discussed by Altmann *et al.* (1983) for the case of the *unreconstructed* 90° partial.

core is far from insignificant (Teichler and Marheine, 1987; Wang and Teichler, 1989; Teichler, 1989a). The stability of this structure has been illustrated by some classical potentials but in general these are unable to describe the very different electronic rehybridisation that will occur at the quasi-five-fold coordinated atoms. The tight-binding technique and CETEP have been used to analyse the bonding processes involved in this symmetric structure. In all cases the Stillinger Weber relaxed unit cell has been used as the starting configuration. All tight-binding relaxations have been performed at a temperature of 100°K to avoid discontinuities in the forces occurring due to state crossing at the Fermi level (see chapter 3, section 3.4.2).

The Chadi Hamiltonian results in an opening of the core and the atoms on either side of the core moving back towards the elastic solution of fig. 5.3a. Since an arbitrary cutoff must be assigned to the Hamiltonian and pair potential, this core opening must be investigated as a function of r_t. Various Hamiltonian cutoffs, r_t=2.79Å, 3.0Å and 3.25Å, were considered and the results are shown in table 5.6.

Cutoff, r_t (Å)	Binding Energy (eV)	Cross core Bond Length	Max/min Bond angles
2.79	-4.678	2.71Å (15.3%)	154.8° 77.1°
3.00	-4.684	2.94Å (25.0%)	151.3° 79.2°
3.25	-4.685	2.99Å (27.3%)	150.2° 79.6°

Table 5.6 Relaxation from the Stillinger Weber quasi-five-fold reconstruction using the Chadi Hamiltonian with various values of r_t.

The degree of core opening can be seen from table 5.6 to be dependent on the chosen cutoff and conclusively demonstrates the disadvantage of having to assign an arbitrary cutoff. Unfortunately there is no liberty to assign a much larger cutoff since the Chadi Hamiltonian

is a nearest neighbour prescription with a $1/d^2$ scaling which is inappropriate for describing second neighbour interactions.

It can be seen from table 5.6 that for r_t=2.79 and 3.0Å the core has opened to the limit allowed by the cutoff to maintain the bonding across the core as weak first neighbour interactions. However, for r_t=3.25Å there is only a minor change in both the structure and binding energy from the r_t=3.0Å result indicating the cutoff has become sufficiently large to allow the core to find its equilibrium structure. The cross core bonds are much more highly stretched than in the Stillinger Weber result.

The mirror symmetry present in this structure (see fig 5.3c) could be responsible for locking the system into an unstable state, and this was investigated by applying a small shift (0.05Å) towards the asymmetric four-fold reconstruction. The system was found to return to the symmetric quasi-five-fold state. This implies that this structure is stable as predicted by the Chadi Hamiltonian but it is only a local minimum when compared to the asymmetric four-fold relaxed core (table 5.3). The four-fold result is found to be about 0.75eV *lower* in energy per dislocation per repeat period down the dislocation line.

Relaxation from the quasi-five-fold state using the GSP Hamiltonian constricts the core, spontaneously introducing the shear along the dislocation required to recover four-fold coordination. No attempt to stabilise the symmetric core was successful and clearly the GSP Hamiltonian predicts this symmetric state to be *unstable*.

The ability to describe five-fold bonding using a minimal sp^3 basis is questionable. The Vogl Hamiltonian, which contains an extra excited *s* orbital, has also been used together with an inverse square scaling. The results obtained were similar to the Chadi Hamiltonian predictions which seems to imply that the scaling law dictates whether or not this symmetric core is stable.

Nonetheless these results all imply that the tight-binding model predicts the quasi-five-fold core to be energetically unstable with respect to a shear across and along the core which recovers full four-fold coordination.

Expansion of the valence wavefunctions in a large plane wave basis, as occurs in CETEP, offers the advantage that contributions from not only *s* and *p* but also *d*, *f* etc. components are implicitly included. A proper description of such a distorted structure should include higher angular momentum states since electronic rehybridisation involving *d* states could stabilise the quasi-five-fold bonding. The stability can be tested by applying a small atomic displacement to break the mirror symmetry and seeing if the relaxation returns to the original state. It was deemed wise to introduce a small symmetry lowering displacement since there is always a certain degree of error in the forces calculated using CETEP[6]. A small displacement to break the symmetry will ensure that the forces are large enough to be reliably described. Movement back to a symmetric state will properly indicate the stability of the quasi-five-fold core. As with the Chadi Hamiltonian work the atomic displacement was small (0.05Å).

Relaxation using CETEP transformed the quasi-five-fold structure into the asymmetric reconstruction. This work therefore also implies that the classically predicted symmetric core is unstable.

5.4.3.2 Electronic structure

Considerable insight into the mechanism that drives this asymmetric shift into the four-fold reconstruction can be gained by using the band-structure techniques of the k-space tight-binding model. The projected band-structures, using the Vogl Hamiltonian, are shown in fig. 5.5 for the quasi-five-fold symmetric core obtained with the Stillinger Weber potential and the four-fold asymmetric core obtained using CETEP (section 5.4.1).

For the symmetric configuration, fig. 5.5a, two bands split away from the valence and conduction bands and *nearly* meet at the Brillouin zone boundary. Analysis of the eigenvectors shows that these states are concentrated on the quasi-five-fold coordinated atoms in each

---

[6] The Hellmann-Feynman forces are exact derivatives of the total energy only when computed at the self-consistent charge density. During a relaxation the electronic contribution to the total energy is minimised at each ionic step but the charge density will never be exactly self-consistent.

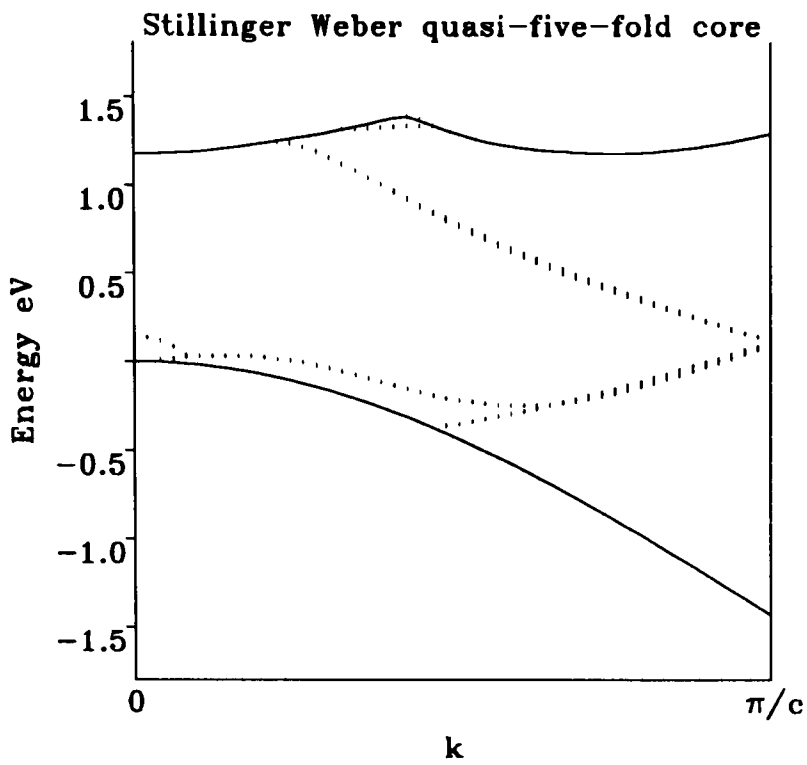

(a)

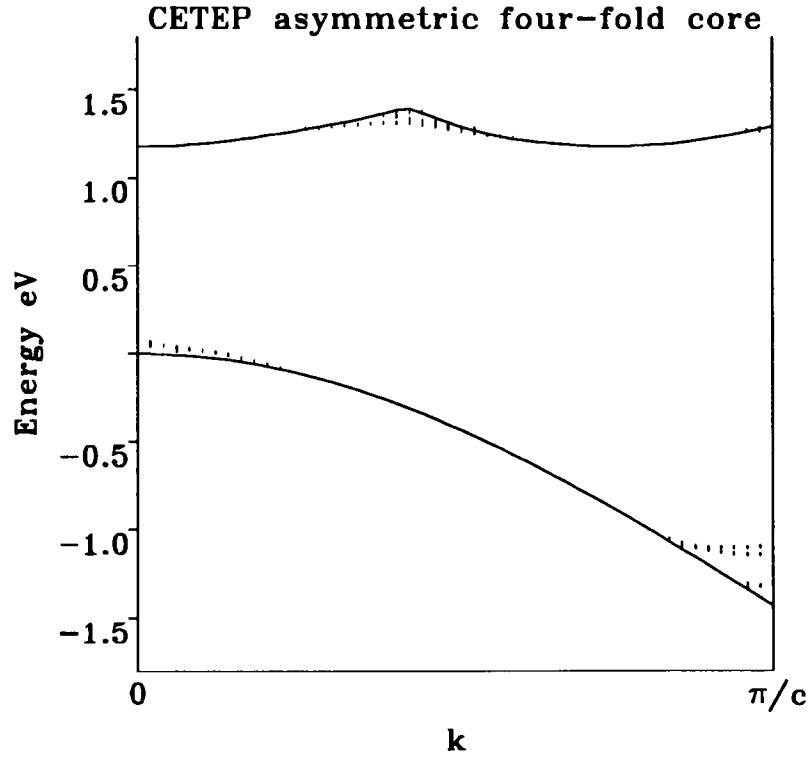

(b)

Fig. 5.5 Band-structures calculated using the Vogl Hamiltonian and the oblique 64 atom unit cell. (a) Stillinger Weber relaxed symmetric quasi-five-fold reconstruction, and (b) CETEP relaxed asymmetric four-fold reconstruction.

dislocation core. Table 5.7 also shows that these states are sp-hybrids oriented almost *normal* to the dislocation line rather than towards each other, the weighting being primarily with the s and p_x components and much less so for p_y and p_z.

Atom place in core	s	p_x	p_y	p_z	s^*
Stacking fault side	0.11	0.26	0.0004	0.035	0.083
Perfect crystal side	0.10	0.29	0.0016	0.032	0.079

Table 5.7 Relative state weightings for the two quasi-five-fold coordinated atoms in one of the 90° partial cores. The other core produces identical results.

Since the hybrids are non-directional the bonding across the core consists of weakly interacting dangling bonds and explains why the band-structure closely resembles that obtained for the *unreconstructed* 90° partial (Teichler and Marheine, 1987; Wang and Teichler, 1989). Each line of these weakly interacting hybrids gives rise to a band spanning the gap. But one period of the dislocation contains *two* inequivalent quasi-five-fold atoms, as can be seen from table 5.7, and therefore a small gap is opened at the zone boundary[7]. The gap is small because the environments of the two atoms differ only slightly.

The two bands spanning the gap would be degenerate if the dislocations were sufficiently far apart. There is a splitting of the bands which is a result of the dislocations interacting, but it is small except just above the valence band edge.

For the asymmetric configuration, fig. 5.5b, the band gap is almost cleared of states. The displacement along the dislocation line, shown in fig. 5.3b, opens the small gap at the Brillouin zone boundary of fig. 5.5a to such an extent that the upper pair of bands move into the bulk conduction band and the lower pair into the bulk valence band. A more chemical viewpoint is that this band splitting arises from the sp-hybrids on the atoms that were quasi-five-fold coordinated pairing up to form *directed* bonds to each other, as originally envisaged

[7] It is difficult to see this gap from fig. 5.5a, but a much larger plotter output has indicated it does exist.

by Hirsch (1979) and Jones (1979). Therefore, it is the electronic contribution to the total energy that stabilises the asymmetric reconstruction.

5.5 Bond angle versus bond stretching distortion

In section 5.3 the atomic structure of the dislocation core was investigated using various relaxation techniques all restricted to nearest neighbour four-fold interactions. The Tersoff (1988a) potential was sectioned off in table 5.3 because of its significantly different results. Specifically, this potential predicts a strongly reconstructed core with bond deviations of only -1% to 2%, but at the expense of a greater bond angle deviation, 90° to 146° (see table 5.3). This greater bond bending results because bonds 8 and 9, in the seven-fold ring, and 10 and 11, in the five-fold ring, are significantly less distorted than with the other relaxation techniques. These less distorted bonds are consistent with the *excessive* bond stretching stiffness of this form of Tersoff's potential (Teichler, 1989c; Tersoff, 1988b; Tersoff, 1989).

In light of these results it is proposed that the parameterisation given by Tersoff (1988a) for his potential developed there, provides an unsuitable description of the bonding present in the 90° partial core. Several observations support this statement:

1) as noted by Teichler (1989c) and Tersoff (1988b, 1989) the original parameters (Tersoff, 1988a) significantly underestimate the bond-bending versus bond-stretching stiffness and hence underestimate the energy contributions from shear deformation so important in the dislocation core.

2) the new parameter set suggested by Tersoff (1988b) to overcome this inadequacy produces a core structure typical of other relaxation techniques (see table 5.3). These methods include other classical potentials and a tight-binding scheme.

3) relaxation using the ab initio code, CETEP, produced an asymmetry around the dislocation cores but there was no evidence for extremely short bond deviations and wide bond angle distortions.

Marklund and Wang (1992) using the same potential and periodic boundary conditions

have obtained a different reconstructed geometry. They find the reconstructed bond is stretched by 4.4% with an even wider bond angle spread (85° to 152°). They propose that their large 256 atom unit cell could be a reason for these highly distorted angles not having been seen in all earlier work. However in section 5.2.1 it was shown that there is negligible structural change between a 64 and 224 oblique unit cell for the Tersoff (1988b) potential. As noted there, similar results were obtained with the other classical prescriptions which includes the Tersoff (1988a) potential. Furthermore, the results obtained here are also in excellent agreement with Heggie and Jones (1987), who modelled a *single* dislocation embedded in a cluster using the same potential. They obtained a core reconstruction where bond lengths were distorted by 1% over bulk values and bond angles by 34% (146°).

The exact reason why Marklund and Wang (1992) have obtained a different core structure is unclear. However the results obtained using this form of Tersoff's potential have illustrated an interesting point which regards the importance of bond angle distortions in determining the electronic structure. Fig. 5.6 shows the Chadi and Vogl Hamiltonian band-structures as calculated for the oblique unit cell relaxed with the Tersoff (1988a) potential. The significant finding is that there exists a *deeper* penetration of the dislocation states into the band-gap than all other cases so far considered in which bond distortions are *much greater* (see chapter 4, figs. 4.16 and 4.17). Even in the cases where the use of an extended cutoff gave bond distortions of up to 12% (see section 5.4.2 and fig. 5.4) there is a comparable penetration of states with the Tersoff (1988a) result here where bond distortions are between -1% and 2% only. This demonstrates that bond length distortions are not the only significant contribution to states in the gap. The consequence of the diminished bond stretching in the case of the Tersoff (1988a) potential is greater bond angle distortions and this clearly has a significant effect.

The reason for this is not difficult to understand by returning to the origins of the diamond-cubic type bonding in Si. This involves the formation of sp^3 hybrids which are *directional* in nature and maximise the overlap of neighbouring orbitals. Overlap is also

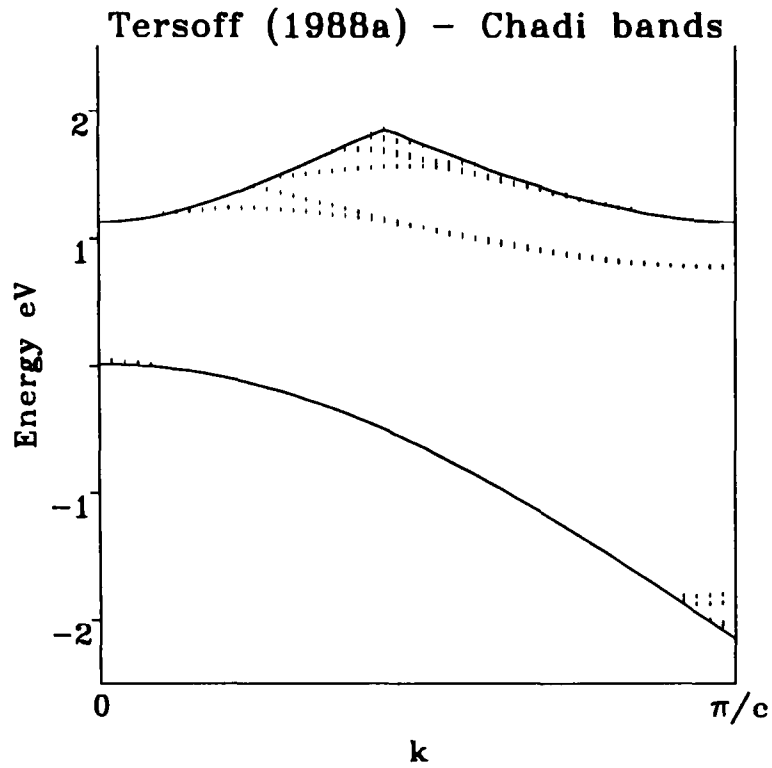

(a)

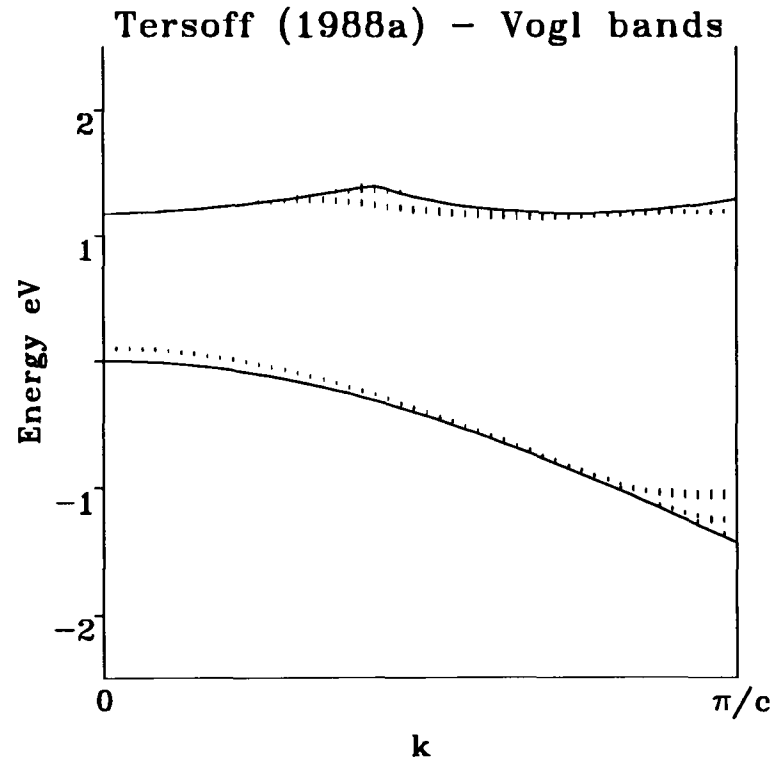

(b)

Fig. 5.6 Band-structures calculated for the oblique 64 atom unit cell relaxed with the Tersoff (1988a) potential. (a) Chadi Hamiltonian bands, and (b) Vogl Hamiltonian bands.

increased, and hence the strength of the bond as well, by bringing the atoms closer together. There is thus a clear desire to maximise orbital overlap which has both a distance *and* directional dependence. It thus seems likely that the core of the 90° partial involves a compromise between the effectiveness of overlap in terms of the spatial distance of two atoms and their directional disposition. The results here indicate that the bond angle distortions, which are often treated with secondary importance, are highly significant in determining the energy of a bond in the core and hence the degree of splitting of the dislocation bands.

A similar result was obtained by Marklund and Wang (1992), where the penetration increased to mid-gap as a result of their larger bond angle distortions, as discussed above, even though the reconstructed bond was stretched by only 4.4%.

As a note, in studies on amorphous Si, angular disorder has been shown to dominate over bond length distortion in terms of its effect on the electronic structure (Joannopoulos, 1977). Further work has shown that dihedral-angle disorder has even greater consequences (Cohen *et al.*, 1980; Singh, 1981).

5.6 Discussion

It has been shown that the reconstruction mechanism in the core of a 90° partial is driven by a purely electronic effect. For this reason, the use of classical potentials in this environment as predictive tools for finding the lowest energy configuration must be questioned. Wilson *et al.* (1990) have also raised this point in their simulations of low index Si surfaces. The result of a symmetric quasi-five-fold reconstructed core, as predicted by the Stillinger Weber and Kaxiras and Pandey potentials, is proposed to be part of a general failing of a classical description of bonding.

In a simple classical prescription, the bond energy is described in terms of its length and angles to neighbouring bonds. This omits essential physics; the strength of a bond not only depends on its distortion, which is usually described in terms of two and three body interactions, but also critically on its local environment which requires the use of a more

general N-body interaction term. Specifically, an atom with many neighbours forms weaker bonds than an atom with few neighbours (see for example Abell, 1985). The quasi-five-fold core contains another difficult property to model, namely the highly stretched bonds will be weakened further by the need to compete with the three shorter bonds. A simple description of the bond energy based purely in terms of its length is clearly inadequate in this case. It thus seems critical, in order to make accurate predictions of the cohesive energy for a particular structure, to involve an effective description of the dependence of the energy of a bond on the local environment.

The Tersoff potential has been shown to be partially successful over other classical attempts to describe the bonding in Si, which is almost certainly because it was constructed around the importance of local bond order. It therefore seems reasonable to suggest that future classical potentials should attempt to describe this physical effect. One particular scheme worthy of note is the Pettifor bond order potential (see chapter 2, section 2.4.1).

The Tersoff (1988a) potential was found to give a core reconstruction significantly different to all other techniques used, giving rise to large bond angle distortions. This type of distortion was shown to be *more* significant over simple bond stretching in its effect on the electronic structure.

The predictions of the Tersoff (1988b) classical potential and two tight-binding Hamiltonians were in general agreement with the ab initio relaxation provided the range of interaction used in these methods was restricted to include no more than the four nearest neighbours. Attempts to include more distant interactions using the Tersoff (1988b) potential and the GSP Hamiltonian led to unreliable results. Both these schemes provide too much weight to second neighbour interactions.

The energetically most stable configuration is the asymmetric four-fold reconstruction as proposed by Jones (1979) and Hirsch (1979). The electronic structure has been shown to clear the indirect band-gap except for the possible existence of very shallow levels near both band edges. The predicted core structure of Marklund and Wang (1992) has been questioned and

the quasi-five-fold core, as discovered by Duesbery *et al.* (1991) and in this work, has been shown to be unstable for electronic reasons.

CHAPTER 6

The effect of phosphorous contamination at dislocations

6.1 Introduction

Using a cluster method with local density functional pseudopotential theory, Heggie *et al.* (1989) found that P is strongly attracted to solitonic sites at the core of a 90° partial (binding energy of between 1 and 1.5eV) resulting in no electronic states in the gap. This lack of electrical activity occurs because the solitonic site is three-fold coordinated. When this site is occupied by a P atom the remaining two electrons pair up to form a lone pair which sits deep in the valence band as originally postulated by Heggie (1987). In later work Heggie *et al.* (1991) showed that if two P atoms take up sites at either end of the reconstructed bond in the 90° partial, the bond breaks allowing both P atoms to adopt the preferred three-fold coordination. This mechanism had a binding energy of 2.3eV and could explain the strong locking effect of P on dislocations in Si (see chapter 1, section 1.3 and 1.4). Electrically the indirect band-gap was again found to be clear of states except for two filled levels close to the valence band edge.

It is intended here to try and reproduce these ab initio results using the more approximate

tight-binding scheme. There are several reasons for this work:

(1) the tight-binding scheme involves 3D periodic boundary conditions and not a cluster.

(2) the programs developed so far have been tested on clean dislocations with reference to earlier work. A similar approach is needed for extension to impurity interactions.

(3) the tight-binding model provides physical and chemical insight into the bonding processes.

(4) the tight-binding scheme is computationally much more efficient than ab initio studies.

An appealing feature of investigating P impurity atoms is that P is expected to be reasonably simple to implement in the current tight-binding scheme. It diffuses substitutionally, is very similar in size to Si, and its bonding is well described by a minimal sp^3 basis (the ab initio studies also used a local basis of s-,p_x-,p_y- and p_z- Gaussian orbitals).

6.2 Generating P-P and Si-P hopping parameters

Three possible interactions must be considered for P impurity atoms in Si, namely Si-Si, P-Si and P-P. The Si-Si interactions will be represented by the Chadi (1984) Hamiltonian. It is thus necessary to obtain hopping parameters to describe the Si-P and P-P interactions.

By studying the form of valence bands Pantelides and Harrison (1975) found that the hopping parameters for covalently bonded materials varied approximately as $1/d^2$. Froyen and Harrison (1979) provided an explanation for this empirical observation by noting the similarity between bands predicted by the Linear Combination of Atomic Orbitals (LCAO) scheme and free-electron bands. Specifically, the shapes of the bands in the two models are very similar, except for band-gaps appearing in the LCAO scheme, and in particular the valence band widths are quite close in both methods. In the LCAO treatment the width of a band scales with the hopping integral, whereas it scales as k^2, or $1/d^2$, in the free electron model, which implies that the hopping integrals should have an inverse square scaling as observed. By equating selected energy differences in the two methods Froyen and Harrison (1979) went on

to derive formulae for a nearest neighbour minimal sp^3 basis which had this inverse square scaling dependence for all the hopping parameters, $h_{ss\sigma}$, $h_{sp\sigma}$, $h_{pp\sigma}$ and $h_{pp\pi}$. This universal formula for generating these hopping parameters based only on the equilibrium bond length is tabulated in Harrison (1980).

The hopping parameters for the Si-P and P-P interactions will be generated by using this table. These interactions thus scale as $1/d^2$ together with the Chadi (1984) Si-Si parameters. The justification for generating parameters from this table is based on P being well described by sp^3 bonding in Si.

6.3 Matching ε_s and ε_p

Care must be taken in using Si-P and P-P hopping parameters generated from the Harrison (1980) table together with those of Chadi (1984) which describe the Si-Si interactions. Chadi assigned ε_s=-5.25eV and ε_p=1.20eV for Si whereas the values given in the Harrison table are -13.55eV and -6.52eV respectively. These values imply a similar s-p splitting in each case (6.45eV for Chadi and 7.03eV for Harrison) but they are clearly placed differently in absolute terms. In considering Si on its own the s-p splitting is important but the absolute values are not. For example, Chadi rigidly shifted ε_s and ε_p to place the valence band edge maximum at 0eV. However, the absolute positions of these two parameters *are* important when considering impurity atoms in Si. If, for example, the values of ε_s and ε_p for P are too low, relative to those for Si, then P will hold on to its fifth electron and will not be readily ionised.

It is not clear how the shift required to match ε_s and ε_p for Si and P should be calculated. A simple shift of the Harrison Si values to the relative position of the Chadi (1984) values would not result in a similar placement of the bands, since this also depends on the hopping integrals themselves. A better approach would be to calculate the shift required to bring the valence band edges of the Si Harrison and Chadi parameters in line. This rigid shift could then be applied to the values of ε_s and ε_p for P.

From Harrison (1980, p.78) the valence band edge maximum is given by

$$E_v=\varepsilon_p-4(1/3h_{pp\sigma}+2/3h_{pp\pi}) \tag{6.1}$$

which using Chadi's Si parameters gives E_v=0eV and with the universal Harrison parameters for Si gives E_v=-9.5eV. The values of the free atomic energies given for P in the Harrison table are thus shifted by +9.5eV to be commensurate with the Chadi Si Hamiltonian values, and become ε_s=-7.6eV and ε_p=1.17eV.

6.4 An initial parameterisation

The hopping parameters can be generated from the Harrison (1980) table by using the equilibrium bond lengths for Si-P and P-P. P exists in several allotropes but the most common is the white P_4 form (Greenwood and Earnshaw, 1984). The P_4 tetrahedrons have each P atom three-fold coordinated to the other three P atoms, with a P-P bond length of 2.21Å and P-P-P angles of 60°. The universal hopping parameters for this equilibrium bond length were generated from the Harrison table.

There was no similar experimental reference point for the Si-P equilibrium bond length. Heggie *et al.* (1991) had considered a lone P substitutional atom in crystalline Si, and found an equilibrium bond length for Si-P of 2.41Å. However, P is known to diffuse substitutionally giving rise to lattice *contraction* (EMIS datareviews No.4, 1988). Following Robertson (1983b), who used the work of Van Vechten and Phillips (1970) in which covalent radii in tetrahedrally coordinated crystals were calculated, an equilibrium bond length for Si-P of 2.34Å has also been considered here. Hopping parameters for an Si-P bond length of both 2.34Å and 2.41Å were generated from the Harrison table.

As with the Chadi Hamiltonian a simple A/d^4 pair potential is assumed for both the Si-P and P-P interactions. The parameter A is fitted to produce the required equilibrium bond length for the appropriate hopping parameters. For the P-P interaction, simulations were performed on a P_4 molecule at the centre of a large unit cell to avoid interactions with periodic

images. The pair potential parameter was adjusted so that the structure gave a P-P bond length of 2.21Å as required.

A single P atom in a cubic unit cell of 64 atoms was used to calculate the pair potential parameters for the two sets of Si-P hopping integrals. A k-point sampling of $q=3$ was adopted and the structure minimised to obtain the Si-P bond length in each case. The pair potential parameters were adjusted to produce relaxed structures with Si-P bond lengths of 2.34Å and 2.41Å using the hopping parameters generated for these respective bond lengths.

6.4.1 P as a donor dopant atom

These simulations of a single P atom in a unit cell of perfect diamond cubic Si were used to investigate the donor atom properties of the P impurity. The presence of the P atom was found to give a clear gap except for a state lying approximately 0.01eV and 0.017eV[1] below the conduction band edge for the 2.34Å and 2.41Å hopping parameters respectively. Further analysis indicated that the P atom had lost some charge which had been reasonably evenly distributed over all the Si atoms. For example, the 2.41Å hopping parameters predicted a charge on the P atom of 4.17 electrons, with a typical value of 4.013 electrons being found on each Si. The 2.34Å hopping parameters gave similar results with slightly more charge leaving the P atom (4.12 electrons remained).

These results are typical of the effect due to a chemical donor impurity, containing five valence electrons, in a semiconductor. The resulting shallow donor level below the conduction band edge gives rise to a weakly bound fifth electron with a large *effective* Bohr radius. These results indicate that the matching of ε_s and ε_p has been qualitatively successful.

6.4.2 P at the core of a 90° partial dislocation

The P impurity interaction with the 90° partial is modelled within the 64 atom *oblique* unit

---

[1] Kittel (1986), *Introduction to Solid State Physics*, gives a value of 0.045eV for the P donor level in Si.

cell containing a dislocation dipole (see chapter 4, fig. 4.8b). The starting configuration is the Chadi (1984) Hamiltonian relaxed structure given in chapter 5, table 5.3. The same *k*-point sampling (*set 3*, see table 5.2) used to obtain this starting structure is used here. To avoid any possible discontinuities in the forces all states are occupied according to the Fermi-Dirac distribution at a temperature of 100°K (see chapter 3, section 3.4.2).

A system which involves two P atoms interacting will also involve Si-P interactions. It is thus sensible to test the Si-P hopping parameters first by considering a single P atom at each dislocation core within the unit cell. Following the work of Heggie *et al.* (1991) the P impurity is placed at one of the Si core sites, illustrated in fig. 6.1a for one of the dislocations. Notice that use of periodic boundary conditions implies a line of P atoms down the dislocation. Using both the 2.34Å and 2.41Å hopping parameters the Si-P bond was found to become significantly stretched. The length of this bond was similar in both cases (2.9Å for the 2.34Å hopping parameters and 3.0Å for the 2.41Å hopping parameters). These findings are in reasonable agreement with the ab initio work which also predicted this lengthening, or "breaking", of the Si-P bond (2.8Å). These results indicate a qualitatively correct description is provided by the Si-P hopping parameters.

Fig. 6.1b illustrates the situation where two P atoms have migrated to positions on either end of the same reconstructed bond. Note that the model consists of a chain of P atoms down the dislocation line as a result of the periodic conditions. This illustrates a disadvantage of the supercell scheme over the cluster method, and a better description would be provided by considering several periods down the dislocation line to separate the P-P bonds[2].

The P-P cross-core bond was found to *shorten* using both hopping parameter sets in disagreement with Heggie *et al.* (1991) in which the P-P bond broke by lengthening to 3.14Å. The above results on one P atom at the core had resulted in the P atom moving toward a state of three-fold coordination and so doubt was cast on the P-P hopping parameters.

---

[2] unfortunately to properly separate the P atoms leads to unit cells that are too large to be considered with the present computing resources.

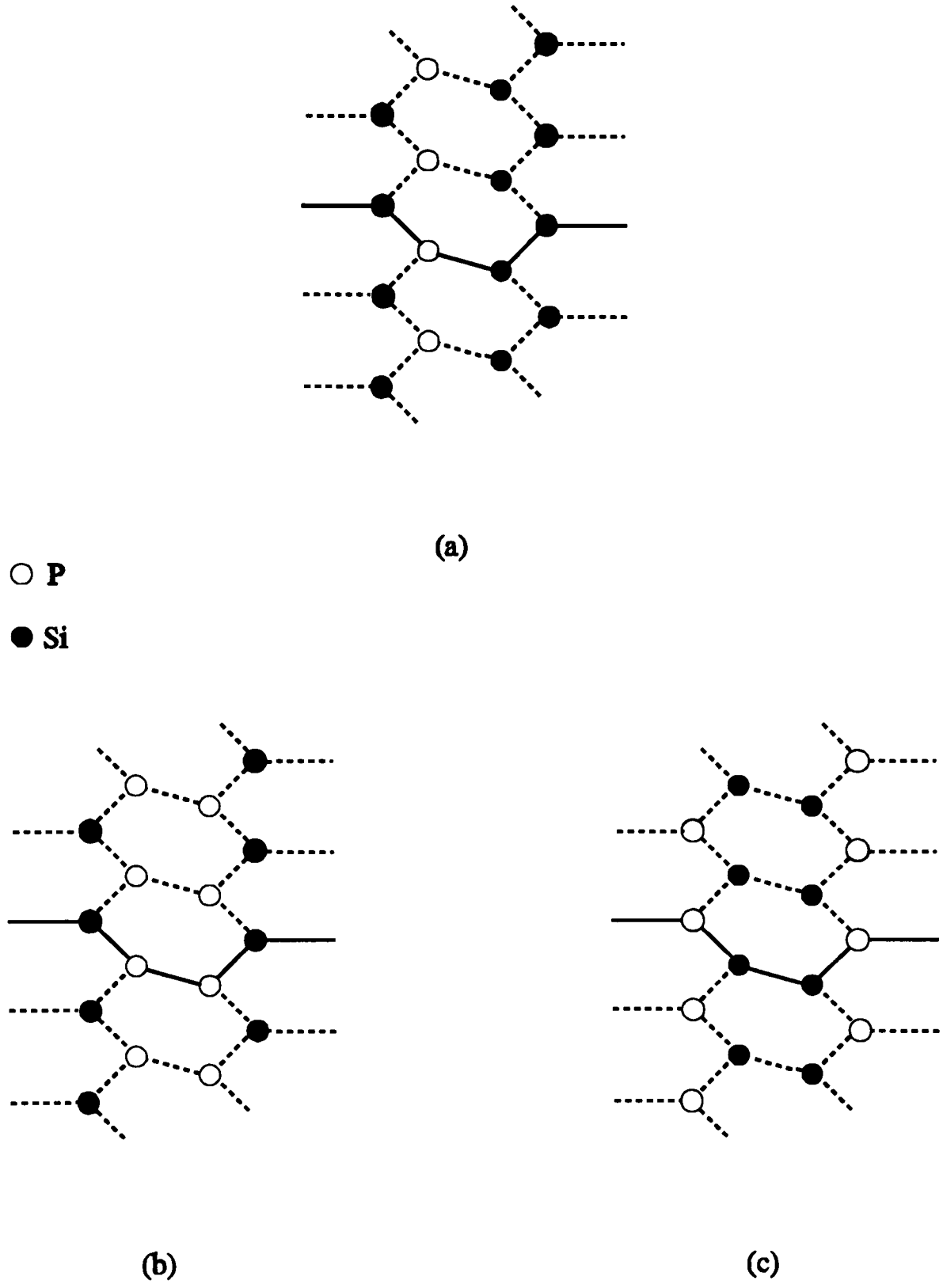

Fig. 6.1 Schematic illustration of the atomic coordinates within the core of a 90° partial dislocation on the (111) slip plane. The unit cell contains only one period down the dislocation line and contains the atoms linked by the solid bonds. The dashed bonds represent periodic images. (a) single P at the core, (b) two P atoms on either end of the reconstructed bond and (c) two P atoms on sites just off the reconstructed bond.

The problem is related to the parameterisation of the P-P interaction using the bond length in the P_4 molecule to generate the hopping integrals. The P_4 molecule is highly stable because each P is bonded to three others leaving a lone pair on each P atom on the opposite side to the three bonds (see Greenwood and Earnshaw, 1984). The short bond length of 2.21Å reflects the stability of the structure. A P-P bond in tetrahedrally coordinated Si will be longer and weaker, because the P atoms must take part in sp^3 hybridisation. Furthermore, it should be noted that the bond angle of 60° in the P_4 molecule is not applicable to a substitutional site in Si.

The strength of the hopping integrals generated by the table of Harrison (1980) are directly related to the equilibrium bond length. The resulting parameters obtained for the short P-P bond length of 2.21Å will result in a very strong bonding interaction. While this is appropriate for the P-P bond in the P_4 molecule it is likely to overestimate significantly the actual bond energy applicable in a tetrahedral environment. This is consistent with the findings that the P-P cross-core bond does not want to break.

The findings here illustrate the familiar requirement that the fitting of hopping integrals should be performed in the environment to be modelled.

6.5 A second parameterisation

A more realistic approach would be to generate hopping parameters based on the P-P equilibrium bond length in a tetrahedral environment. Unfortunately the ab initio work by Heggie *et al.* had no reason to calculate this bond length and there are no experimental results for this situation. A very simple estimate of the P-P bond length can be provided by again considering the covalent radii of P in a tetrahedral site in Si (Robertson, 1983b). This implies a P-P bond length of 2.34Å. In this new approach then, the Si-P and P-P bond lengths are assumed to be the same. Since the ab initio work predicted a Si-P bond length of 2.41Å a P-P equilibrium bond of this length has also been considered.

Parameterisation is considerably easier under the assumption that the Si-P and P-P

equilibrium bond lengths in a tetrahedral environment are the same. The universal Harrison hopping parameters depend only on the bond length and this implies that the hopping parameters to describe the Si-P and P-P interactions are the same. The hopping integrals used are those generated for the Si-P interactions in the initial parameterisation.

As described in section 6.4, the pair potential parameter for the Si-P interaction was adjusted to obtain the appropriate equilibrium bond length for a single P atom in a cubic unit cell of perfect diamond cubic Si containing 64 atoms. With this parameter obtained for the two hopping parameter sets generated at 2.34Å and 2.41Å, the P-P pair potential parameter is then similarly obtained; this time two P atoms in adjacent sites are relaxed in the same cubic unit cell and the pair potential parameter adjusted to obtain the appropriate bond length for the set of hopping parameters used (ie. 2.34Å or 2.41Å).

6.5.1 P at the core of a 90° partial dislocation

The predictions of a single P atom at the core have already been discussed in section 6.4.2. The new P-P parameters are tested by again considering two P atoms at the core as illustrated in fig. 6.1b. Both the 2.34Å and 2.41Å Hamiltonian parameters resulted in the P-P bond stretching to a point where it could be considered broken (2.98Å and 3.06Å respectively). These results are consistent with the ab initio findings, although Heggie *et al.* (1991) found the P atoms moved even further apart (3.14Å). However, the promise of this new parameterisation was short lived when the situation in fig. 6.1c was considered, to investigate the locking effect predicted by the tight-binding model. In contradiction to the ab initio work the binding energy of this configuration was found to be significantly lower than when the P atoms occupy the sites in fig. 6.1b. Thus while these tight-binding parameters seem to predict correctly the P atoms preferring a state of three-fold coordination when at the core, they also predict that the P atoms will never migrate to these positions but will remain four-fold coordinated in the bulk!

The problem can be traced to an inconsistency in matching the Chadi (1984) Si-Si

parameters and those generated from the Harrison (1980) table for the Si-P and P-P interactions. While the values of ε_s and ε_p were shifted to be consistent (section 6.3) there is still a problem with the hopping integrals themselves. This can be understood by comparing the Si-Si hopping parameters of Chadi (1984) with those generated from Harrison (1980) and this is done in table 6.1.

Parameter	Chadi (1984)	Harrison (1980)
$h_{ss\sigma}$ (eV)	-1.938	-1.93
$h_{sp\sigma}$ (eV)	1.745	2.54
$h_{pp\sigma}$ (eV)	3.050	4.47
$h_{pp\pi}$ (eV)	-1.075	-1.12

Table 6.1 Comparison of Chadi (1984) Si-Si hopping parameters and those generated from the Harrison (1980) table. Note the significant difference between $h_{sp\sigma}$ in the two prescriptions and also between $h_{pp\sigma}$.

The Harrison generated parameters were originally adjusted to reproduce the hopping parameters obtained by Chadi and Cohen (1975) for Si and Ge. Chadi (1984) altered these Si parameters in his work on structural and energy calculations on Si surfaces. It can be seen from table 6.1 that $h_{ss\sigma}$ and $h_{pp\pi}$ are very similar in the two prescriptions, but $h_{sp\sigma}$ and $h_{pp\sigma}$ are significantly different. However, it is these latter two hopping integrals that provide nearly all the bonding energy in diamond cubic (Paxton and Sutton, 1989; see table 6.2), which illustrates the highly directional nature of the bonding. The result is that the Harrison Si-Si parameters predict lower bonding energies than the Chadi (1984) Hamiltonian. Since the Si-P and P-P parameters are generated from the Harrison table, this inconsistency is carried through to the current work. This can be seen from table 6.2.

The energy of the Si-P and P-P bonds, being almost entirely determined by $h_{sp\sigma}$ and $h_{pp\sigma}$, are clearly much more negative than the Si-Si bond energy predicted by the Chadi parameters. The consequence of this improper matching of the two sets of parameters is that two P atoms will contribute the greatest bonding energy to the system when each is able to form four

Interaction	$B_{ss\sigma}$ (eV)	$B_{sp\sigma}$ (eV)	$B_{pp\sigma}$ (eV)	$B_{pp\pi}$ (eV)
Si-Si Chadi (1984)	-0.81	-2.47	-4.25	-0.60
Si-P (2.34Å)	-0.64	-3.72	-6.52	-0.55
Si-P (2.41Å)	-0.56	-3.44	-6.19	-0.51
P-P (2.34Å)	-0.60	-3.65	-6.51	-0.46
P-P (2.41Å)	-0.49	-3.30	-6.15	-0.43

Table 6.2 Comparison of the component bond energies for the Chadi (1984) Si-Si interaction and the Si-P, P-P interactions given by the two sets of Si-P and P-P hopping parameters generated at 2.34Å and 2.41Å. Note the significantly lower bond energies for $B_{sp\sigma}$ and $B_{pp\sigma}$ given by the Si-P and P-P parameterisations, generated from the Harrison (1980) table, compared to those given by the Chadi (1984) Hamiltonian.

bonds. It is thus energetically favourable for each P to remain surrounded by four Si neighbours rather than migrating to the core to adopt the three-fold coordination that is predicted if they arrive there. Consequently the situation illustrated in fig. 6.1c is lower in energy than that of fig. 6.1b, and there is no tendency for the P to segregate to the dislocation core.

6.6 Final Hamiltonian hopping parameters developed

One solution to this problem would be to dispense with the Chadi (1984) Hamiltonian and to generate Si-Si parameters from the Harrison table. In this way everything would be consistent. However, Chadi (1984) adjusted the Chadi and Cohen (1975) parameters to produce better structural predictions and further it is these parameters that have been used throughout the rest of this thesis. It is therefore desirable to maintain the Chadi (1984) parameters, and thus the Si-P and P-P hopping parameters must be scaled to match these.

Both previous parameterisations have indicated insignificant differences in the results predicted by the hopping parameters generated at 2.34Å and 2.41Å. The new parameters considered here are generated for an equilibrium bond length of 2.41Å only, this being the length of the Si-P bond found in the ab initio studies. The matching can be performed by

suitably scaling the $h_{sp\sigma}$ and $h_{pp\sigma}$ parameters of the Si-P and P-P hopping parameters to be consistent with the Chadi (1984) set. From table 6.1 it can be seen that the Harrison (1980) values of $h_{sp\sigma}$ and $h_{pp\sigma}$ can be scaled to those given by Chadi (1984) by multiplying them by 1.745/2.54=0.687 and 3.05/4.47=0.682 respectively. This same scaling is then imposed on the Si-P and P-P parameters.

The question of what values of ε_s and ε_p for P are appropriate must be reconsidered having scaled these hopping integrals. The Harrison (1980) value for $h_{pp\pi}$ is the same but the scaled value of $h_{pp\sigma}$ is now 3.05eV as opposed to 4.47eV. Use of eqn. 6.1 now predicts a valence band edge at -7.6eV. Consequently a shift of +7.6eV is applied and gives values of ε_s=-9.5eV and ε_p=-0.73eV. The inconsistency of applying this shift as calculated for a Si-Si bond length of 2.3517Å and then considering Si-P and P-P hopping parameters generated at 2.34Å and 2.41Å may have been already noted by the reader. Clearly the attempt here is to produce as reliable an estimate as possible, but these inconsistencies can only be eliminated by having more appropriate experimental or theoretical results to fit to. In this case, the best indication of the effectiveness of the matching of ε_s and ε_p is to investigate how well the parameters describe the donor properties of substitutional P in diamond cubic Si, as discussed in section 6.4.1. Using the new hopping parameters and values of ε_s and ε_p gave a very poor description of the donor properties of P. Specifically, a single P atom in a unit cell of diamond cubic Si was found to gain even more charge (5.1 electrons) rather than donating its extra electron. This clearly indicates that the new placement of ε_s and ε_p is incorrect. By lowering the absolute placement of ε_s and ε_p more charge can be made to leave the P atoms, and hence a second parameterisation was considered using the old values of ε_s and ε_p. A donor level was found at 0.14eV below the conduction band edge and the P atom had donated most of its charge (4.25 electrons remained). The ab initio studies found the P donor level to be 0.6eV below the conduction band edge (the gap is enlarged to 4.5eV in this work due to interactions with the terminating H atoms, see Heggie *et al.*, 1989). By assuming a linear scaling of this

level with the band gap, this implies a donor level of 0.13eV. This second parameter set thus provides good agreement with the ab initio studies, and is listed in table 6.3, together with the Chadi (1984) parameters for reference.

Parameter	Chadi (1984) Si-Si	Si-P / P-P
$h_{ss\sigma}$ (eV)	-1.938	-1.84
$h_{sp\sigma}$ (eV)	1.745	1.66
$h_{pp\sigma}$ (eV)	3.050	2.90
$h_{pp\pi}$ (eV)	-1.075	-1.07
ε_s for Si (eV)	-5.25	-
ε_p for Si (eV)	1.20	-
ε_s for P (eV)	-	-7.6
ε_p for P (eV)	-	1.17
Pair potential parameter for Si-Si (eVÅ^4)	4.065494	-
Pair potential parameter for Si-P (eVÅ^4)	-	3.763
Pair potential parameter for P-P (eVÅ^4)	-	3.54

Table 6.3 The final parameterisations considered for describing Si-Si, Si-P and P-P interactions. The Si-Si parameters are from Chadi (1984). The Si-P and P-P parameters are generated from the Harrison (1980) table assuming an equilibrium bond length of 2.41Å for both interactions. These parameters are then scaled to make them consistent with the Chadi ones, as described in the text.

The pair potential parameters are again fitted by performing simulations on a single P and two P atoms in a unit cell of diamond cubic Si, as discussed earlier. The pair potential parameter for the Chadi Hamiltonian is determined by the equilibrium condition for the bulk Si crystal at the experimentally observed lattice parameter.

6.6.1 P at the core of a 90° partial dislocation

The predictions of the Si-P hopping parameters are tested by considering a single P atom at the core of the 90° partial, as illustrated in fig. 6.1a. The reconstructed bond was found to

"break", increasing to a length of 3.0Å, which agrees with the findings of earlier parameterisations and reasonably well with the ab initio work (2.8Å bond length in this case). This is a surprising result, since the Si atom at the end of this broken bond is also in a state of three-fold coordination. Heggie *et al.* (1991) found that the extra electron on the Si preferred to sit close to the P atom! These results demonstrate that the P atom clearly prefers to sit in a state of three-fold coordination at the core.

The migration of two P atoms to the core was found to be energetically unfavourable using an earlier parameterisation (section 6.5.1), and the possible reasons for this were discussed there. A similar analysis is undertaken here using the Hamiltonian parameters of table 6.3.

Following the work of Heggie *et al.* (1991) two P atoms are placed at sites just off the reconstructed bond, as illustrated in fig. 6.1c. The relaxation resulted in some distorted bonds; the reconstructed Si-Si bond lengthened to 2.48Å and stretched bonds of 2.43Å and 2.63Å were found in the Si-P back bonds. The use of periodic boundary conditions results in lines of P atoms, see fig. 6.1c, and so a direct comparison with the ab initio cluster results is inappropriate. However, in their simulation of two P atoms occupying these sites just off the reconstructed bond Heggie *et al.* obtained a reconstructed bond length of 2.46Å and lengthening in the back bonds of 2.48Å and 2.54Å. This indicates that the tight-binding scheme is providing reasonable results. The resulting band-structure for the tight-binding relaxed structure is shown in fig. 6.2a. The existence of a band of states that lies at a mid-gap level is again in agreement with the ab initio findings.

The two P atoms were now placed at the core sites, as in fig. 6.1b. As found in the earlier parameterisation (section 6.5.1) the P-P bond was found to spontaneously "break" having lengthened to 2.95Å. Unlike the predictions of the previous parameters, this relaxed structure was found to be 0.64eV *lower* in energy per dislocation per repeat period, than the relaxed structure of fig. 6.1c. This is consistent with the ab initio findings, although Heggie *et al.* find a much greater binding energy difference of 2.3eV. The new parameters thus correctly predict that not only will two P atoms adopt three-fold coordination at the core, they will move from

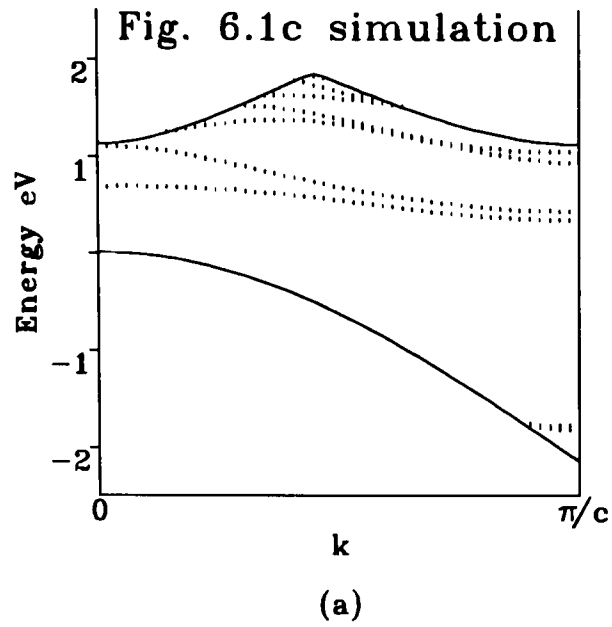

(a)

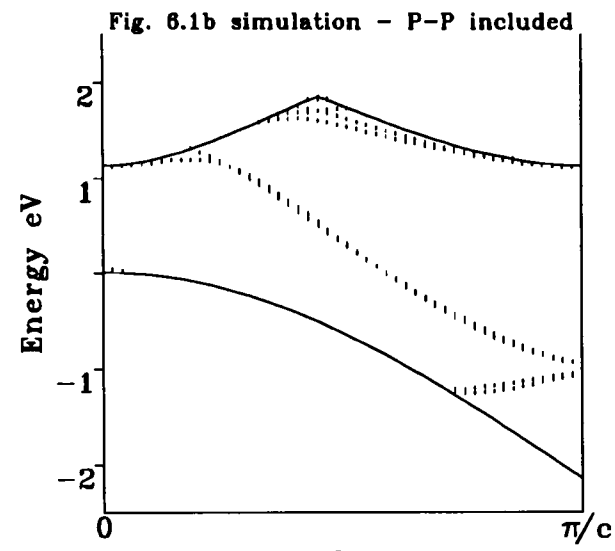

(b)

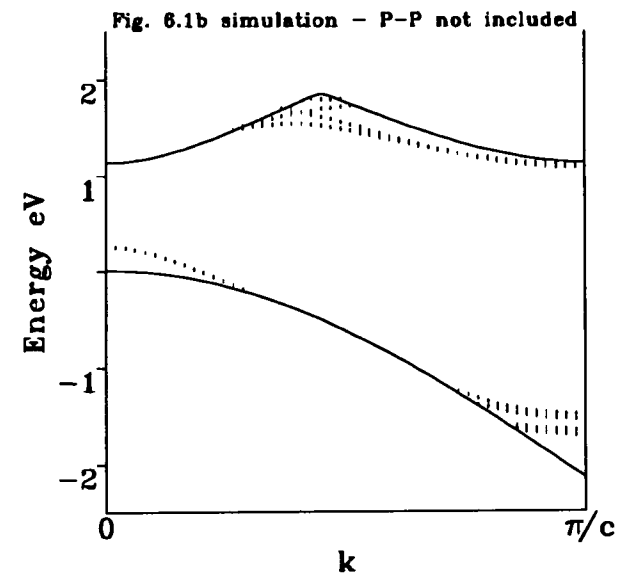

(c)

Fig. 6.2 Projected band-structures in eV for the reconstructed 90° partial along the dislocation line. The solid lines show the edges of the bulk valence and conduction bands. $c=a_0/\sqrt{2}$ is the repeat period along the dislocation. (a) 2 P atoms placed as in fig. 6.1c, (b) two P atoms as in fig. 6.1b with the P-P bond included in the Hamiltonian, and (c) the same case as (b) but with the P-P interaction *not* included in the Hamiltonian.

the bulk to do so. The band-structure for this case is shown in fig. 6.2b. Unfortunately a band of states spanning the gap is not consistent with the findings of the ab initio work, which found a virtually clear band-gap as a result of the three-fold coordinated P atoms.

The problem lies again with the simple $1/d^2$ hopping parameter scaling which does not decay realistically with distance and significantly overestimates highly stretched bonds, as occur here. The overestimation of distant interactions by simple scaling laws, like an inverse square scaling, was the motivation for producing a more realistic functional form for Goodwin *et al.* (1989).

In anticipation of the breaking of the P-P bond, a large cutoff, r_t=3.26Å, was used. By reducing this to r_t=2.9Å the P-P interaction can be de-coupled from the Hamiltonian, and the P atoms have become truly three-fold coordinated. The important finding is that by simply eliminating this interaction the energy is *lowered* by 0.83eV per dislocation per repeat period down the dislocation. This can be understood from fig. 6.2c, in which the band-gap has become broadly clear as a result of *not* including the P-P interaction in the Hamiltonian[3]. Relaxation using this lower cutoff leads to the P atoms moving in until the moment that the P-P interaction starts to be included[4]. The resulting band-structure is virtually indistinguishable to fig. 6.2c, since the P atoms are still three-fold coordinated. These findings demonstrate that the P-P bond does indeed want to break, since any interaction between the P atoms leads to an increase in energy. The problem with trying to describe a bond "breaking" process using a $1/d^2$ scaling is clearly unrealistic. A more realistic hopping parameter scaling law needs to be developed for future work.

By treating the P atoms as three-fold coordinated in this case, fig. 6.1b, a different energy comparison to the configuration of fig. 6.1c can be made. The binding energy of the first case is now found to be 1.5eV per dislocation per repeat period down the dislocation line *lower*

---

[3] Similar results were found with the previous parameters of section 6.5.

[4] Recall that the hopping integral and pair potential scalings are smoothly brought to zero at r_t (see chapter 3, section 3.4 and fig. 3.2).

than the second. The original finding of 0.64eV will be too small, due to the overestimation of the P-P interaction using the inverse square scaling, and the value of 1.5eV is likely to be too large because in practise there will be some interaction between the P atoms. Regardless of this point, the tight-binding scheme underestimates the binding energy gained by having the two P atoms three-fold coordinated at the core when compared to the ab initio findings. The reason for this is discussed below in section 6.7.

6.6.2 P at the core of an unreconstructed 30° partial dislocation

A preliminary investigation of P interaction at the 30° partial has been undertaken. The parameters listed in table 6.3 have been used and the analysis has been performed on the unreconstructed 30° partial, since the number of atoms that needs to be considered is half that for the reconstructed configuration. The analysis is thus aimed at investigating the affinity for P atoms to three-fold coordinated sites in the 30° partial. The unit cell is rectangular and contains 128 atoms and a 30° partial quadrupole, see chapter 4, fig. 4.18b.

Fig. 6.3a illustrates the band-structure of the clean unreconstructed 30° partial dislocation. The dispersion obtained in other schemes (Northrup *et al.*, 1981; Veth and Teichler, 1984) is lacking here probably because the Hamiltonian cutoff does not include the interacting dangling bonds down the dislocation line. These lie a full second neighbour bonding distance away from each other. Nonetheless, the Si dangling-bond gives rise to a band of states penetrating into the indirect band-gap below the conduction band edge.

Four P atoms, one for each partial, were now placed at the dangling-bond sites as illustrated in fig. 6.4a. The significant result is that the band-gap is now found to be clear of states, fig. 6.3b. The P atoms are thus able to passivate dangling-bond sites, and a similar result is expected for a 30° partial soliton.

To investigate the tendency for P to migrate to these dangling-bond sites a second simulation involving four P atoms was performed. In this case the P atoms were placed just off the dangling-bond sites, as illustrated in fig. 6.4b. The relaxed configuration was found

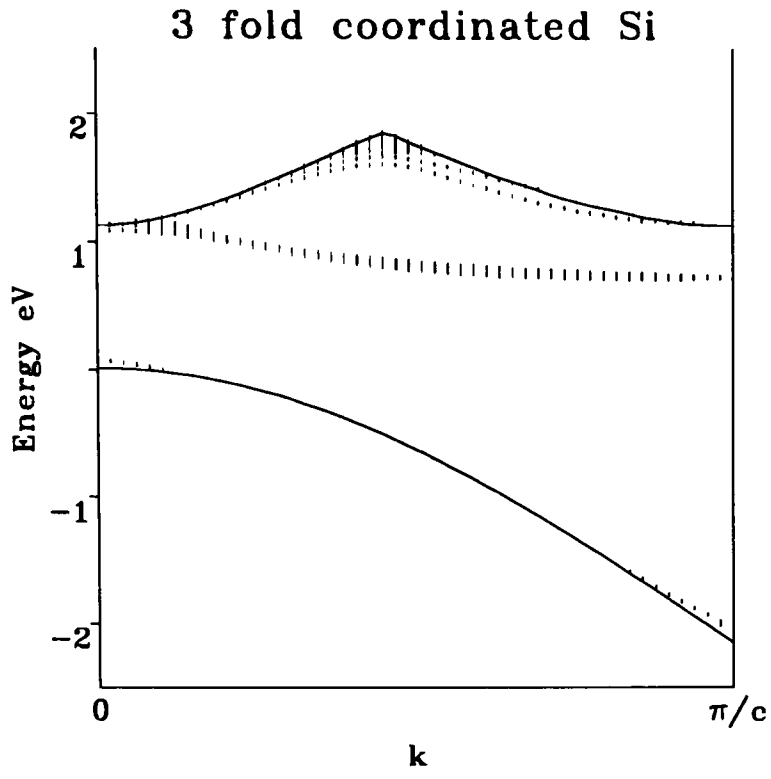

Fig. 6.3 Band-structures calculated for a 128 atom rectangular unit cell containing an unreconstructed 30° dislocation quadrupole. (a) the clean dislocation, and (b) P atoms occupying the three-fold coordinated sites, as in fig. 6.3a.

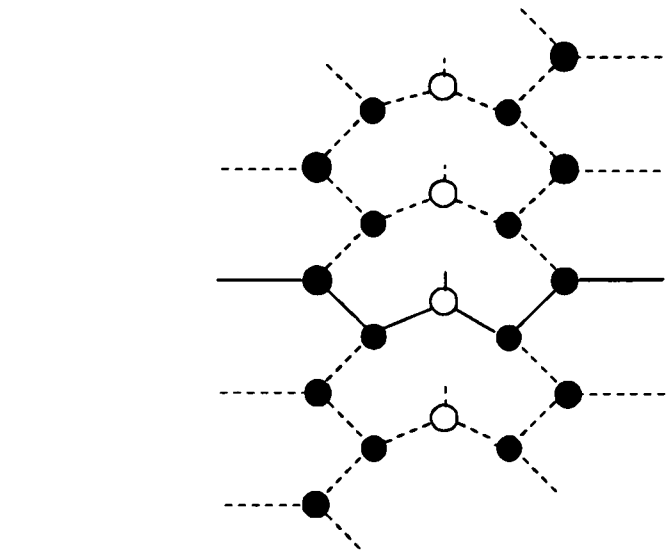

(a)

○ P

● Si

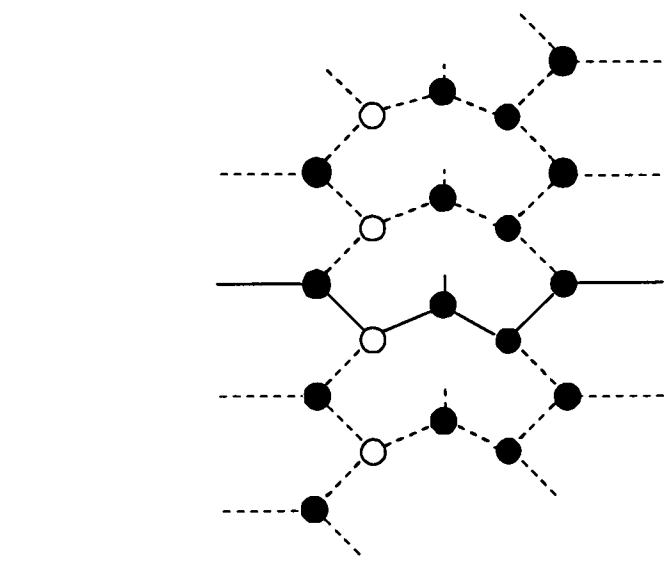

(b)

Fig. 6.4 Schematic illustration of the atomic coordinates within the core of a 30° partial dislocation on the (111) slip plane. The unit cell contains only one period down the dislocation line and contains the atoms linked by the solid bonds. The dashed bonds represent periodic images. (a) single P at the three-fold coordinated core site, (b) P atom positioned just off the dangling-bond site.

to be 0.63eV per dislocation per repeat period along the dislocation *higher* in energy than when the P atoms occupy the dangling-bond sites. There is thus a significant energy gain by having the P atoms migrate to the core to replace the three-fold coordinated Si atoms.

6.7 Discussion

In principle P represents one of the simplest impurity atoms that can be considered in a tight-binding scheme. However, the lack of ab initio and experimental data for substitutional P in Si leads to severe difficulties in obtaining a reliable Hamiltonian parameterisation. For example, hopping parameters for Si, Ge, GaAs etc. can all be generated to optimise the fit to an accurate ab initio calculation of the band-structure. This would eliminate the difficulties in realistically matching parameterisations generated with different schemes, which has clearly been a problem here. An ab initio calculation on the length of the P-P bond for substitutional P in Si would be useful. Currently the equilibrium bond length has been based on the covalent radii for tetrahedral sites in Si; this leads to the use of identical Si-P and P-P bond lengths.

Despite these difficulties, the final parameterisation listed in table 6.3 provides good qualitative agreement with the ab initio findings of Heggie *et al.* (1991). Substitutional P in Si involves the four-fold coordination sp^3 hybridisation and results in the extra electron of the P being donated. However, a single P atom that migrates to the core, fig. 6.1a, is found to adopt three-fold coordination. Two P atoms at the end of one reconstructed bond are found to break this bond and essentially to clear the band-gap of states, although the problems with this analysis, due to the inverse square scaling used here, have been discussed. The binding energy for this process lies between 0.64 and 1.5eV per dislocation per repeat period down the dislocation, which indicates that two P atoms can lead to a significant locking effect.

The P atoms have also been found to be drawn to dangling-bond sites in the unreconstructed 30° partial. They are strongly bound to these three-fold coordinated sites, with a binding energy of about 0.63eV per dislocation per repeat period down the dislocation line. Having replaced the three-fold coordinated Si, the P atoms lead to essentially no states within

the indirect band-gap.

The tight-binding model will always underestimate this binding energy because it is unable to describe some important quantities that are incorporated in an ab initio scheme. Movement into a state of three-fold coordination leaves the P atoms with a lone pair. The exchange-correlation interaction will lead to a lowering of the total energy because the electrons in this lone pair have opposite spins. The tight-binding scheme is unable to describe this energy lowering. In the case where two P atoms sit on either end of the reconstructed bond in the 90° partial, fig. 6.1b, there is also an electrostatic repulsion that will act to move the P atoms apart, because they are positively charged. This type of interaction is also absent from the tight-binding scheme. Clearly the stability of the three-fold coordinated P atoms that result from the breaking of this bond will be strongly dependent on the energy lowering from both the exchange-correlation and electrostatic interactions.

It is however significant that the tight-binding scheme, which lacks these interactions, produces a qualitatively good description of the P impurity and its desire to become three-fold coordinated. This implies that the underlying mechanism that leads to the stability of the three-fold over the four-fold P state is present in the tight-binding scheme. It is also readily understood. Formation of sp^3 hybrids for P results in only four of its electrons being able to "bond" and leads to its donor properties. However, in a three-fold coordinated site the P atom forms three covalent bonds and the two electrons remaining form a lone pair; in ideal circumstances the three-fold bonding is p-like at roughly 90°, leaving an s-like lone pair that sits deep in the valence band (Robertson, 1983a). In a defect environment, such as a dislocation, the P atom might be able to move from a state of sp^3 hybridisation, which gives rise to a high energy occupied state, toward a three-fold bonding state involving the formation of new hybrids. In general the P atom will be in a state of hybridisation which is somewhere between the ideal p-type three-fold and the four-fold sp^3, but this configuration will necessarily lead to occupied states that are lower than in the donor case. The resulting gain in band energy can be considerable.

A good example of this strong affinity for three-fold coordinated sites is given by the doping of amorphous Si. This was found to be particularly difficult because donor atoms like P immediately segregated to three-fold coordinated sites, thereby lowering the total system energy.

6.8 Boron

Unlike P, B is found to have a very weak locking strength (Imai and Sumino, 1983). A possible explanation for this experimental finding is postulated here based on the unique chemistry of B. Only a brief introduction to B is given here and the reader is referred to Greenwood and Earnshaw (1984) for a comprehensive description of its chemistry.

B is the only non-metal in group III of the periodic table. It tends to form covalent, molecular compounds, but it differs from elements such as Si in having one less valence electron than the number of valence orbitals (electron deficiency). The resulting covalent bonding thus tends to consist of multicentre bonding. The boranes are characterised by this type of bonding, B_2H_6 consisting of two BH_2 groups linked by two bridging H atoms which form a 3 centre 2 electron bond.

B does exist in a three-fold coordinated state in, for example, the trihalides, BX_3. However, these boron trihalides form many molecular addition compounds, LBX_3, with molecules, L, possessing a lone-pair of electrons. The tetrahalogeno borates, BX_4^- are the special case in which the ligand is X^-. Thus the chemistry of B is dominated by its desire to obtain a share of sufficient electrons, under the constraint of covalent-type bonding.

A substitutional B atom in Si will act as an acceptor because of its valence of just three electrons. Evidence from Nuclear Magnetic Resonance (Greenbaum and Carlos, 1984) illustrates that B and P exist predominantly in a three-fold coordinated state in amorphous Si. It is tempting to deduce from this that the three-fold coordinated state is much more stable than four-fold sites. However, it is likely that B occupies three-fold coordinated sites because the *total system energy* is reduced in comparison to the case where a Si atom, and its

associated dangling-bond, occupy the site.

It is clear from the brief discussion above that B is electron deficient. It is thus almost certain that if two B atoms were to find themselves at either end of a reconstructed bond, as in the configuration of fig. 6.1b, the B atoms would move apart and the bond would break. The only conceivable way in which these two B atoms would remain four-fold coordinated is if multicentre bonding with surrounding Si atoms could be established. This seems unlikely and the belief is that two B atoms would break the reconstructed bond and adopt three-fold coordination, as in the case of P.

So why is there only a weak locking effect? The crucial difference is that the valence of P makes this bond breaking highly favourable. In a tetrahedral environment P must partake in the formation of sp^3 hybrids which leads to a highest filled state just below the conduction band. However, by adopting three-fold coordination the P has two extra electrons which can pair up in a lone pair and the gap is essentially cleared of states. It is thus energetically favourable for two P atoms to migrate from the bulk and break an existing Si-Si bond, since both P atoms move from a four-fold to the chemically preferred three-fold coordination.

Thus while the total system energy will be lowered by P or B atoms replacing Si atoms at any three-fold coordinated soliton sites, the locking effect in terms of two impurity atoms breaking a reconstructed bond will be different. Indeed, it seems unlikely that two B atoms will ever migrate to positions at either end of the reconstructed bond. This is because the B atoms are likely to remain in the bulk where they have a share of more electrons. Fundamentally, there is no similar chemical advantage for B to break bonds to adopt three-fold coordination as there is for P. Any locking due to the presence of B at or near the dislocation core is likely to be weak.

CHAPTER 7

Copper and its interaction with the 90° partial dislocation

7.1 Introduction

Cu is the fastest diffusing transition element in Si (EMIS datareviews No.4, 1988). It diffuses interstitially and stays predominantly on interstitial sites at high temperature in thermal equilibrium. Combined with a low solubility, Cu and transition metals in general have serious consequences during device manufacture. They invariably lead to the introduction of deep levels and are excellent recombination centres (Bergholz *et al.*, 1991). Transition metal contamination control is thus a key factor for high and stable device yields.

Cu segregates to dislocations and leads to changes in the electrical activity. EBIC work indicates that contamination by transition metal impurities causes strong electrical activity at dislocations (Fell and Wilshaw, 1991; Radzimski *et al.*, 1991). Photoluminescence work by Lightowlers *et al.* (1989) and Higgs *et al.* (1992) has shown that very low contamination by transition metals, including Cu, leads to strong luminescence.

An understanding of the mechanisms that lead to electrical activity at dislocations as a result of transition metal contamination would be of significant importance. A preliminary investigation of interstitial Cu at the core of a 90° partial dislocation is undertaken here.

7.2 The proposed simulation and its approximations

The proposed machine space that would be allocated for the Cu calculation was 32 out of the 64 nodes on the Edinburgh Meiko parallel computer. This translates to a Random Access Memory (RAM) allocation of 512Mb (megabytes) and a processing speed typically four times the speed of a Cray 2. While this is clearly a formidable amount of computing power, the calculation involving Cu is computationally extremely demanding. The hard nature of its pseudopotential implies the need for a large plane wave basis set to represent the valence wavefunctions. The choice of a suitable energy cutoff, which defines the number of plane waves, must be established first and is described in section 7.2.1. The implication of such a large plane wave expansion is that a set of restrictions has to be made to make the calculation tenable. Most of these will be expanded upon, but they are listed together to provide a clear reference of the conditions and approximations inherent in the current Cu simulation.

(1) the Cu pseudopotential has been optimised to minimise the number of plane waves needed. Part of this optimisation involves extending the core cutoff point, beyond which the true valence and pseudo wavefunctions must become exact. Tests must be performed to check the realism of the results and the minimum number of plane waves required for consistent results. This latter quantity is found to correspond to a plane wave cutoff energy of 350eV, which implies approximately 20,000 plane waves, and this directly dictates the restrictions that are placed on the rest of the calculation.

(2) as a result of the tests performed for (1), the number of atoms in the unit cell is limited to no more than 65-70. The shape of the unit cell involves a compromise between keeping the Cu atoms well separated and obtaining a reliable core structure.

(3) the computational limitations also restrict the k-point sampling to a calculation at *one* point only, (0,0,1/4).

(4) the unit cell size and shape is fixed. This is not a time or memory constraint but a limitation of CETEP which, at the time of writing, is unable to calculate stresses.

7.2.1 A limited plane wave basis set

Expansion of the valence wavefunctions in a limited basis set will lead to errors in the total energy calculated. The technique used to locate the point at which a sufficient number of plane waves has been chosen was introduced in chapter 3, section 3.5. It was shown there that the expansion was terminated when a converged description of energy *differences* was obtained, rather than absolute energies. A similar approach is taken here in the tests on the Cu pseudopotential, since the requirement of absolute energy convergence would make the calculation completely unmanageable.

Pseudopotentials are normally generated in k-space and in this form can be used with any energy cutoff. The greater this cutoff the more plane waves in the expansion and the better the convergence. As discussed in chapter 3, section 3.5, the non-local components of the pseudopotential can also be projected using a real-space technique which is computationally more efficient. The serial, CASTEP, code uses k-space pseudopotentials, whereas the parallel, CETEP, code uses real-space versions which are constructed from the k-space form. Unlike the k-space pseudopotential, the real-space forms can only be used to a maximum cutoff energy which was originally specified in their construction. For example, it was necessary for a new real-space Si pseudopotential to be constructed that could operate at the cutoff energy appropriate to the Cu, since the existing form of the Si pseudopotential was not constructed to be used at such high cutoffs.

7.2.1.1 The Cu pseudopotential

A completely new Cu pseudopotential has been developed for this work[1] and its testing has been undertaken here.

It is first necessary to test the k-space form of this new pseudopotential. This was performed using the serial code, CASTEP, which has been converted to run on the Stardent

[1] I am grateful to M.C. Payne and M.H. Lee at the Cavendish Laboratory in Cambridge for providing me with this potential.

computer here at Oxford.

The test chosen was on a Cu dimer which has been widely studied using similar local density functional pseudopotential schemes (see Ballone and Galli, 1990). The dimer is modelled as two Cu atoms at the centre of a large cubic unit cell. Periodic boundary conditions implies this is equivalent to a superlattice of dimers, and the unit cell must be made large enough to minimise dimer-dimer interactions. A cubic unit cell of sides 7.5Å was chosen, since earlier calculations on a Si dimer, chapter 3, section 3.5, had shown that larger unit cells gave rise to little change in the results obtained. The lack of interaction between the dimers results in negligible dispersion and all calculations have been obtained using one k-point (the gamma point).

A 400eV cutoff was initially adopted which represented the maximum number of plane waves that the eventual Cu calculation would be restricted to, based on the computing resources allocated. At this cutoff energy, several bond lengths for the Cu dimer were chosen and CASTEP run to obtain a converged total energy. No ionic relaxation was performed. The process was then repeated at a *lower* cutoff and the resulting energy versus bond length curves compared.

The results for three cutoffs, 400eV, 350eV and 300eV are illustrated in fig. 7.1. The following points should be noted:

(1) the 350eV curve is moved by -3.3eV, and the 300eV cutoff curve by -20.5eV to match the placement on the energy scale of the 400eV curve. This implies that total energies are not converged.

(2) the position of the minimum and the curvature of the 350eV cutoff curve are in excellent agreement with those obtained at 400eV, but a cutoff of 300eV is too low and provides unreliable results.

While these results imply that a suitable convergence of the Cu pseudopotential is obtained at 350eV they provide no information on the physical reliability of the results. Contact with experiment can be obtained by noting that the position of the minimum corresponds to the

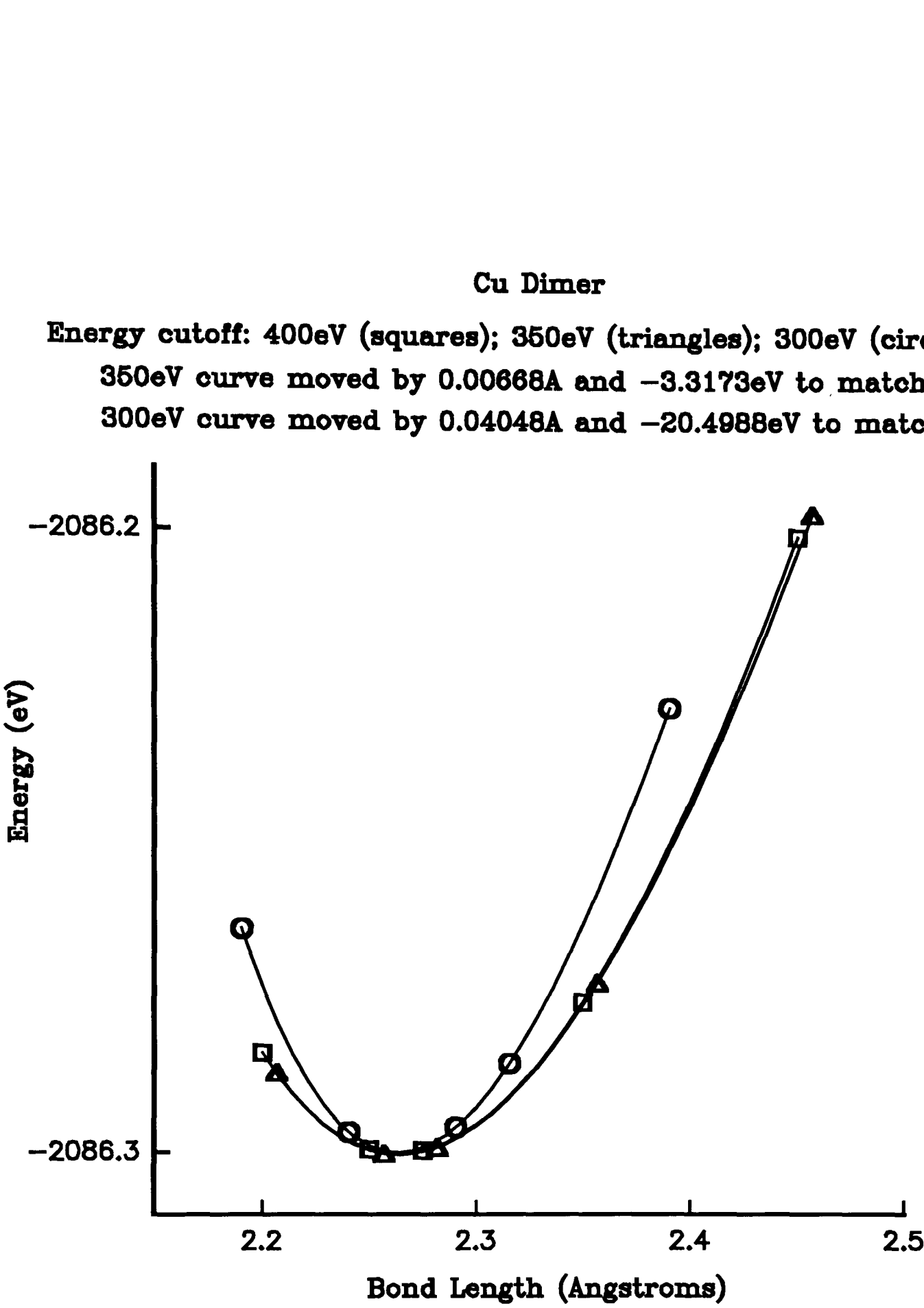

Fig. 7.1 Cu dimer calculations using **CASTEP**.

equilibrium dimer bond length and that the vibrational frequency can be calculated from the curvature at the minimum[2]. These have been calculated for all three cutoffs and are compared to experiment in table 7.1.

Technique	Dimer Bond Length r_e (Å)	Vibrational Frequency w_e (cm^{-1})
Experiment	2.2197	264.55
400eV cutoff	2.263	250.70
350eV cutoff	2.257	251.97
300eV cutoff	2.223	318.72

Table 7.1 Comparison of equilibrium Cu dimer bond length and vibrational frequency as calculated at three cutoffs. Also shown are the experimental values (Huber and Herzberg, 1979).

Table 7.1 illustrates the large difference from the 400eV results obtained with a 300eV cutoff. It also demonstrates that the 350 and 400eV results are in good agreement with experiment. The errors in the calculated values as compared with experiment are typical of other similar calculations (Ballone and Galli, 1990).

These tests have shown that the k-space form of the Cu pseudopotential provides a realistic description for a cutoff energy of 350eV or higher. This lower limit was chosen for the construction of the real-space form of the pseudopotential.

It might appear strange that the k-space to real-space conversion must be checked. However, the conversion involves a number of "tweaking" parameters[3] and its effectiveness needs to be verified. Indeed the first real-space form provided, gave very poor agreement with the k-space results and in particular unphysical forces. A second form was found to be much

---

[2] The vibrational frequency is given by $w_e=\sqrt{k/\mu}$. μ is the reduced mass which for a dimer is just half the mass of one of the atoms. k is equal to the curvature, $\frac{\partial^2 E}{\partial r^2}$, at the minimum.

[3] The conversions were performed at Cambridge.

more successful and reproduced the k-space 350eV cutoff results to within 0.1% (r_e=2.257Å and w_e=251.72cm^{-1}).

This second real-space form of the Cu pseudopotential has been used in the rest of this work at a plane wave energy cutoff of 350eV. The tests described here are important not only to the present work but also to various future studies which are going to make use of this Cu pseudopotential.

7.2.1.2 The Si pseudopotential

There is a more tried and tested knowledge for Si, than in the case of Cu, as regards the use of real-space pseudopotentials. It is however unusual to use such a high energy cutoff for an element whose pseudopotential has been used at cutoffs as low as 95eV (Stich *et al.*, 1992). The inclusion of the Cu demands working at a cutoff of 350eV and so the Si pseudopotential must be tested to ensure it provides realistic results at this cutoff.

A real-space Si pseudopotential constructed to operate at cutoffs up to 400eV has been provided for the present work[4]. It was tested by calculating the structural energy curve for a unit cell of 8 Si atoms in the diamond cubic structure. A uniform mesh of k-points is needed to sample the cubic reciprocal lattice generated by the 8 atom unit cell and a q=2 sampling was chosen. The curve was generated by obtaining the converged total energy, using CETEP, for a range of unit cell volumes (i.e. changing the length of the unit cell edges isotropically).

Fig. 7.2 illustrates the results obtained. In this case, the position of the minimum determines the equilibrium lattice parameter and the curvature at the minimum is used to calculate the bulk modulus[5]. This gives a_0=5.39Å and B=0.968x10^{11}J/m^3. The experimental values are a_0=5.431Å and B=0.978x10^{11}J/m^3 (EMIS datareviews No.4, 1988) which implies

---

[4] I am grateful to D.M. Bird, at the University of Bath, for providing me with this pseudopotential.

[5] For an equilibrium volume, V_o, the equilibrium lattice parameter is given by $a_o=V_o^{1/3}$. The bulk modulus is defined by $B=-V\frac{\partial p}{\partial V}$. Using $p=-\frac{\partial E}{\partial V}$ this gives $B=V_o\left.\frac{\partial^2 E}{\partial V^2}\right|_{V_o}$.

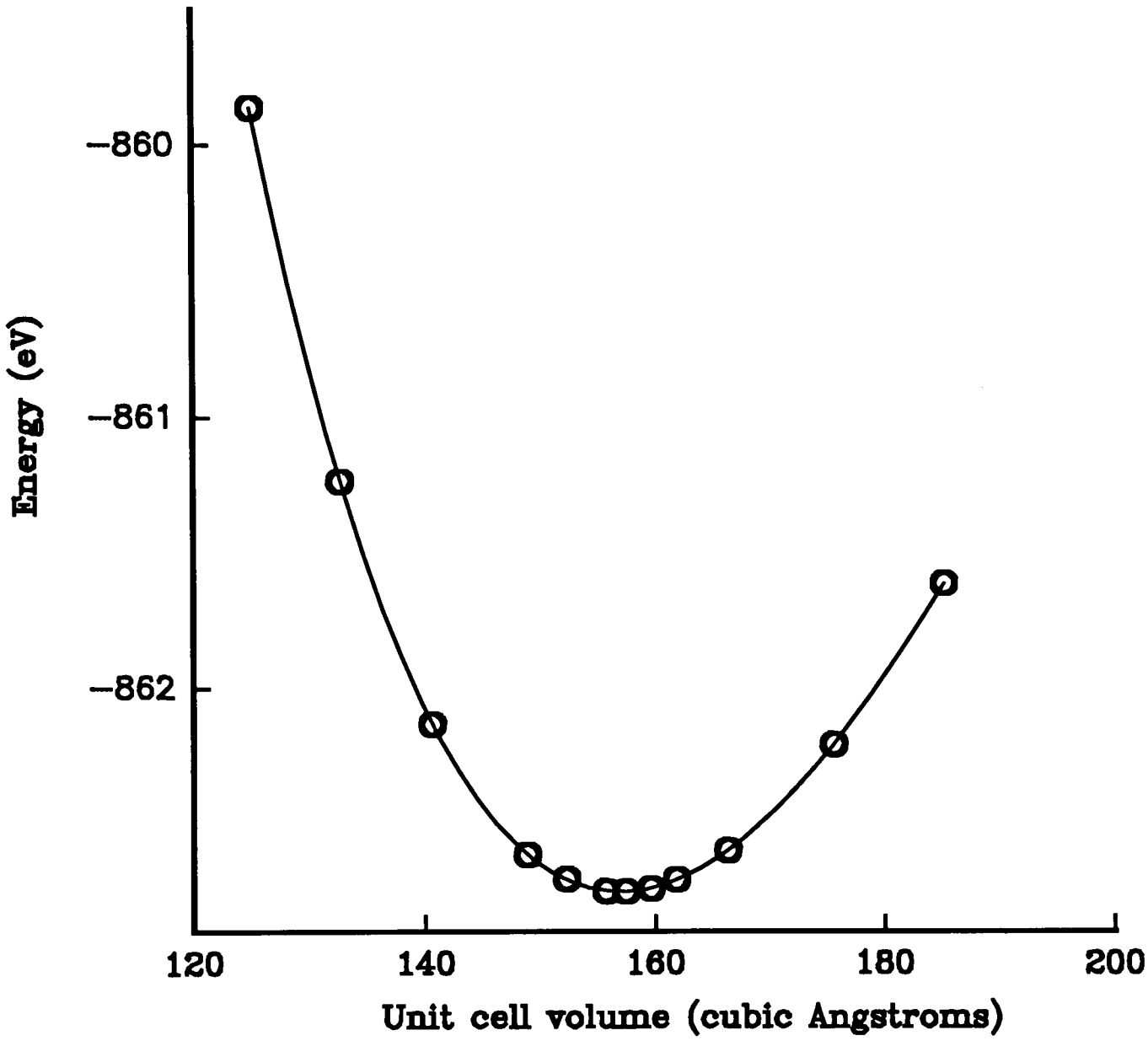

Fig. 7.2 Diamond cubic Si structural energy curve calculations using **CETEP**.

the calculated values are in error by -0.7% and -1.0% respectively. This indicates that this new real-space Si pseudopotential, used at 350eV, provides good results.

7.2.2 The unit cell

The need to consider a cutoff of 350eV demands a maximum unit cell size of about 65-70 atoms. It might seem sensible to use the *oblique* 64 atom unit cell used throughout the rest of this work since this has been shown to produce reliable core structures and band-structures. Unfortunately this cell only involves one crystal repeat period down the dislocation line. While in most cases this is desirable, it is not so here since a Cu atom in one of the cores will only lie 3.84Å apart from its periodic neighbour in this direction. This will lead to a large Cu-Cu interaction, which is reduced here by doubling the unit cell period down the dislocation line. A unit cell of 64 atoms is maintained by halving the separation of the two 90° partials in the $[1\bar{2}1]$ direction. This however leaves a unit cell which is identical in shape to the 32 atom unit cell described in chapter 5, section 5.2.1, except it is double the length in the dislocation line, or *Z*, direction. It was shown there that this 32 atom unit cell had the partials too close, and a different atomic and electronic structure was obtained in comparison to several larger unit cells. A similar problem is encountered here as can be seen from table 7.2.

The results on the left for the current unit cell, which has 2 *Z* periods, are the product of a relaxation using CETEP to a maximum force of 0.05eV/Å from a starting unit cell relaxed with the tight-binding Chadi Hamiltonian. Since the intention is to provide a starting relaxed core structure for the Cu calculation, the relaxation was performed using the 350eV real-space Si pseudopotential described above. The results on the right illustrate the core structure obtained by relaxing the 64 atom unit cell with only 1 *Z* period, which was obtained using a real-space Si pseudopotential at a 120eV cutoff (see chapter 5, section 5.4.1 for details of this calculation). This implies that the comparison in table 7.2 is not exact since the two unit cells have been relaxed with real-space Si pseudopotentials constructed to work at different cutoffs. However, the differences are expected to be minor since both real-space pseudopotentials have

Bond	**Current 64 atom cell 2 *Z* periods cutoff=350eV**	**Original 64 atom cell 1 *Z* period cutoff=120eV**
Bond 1	2.430 (3.3)	2.412 (2.6)
Bond 2	2.332 (-0.9)	2.328 (-1.0)
Bond 2'	2.387 (1.5)	2.440 (3.8)
Bond 3	2.389 (1.6)	2.423 (3.0)
Bond 3'	2.328 (-1.0)	2.315 (-1.5)
Bond 6	2.344 (-0.3)	2.342 (-0.4)
Bond 7	2.349 (-0.1)	2.359 (0.3)
Normal Crystal Side		
Angle 213	98.6	96.2
Angle 214	131.4	134.9
Angle 215	104.4	103.7
Angle 314	108.9	107.3
Angle 315	116.0	115.2
Angle 415	98.4	100.2
Stacking Fault Side		
Angle 127	98.8	98.4
Angle 126	131.6	138.4
Angle 128	104.2	102.5
Angle 627	109.0	108.3
Angle 728	117.0	112.9
Angle 628	97.5	95.9

Table 7.2 Comparison of the local bonding around the reconstructed bond 1 for relaxations using CETEP. The unit cell to be used in the Cu calculation involves two *Z* periods down the dislocation line and is relaxed with a real space Si pseudopotential at an energy cutoff of 350eV. The results on the right are those described in chapter 5, section 5.4.1, and are obtained with a real space Si pseudopotential at a cutoff of 120eV. The bond and angle notation used is as depicted in chapter 4, fig 4.9, where, for example, angle 123 means the angle subtended by atoms 1 and 3 at atom 2. The bond lengths are given in Å and the percentage distortions from the perfect Si bond length (2.3517Å) are in brackets.

been constructed from the *same* k-space version.

Table 7.2 shows that the two unit cells differ in atomic structure in a very similar way to that described in chapter 5, section 5.2.1. Specifically, some of the back bonds, 2' and 3, and some of the angles are considerably less distorted in the current unit cell. As discussed before, this reflects the fact that the close proximity of the partials does not allow the cores sufficient freedom to "breathe". It can also be seen that the asymmetry present in the original 64 atom

oblique cell is also restricted in the current case.

Although the core structure is modified by the close proximity of the partials, this preliminary study is intended to reveal mechanisms by which Cu affects the core structure and not to provide accurate quantitative predictions. These can be obtained only when computing power has advanced to allow larger unit cells to be used, or alternatively, if the full 64 nodes on the Meiko computing surface are available for the calculation. The assumption is that the close proximity of the partials will still allow a good qualitative description.

7.2.3 k-point sampling

The internal storage of the wavefunctions is demanding on computing resources. Since an adequate description of Cu requires such a large expansion of plane waves, another immediate consequence is that there is memory available for storing only one wavefunction and limits the calculation to a single k-point.

In chapter 5, section 5.2.2, it was shown that the oblique unit cell, which contains just one repeat period down the dislocation line had only significant k-point dispersion in this direction. For the present unit cell this direction is now twice as long and the dispersion will be less. However, in order to double the length in this Z direction, the X direction had to be halved in length. This may well result in a significant dispersion now existing in directions other than just down the dislocation line and the question of which *single* k-point to use is not so obvious.

As introduced in chapter 3, section 3.4.3.1, a symmetric mesh of k-points is used following the scheme of Monkhurst and Pack (1978). The need to consider a *symmetric* mesh arises since the eigenvectors will be *different* for each symmetry related k-point[6] and the forces will be correct only when the weighted average is taken. For example a k-point (0,1/4,1/4) has symmetry partners (0,-1/4,-1/4), (0,1/4,-1/4) and (0,-1/4,1/4). This plane averaging is thus correctly performed only when any *two* of these k-points are used, provided

---

[6] unless they are related by time-reversal symmetry which is the special case where the eigenvectors are complex conjugates of each other and it is therefore only necessary to consider one of them, as previously discussed.

they are not related by time-reversal symmetry.

The current Cu calculation is restricted to one k-point only. From the above discussion this therefore leads to just four possibilities, (0,0,0), (1/4,0,0), (0,1/4,0) and (0,0,1/4).

An understanding of the effective convergence that will be obtained in the Cu calculation using CETEP can be investigated using the tight-binding scheme. The convergence results obtained, arbitrarily using the GSP Hamiltonian, for each of these k-points are listed in table 7.3.

k-point sampling	Binding Energy (eV)	Max/min Bond Lengths	Max/min Bond angles
(0,0,0)	-4.473	2.74% -1.72%	130.8° 95.0°
(1/4,0,0)	-4.488	3.11% -1.73%	131.2° 95.5°
(0,1/4,0)	-4.478	2.61% -1.68%	130.6° 95.0°
(0,0,1/4)	-4.574	2.68% -2.03%	131.4° 95.3°
q=2 (4 k-points)	-4.577	2.82% -1.99%	131.4° 95.5°
q=4 (32 k-points)	-4.573	2.84% -1.97%	131.3° 95.5°

Table 7.3 Comparison of the convergence obtained by using *one* k-point for sampling the Brillouin zone. Also shown are the results obtained for a uniform sampling at q=2 and q=4 for reference. All results have been obtained by relaxing the 64 atom oblique unit cell described in section 7.2.2 using the GSP Hamiltonian with r_t=3.0Å.

These results indicate that the best energy and structural convergence is obtained by using the k-point (0,0,1/4). Its results are close to those obtained at a q=2 uniform sampling over the 3D Brillouin zone and indicate that dispersion is still mainly contained along the Z direction. The other important result is that there is negligible change by increasing the sampling to q=4.

The single k-point used in the Cu calculation is thus (0,0,1/4) and these results have

indicated that it should provide a reliable Brillouin zone averaging.

7.3 Introducing the Cu

As discussed above, Higgs *et al.* (1992) find that very low levels of transition metal contamination leads to a drastic increase in the photoluminescence, but also find that at higher concentrations the onset of transition metal precipitates eventually quenched the luminescence. They postulated that these precipitates absorb the centres responsible for the luminescence. These effects were found to be independent of the identity of the transition metal. Weronek *et al.* (1992) found that the intensities and polarisations of the luminescence depend strongly on the direction of detection, although they came to a different conclusion as regards the effect of the transition metal contamination, see chapter 1, section 1.3.

A possible mechanism to explain the results of Higgs *et al.* has been suggested (Jones, 1992). Transition metal impurities diffuse to a dislocation core and could be responsible for the production of interstitials. These interstitials could diffuse along the dislocation line until they meet others causing the dislocation to climb. This would result in a small *shuffle* segment which involves dangling bonds lying almost normal to the glide plane. The resulting luminescence is thus associated with a Si dangling bond and has the observed polarisation. The luminescence is also independent of the identity of the transition metal.

It should be noted that the photoluminescence results of Higgs *et al.* are *not* in agreement with EBIC findings (Fell and Wilshaw, 1991; Fell, 1992; Radzimski, 1991). EBIC finds deep levels associated with transition metals which are dependent on the identity of the impurity. These levels are also much deeper (mid-gap) than those observed in Photoluminescence (all within 0.3eV of the valence band edge). Another key difference with EBIC is that Photoluminescence only detects states that take part in radiative recombination processes. Due to the indirect nature of the band-gap in Si, these processes account for only typically 1 in 1000, or less, of the recombination activity present. These differences indicate it is likely that EBIC and Photoluminescence are observing different states. It is thus possible that there are

at least two mechanisms by which transition metals introduce deep levels into the gap. Some levels may be introduced by the transition metal inducing a core structure change that may involve Si dangling-bonds in a similar manner to that described above, and secondly deeper levels are introduced that are associated with the transition metal itself.

Experimental work on Cu-Si precipitates (Mukherjee *et al.*, 1969; Solberg, 1978) indicate that there exists an equilibrium phase Cu_3Si. No equilibrium silicide exists for a concentration of Cu less than three times that of Si. It is thus clear that Cu likes to form precipitates in which it can surround the Si. The crystal structure of the low-temperature (room temperature and below) Cu_3Si phase is suggested to be based on a trigonally distorted b.c.c. arrangement with an orthorhombic lattice (Solberg, 1978).

The diffusion of Cu to a dislocation core and the mechanism of precipitation is thus likely to be an extremely complicated task to model. Under the constraints of the present computing resources the simulation is restricted to considering only a small number of Cu atoms and is therefore currently unable to consider Cu precipitates at dislocations. However, as discussed earlier, Cu diffuses interstitially and an investigation of the effect that an interstitial Cu atom has on the core would be a useful initial step. Specifically, an interstitial Cu atom might lead to the possibility of Si interstitials or dangling-bonds being created.

The 90° partial consists of 5 and 7-membered rings, which are regions of elastic compression and expansion respectively. These dislocation "pipes" are regions that are likely to attract interstitial impurities because of the possibility of reducing the elastic strain of the system. It is not clear whether the Cu will prefer the 5-membered ring interstitial site or that of the 7-membered ring. Since the computing time allocated to the simulation was restricted it seemed appropriate to consider the Cu atom at the centre of the 5-membered ring, because it is almost certainly going to result in structural damage and Si bond breaking being a region of elastic compression.

Two Cu atoms, one in each core, need to be considered for the usual reasons (see chapter 4, section 4.1). This implies an even number of Cu atoms in the simulation cell which

is important here for computational simplicity[7]. The starting configuration thus consists of the relaxed unit cell of table 7.2, with one Cu atom at the centre of each 5-membered ring. The Cu atoms are kept as far apart as possible by placing them symmetrically either side of the origin in the dislocation line direction (ie. at $-Z/4$ and $+Z/4$ where Z is the unit cell length along the dislocation line). This starting configuration is illustrated in fig. 7.3a.

7.4 Simulation results

By introducing two Cu atoms into the relaxed unit cell of table 7.2 implies a new charge density which will not be self-consistent. The simulation must begin with the minimisation of the total energy with respect to the electronic system. After 25 iterations the forces and energies had converged indicating self-consistency had been reached. The total energy and maximum force in the system at this point (*stage 1*) are listed in table 7.4.

Simulation stage	Ionic relaxation iteration number	Total energy (eV)	Max. Force (eV/Å)
stage 1 (fig. 7.3a)	0	-7782.4	106.0
stage 2 (fig. 7.3b)	80	-8585.1	29.3
stage 3 (fig. 7.4a)	110	-8856.8	24.4
stage 4 (fig. 7.4b)	175	-9388.2	23.5

Table 7.4 Four stages of the Cu simulation showing the total energy and maximum force in the system at each stage. The structure at each stage is illustrated by the figure in brackets.

The maximum force of 106.0eV/Å is very large and generally the forces in the system

[7] For a system containing an even number of electrons, CETEP occupies each level with two electrons up to the highest occupied state that needs to be considered. For an odd number of electrons the system becomes metallic and levels must be occupied by using the Fermi-Dirac distribution, the resulting electronic minimisation being much more difficult. Neutral Cu is considered here and has eleven valence electrons. Thus an even number of Cu atoms must be considered to keep all states fully occupied.

Fig. 7.3a Starting point for the simulation, *stage 1*. One Cu atom lies at the centre of each 5-membered ring for the 90° dislocation dipole.

Fig. 7.3b *Stage 2* of the simulation (80 ionic relaxations).

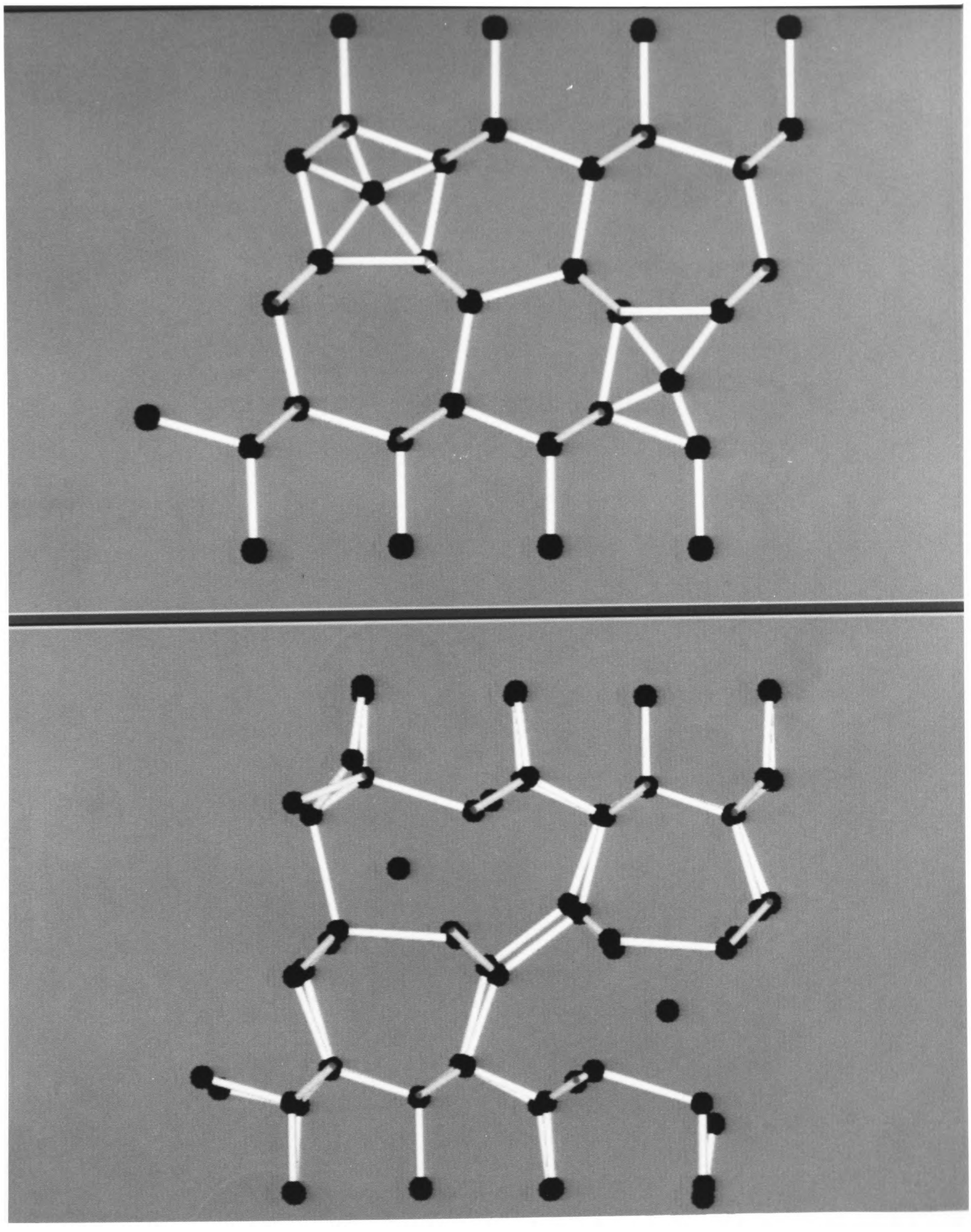

Fig. 7.3a Starting point for the simulation, *stage 1*. One Cu atom lies at the centre of each 5-membered ring for the 90° dislocation dipole.

Fig. 7.3b *Stage 2* of the simulation (80 ionic relaxations).

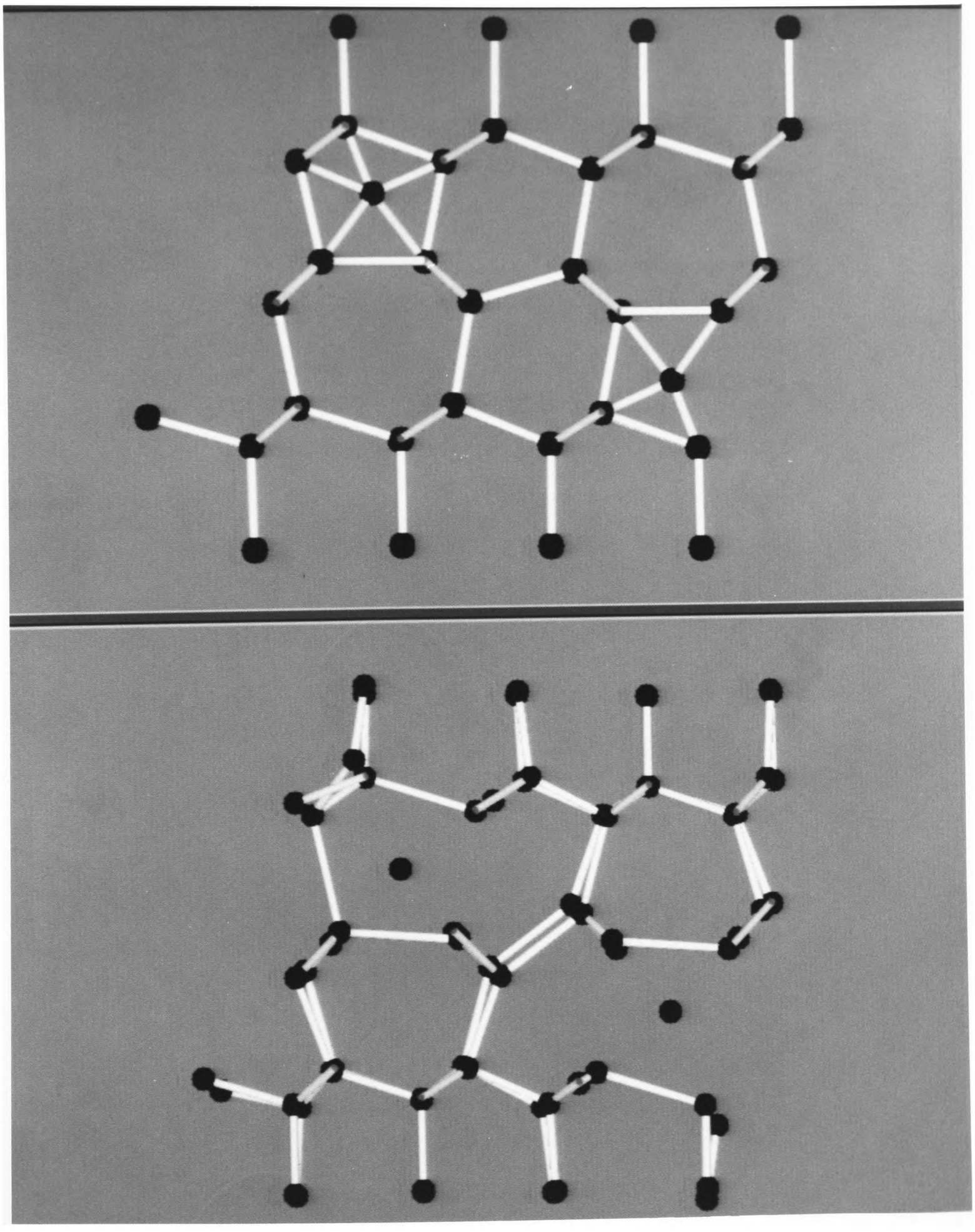

Fig. 7.4a *Stage 3* of the simulation (110 ionic relaxations).

Fig. 7.4b *Stage 4* of the simulation (175 ionic relaxations).

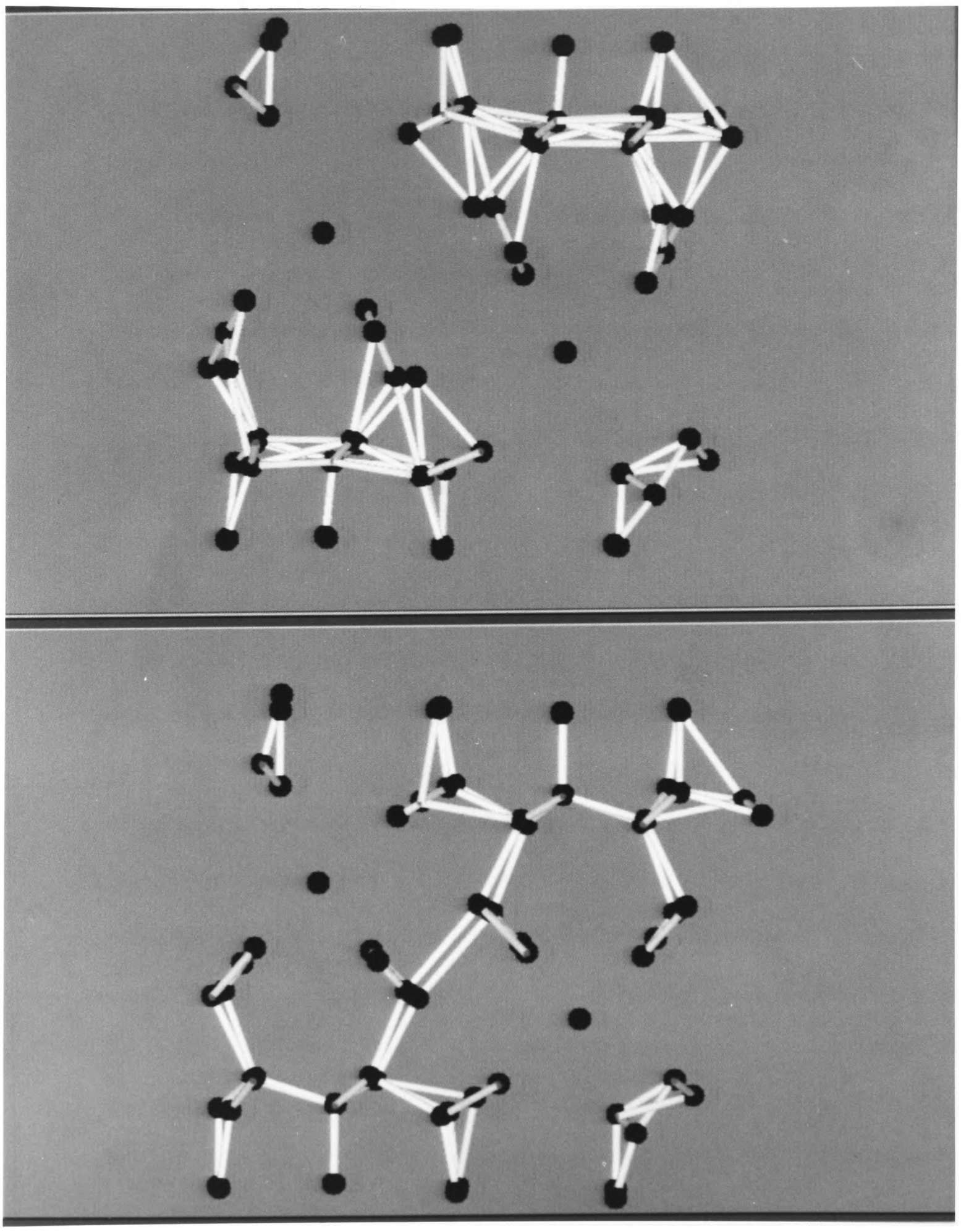

were large in the region of the 5-membered ring as hoped. The ions were then allowed to relax and three further stages have been examined in table 7.4 and are illustrated in figs. 7.3b, 7.4a and 7.4b.

Table 7.4 indicates that there is initially a very rapid drop in the forces within the unit cell but that from stages 2 to 4 the change is much smaller. This indicates that the system is undergoing a large structural change which is consistent with the rapid and steady drop in the total energy throughout the whole simulation.

Fig. 7.3b illustrates the structural state of the unit cell at *stage 2* (after 80 ionic iterations). The Cu atoms have clearly induced some bond breaking in the 5-membered rings and are themselves reasonably stationary. It seemed hopeful that continued relaxation could result in the ejection of a Si interstitial or a relaxation around a Si dangling-bond. However, figs. 7.4a and 7.4b illustrate a major structural change has occurred in the unit cell with the loss of the dislocation core structure. Table 7.4 indicates that the relaxation is far from completion at *stage 4*, fig. 7.4b, (forces still as high as 23.5eV/Å) and yet this was the point reached in the computer time provided.

There is no point trying to say otherwise; the first impression is that the system has moved into a completely unphysical mess! However, analysis of the bonding indicates that the Si atoms have actually moved toward a close-packed structure, although the simulation is still far from completion. The number of bonds to each Si atom is typically 10 for neighbours within a nearest-neighbour cutoff range of 2.8Å. The bond lengths are becoming smaller and approaching an average value of 1.9Å, which is typical of Si close-packed structures. The conclusion is that the presence of the Cu atoms has forced a complete Si phase change. This indicates that the unit cell is under a large compressive pressure and the simulation has moved the Si atoms towards the lowest total energy crystal structure under these conditions, which is close packed (Yin and Cohen, 1982a; 1984).

A more valuable result is the clear evidence that the Cu atoms strongly repel the surrounding Si atoms. Analysis of the charge density provides further information. Fig. 7.5

Fig. 7.5 A slice of the charge density normal to $[1\,0\,\bar{1}]$. The colouring from blue through to red represents increasing charge density. The two red areas correspond to two Cu atoms. The unit cell depicted is the *rectangular quadrupole* unit cell generated from the *oblique dipole* unit cell shown in fig. 7.4b. The top Cu atom corresponds to the left one in fig. 7.4b (the lower Cu atom here is the periodic image of the upper one formed when generating the rectangular quadrupole cell). The Cu atom on the right of fig. 7.4b is separated from the left one along $[1\,0\,\bar{1}]$, see section 7.3, and so is not visible in this picture. The yellow areas represent Si atoms and the formation of bonds between them is clearly visible; note this is even more apparent when viewing different charge density slices since the Si atoms, such as the one located at the black pointer in the lower right corner, generally lie in different positions along $[1\,0\,\bar{1}]$. No such bond formation is apparent with the Cu.

display image

Fig. 7.5 A slice of the charge density normal to $[1\,0\bar{1}]$. The colouring from blue through to red represents increasing charge density. The two red areas correspond to two Cu atoms. The unit cell depicted is the *rectangular quadrupole* unit cell generated from the *oblique dipole* unit cell shown in fig. 7.4b. The top Cu atom corresponds to the left one in fig. 7.4b (the lower Cu atom here is the periodic image of the upper one formed when generating the rectangular quadrupole cell). The Cu atom on the right of fig. 7.4b is separated from the left one along $[1\,0\bar{1}]$, see section 7.3, and so is not visible in this picture. The yellow areas represent Si atoms and the formation of bonds between them is clearly visible; note this is even more apparent when viewing different charge density slices since the Si atoms, such as the one located at the black pointer in the lower right corner, generally lie in different positions along $[1\,0\bar{1}]$. No such bond formation is apparent with the Cu.

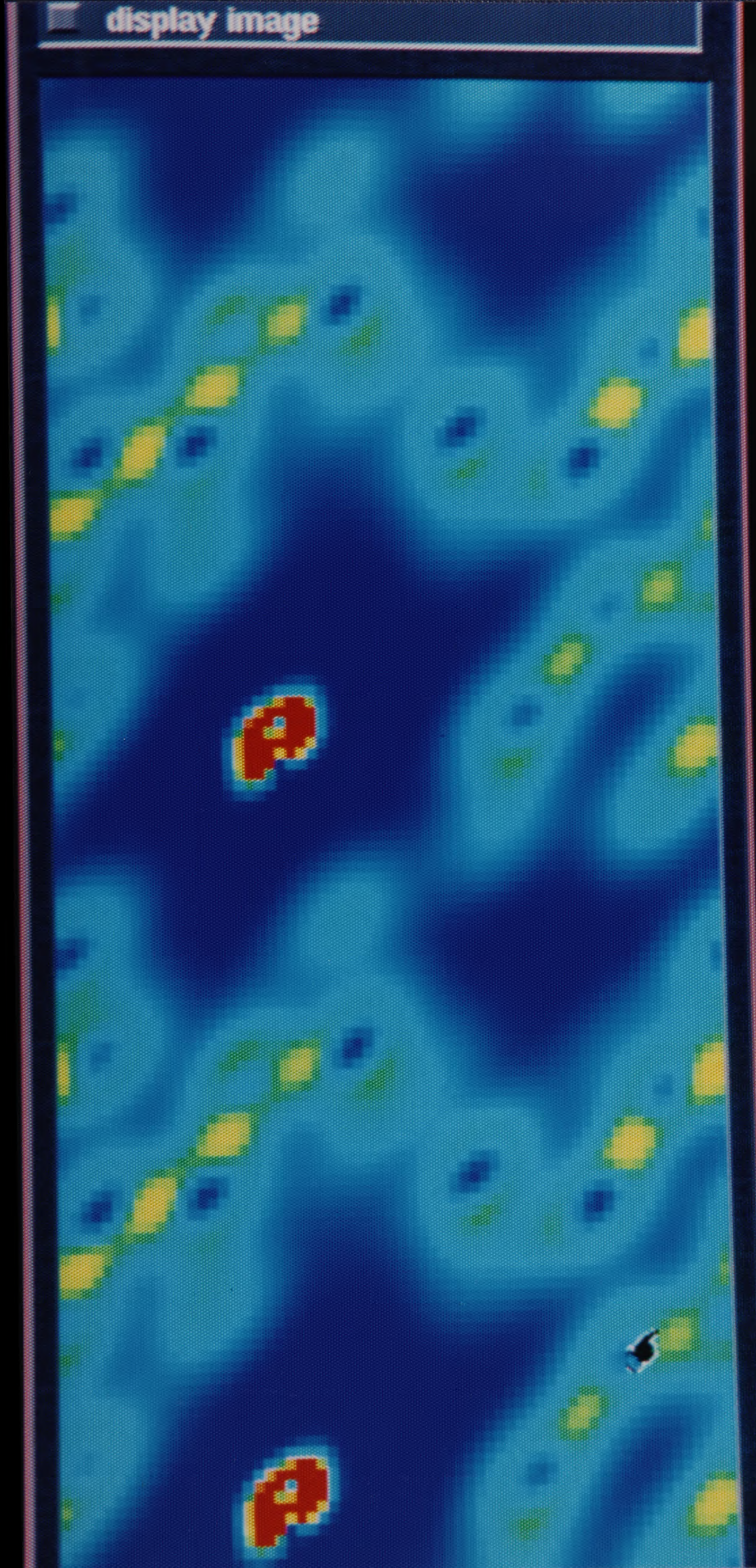
display image

represents a slice through the charge density normal to $[10\bar{1}]$. For the purposes of viewing the charge density an orthogonal unit cell is required; fig. 7.5 thus depicts the charge density present in the *oblique dipole* unit cell of fig. 7.4b, but in the related *rectangular quadrupole* unit cell which contains twice as many atoms (see chapter 4, section 4.2). The unit cell illustrated in fig. 7.5 thus contains four Cu atoms, two of which are visible and represented by the red areas. The top Cu atom is equivalent to the left one in fig. 7.4b, the lower one here being the periodic image of this upper one formed when generating the *rectangular* unit cell from the *oblique* one. The Cu atom on the right of fig. 7.4b is separated along $[10\bar{1}]$ from the left Cu atom, and hence it, and its periodic image, appear on a different slice of the charge density.

Since the colouring from blue through to red indicates increasing charge density, the Cu atoms represent the most dense regions of charge. This indicates the Cu atoms have held tightly onto their charge, since the red regions are highly local and predominantly circular as can be checked by viewing other slices. The other important point is that the Cu atoms are surrounded by a void in the charge density. This is contrasted with Si-Si bonds which can be observed as yellow regions between the bright yellow Si atoms, this being particularly evident for different slices. The conclusion from fig. 7.5 is that the Cu atoms not only strongly repel the surrounding Si atoms, but also make no attempt to form bonds to them.

7.5 Discussion

The presence of the Cu atoms in the 5-membered rings will lead to an internal pressure of the system, but there was no feel for the magnitude of this effect. The simulation clearly *must* allow the volume of the unit cell to change to accommodate the extra atoms. As mentioned earlier, the current version of CETEP is unable to include this effect. By placing the Cu atoms in the 5-membered as opposed to the 7-membered rings has compounded this problem. The conclusion is that within a fixed unit cell it is impossible to include the two Cu atoms in the elastic compressive region of the 90° partial cores and to maintain simultaneously

the open diamond-cubic structure as the lowest energy phase.

Despite these problems, the current simulation has indicated that neutral interstitial Cu seems to strongly repel the surrounding Si atoms and does not take part in bond formation. It is not clear why this is the case and further investigation, with various charge states for the Cu, would be useful.

Initial theoretical and experimental investigations are usually learning processes that allow an understanding of the problems involved in the simulation. This is certainly the case here. I was happy to hear that the work described in this chapter is to be continued at Cambridge[8], in the form tested and developed here. The Cu atoms will be placed in the 7-membered rings and the Cu pseudopotential is likely to be of the Cu^+ ion and not of the neutral atom. This is mainly because the Cu ion will be smaller and also there is some belief, though no real evidence, that Cu diffuses in this electronic state. The problem of allowing the unit cell to change size and shape is as yet unresolved. This is a point that must be considered for future applications.

---

[8] Victor Milman is interested in the interstitial diffusion of Cu in Si.

CHAPTER 8

Other work and suggestions for the future

8.1 Introduction

Two other areas of work that have been investigated are described in sections 8.2 and 8.3. The remainder of this chapter outlines suggestions for the possible direction of future work.

8.2 Vacancy interaction with dislocations

The strain energy involved at the core of a dislocation may result in point defects tending to migrate to the core in preference to a site in the bulk. For example, in the 90° partial dislocation the five-fold ring is a region of elastic compression as a result of the two extra {224} half planes that are squeezed into the regular structure. Vacancies will therefore be attracted to this region. Conversely, a large impurity atom can lower the strain energy of the system by taking up a position in the seven-fold ring, which is a region of elastic expansion.

Marklund (1989) investigated the tendency for vacancies to migrate to a 90° partial dislocation. He used the Tersoff (1988a) potential to obtain the energy of a *relaxed* vacancy at sites near the dislocation compared to those in the bulk. These relaxations were performed at 0°K and then temperature was introduced to the analysis by using the expression

$$C/C_0 = \exp(\Delta S_f/k)\exp(-\Delta U_f/kT) \qquad (8.1)$$

Here C/C_0 is the relative concentration of vacancies at the dislocation compared to the bulk, ΔU_f is the difference in formation energy of the vacancy at the dislocation site compared

to the bulk and ΔS_f is the corresponding difference in the vibrational entropy.

Marklund found that C/C_0 decreased rapidly with both temperature and distance from the dislocation line. This was also found by Panteleev *et al.* (1974) using continuum elasticity theory.

The disadvantage of this scheme is that no account is taken of the temperature dependence of the vacancy formation energy, ΔU_f, and the change in vibrational entropy that will result in a simulation performed at temperature. A vacancy introduced at a finite temperature could well cause a different atomic rearrangement from what occurs with a simple 0°K relaxation, particularly at the dislocation core. A better approach would be to model the introduction of vacancies at a finite temperature so that both the concentration for this temperature and the resulting atomic structure are simultaneously obtained.

This requires a scheme in which there is freedom to vary both the position of an atomic site and its content (Si atom or vacancy) at a finite temperature. Even when the system is in equilibrium, as time progresses the content and position of a particular site will change. However, by averaging the content and site position over a long time the expectation values of these quantities may be obtained. The problem is therefore reduced to obtaining the time-averaged position and compositional distribution. Two techniques have been developed that perform this averaging.

8.2.1 Monte Carlo

The Monte Carlo technique[1] is used to perform a weighted sampling of phase space using a chosen statistical ensemble. A Monte Carlo (MC) simulation is then used to compute averages over this statistical ensemble.

The technique implemented here is the Metropolis Monte Carlo method (Metropolis *et al.*, 1953; Wood, 1986). At each MC step, this scheme involves the comparison of the relative probabilities of two states, m and n, with energies V_m and V_n respectively. The new state, n,

[1] See Allen and Tildesley (1987) for a full account of the method and its development.

is accepted or rejected according to the following criteria,

1) if $V_n \leq V_m$ then the energy is going down hill and the new state is definitely accepted.

2) if $V_n > V_m$ then the energy is going up hill and the move is accepted only if a randomly generated number lying between 0 and 1 is found to be less than $\exp(-(V_n - V_m)/kT)$. If this is not true then the system returns to state m.

If the probabilities for states m, n are P_m, P_n respectively this method may be summarised by saying that if the ratio P_n/P_m is greater than unity the new configuration, n, is always accepted and if less than one n is retained with a probability given by the ratio P_n/P_m.

The major advantage of the MC approach, over say Molecular Dynamics (MD), is that the simulation is not required to follow the physical dynamics of the system. Computing the segregation of vacancies to the dislocation line using MD would involve a time-scale for simulations which is far in excess of present computing power. MC avoids the need to follow the slow vacancy movement by creating a vacancy at a site without worrying about how the system would get from one state to another. The same principle has been successfully used in obtaining equilibrium alloy concentrations (Foiles, 1985) without the need to wait for slow atomic interchange processes.

The requirement is to compute the relative probabilities of two states. The ensemble chosen involves fixed temperature, and a fixed number of atomic sites. The numbers of Si atoms and vacancies are not fixed, but a given composition can be obtained by suitable choice of their chemical potentials, μ_{Si} and μ_{vac}. Consider a state n which involves one extra vacancy from a state m. The quantity V_n-V_m is obtained as follows:

$$\begin{aligned} V_m &= U_m - N_{Si}\,\mu_{Si} - N_{vac}\,\mu_{vac} \\ V_n &= U_n - (N_{Si}-1)\mu_{Si} - (N_{vac}+1)\mu_{vac} \\ V_n - V_m &= U_n - U_m + \mu_{Si} - \mu_{vac} \end{aligned} \tag{8.2}$$

The chemical potential difference, $\mu_{diff} = \mu_{Si} - \mu_{vac}$, is central in determining the relative

probability that a vacancy is introduced to the system. For a bulk site, the internal energy difference between this site being occupied by a Si atom and an *unrelaxed* vacancy, $U_n - U_m$, is 8.7eV as calculated using the Stillinger Weber potential. The ideal vacancy formation energy is estimated by assuming the rejected Si atom forms two perfect bonds on the surface, which halves the value of $U_n - U_m$. μ_{diff} is then adjusted to obtain a reasonable probability of vacancy formation over several million MC steps.

The simulation is performed by allowing both vacancy creation and atomic displacements to occur, both accepted or rejected according to the MC decisions outlined above. Following the introduction of a vacancy the simulation is restricted to atomic displacement MC steps for several thousand iterations. This ensures that the system is given time to relax around the newly formed defect before any attempt is made to introduce another vacancy. Over a complete MC run *averages* are built up which indicate the concentrations of vacancies at each site and the atomic rearrangement that results.

Well it did not work! This result is however of significance, since the reason for the failure seems general, rather than specific, to any system in which the difference in energy for a site with and without the unrelaxed defect is very large. In these cases the defect equilibrium concentration will be very small. In practice a non-equilibrium concentration must be considered, such as one vacancy in 1000 Si atoms, because the model is limited to a fixed number of sites. In order for a MC simulation to introduce at least one vacancy in several million time-steps the value of μ_{diff} must be adjusted accordingly. This however introduces a problem. On the occasion that a vacancy is accepted this leaves all atoms surrounding the defect three-fold coordinated. Even after allowing for atomic rearrangement around the vacancy, the binding energies of the Si atoms immediately surrounding the vacancy are much smaller than four-fold coordinated atoms elsewhere. If a random decision is made to try and place a vacancy at one of these sites, it *always* succeeds. This is because energetically the Si atom is more easily replaced, and hence $U_n - U_m$ is much smaller, but the value of μ_{diff} is held fixed and in general is more *negative* than the cost in energy of creating the vacancy at this

site. From eqn. 8.2 this implies $V_n - V_m < 0$ and hence the move is definitely accepted.

There seems no way of getting around this problem. Since the energy of creating an *unrelaxed* vacancy is so large, in order to introduce a vacancy in the first place μ_{diff} must be made large and negative. This amounts to saying that the chemical potential of the vacancy is made so large that equilibrium now involves a whole avalanche of vacancies. Consequently, once one vacancy has been introduced the system is unstable to the introduction of more, the net result being a steady eating away of the simulation cell! Physically this corresponds to a situation in which μ_{diff} leads to a large excess concentration and then those vacancies will produce voids at nucleation centres such as dislocations.

The reason for this finding can actually be physically understood from the other technique that has been developed to model this problem.

8.2.2 An alternative approach to Monte Carlo

A much more computationally efficient approach than the MC technique has been developed by Gyorffy *et al.* (1983) and Lundberg (1987) and applied to the modelling of alloys. In the general *AB* alloy problem the occupancy of a site i at any given instant of time is denoted, p_i. An *A* atom at this site is given by $p_i = 1$ and a *B* atom by $p_i = 0$. Averaged over time, an equilibrium site occupancy, $c_i = \langle p_i \rangle$, defines the average A content of site i, the average *B* content given by $1 - c_i$.

Consider a simple pair potential formalism under the *mean field approximation*[2] which ignores correlations between occupancies on different sites and on the same site. The energy for an atom at site i is obtained by summing over the neighbouring sites. The interaction between an *A* atom on site i and a *B* atom on site j is denoted $\phi_{ij}^{AB} = \phi_{ji}^{AB}$, which are functions of the distance between the two atoms. The respective site energies for an *A* and *B* atom at

[2] The method has recently been taken beyond the mean field approximation by Sutton (1992).

site i are given by

$$E_i^A = \sum_{j \neq i} c_j \phi_{ij}^{AA} + (1-c_j)\phi_{ij}^{AB}$$
$$E_i^B = \sum_{j \neq i} c_j \phi_{ij}^{AB} + (1-c_j)\phi_{ij}^{BB} \qquad (8.3)$$

The energy of site i is then obtained from

$$E_i = c_i E_i^A + (1-c_i)E_i^B \qquad (8.4)$$

and the total energy of the system with a set of site occupancies, c_i, is then given by

$$E = 1/2 \sum_{i,j,\ i \neq j} c_i c_j \phi_{ij}^{AA} + [c_i(1-c_j) + c_j(1-c_i)]\phi_{ij}^{AB} + (1-c_i)(1-c_j)\phi_{ij}^{BB} \qquad (8.4)$$

Since the number of A and B atoms is not fixed it is necessary to work with the grand potential, $\Omega = E - TS - \mu_A N_A - \mu_B N_B$. The configurational entropy is calculated under the Bragg-Williams approximation in which the A and B atoms are assumed to be non-interacting. The grand potential is then given by

$$\Omega = E + kT\sum_i c_i \ln c_i + (1-c_i)\ln(1-c_i) - \mu_A \sum_i c_i - \mu_B \sum_i (1-c_i) \qquad (8.5)$$

The simulation is now performed to obtain the site occupancies $\{c_i\}$ and atomic positions $\{\mathbf{r}_i\}$ that minimise the grand potential of the system. For N sites there are thus $4N$ variables and the minimisation is performed in Molecular Dynamics as two coupled equations of motion

$$-\frac{\partial \Omega}{\partial c_k} = m_c \frac{\partial^2 c_k}{\partial t^2} \quad ; \quad -\frac{\partial \Omega}{\partial r} = m\frac{\partial^2 r}{\partial t^2} \qquad (8.6)$$

where m_c is a fictitious mass assigned to the site occupancies. These forces are given from eqn. 8.5 as follows

$$-\frac{\partial \Omega}{\partial c_k} = -\frac{\partial E}{\partial c_k} - kT \ln \frac{c_k}{1-c_k} + (\mu_A - \mu_B) \qquad (8.7)$$

and

$$-\frac{\partial \Omega}{\partial r} = -\frac{\partial E}{\partial r} \tag{8.8}$$

Note that these equations are coupled because E is a function of both the atomic positions and the site occupancies. It is easily shown by differentiating eqn. 8.4 that

$$-\frac{\partial E}{\partial c_k} = E_k^B - E_k^A \tag{8.9}$$

where the right hand side of this equation represents the energy of replacing an A atom with a B atom at site k.

The vacancy problem can be defined by associating the B atoms in the above analysis with vacancies. The internal energy has again been calculated using the Stillinger Weber potential, which involves two and three body terms. The three body term proceeds in exactly the same way, this time three sites, i, j, k being considered together with three body interaction potentials, $\phi_{ijk}^{AAB}, \phi_{ikj}^{AAB}, \phi_{ijk}^{ABB}$ etc, where it should be noted that $\phi_{ijk}^{AAB} \neq \phi_{ikj}^{AAB}$ etc.

While simulations performed using this technique are able to provide an answer, unlike the failure in MC, a similar inability to obtain useful information was found to occur. The problem is again directly related to the high energy cost of creating the *unrelaxed* vacancy, and can be understood with reference to eqn. 8.7. For a set of site occupancies close to 1 the generalised force in eqn. 8.9 tends to +8.7eV/site, the ideal vacancy formation energy discussed earlier. This force thus drives the system towards a state containing no vacancies. This is opposed by the entropy term which gives rise to a negative generalised force which tends to infinity as the site occupancies tend to unity. However, since the energy change between a site having a Si atom and a vacancy is so large, the force derived from the entropy term becomes large enough to balance this only at points where the site occupancies are very nearly unity. The result is that only a minute fraction of vacancies are, on average, present in the system and as a consequence the system is virtually unaware of their presence. By

increasing the temperature the size of the entropy force term is increased, but the system will have melted well before a reasonable concentration of vacancies is reached.

There is another way that the system can be forced to move from a set of occupancies, c_i, which are close to unity and as a result introduce more vacancies. If the chemical potential difference in eqn. 8.7 is made large and negative, as was also done in the MC simulations, it can eventually overcome the opposing force of eqn. 8.9 and move from the low vacancy concentration regime. The latter force will systematically reduce in size the further the site occupancies move from unity, and in the extreme will tend to zero as all the c_is tend to zero. Thus, the constant force given by the chemical potential difference chosen cannot be stopped by this force once its initial opposition has been overcome. The opposition comes from the entropy term which gives rise to a positive force but only in the region where the site occupancies are less than 0.5. In the limit, as the site occupancies tend to zero, this force tends to infinity. However, just as in the earlier case, since the force to set the system moving was so large the opposing force derived from the entropy term becomes large enough to balance this only at points where the site occupancies are very nearly zero, which corresponds to a unit cell composed of almost entirely vacancies.

This may be better understood with reference to fig. 8.1 in which the grand potential of eqn. 8.5 is illustrated schematically as a function of the site occupancies, c_i. The two extremes of the curve illustrate the points at which the force derived from the configurational entropy term is able to balance the driving force that is moving toward either a system of all Si atoms or all vacancies. As a direct consequence of the high energy cost of introducing an *unrelaxed* vacancy, these points are insignificantly different from the extreme limits. This plot also explains the two findings of the MC simulations, in which either no vacancies were introduced or an avalanche occurred which left no Si atoms. In each case it is the unphysical tampering with the chemical potential difference to obtain a reasonable concentration of vacancies, say 1 in 1000 sites, which places a demand on the system to saturate with vacancies.

The failure of both the MC and statistical methods in the study of vacancies is proposed

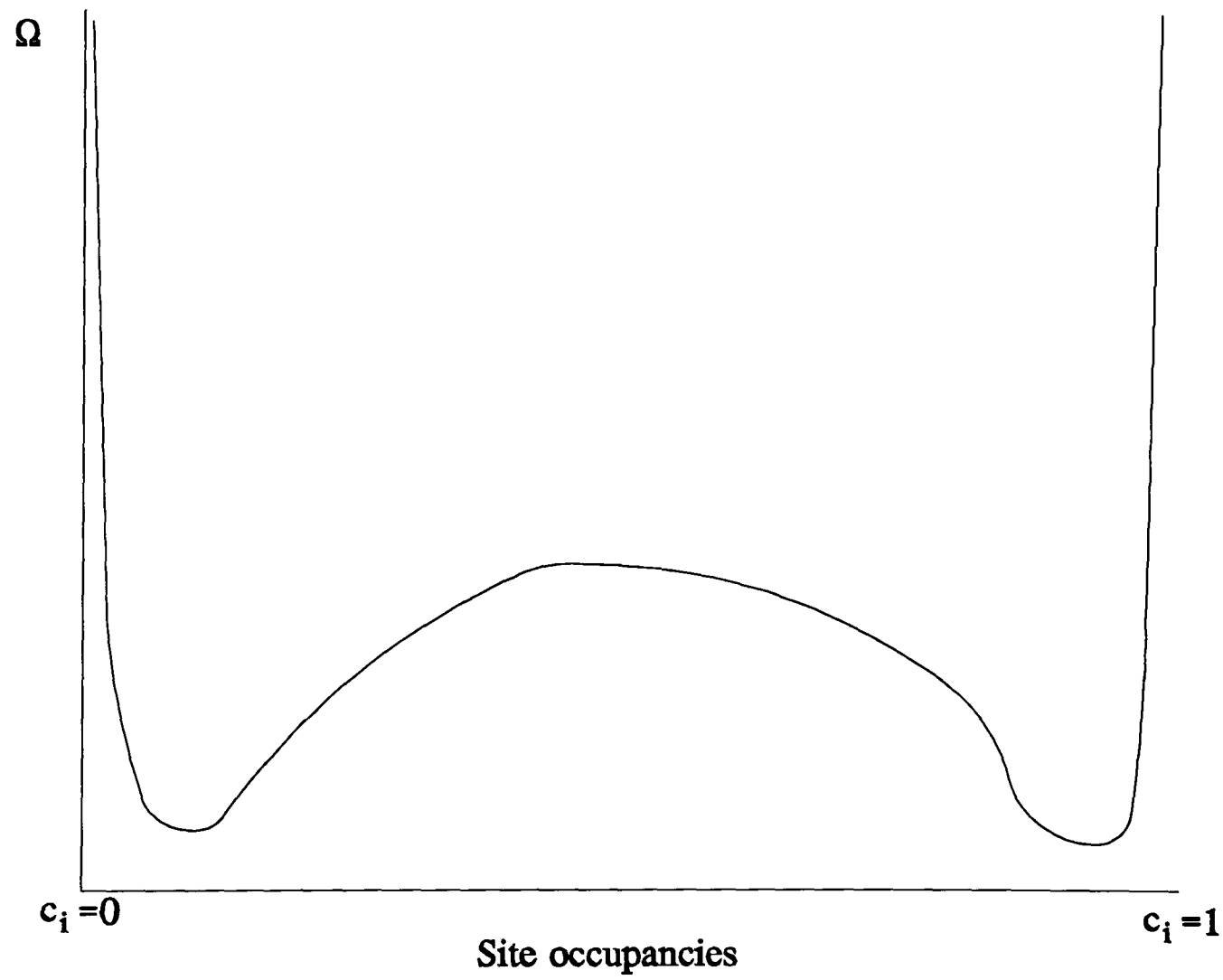

Fig. 8.1 Schematic representation of the variation of the grand potential, Ω, with site occupancy, c_i. The left minimum represents a system state saturated with vacancies, and the one on the right a state in which the vacancy concentration is negligible.

to be more general. Specifically, any system which involves large energy changes when one component is replaced by the other will lead to problems. Part of the difficulty is related to the fact that both the MC and statistical approaches are concerned with the *unrelaxed* energy when the occupancy of a site is changed. In reality there is relaxation around each vacant site which affects the formation energy to a significant degree. It is this relaxed formation energy which in reality describes the equilibrium number of vacancies, *not* the ideal unrelaxed energy. However, even with this reduced formation energy entering into the schemes it is still necessary to consider many more atomic sites to allow at least one vacancy to be introduced in a realistic equilibrium concentration. With the present cell sizes that are feasible for modelling this is not possible and hence the system is almost completely unaware that the vacancies exist, since they can do so only in such minute quantities. As such no real information about how vacancies affect the core structure, and the temperature dependence of this process, can be obtained by these methods.

8.3 The Frank partial dislocation

EBIC work by Wilshaw and Fell (1990) has shown that "clean" oxygen induced stacking faults and their bounding Frank partial dislocation do not act as recombination centres. They further showed that the introduction of transition metal impurities results in an EBIC signal, the recombination activity dependent on the impurity atom. This implies that the basic clean Frank partial should be reconstructed in a manner that leads to no states in the gap, which almost certainly indicates a fully four-fold coordinated structure. A preliminary investigation into the possible atomic structure of a Frank partial has been started here.

The Frank partial dislocation is created as the boundary line of a fault formed by inserting or removing one close packed {1 1 1} layer in FCC crystals. The diamond cubic structure has an FCC lattice but a basis of two atoms, which leads to a stacking sequence of ..AaBbCcAaBbCc.. (see chapter 1, section 1.2 and fig. 1.1a). The Frank partial in Si is thus formed by the insertion or removal of a double layer, such as Aa. The latter leads to an

intrinsic fault with stacking sequence ..AaBbCcBbCc.., whereas insertion of this layer leads to an *extrinsic* fault with stacking sequence ..AaBbAaCcAaBbCc.. The Frank partial has a Burgers vector *normal* to the {1 1 1} plane of the fault and the magnitude of the vector is equal to the change in lattice spacing produced by one of these double layers, $\boldsymbol{b}=1/3<1\,1\,1>$.

Two Frank partials of equal and opposite Burgers vectors in the usual dipolar arrangement can be used to bound a region inside a unit cell which has either lost or gained a double layer. However, due to the addition or loss of atoms to the system in forming these partials a quadrupolar type of unit cell must again be considered to enable the use of periodic boundary conditions. The lower dipole, in terms of the $<1\,1\,1>$ direction, bounds a region where a double layer has been removed, and the upper dipole then bounds the region in which these atoms are inserted. The generation of an appropriate starting configuration is illustrated in figs. 8.2a, 8.2b and 8.3.

An initial unit cell of perfect diamond cubic is generated using **GEN3D**. The unit cell is rectangular and contains 192 atoms, with box vectors $2[1\bar{2}1]$, $4[\bar{1}\,1\,\bar{1}]$ and $[1\,0\,\bar{1}]/2$. 8 atoms are removed from this unit cell as shown in fig. 8.2a. The atoms are then moved according to the displacements predicted by anisotropic elasticity theory using **AESOL_QUAD** and the resulting structure is illustrated in fig. 8.2b. It can be seen that the lower Frank partial dipole has collapsed the atoms to fill the original hole in fig. 8.2a, and the upper dipole of opposite sense has opened up a region to accommodate a new double layer. The 8 atoms initially removed can now be replaced and the resulting configuration is shown in fig. 8.3. The lower dipole gives rise to an intrinsic stacking fault and the upper one to an extrinsic fault as required.

A significant amount of time and effort was concentrated on trying to find how a four-fold reconstructed structure could be obtained from this starting configuration. The possibility of three-fold coordinated atoms that could undergo a Peierls distortion to bond along the core, as in the 30° partial, was also considered. The analysis always produced under or over coordinated atoms, and in general energetically unfavourable ring structures. A different

Fig. 8.2a A unit cell of perfect diamond cubic with 8 atoms removed in preparation for the elastic solution.

Fig. 8.2b The same unit cell after the atoms have been displaced according to anisotropic elasticity theory. Note that the lower hole has been filled, due to the bounding Frank partial dipole, and an upper one has opened due to the bounding Frank partial dipole of opposite sense.

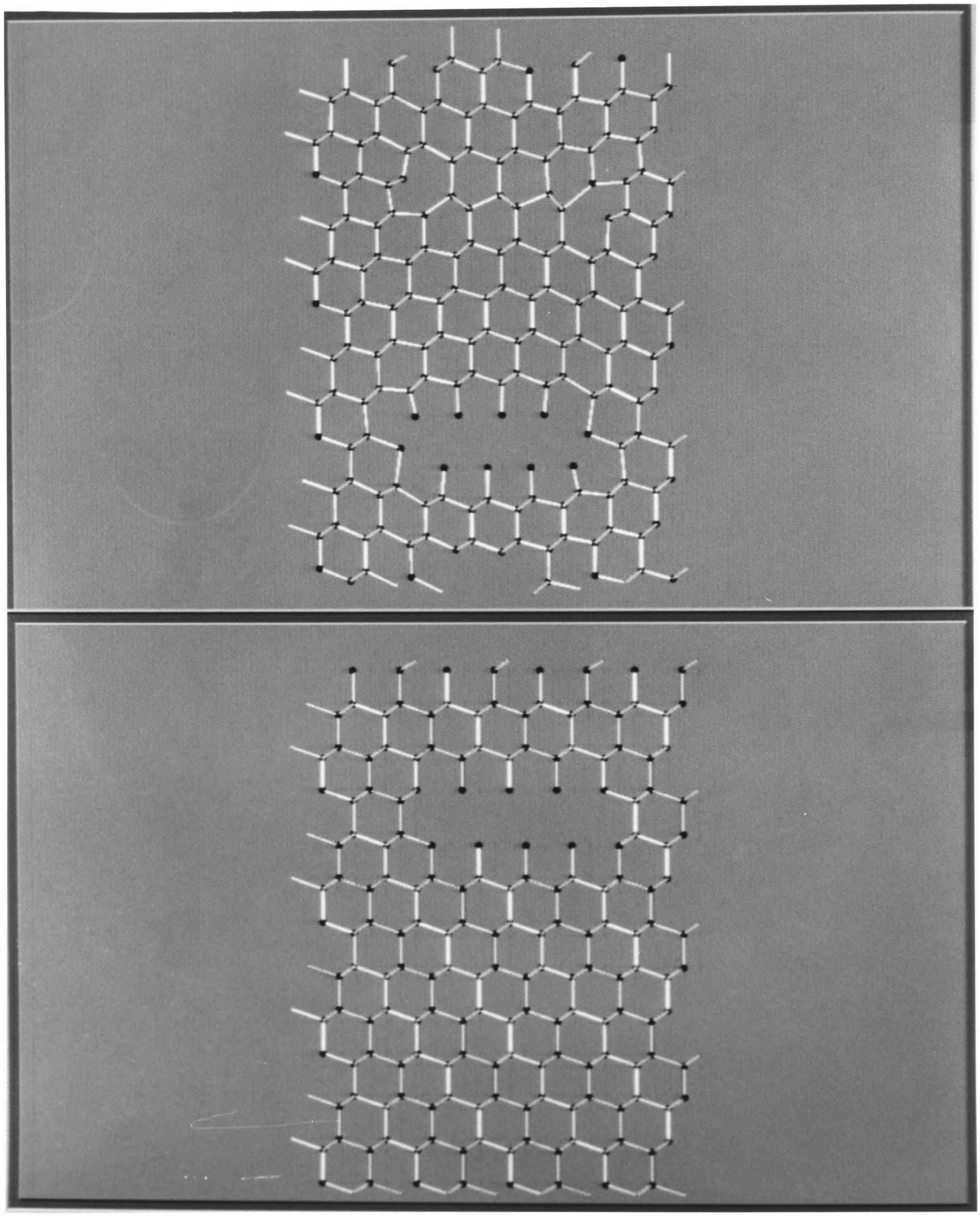

Fig. 8.3 The 8 atoms initially removed have now been replaced. Note the intrinsic stacking fault in the lower part of the unit cell due to the removal of a close-packed layer, and the extrinsic fault in the upper part of the unit cell due to the addition of this layer.

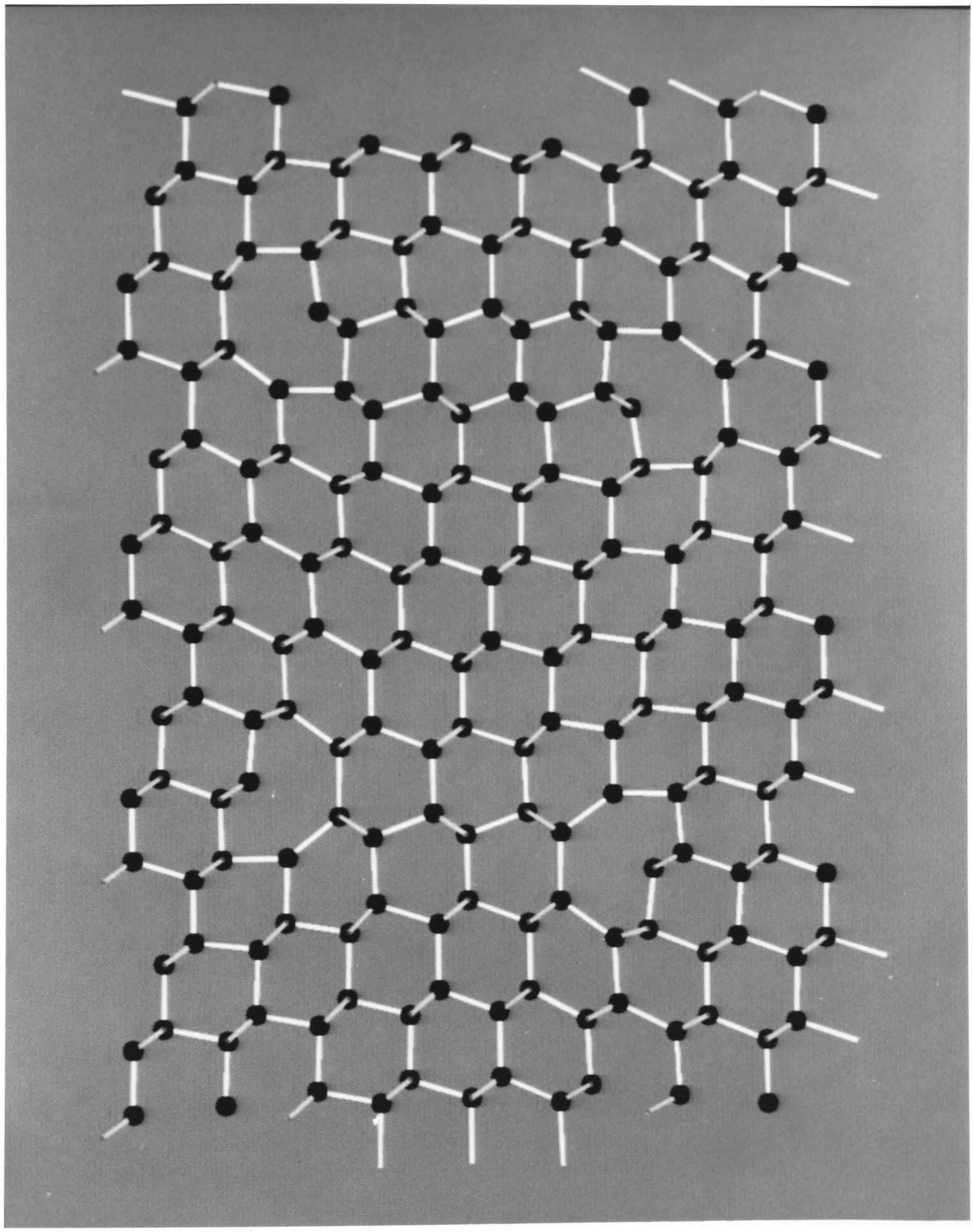

approach has also been considered which involves annealing this starting configuration at a high temperature using MD, with the intention to sample the phase space for the minimum structure which can then be cooled or "quenched" out as described in chapter 3, section 3.3.1.4. Simulations using the Stillinger Weber and Tersoff (1988b) potentials have not been able to find a four-fold reconstructed configuration, or a structure involving three-fold coordinated atoms similar to the 30° partial, although several different structural possibilities have been found. It is likely that some form of four-fold reconstructed core does exist based on the experimental evidence, but this initial analysis indicates its structure is not obvious.

A similar approach has been more successful in the modelling of a $[1\,1\,\bar{1}4]$ symmetric tilt grain boundary. From the discussion in chapter 4, section 4.2, it was decided to introduce the grain boundary by modelling a dislocation dipole in a rectangular unit cell. The grain boundary is composed of [001] perfect lattice dislocations, and the unit cell height is given by the *repeat period of the tilt grain boundary*. The elastic solution was obtained using the program **AESOL** and an initial relaxation was performed using the Stillinger Weber potential. This produced a structure consisting of an 8-membered and two 5-membered rings around each core which was completely four-fold coordinated except for two atoms on either side of the core. These atoms are placed in an exact analogy to those in the core of the 90° partial. Using the Stillinger Weber potential they remain symmetrically placed down the dislocation line and a quasi-five-fold bonding results. Use of the Tersoff (1988b) potential stabilises the structure which involves the asymmetric shift across and along the core, as in the 90° partial reconstruction, recovering full four-fold coordination. This symmetric tilt grain boundary is thus expected to behave in a similar manner to the reconstructed 90° partial (see chapter 5). Much more detailed work on this result will appear in the D.Phil. thesis of Krishna (1993).

8.4 Suggestions for the future

Point defect interactions with dislocations in semiconductors is a new area of theoretical

research. It is also an intense area of current experimental work, and there is promise of a parallel application of theoretical methods. The combined approach could reveal a real understanding of the electrical activity associated with clean and contaminated dislocations.

Suggestions for the future fall into two categories, those which take off immediately from the current work and those which could be the subject of future investigations.

The temperature dependence of the concentration and resulting atomic structure due to vacancies at dislocations has been investigated in section 8.2. The difficulties in obtaining results for this problem has been discussed there. There is another way in which the thermally averaged structure of an *isolated* vacancy at a dislocation at a finite temperature may be obtained. This can be achieved by augmenting the interatomic forces that apply at 0°K with temperature dependent contributions that arise from the minimisation of the free energy at a finite temperature, resulting in so called temperature-dependent forces (Sutton, 1989). The structure, at temperature, can then be obtained by a simple *static* minimisation.

The 30° and Frank partial dislocations have been preliminarily investigated but it would be useful to perform a detailed analysis similar to the 90° partial. The 60° Shockley partial (see Hirsch, 1979, 1980; Jones and Marklund, 1980; Veth and Teichler, 1984) involves highly stretched bonds which will clearly give the core of this dislocation a particular affinity to bond breaking or atomic rearrangement. The P calculations could be extended to consider these partials.

The tight-binding calculations could be continued using other impurity atoms such as B and As to compare the results obtained with the P. The ab initio, *CETEP*, calculations on Cu are to continue by looking at interstitial Cu^+ ions in the seven-fold ring of the 90° partial. The extension to different partials will also be useful and important research. Simulations using different transition metals should lead to an understanding of how these elements introduce deep gap states; for example, are these states dependent on the identity of the transition metal? As a note, however, transition metals such as Fe lead to the added complication of how to treat the magnetic interactions.

As computing power develops larger calculations may be undertaken. The size of the unit cell in the current Cu simulation has been questioned. Use of larger cells will certainly provide more realistic results, although it is stressed again that the equilibrium unit cell volume should be investigated and obtained. This will require the future development of techniques in *CETEP* to calculate stresses. Another useful result of enhanced computing resources could be an investigation into transition metal precipitation and its structural and electrical consequences.

The work described in this thesis has been exclusively concerned with Si. Similar work for Ge, GaAs and other semiconducting materials should be undertaken. In general, the possibilities for future research in this field are limited only by the constraints of the computing "apparatus" and the imagination of the researcher.

The direction for theoretical investigations in this area should ultimately be linked to the experimental findings. However, general ab initio schemes are capable, although they are not infallible, for accurate quantitative results in this and other areas of research. Given the guarantee of greater computing power there is the promise of theoretical simulations providing predictions for the experimentalists to verify!

APPENDICES AND REFERENCES

APPENDIX A

Lifson Warshell, Stillinger Weber and Tersoff potentials

The modified Lifson Warshell potential

This potential is as developed by Altmann *et al.* (1983) and contains the following terms:

(1) Bond Stretching:

$$\sum_{b_i} D_b\{\exp[-2\alpha(b_i-b_0)]-2\exp[-\alpha(b_i-b_0)]\}, \tag{A.1}$$

where

$$\alpha=(K_b/2D_b)^{1/2}. \tag{A.2}$$

(2) Bond Bending:

$$\sum_{\theta_i} [1/2K_\theta(\theta_i-\theta_0)^2+1/2K_q(q_i-q_0)^2]. \tag{A.3}$$

where θ is the angle between two bonds at a common atom and q is the distance between the two atoms bonded to this common atom, q being a function of θ.

(3) Torsional Term:

$$\sum_{\phi_i} [K_\phi/18(1+\cos 3\phi_i)+K_{\theta\theta}(\theta_1-\theta_0)(\theta_2-\theta_0)\cos\phi_i]. \tag{A.4}$$

where ϕ_i is one of the 9 torsional angles related to each bond. (for an explanation of the meaning of a torsional angle see Altmann *et al.* (1982)).

(4) Van der Waals interactions:

$$\sum\{8.28\times10^5\varepsilon\exp[-r/(0.0736r^*)]-2.25\varepsilon(r^*/r)^6\}, \tag{A.5}$$

where the summation is over all non-bonded pairs.

The parameters fitted by Altmann *et al.* (1983) are:

Parameter	Value
b_0 (Å)	2.3513
D_b (eV)	3.51
K_b (eV/Å^2)	7.99
K_θ (eV/rad^2)	-0.104
K_q (eV/Å^2)	0.296
K_ϕ (eV)	0.0278
$K_{\theta\theta}$ (eV/rad^2)	-0.778
ε (eV)	0.00191
r^* (Å)	3.560

The Stillinger Weber potential

The Stillinger Weber potential contains two and three body terms. Energy and length units ε and σ were introduced such that,

$$v_2(r_{ij}) = \varepsilon f_2(r_{ij}/\sigma) \ , \qquad v_3(r_i,r_j,r_k) = \varepsilon f_3(r_i/\sigma, r_j/\sigma, r_k/\sigma) \ , \tag{A.6}$$

where r_i is the position of atom i and r_{ij} is the ij bond length. The scaled pair potential is

$$f_2(r) = \begin{cases} A\left(\frac{B}{r^p} - \frac{1}{r^q}\right)\exp\left[\frac{1}{(r-a)}\right], & r<a, \\ 0, & r \geq a. \end{cases} \tag{A.7}$$

Here a sets the range of the potential, B is adjusted so that the potential minimum occurs at $r=2^{1/6}$, and A is set so that the value of f_2 at the potential minimum is -1. This potential automatically cuts off at $r=a$ without discontinuities in any derivatives. The same cutoff advantage can be extended to the three-body interactions f_3. This term is required to have rotational and translational symmetry and is thus expressed as a symmetrised sum:

$$f_3(r_i,r_j,r_k) = h(r_{ij},r_{ik},\theta_{jik}) + h(r_{ji},r_{jk},\theta_{ijk}) + h(r_{ki},r_{kj},\theta_{ikj}) \tag{A.8}$$

where θ_{jik} is the angle between r_j and r_k subtended at i. Provided that both r_{ij} and r_{ik} are less than the cutoff a, then h has the following form:

$$h(r_{ij},r_{ik},\theta_{jik}) = \lambda \exp\left[\frac{\gamma}{(r_{ij}-a)} + \frac{\gamma}{(r_{ik}-a)}\right] \times \left(\cos\theta_{jik} + \frac{1}{3}\right)^2 \tag{A.9}$$

otherwise h is zero. Since the ideal tetrahedral angle, θ_t, is such that $\cos\theta_t = -1/3$, the angular term discriminates in favour of a perfect tetrahedral geometry.

The parameters chosen by Stillinger and Weber (1985) are:

Parameter	Value
A	7.049556277
B	0.6022245584
p	4
q	0
a	1.80
λ	21.0
γ	1.20
ε (eV/atom pair)	2.1672
σ (Å)	2.0951

The Tersoff potential

The functional form as derived by Tersoff (1988a) is as follows:

$$
\begin{aligned}
&E=\sum_i E_i=\frac{1}{2}\sum_{i\neq j} V_{ij},\\
&V_{ij}=f_c(r_{ij})[a_{ij}\,Aexp(-\lambda_1 r_{ij})-b_{ij}\,Bexp(-\lambda_2 r_{ij})],\\
&f_c(r)=\begin{cases}1, & r < R-D\\ \frac{1}{2}-\frac{1}{2}\sin\left[\frac{\pi}{2}(r-R)/D\right], & R-D < r < R+D\\ 0, & r > R+D\end{cases}\\
&b_{ij}=(1+\beta^n\zeta_{ij}^n)^{-1/2n},\\
&\zeta_{ij}=\sum_{k\,(\neq i,j)} f_c(r_{ik})g(\theta_{jik})\exp[\lambda_3^3(r_{ij}-r_{ik})^3],\\
&g(\theta)=1+\frac{c^2}{d^2}-\frac{c^2}{d^2+(h-\cos\theta)^2},\\
&a_{ij}=(1+\alpha^n\eta_{ij}^n)^{-1/2n},\\
&\eta_{ij}=\sum_{k\,(\neq i,j)} f_c(r_{ik})\exp[\lambda_3^3(r_{ij}-r_{ik})^3].
\end{aligned}
\qquad (A.10)
$$

Here, i, j, and k label the atoms of the system, r_{ij} is the length of the ij bond, and θ_{jik} is the bond angle between bonds ij and ik.

The two parameter sets used in this work (Tersoff 1988a, 1988b) are:

Parameter	Tersoff (1988a)	Tersoff (1988b)
A (eV)	3.2647×10^{3}	1.8308×10^{3}
B (eV)	9.5373×10^{1}	4.7118×10^{2}
λ_1 (Å^{-1})	3.2394	2.4799
λ_2 (Å^{-1})	1.3258	1.7322
α	0.0	0.0
β	3.3675×10^{-1}	1.0999×10^{-6}
η	2.2956×10^{1}	7.8734×10^{-1}
c	4.8381	1.0039×10^{5}
d	2.0417	1.6218×10^{1}
h	0.0000	-5.9826×10^{-1}
λ_3 (Å^{-1})	1.3258	1.7322
R (Å)	3.0	2.85
D (Å)	0.2	0.15

APPENDIX B

Glossary of programs developed

The input files required for some of these programs are listed in appendix C. In particular there exist two types of atomic configuration file which have been called *type 1* and *type 2* in appendix C. The required type is indicated here in brackets for the relevant programs.

AESOL: Anisotropic elasticity theory solution for a dislocation dipole in an orthogonal unit cell. (*type 1*).

AESOL_QUAD: Anisotropic elasticity theory solution for a dislocation quadrupole in an orthogonal unit cell. (*type 1*).

AESOL_SKEWDIPOLE: Anisotropic elasticity theory solution for a dislocation dipole in a skew unit cell. (*type 1*).

BANDPLOT: Plots the direct band-structure output from the tight-binding program (VAX).

GAPSTATES: Strips out all information from a band-structure plot using Chadi's Hamiltonian except for the projected bulk band edges and states within the gap. Needs two band-structure plots - a perfect crystal plot and the defect structure plot. The format for these plots comes straight out of the tight-binding program.

GAPPLOT: Plots the output from **GAPSTATES** or **GAPSPSSTATES** (VAX).

GAPSPSSTATES: Strips out all information from a band-structure plot using Vogl's Hamiltonian except for the projected bulk band edges and states within the gap. Needs two band-structure plots - a perfect crystal plot and the defect structure plot. The format for these plots comes straight out of the tight-binding program.

GEN3D: Generates a perfect 3D periodic cell of diamond cubic crystal (see chapter 3, section 3.2). Output is an atomic configuration file of *type 1*.

MCARLO: Monte Carlo code developed to investigate vacancy concentrations at the core of dislocations (see chapter 8, section 8.2.1). See the code for details of its use.

MDLW: Molecular Dynamics code using the modified Lifson Warshell potential for orthogonal unit cells large enough to satisfy the *minimum image condition*. (*type 1*).

MDLW_NOMI: Molecular Dynamics code using the modified Lifson Warshell potential for orthogonal unit cells that does not rely on the *minimum image condition*. (*type 1*).

MDSTATS: Molecular Dynamics scheme using the Stillinger Weber potential AND a statistical weighting on the occupation of each atom. Used to investigate the concentration of vacancies at dislocation cores, to compare with the Monte Carlo predictions (see chapter 8. section 8.2.2). See the code for details of its use.

MDSW: Molecular Dynamics code using the Stillinger Weber potential for orthogonal unit cells large enough to satisfy the *minimum image condition*. (*type 1*).

MDSW_NOMI: Molecular Dynamics code using the Stillinger Weber potential for orthogonal unit cells that does not rely on the *minimum image condition.* (*type 1*).

MDSW_NOMI_SKEW: Molecular Dynamics code using the Stillinger Weber potential for the skew unit cells described in chapter 4, section 1.2 and 1.3. It does not rely on the *minimum image condition.* (*type 1*).

MDTERSOFF: Molecular Dynamics code using the Tersoff potential for orthogonal unit cells large enough to satisfy the *minimum image condition.* (*type 1*).

MDTERSOFF_NOMI: Molecular Dynamics code using the Tersoff potential for orthogonal unit cells that does not rely on the *minimum image condition.* (*type 1*).

MDTERSOFF_NOMI_SKEW: Molecular Dynamics code using the Tersoff potential for the skew unit cells described in chapter 4, section 1.2 and 1.3. It does not rely on the *minimum image condition.* (*type 1*).

MDTETRABOND: Bond length and angle analysis for an orthogonal unit cell large enough to satisfy the *minimum image condition.* (*type 1*).

MULTSLAB: Written by M^{c}Innes (1992). Allows any orthogonal unit cell to be multiplied in any of its three box directions. (*type 2*).

ORTHOG_CSTP_TO_TB: Converts any orthogonal unit cell from the *CASTEP* and *CETEP* format (see appendix C) back to *type 2* format.

ORTHOG_TB_TO_CSTP: Converts any orthogonal unit cell into the format required by *CASTEP* and *CETEP* (see appendix D). (*type 2*).

SKEW_CSTP_TO_TB: Converts a skew cell from the *CASTEP* and *CETEP* format (see appendix D) back to *type 2* format.

SKEW_FROM_QUAD: Generates a skew cell from an orthogonal unit cell containing a quadrupole. (*type 2*).

SKEW_TB_TO_CSTP: Converts a skew cell into the format required by *CASTEP* and *CETEP* (see appendix D). (*type 2*).

TBOND_SKEWDIPOLE: Bond length and angle analysis for the skew cells - these cells don't rely on the *minimum image condition.* (*type 2*).

TETRABOND: Bond length and angle analysis for an orthogonal unit cell large enough to satisfy the *minimum image condition.* (*type 2*).

APPENDIX C

Atomic and resource files

Atomic configuration files

There exist two types of file that contain the unit cell and atomic information:

Type 1: This is the form output from the unit cell generation program **GEN3D**. It is input to all classical Molecular Dynamics programs and the anisotropic elasticity theory programs.

integer	:	*iteration no*
character*80	:	*title*
integer	:	*Number of atoms (N)*
real*8 x 3	:	*box_x, box_y, box_z - Cell size*
real*8 x 3	:	*box_x direction vector in i, j, k coordinate system*
real*8 x 3	:	*box_y direction vector in i, j, k coordinate system*
real*8 x 3	:	*box_z direction vector in i, j, k coordinate system*
real*8 x 3, integer	:	*x, y and z coordinates of atom 1; atomic type*
real*8 x 3, integer	:	*x, y and z coordinates of atom 2; atomic type*
.		
.		
real*8 x 3, integer	:	*x, y and z coordinates of atom N; atomic type*

Type 2: This is the style as required by the tight-binding code (see M^{c}Innes, 1992). It is also the form used to convert files into *CASTEP* and *CETEP* format (see Appendix D).

integer	:	*iteration no*
character*80	:	*title*
integer x 3	:	*Total no of atoms (N), no of host atoms (N), dummy*
real*8 x 3	:	*box_x, box_y, box_z - Cell size*
real*8 x 3, integer	:	*x, y and z coordinates of atom 1; atomic type*
real*8 x 3, integer	:	*x, y and z coordinates of atom 2; atomic type*
.		
.		
real*8 x 3, integer	:	*x, y and z coordinates of atom N; atomic type*
character*10	:	*noself/self - tag for self consistency data*

If self-consistency and Molecular Dynamics are in use then atom charges and velocities etc. are written to the end of this file. Specific k-points, read in when $q < 0$ in the resource file (see M^{c}Innes, 1992), must be added to the end of this file in fractions of the reciprocal lattice:

integer	:	*Number of k-points* (N)
real*8 x 3	:	k_x, k_y, k_z *for k-point 1 (eg. 0.0, 0.0, 0.25)*
real*8 x 3	:	k_x, k_y, k_z *for k-point 2*
.		
.		
real*8 x 3	:	k_x, k_y, k_z *for k-point N*
real*8	:	*Weight of k-point 1 (eg. 0.25)*
real*8	:	*Weight of k-point 2*
.		
.		
real*8	:	*Weight of k-point N*

Resource file for anisotropic elasticity programs

These programs can be run on line or will read this file from standard input.

elastic constant, c_{11}
elastic constant, c_{12}
elastic constant, c_{44}
box x direction in i, j, k coordinate system
box z direction in i, j, k coordinate system
Burger's vector in new coordinate system of the unit cell, ie. (box_x,0,0) etc.
input channel number, eg. 2
*title of the atomic configuration file - **type 1** (see above)*
number of slabs to repeat in the box_x direction
number of slabs to repeat in the box_y direction
X and Y coordinates of left dislocation
X and Y coordinates of right dislocation
{X and Y coordinates of upper right dislocation - only for Quadrupole}
{X and Y coordinates of upper left dislocation - only for Quadrupole}
output channel number, eg. 3
title of output file

Resource file for Stillinger Weber and modified Lifson Warshell MD programs

This file is called **mdpars.dat** and is read in by these programs.

descriptive text - eg. Stillinger Weber simulation at 1000K.
title of the atomic configuration file
number of MD iterations required
total CPU time for the simulation - this is only of relevance for the VAX versions
temperature (°K)
MD time step x 10^{-14} seconds
quenching flag - 0 off; 1 on
pressure time constant - used in volume equilibration
number of MD steps between output of atomic configuration file
number of MD steps between information output - ie. KE, PE etc.
temperature equilibration flag - 0 off; 1 on
volume equilibration flag - 0 off; 1 on
cooling flag - 0 off; 1 on
cooling rate (°K/time-step) if cooling flag set to 1

Resource file for Tersoff MD programs

descriptive text - eg. Tersoff simulation at 1000K.
title of the atomic configuration file
number of MD iterations required
total CPU time for the simulation - this is only of relevance for the VAX versions
temperature (°K)
MD time step x 10^{-14} seconds
quenching flag - 0 off; 1 on
number of MD steps between output of atomic configuration file
number of MD steps between information output - ie. KE, PE etc.
temperature equilibration flag - 0 off; 1 on
cooling flag - 0 off; 1 on
cooling rate (°K/time-step) if cooling flag set to 1
parameter set flag - 1 = Tersoff (1988a); 2 = Tersoff (1988b)

This file is also called **mdpars.dat** and is read in by these programs. Parameters related to volume equilibration have been removed in the case of the Tersoff codes. Note the new parameter at the end of the file that picks out the two possible parameter sets (Tersoff 1988a, 1988b).

For information on how to run the tight-binding codes, see M^{c}Innes (1992).

APPENDIX D

Using CASTEP and CETEP

Input files

fort.3: Symmetrisation data (reduces the number of k-points needed in structures exhibiting symmetry).

fort.10: data for interpolating the Ewald integral.

fort.11: data for interpolating the pseudopotential - for two atomic species just add the *fort.11* of the second to the end of the *fort.11* of the first.

fort.14: resource file - explanatory text exists within this file. (see below for other details)

fort.15: atomic configuration file and **k**-points - see below.

fort.18: non-local pseudopotential data for real-space version of *CETEP* - for two atomic species just add the *fort.18* of the second to the end of the *fort.18* of the first.

Atomic configuration file
Be careful with the form of the box vectors, and note that everything is doubled up:

real*8 x 3 : ***i*** *component of the box_x, box_y and box_z vectors.*
real*8 x 3 : ***j*** *component of the box_x, box_y and box_z vectors.*
real*8 x 3 : ***k*** *component of the box_x, box_y and box_z vectors.*
real*8 x 3 : ***i*** *component of the box_x, box_y and box_z vectors.*
real*8 x 3 : ***j*** *component of the box_x, box_y and box_z vectors.*
real*8 x 3 : ***k*** *component of the box_x, box_y and box_z vectors.*
real*8 x 4 : *x, y and z positions of atom 1 as fractions of the respective box sides, atom movement? - 1.0=on; 0.0=off.*
real*8 x 4 : *x, y and z positions of atom 2 as fractions of the respective box sides, atom movement? - 1.0=on; 0.0=off.*
.
.
real*8 x 4 : *x, y and z positions of atom N as fractions of the respective box sides, atom movement? - 1.0=on; 0.0=off.*
real*8 x 3 : *x, y and z positions of atom 1 as fractions of the respective box sides.*
real*8 x 3 : *x, y and z positions of atom 2 as fractions of the respective box sides.*
.
.
real*8 x 3 : *x, y and z positions of atom N as fractions of the respective box sides.*

k-points are placed at the end of this file. They have different formats in the serial and parallel codes. For *CETEP*:
real*8 x 4 : k_x, k_y, k_z *for k-point 1 (eg. 0.0, 0.0, 0.25); weight (eg. 0.25)*
real*8 x 4 : k_x, k_y, k_z *for k-point 2*; weight
.
.
real*8 x 4 : k_x, k_y, k_z *for k-point N*; weight

For *CASTEP*:

real*8 x 3	:	k_x, k_y, k_z *for k-point 1 (eg. 0.0, 0.0, 0.25)*
real*8 x 3	:	k_x, k_y, k_z *for k-point 2*
.		
.		
real*8 x 3	:	k_x, k_y, k_z *for k-point N*
real*8	:	*Weight of k-point 1 (eg. 0.25)*
real*8	:	*Weight of k-point 2*
.		
.		
real*8	:	*Weight of k-point N*

Notes on using CASTEP

The include file *param* is used to specify and allocate space for all the major parameters. When changed the code *CGION8.F* must be recompiled and linked with all other object modules. This is achieved by using: *f77 -72 -O2 -c cgion8.f; f77 -72 -O2 -o outputname *.o -lnag*. Param declares - the number of k-points; the number of ions; the number of ions of species 1 and 2 etc.; the energy cutoff; the number of plane waves; the fourier transform parameters and ewald integral parameters to name but a few.

CASTEP is easy to use. Choose the number of ions/k-points etc required, compile and then run. The code will tell you which parameters need changing and what their values should be. Make the changes in *param*, recompile and go.

Notes on using CETEP

Use *makefile* to compile and link, which will take care of everything for you whatever changes have been made. There are three include files to be aware of:

cubeparm.inc: to specify the number of nodes to be used - changing this file will cause makefile to recompile the whole code.

ewaltrp.inc: file for ewald integral parameters. *CETEP* is not so helpful in telling you what these should be and there have seemed to be problems if you get them wrong. My advice is run on *CASTEP* to find out what they should be. NOTE - the number of ions must also be specified in this include file.

mainp.inc: this is similar to *param* above. Again the number of ions must be declared, number of species, number of ions per species etc. Other parameters of importance are:

NGX, NGY, NGZ: the program will tell you what these should be, but note that these are suggested values for *orthogonal* cells only. Try and make *NGX* a multiple of the number of nodes you are using (ie. if 16 nodes, NGX=16, 32 etc.). This is because the distribution on the nodes is performed sequentially with *NGX*, so that a multiple of the number of nodes will distribute all nodes equally.

NIONPN: the number of ions per node - reduce this as far as you can since it is expensive on memory requirements - the program will tell you what it must be.

NGRPT: as with the parameter above, try and reduce this as much as possible since it uses a lot of memory - again the program will tell you what it must be.

MRPLWV: max number of plane waves - be careful here and check that the number of plane

waves distributed over all nodes is less than the value of this parameter.

fort.14: this has explanatory text - some specific parameters are:

NDELAY: ions will move, assuming *IION*=1, only after *NDELAY* initial iterations - this is used to minimise the electronic system prior to letting the ions move.

Time-step for ion dynamics: this is what actually specifies the maximum displacement allowed by the ions - this displacement is given by the value of this parameter multiplied by the maximum force in the system.

Useful commands on Maxwell

TPS informs you of the jobs running on Maxwell and the number of nodes taken by each. *Cube* loads the code onto the nodes and takes as its input a number specifying the number of nodes (see cubeparm.inc), eg. *cube -d4 parcarp > out* will load the program parcarp onto 16 nodes and write the output to the file out. Maxwell is a unix-based machine.

Final comments on running on Maxwell

The code can only practically output wavefunctions etc at the end of a run. Maxwell is prone to stopping halfway through a run at times resulting in no output, so keep runs to about 12 hours or so for safety. Keep an eye on the energy and forces as the ions move - if the electrons can't keep up the energy tends to blow up, but I have had an occasion when it has just slowly and subtly crept back up!

APPENDIX E

CETEP relaxed cell - tabulated coordinates

The details of the relaxation are given in chapter 5, section 5.4.1. The unit cell is *oblique* containing 64 atoms and a 90° partial dislocation dipole. The box vectors are expressed in the usual **i**, **j**, **k** orthogonal coordinate system and are given in units of Å. The atomic positions are given in terms of fractions of these box vectors (ie. 0.5 0.4 0.3 implies the atom lies at the position given by $0.5\boldsymbol{X} + 0.4\boldsymbol{Y} + 0.3\boldsymbol{Z}$).

X box vector (**i**, **j**, **k**)	10.8580	-21.7160	10.8580
Y box vector (**i**, **j**, **k**)	-0.4524	-18.0967	-3.1669
Z box vector (**i**, **j**, **k**)	2.7145	0.0000	-2.7145
atom 1	-0.4324	0.0310	-0.3350
atom 2	0.4624	0.2160	-0.3875
atom 3	-0.2104	-0.2175	-0.1674
atom 4	-0.3174	-0.0319	-0.3435
atom 5	0.0032	-0.4644	-0.0052
atom 6	-0.0945	-0.2703	-0.0957
atom 7	-0.4181	0.2895	-0.4273
atom 8	0.4924	0.4715	0.4917
atom 9	-0.2293	0.0390	-0.1372
atom 10	-0.3039	0.2211	-0.3322
atom 11	0.0534	-0.2180	-0.1153
atom 12	-0.0262	-0.0310	-0.1652
atom 13	0.2571	-0.4688	-0.0163
atom 14	0.1675	-0.2828	-0.0862
atom 15	-0.1674	0.2827	-0.3694
atom 16	-0.2570	0.4687	-0.4856
atom 17	0.0261	0.0311	-0.1964
atom 18	-0.0534	0.2180	-0.3338
atom 19	0.3040	-0.2211	-0.1108
atom 20	0.2293	-0.0391	-0.0973
atom 21	-0.4923	-0.4716	-0.0368

atom 22	0.4182	-0.2896	-0.1380
atom 23	0.0945	0.2702	-0.3672
atom 24	-0.0032	0.4644	-0.4698
atom 25	0.3174	0.0318	-0.3737
atom 26	0.2104	0.2176	-0.3853
atom 27	-0.4624	-0.2159	-0.1715
atom 28	0.4324	-0.0312	-0.3043
atom 29	-0.2462	-0.4679	-0.0197
atom 30	-0.3466	-0.2827	-0.1342
atom 31	0.3466	0.2827	-0.4170
atom 32	0.2462	0.4679	-0.4877
atom 33	-0.3362	-0.2197	0.3327
atom 34	-0.4415	-0.0338	0.2016
atom 35	-0.1193	-0.4694	0.4807
atom 36	-0.2202	-0.2819	0.3667
atom 37	0.4671	0.2804	0.0828
atom 38	0.3713	0.4665	0.0126
atom 39	-0.3148	0.0426	0.1005
atom 40	-0.4211	0.2244	0.1003
atom 41	-0.0761	-0.2124	0.3845
atom 42	-0.1545	-0.0263	0.3786
atom 43	0.1319	-0.4687	0.4837
atom 44	0.0406	-0.2813	0.4115
atom 45	-0.2917	0.2830	0.1327
atom 46	-0.3804	0.4677	0.0155
atom 47	-0.0988	0.0308	0.3083
atom 48	-0.1778	0.2172	0.1673
atom 49	0.1778	-0.2173	0.3849
atom 50	0.0988	-0.0307	0.3381
atom 51	0.3805	-0.4677	0.4838
atom 52	0.2918	-0.2830	0.4158
atom 53	-0.0406	0.2813	0.1295

atom 54	-0.1319	0.4688	0.0143
atom 55	0.1546	0.0262	0.3527
atom 56	0.0762	0.2123	0.1712
atom 57	0.4212	-0.2245	0.3251
atom 58	0.3148	-0.0427	0.1454
atom 59	-0.3712	-0.4665	0.4792
atom 60	-0.4670	-0.2804	0.3630
atom 61	0.2203	0.2821	0.0844
atom 62	0.1193	0.4694	0.0113
atom 63	0.4416	0.0337	0.1674
atom 64	0.3363	0.2196	0.1126

REFERENCES

Abell GC, (1985), *Phys. Rev. B*, **31**, 6184.

Alexander H, (1979), *J. Phys. (Paris)*, **40**, C6-1.

Alexander H, (1986), *Dislocations in Solids*, Vol. 7 Ed. Nabarro FRN, North Holland, Amsterdam, 146.

Allen PB and Tildesley FJ, (1987), *Computer Simulation of Liquids*, Clarendon Press: Oxford.

Altmann SL, Lapiccirella A and Lodge KW, (1983), *Int. J. Quant. Chem.*, **23**, 1057.

Altmann SL, Lapiccirella A, Lodge KW and Tomassini N, (1982), *J. Phys. C: sol. stat. phys.*, **15**, 5581.

Anstis GR, Hirsch PB, Humphreys CJ, Hutchinson JL and Ourmazd A, (1981), *Inst. Phys. Conf. Ser.*, **60**, p. 15.

Ashcroft NW and Mermin ND, (1976), *Solid State Physics*, Holt, Reinhart and Winston.

Bachelet GB, Hamann DR and Schluter M, (1982), *Phys. Rev. B*, **26**, 4199.

Ball MA and Hajaig S, (1981), *Philos. Mag. B*, **43**, 309.

Ballone P and Galli G, (1990), *Phys. Rev. B*, **42**, 1112.

Baraff GA, Kane EO and Schlüter M, (1980), *Phys. Rev. B*, **21**, 5662.

Bergholz W, Zoth G, Gelsdorf F and Kolbesen BO, (1991), *Defects in Silicon II*, The Electrochem. Soc., Penington, N.J.

Bloch F, (1928), *Z Phys.*, **52**, 555.

Bonapasta AA, Battistoni C, Lapiccirella A, Tomassini N, Altmann SL and Lodge KW, (1988), *Phys. Rev. B*, **37**, 3058.

Bourret A, Thibault-Desseaux J and Lancon FJ (1983), *J. Phys. (Paris)*, **44**, C4-15.

Bull C, Ashburn P, Booker GR and Nicholas KH, (1979), *Sol. Stat. Electron*, **22**, 95.

Car R and Parrinello M, (1985), *Phys. Rev. Lett.*, **55**, 2471.

Chadi DJ, (1978), *Phys. Rev. Lett.*, **41**, 1062.

Chadi DJ, (1979a), *Phys. Rev. B*, **19**, 2074.

Chadi DJ, (1979b), *Phys. Rev. Lett.*, **43**, 43.

Chadi DJ, (1984), *Phys. Rev. B*, **29**, 785.

Chadi DJ and Cohen ML, (1975), *Phys. Status Solidi B*, **68**, 405.

Chelikowsky JR, (1982), *Phys. Rev. Lett.*, **49**, 1569.

Chelikowsky JR and Spence JCH, (1984), *Phys. Rev. B*, **30**, 694.

Cohen MH, Singh J and Yonezawa F, (1980), *J. Non-Cryst. Solids*, **35-36**, 55.

Denteneer P and van Haeringen W, (1985), *J. Phys. C: sol. stat. phys.*, **18**, 4127.

Dodson BW, (1987), *Phys. Rev. B*, **35**, 2795.

Duesbery MS, Joos B and Michel DJ, (1991), *Phys. Rev. B*, **43**, 5143.

Duesbery MS, (1991), *private communication.*

EMIS Datareviews Series No. 4, (1988), *Properties of Silicon*, Inspec Publication, London.

Eshelby JD, Read WT and Shockley W, (1953), *Acta. Met.*, **1**, 251.

Fell TS, (1992), PhD Thesis, University of Oxford, England.

Fell TS and Wilshaw PR, (1991), *Inst. Phys. Conf. Ser.*, **117**, 733.

Finnis MW, (1990), *private communication.*

Foiles SM, (1985), *Phys. Rev. B*, **32**, 7685.

Foulkes WMC, (1987), PhD thesis, University of Cambridge, England.

Froyen S and Harrison WA, (1979), *Phys. Rev. B*, **20**, 2420.

Gomez A and Hirsch PB, (1977), *Philos. Mag.*, **36**, 169.

Gomez A, Cockayne DJH, Hirsch PB and Vitek V, (1975), *Philos. Mag.*, **31**, 105.

Goodwin L, Skinner AJ and Pettifor DG, (1989), *Europhys. Lett.*, **9**, 701.

Grazhulis VA, Kveder VV and Ossipyan YuA, (1981), *Soviet Phys. JTEP*, **53**, 618.

Greenbaum SG and Carlos WE, (1984), *J. Appl. Phys.*, **56**, 1874.

Greenwood NN and Earnshaw A, (1984), *Chemistry of the Elements*, Pergamon Press, Oxford.

Gyorffy BL and Stocks GM, (1983), *Phys. Rev. Lett.*, **50**, 374.

Hairie A, (1992), *private communication with AP Sutton.*

Halicioglu T, Pamuk HO and Erkoc S, (1988), *Phys. Status Solidi B*, **149**, 81.

Harris J, (1985), *Phys. Rev. B*, **31**, 1770.

Harrison WA, (1980), *Electronic Structure and the Properties of Solids*, San Francisco: Freeman.

Häussermann F and Schaumburg H, (1973), *Philos. Mag.*, **27**, 745.

Haydock R, Heine V and Kelly MJ, (1972), *J. Phys. C: sol. stat. phys.*, **5**, 2845.

Heine V, (1980), *Solid State Physics*, **35**, 1.

Heggie MI, (1987), *Izv. Akad. Nauk. SSSR Ser. Fiz.*, **51**, 693.

Heggie MI and Jones R, (1982), *J. Phys. (Paris)*, **43**, C1-45.

Heggie MI and Jones R, (1983a), *Philos. Mag. B*, **48**, 365.

Heggie MI and Jones R, (1983b), *Philos. Mag. B*, **48**, 379.

Heggie MI and Jones R, (1983c), *J. Phys. (Paris)*, **44**, C4-43.

Heggie MI and Jones R, (1987), *Inst. Phys. Conf. Ser.*, **87**, p. 367.

Heggie MI, Jones R, Lister GMS and Umerski A, (1989), *Inst. Phys. Conf. Ser.*, **104**, p. 43.

Heggie MI, Jones R and Umerski A, (1991), *Inst. Phys. Conf. Ser.*, **117**, 125.

Higgs V, Lightowlers EC, Norman CE and Kightley P, (1992), *Mater. Sci. Forum*, **83-87**, 1309.

Hirsch PB, (1979), *J. Phys. (Paris)*, **40**, C6-27.

Hirsch PB, (1980), *J. Microsc.*, **118**, 3.

Hirsch PB, (1985), *Mater. Sci. Technol.*, **1**, 666.

Hirth JP and Lothe J, (1982), *Theory of Dislocations*, McGraw-Hill, New York, 2nd Edition.

Hockney RW and Eastwood JW, (1981), *Computer simulation using particles*, McGraw-Hill, New York.

Hoffmann R, (1963), *J. Chem. Phys.*, **39**, 1397.

Hohenberg P and Kohn W, (1964), *Phys. Rev.*, **136**, B864.

Hornstra J, (1958), *J. Phys. Chem. Solids*, **5**, 129.

Huber KP and Herzberg G, (1979), *Molecular Spectra and Molecular Structure. IV Constants of Diatomic Molecules*, Van Nostrand, Princeton.

Huff HR and Shimura F, (1985), *Solid State Technol. March*, 103.

Hull D and Bacon DJ, (1984), *Introduction to Dislocations*, Pergamon Press, Oxford.

Ihm J, Zunger A and Cohen ML, (1979), *J. Phys. C: sol. stat. phys.*, **12**, 4409.

Imai M and Sumino K, (1983), *Phil. Mag. A*, **47**, 599.

Jaros M and Kirton MJ, (1982), *Philos. Mag. B*, **46**, 85.

Jian Z, Kaiming Z and Xide X, (1990), *Phys. Rev. B*, **41**, 12915.

Joannopoulos JD, (1977), *Phys. Rev. B*, **16**, 2764.

Jones R, (1979), *J. Phys. (Paris)*, **40**, C6-33.

Jones R, (1981), *Inst. Phys. Conf. Ser.*, **60**, p. 45.

Jones R, (1985), *Yamada Science Foundation*, 343.

Jones R, (1987), *J. Phys. C: sol. stat. phys.*, **20**, L271.

Jones R, (1992), *private communication.*

Jones R and King TEG, (1983), *Phil. Mag. B*, **47**, 481.

Jones R and Marklund S, (1980), *Phys. Status Solidi B*, **101**, 585.

Kamiyama H and Sumino K, (1985), *Yamada Conf. on Dislocs. in Solids*, Ed: Suzuki H, Nonomiya T, Sumino K and Takeuchi S, Univ. Tokyo Press, p.399.

Kane EO, (1976), *Phys. Rev. B*, **13**, 3478.

Kaxiras E and Pandey KC, (1988), *Phys. Rev. B*, **38**, 12736.

Keating PN, (1966), *Phys. Rev.*, **145**, 637.

Kerker GP, (1980), *J. Phys. C: sol. stat. phys.*, **13**, L189.

Kimerling LC, Patel JR, Benton JL and Freeland PE, (1981), *Inst. Phys. Conf. Ser.*, **59**, p. 401.

King-Smith RD, Payne MC and Lin JS, (1991), *Phys. Rev. B*, **44**, 13063.

Kirton MJ and Jaros M, (1981), *J. Phys. C: sol. stat. phys.*, **14**, 2099.

Kisielowski-Kemmerich C, Weber ER and Omling P, (1987), *Bull. Acad. Sci. USSR*, **51**, 18.

Kittel C, (1986), *Introduction to Solid State Physics*, Wiley, 6th Edition.

Kleinman L and Bylander DM, (1980), *Phys. Rev. Lett.*, **48**, 1425.

Klenova TV and Moloskii MI, (1986), *Sov. Phys. Solid State*, **28**, 1768.

Kohn W and Sham LJ, (1965), *Phys. Rev. A*, **140**, 1133.

Kohyama M, (1991), *J. Phys.: Condens. Matter*, **3**, 2193.

Kohyama M, Yamamoto R, Ebata Y and Kinoshita M, (1988a), *J. Phys. C: sol. stat. phys.*, **21**, 3205.

Kohyama M, Yamamoto R, Watanabe Y, Ebata Y and Kinoshita M, (1988b), *J. Phys. C: sol. stat. phys.*, **21**, L695.

Koizumi H and Ninomiya T, (1978), *J. Phys. Soc. Japan*, **44**, 898.

Krishna S, (1993), PhD Thesis, University of Oxford, England, *to be published.*

Kveder VV, Ossipyan YuA, Schröter W and Zoth G, (1982), *Phys Stat. Sol. A*, **72**, 701.

Lee JG and Morrison SR, (1988), *J. Appl. Phys.*, **64**, 12.

Lifson S and Warshell A, (1968), *J. Chem. Phys*, **49**, 5116.

Lightowlers EC, Higgs V, Gregson MJ, Davies G, Davey ST, Gibbings CJ, Tuppen CG, Schaffler F and Kasper A, (1989), *Thin Solid Films*, **183**, 235.

Lodge KW, (1986), *J. Phys. C: sol. stat. phys.*, **19**, 151.

Lodge KW, Altmann SL, Lapiccirella A and Tomassini N, (1984), *Philos. Mag. B*, **49**, 41.

Lodge KW, Lapiccirella A and Altmann S, (1983), *Inst. Phys. Conf. Ser.*, **67**, p. 55.

Lodge KW, Lapiccirella A, Battistoni C, Altmann SL and Tomassini N, (1989), *Philos. Mag. A*, **60**, 643.

Louchet F and Thibault-Desseaux J, (1987), *Revue de Physique Appliquee*, **22**, 207.

Louie SG, (1980), *Phys. Rev. B*, **22**, 1933.

Louie SG, (1989), *in Atomistic simulation of materials, eds. V. Vitek and D.J. Srolovitz, Plenum: New York*, p 125.

Lundberg M, (1987), *Phys. Rev. B*, **36**, 4692.

Marklund S, (1978), *Phys. Status Solidi B*, **85**, 673.

Marklund S, (1979), *Phys. Status Solidi B*, **92**, 83.

Marklund S, (1980), *Phys. Status Solidi B*, **100**, 77.

Marklund S, (1983), *J. Phys. (Paris)*, **44**, C4-25.

Marklund S, (1989), *Solid State Communications*, **72**, 609.

Marklund S and Wang YL, (1992), *Solid State Comm.*, **82**, 137.

McInnes DA, (1992), PhD Thesis, University of Oxford, England.

Metropolis N, Rosenbluth AW, Rosenbluth MN, Teller AH and Teller E, (1953), *J. Chem. Phys.*, **21**, 1087.

Monkhurst HJ and Pack JD, (1978), *Phys. Rev. B*, **13**, 5188.

Mukherjee KP, Bandyopadhyaya J and Gupta KP, (1969), *Trans. Metall. Societ. Aime*, **245**, 2335.

Nabarro FRN, (1947), *Proc. Phys. Soc.*, **59**, 256.

Nielsen OH and Martin RM, (1983), *Phys. Rev. Lett.*, **50**, 697.

Northrup JE, Cohen ML, Chelikowsky JR, Spence J and Olsen A, (1981), *Phys. Rev. B*, **24**, 4623.

Olsen A and Spence JCH, (1981), *Philos. Mag. A*, **43**, 945.

Omling P, Weber ER, Montelius L, Alexander H and Michel J, (1985), *Phys. Rev. B*, **32**, 6571.

Pandey KC and Phillips JC, (1974a), *Solid State Commun.*, **14**, 439.

Pandey KC and Phillips JC, (1974b), *Phys. Rev. Lett.*, **32**, 1433.

Pandey KC and Phillips JC, (1976), *Phys. Rev. B*, **13**, 750.

Panteleev VA, Baryshev RS, Akinkina EI and Volovskaya ND, (1974), *Sov. Phys. Solid State*, **16**, 356.

Pantelides ST and Harrison WA, (1975), *Phys. Rev. B*, **11**, 3006.

Patel JR and Kimerling LC, (1981), *Cryst. Res. Technol.*, **16**, 187.

Paxton AT and Sutton AP, (1988), *J. Phys. C: sol. stat. phys.*, **21**, L481.

Paxton AT and Sutton AP, (1989), *Acta Metall.*, **37**, 1693.

Payne MC, Teter MP, Allan DC, Arias T and Joannopoulos JD, (1992), *to be published.*

Peaker AR, Kaniewski M, Kaniewski J, Evans JH, Hamilton B and Lorimer G, (1991), *Proc. Electrochem. Soc. Symposium on "Defects in Silicon"*, Washington.

Peierls RE, (1940), *Proc. Phys. Soc.*, **52**, 23.

Perdew JP and Zunger A, (1981), *Phys. Rev. B*, **23**, 5048.

Persson A, (1983), *J. Phys. (Paris)*, **44**, C4-453.

Pettifor DG, (1977), *J. Phys. F*, **7**, 613.

Pettifor DG, (1987), *Sol. Stat. Phys.*, **40**, 43.

Pettifor DG, (1989), *Phys. Rev. Lett.*, **63**, 2480.

Pettifor DG, (1990), *Springer Proc. Phys.*, **48**, 64.

Pettifor DG and Podloucky R, (1986), *J. Phys. C: sol. stat. phys.*, **19**, 285.

Pettifor DG and Aoki M, (1991), *Phil. Trans. R. Soc. Lon.*, **A334**, 439.

Pohoryles B, (1986), *Mater. Sci. Forum*, **10-12**, 815.

Pohoryles B, (1987), *Izv. Akad. Nauk. SSSR Ser. Fiz.*, **51**, 1490.

Pohoryles B, (1988a), *Philos. Mag. Lett.*, **58**, 1.

Pohoryles B, (1988b), *Philos. Mag. Lett.*, **58**, 7.

Pohoryles B, (1989), *Inst. Phys. Conf. Ser.*, **104**, p. 175.

Press WH, Flaner BP, Teukolsky SA and Vertterling WT, (1986), *Numerical Recipes - The Art of Scientific Computing*, CUP.

Radzimski ZJ, Zhou TQ, Buczkowski A, Rozgonyi GA, Finn D, Hellwig LG and Ross JA, (1991), *Appl. Phys. Lett.*, **60**, 1096.

Ray ILF and Cockayne DJH, (1971), *Proc. Roy. Soc.*, **A325**, 543.

Ravi KV, (1981), *Imperfections and Impurities in Semiconductor Silicon*, (J. Wiley & Sons, New York), p.234.

Robertson J, (1983a), *Phys. Rev. B*, **28**, 4666.

Robertson J, (1983b), *Phys. Rev. B*, **28**, 4647.

Sato M and Sumino K, (1985), *Yamada Conf. on Dislocs. in Solids*, Ed. Suzuki H, Nonomiya T, Sumino K and Takeuchi S, Univ. Tokyo Press, p.391.

Sauer R, Weber J, Stolz J, Weber ER, Kosters KH and Alexander H, (1985), *Appl. Phys. A*, **36**, 1.

Schröter W, Scheibe E and Schoen H, (1980), *J. Microsc.*, **118**, 23.

Seeger K, (1982), *Semiconductor Physics*, Springer, New York, 217, 260.

Shockley W, (1953), *Phys. Rev.*, **91**, 228.

Singh J, (1981), *Phys. Rev. B*, **23**, 4156.

Slater JC and Koster GF, (1954), *Phys. Rev.*, **94**, 1498.

Solberg JK, (1978), *Acta. Cryst. A*, **34**, 684.

Stich I, Payne MC, King-Smith RD, Lin J-S and Clarke LJ, (1992), *Phys. Rev. Lett.*, **68**, 1351.

Stillinger FH and Weber TA, (1985), *Phys. Rev. B*, **31**, 5262.

Stoneham AM, Torres VTB, Masri PM and Schober HR, (1988), *Philos. Mag. A*, **58**, 93.

Suezawa M, Sumino K and Iwaizumi M, (1981), *Inst. Phys. Conf. Ser.*, **59**, 407.

Sumino K, (1989), *Mat. Sci. and Eng.*, **B4**, 335.

Sumino K and Imai M, (1983), *Phil. Mag. A*, **47**, 753.

Sutton AP, (1989), *Phil. Mag. A*, **60**, 147.

Sutton AP, (1992), *Phil. Trans. Roy. Soc.*, to appear.

Sutton AP, Finnis MW, Pettifor DG and Ohta Y, (1988), *J. Phys. C: sol. stat. phys.*, **21**, 35.

Swope WC, Andersen HC, Berens PH and Wilson KR, (1982), *J. Chem. Phys.*, **76**, 637.

Szielko W, Breitenstein O and Pickenhein R, (1981), *Cryst. Res. Technol.*, **16**, 197.

Teichler H, (1989a), *Presented at the 6th Internat. Symposium on Structure and Properties of Dislocations in Semiconductors, Oxford, 1989*

Teichler H, (1989b), *Inst. Phys. Conf. Ser.*, **104**, 57.

Teichler H, (1989c), *Polycrystalline Semiconductors*, (ed J.H.Werner, H.P.Strunk,and H.J.Möller, Springer Proc. Physics, Springer, Heidelberg) **Vol 35**, p. 25.

Teichler H and Marheine C, (1987), *Izv. Akad. Nauk. SSSR Ser. Fiz.*, **51**, 663.

Teichler H and Veth H, (1983), *J. Phys. (Paris)*, **44**, C4-93.

Tersoff J, (1986), *Phys. Rev. Lett.*, **56**, 632.

Tersoff J, (1988a), *Phys. Rev. B*, **37**, 6991.

Tersoff J, (1988b), *Phys. Rev. B*, **38**, 9902.

Tersoff J, (1989), *Phys. Rev. B*, **39**, 5566.

Teter MP, Payne MC and Allan DC, (1989), *Phys. Rev. B*, **40**, 12255.

Umerski A, (1992), *private communication.*

Van Vechten JA and Phillips JC, (1970), *Phys. Rev. B*, **2**, 2160.

Verlet L, (1967), *Phys. Rev.*, **159**, 98.

Veth H and Teichler H, (1984), *Philos. Mag. B*, **49**, 371.

Vogl P, Hjalmarson HJ and Dow JD, (1983), *J. Phys. Chem. Solids*, **44**, 365.

Wang YL and Teichler H, (1989), *Phys. Status Solidi B*, **154**, 649.

Weber ER and Alexander H, (1979), *J. Phys. (Paris)*, **40**, C6-101.

Weber ER and Alexander H, (1983), *J. Phys. (Paris)*, **44**, C4-319.

Weronek K, Weber J, Höpner A, Ernst F, Buchner R, Stefaniak M and Alexander H, (1992), *Mater. Sci. Forum*, **83-87**, 1315.

Wilshaw PR and Booker GR, (1985), *Inst. Phys. Conf. Ser.*, **76**, 329.

Wilshaw PR and Booker GR, (1987), *Izv. Akad. Nauk. SSSR Ser. Fiz.*, **51**, 1587.

Wilshaw PR and Fell TS, (1989), *Inst. Phys. Conf. Ser.*, **104**, 85.

Wilshaw PR and Fell TS, (1990), *presented at the 20th International Conference on the Physics of Semiconductors, POLYSE '90*

Wilson JH, Todd JD and Sutton AP, (1990), *J. Phys.:Condens. Matter*, **2**, 10259.

Wood WW, (1986), *Proceedings of the Enricho Fermi summer school, Varenna 1985*, 3.

Woodham R and Booker GR, (1987), *Proc. 5th Oxford Conf. Micro. Semicon. Mats.*

Yin MT and Cohen ML, (1982a), *Phys. Rev. B*, **26**, 5668.

Yin MT and Cohen ML, (1982b), *Phys. Rev. B*, **25**, 4317.

Yin MT and Cohen ML, (1984), *Phys. Rev. B*, **29**, 6996.

Yonenaga I and Sumino K, (1985), *Yamada Conf. on Dislocs. in Solids*, Ed. Suzuki H, Nonomiya T, Sumino K and Takeuchi S, Univ. Tokyo Press, p.385.

3D PERIODIC CODE: MODELLING DISLOCATIONS